Abstract

WEIJUAN NI. Development of Boronic Acid-Based Spectroscopic Sensors for Saccharides. (Under the direction of Professor Binghe Wang)

Boronic acid functional group is used widely as a recognition moiety for the development of sensors for saccharides, due to its unique strong and reversible interaction with diols. The fluorescence and/or UV spectroscopic method are the easiest and most common methods to signal the binding event of these receptors (boronic acid compounds) with saccharides. This dissertation consists of three major parts. First, a series of fluorescent diboronic acid compounds with an anthracene PET (photoinduced electron transfer) system were designed and synthesized (Chapter 1). These compounds can be used as sensors for cell surface carbohydrates, such as sialyl Lewis X (sLex), which are known to be biomarkers for certain cancers. Among these diboronic acid compounds, the lead compound was found to fluorescently label cells expressing sLex selectively. The structure of the lead compound was modified and new conformationally constrained analogs were synthesized. Second, the mechanism of the fluorescent photoinduced electron transfer (PET) system, which was used in our design of fluorescent sensors for sLex, was examined in detail using both density functional calculation (DFT) and model compound fluorescence studies. Based on the study, a new hydrolysis mechanism was proposed (Chapter 2 and 3). Third, novel nitrophenol-based boronic acid reporter compounds, which show significant UV spectroscopic changes upon addition of sugars at neutral pH in aqueous solution, were designed and synthesized (Chapter 4). The design took advantage of the ability of a boronic acid functional group to modulate the pKa

and/or the electron density of a neighboring group. These reporter compounds can be used as the recognition and signaling unit for the construction of polyboronic acid sensors for selective and specific recognitions of saccharides of biological significance.

Development of Boronic Acid-Based Spectroscopic Sensors for Saccharides

By Weijuan Ni

A dissertation submitted to the Graduate Faculty

Of North Carolina State University

In partial fulfillment of the Degree of

Doctor of Philosophy

DEPARTMENT OF CHEMISTRY

Raleigh, NC

2003

Approved by:

Binghe Wang	Daniel L. Comins
Chair of the Advisory Committee	
Stefan Franzen	Suzanne T. Purrington

Dedication

To my son Yifan Andrew Zhang, the best thing ever happened to me, and to my parents Zhong Ni and Jianfang You. I appreciate all of your love, faith, and kindness.

Biography

The author was born in 1971 in Jiangsu Province, China. She grew up on the beautiful and fertile land along the south bank of Yangtze River, Zhangjiagang, Jiangsu Province. She stayed in Jiangsu Province for her first twenty-two years until she graduated from Nanjing University with a BS in Chemistry in 1993. In the same year, she left for Shanghai and entered the graduate school of the East China University of Science and Technology, and there she earned her MS in Fine Chemicals with Professor Kongchang Chen in 1996. In July 1999, she stepped onto the land of United States for the first time, and began her graduate education with Professor Binghe Wang at North Carolina State University. Here she worked on a variety projects based on boronic acid compounds as fluorescent and UV sensors.

Acknowledgements

I would like to thank my advisor, Professor Binghe Wang for his extensive guidance, immense patience and encouragement during my graduate work.

I would like to thank Professor Stefan Franzen for his supervising me on the calculation part of this dissertation, which opened a new window of chemistry --- computational chemistry to me.

I would like to acknowledge Dr. Wenqian Yang, Dr. Shouhai Gao, Dr. Xingming Gao and Dr. Vishnu Vardhan Reddy Karmati for their work on the synthesis of diboronic fluorescence sensors for cell surface carbohydrates project. I would like to acknowledge Dr. Gregory Springsteen for the initial thought on the UV sensor project.

I would like to thank the other former and current members of the Wang group, especially Dr. Wei Wang, who induced me to join Dr. Wang's research group and Dr. Eric Ballard, who gave lots of advice and suggestions.

I would like to thank the other committee members, Professors Daniel Comins and Suzanne Purrington.

I would like to thank my fellow graduate students and postdocs within the department, for their camaraderie.

I would like to acknowledge North Carolina State University Department of Chemistry and the Burroughs Welcome Fund and National Institutes of Health for funding this research.

I would like to acknowledge the support from the North Carolina Supercomputer Center.

Table of Contents **Page**

List of Figures…… ix

List of Tables…….xii

List of Schemes……....xiii

List of Abbreviations……xiv

Chapter 1. Development of Fluorescent Diboronic Acid Sensors for Cell Surface Carbohydrates……. 1

Abstract…….. 1

1.1. Contributions…….. 2

1.2. Introduction…….……..……..……. 2
1.2.1. Targeting on Cell-Surface Sachharides…….. 3
1.2.2. Boronic Acids and Carbohydrate Recognition Chemistry……... 4

1.3. Design of Fluorescent Diboronic Acid Compounds…… 5
1.3.1. Fluorescent Monitoring System…….. 5
1.3.2. Structure Analysis of Cell-Surface Carbohydrates……. 7
1.3.3. Design of Diboronic Acids Compounds…….. 8

1.4. Project Objective…….. 9

1.5. Syntheses…….. 11
1.5.1. Retrosynthetic Route of Diboronic Acid Compounds…….. 12
1.5.2. Synthesis of Common Building Block Anthracene Amines…... 13
1.5.3. Preparation of Linkers…….. 14
1.5.4. Synthesis of Boronic Acid Moiety……... 17
1.5.5. Synthesis of Diboronic Acid Compounds…… 17

1.6. Binding Study…….. 18
1.6.1. Binding Study against Chemically Synthesized Target Carbohydrates in Solution…… 18
1.6.2. *In Vitro* Binding Study……. 21
1.6.2.1. The Selection of Cells that Express sLex and Ley…. 22
1.6.2.2. Fluorescence Studies…….. 23

1.7. Design and synthesis of Constrained Analogs of the Lead Compound for Sensing Sialyl Lewis X and Conformational Study…… 26
1.7.1. Design…….. 26
1.7.2. Synthesis of Constrained Analogs……... 28
1.7.2.1. Synthesis of Two Constrained Building Blocks…… 28
1.7.2.2. Synthesis of Constrained Analogs……. 30

1.8. Conformational Study of the Constrained Analog Diboronic Acid Compounds Using Molecular Mechanics…….31
1.8.1. Low Energy Conformation Study of the Non-constrained Compounds……. 31
1.8.2. Low Energy Conformation Study of the Constrained Analog… 35

1.9. Conclusion……. 38

Experimental……..…….. 39

References……..61

Chapter 2. Study of the Mechanism of Electron-Transfer Quenching by Boron-Nitrogen Adducts in Fluorescent Sensors……. 66

Abstract……. 66

2.1. Introduction…….. 66
2.1.1. Boron-Nitrogen Bond Chemistry……..… 68
2.1.2. Charge Transfer Theory Involved in this Fluorescence Change Mechanism…….. 70

2.2. Method ……. 74

2.3. Results……... 75

2.3.1 B-N interaction ……. 75
2.3.2. Phenyl Boronic Ester Formation Requires a Cp-Cp-B-O Dihedral Angle ($\tau_{C\text{-}C\text{-}B\text{-}O}$) of 90^{o}……...77
2.3.3. The Minimum Energy Structure is Found for O-C-C-O Dihedral Angle $\tau_{O\text{-}C\text{-}C\text{-}O} = 30^{o}$……. 80
2.3.4. Energy of charge transfer states…… 81
2.3.5. Calculation of Solvation Effects…….. 83
2.3.6. Calculation of the Reorganization Energy…… 85
2.3.7. Calculation of the Activation Energy for Electron Transfer……. 87

2.4. Discussion……..88

2.5. Conclusion…… 91

References…….94

Chapter 3. A Study of the Hydrolysis Mechanism for a Photoinduced Electron Transfer (PET) Sensor System for Diol and Saccharides……..97

Abstract…….97

3.1. Introduction.……. 98

3.2. Synthesis……..…….99

3.3. Results and Discussion..…….…….100
3.3.1. The Proposal of a New Hydrolysis Mechanism……..100
3.3.2. Examination of the Hydrolysis Mechanism……..…104
3.3.2.1. pH Profiles of the Acid 1 and Various Complexes…....104
3.3.2.2. The Solvent Effect…….106
3.3.2.3. The Effect of Different Sugars on the Fluorescence Intensity Changes of **1**…….109
3.3.2.4. The B-N Bond Strength…….110
3.3.2.5. DFT Calculation Study…… 111

3.4. Conclusion……...……... 115

Experimental ……..……..…116

References……117

Chapter 4. Development of Nitrophenol-Based Boronic Acid Compounds for Color Sensing of Diols……... 118

Abstract……118

4.1. Introduction……..119

4.2. Design of UV Boronic Acid Sensors for Saccharides…….120
4.2.1. pKa Differences between Boronic Acid and Ester……..120
4.2.2. *p*-Nitrophenol Chemistry…….122

4.2.3. Design of Nitrophenol Boronic Acid……...122

4.3. Synthesis……..123
4.3.1. Synthesis of *p*-Nitrophenol-2-Boronic Acid (**7**)……...…123
4.3.2. Synthesis of 4, 6-Dinitrophenol-2-Boronic Acid (**8**)……124

4.4. Results.……..……...125
4.4.1. Binding Studies of **7** with Diol-containing Compounds……..125
4.4.2. Binding Studies of **8** with Diol-containing Compounds……..127

4.5. Mechanistic studies……...…..……..…128
4.5.1. Ionization States Study……129
4.5.1.1. Analyzation of the Ionization States through pH profiles of **7** the Absence and Presence of Diols……130
4.5.1.2. ^{11}B NMR Studies of Compound **7** and its Ester.……138
4.5.2. Mechanism of the Spectroscopic Change of **7** with the Addition of D-fructose at Neutral pH……...…139
4.5.3. Mechanism of the Spectroscopic Change of **8** with the Addition of D-fructose at Neutral pH……. 140

4.6. Conclusion……...…142

Experimental……143

References……147

Appendices…..……. 151

List of Figures Page

Figure 1.1. Boronic acid compounds bind with diols and form boronate……. 5

Figure 1.2. Mechanism proposed by the Shinkai group of fluorescence intensity change of compound **4** upon binding with saccharides…….. 6

Figure 1.3. Sub-structures of Lewis X, Lewis Y, sialyl Lewis a, and sialyl Lewis X….. 7

Figure 1.4. Designed fluorescent diboronic sensors for cell surface carbohydrates…….. 8

Figure 1.5. Designed and synthesized target diboronic acid compounds…… 11

Figure 1.6. Retrosynthetic route of diboronic acid compounds……... 12

Figure 1.7. The dicarboxylic acids used as the linkers in the diboronic acid compounds I prepared……15

Figure 1.8. The fluorescence intensity change profile of the diboronic acids……. 19

Figure 1.9. Comparison of the binding of the sensor **29** binding with sLex, Ley, sLea, and Lex…….……..20

Figure 1.10. Titration curves of **29** (1×10^{-5} M, MeOH/phosphate buffer (pH 7.4) (1/1, v/v), λ_{ex} = 370 nm, λ_{em} = 426 nm) against sLex...……..… 21

Figure 1.11. Flow cytometry analysis of surface antigens on HEPG2, HEP3B, and COS7 cells……...…….……22

Figure 1.12. Densitometry quantification of fluorescent compounds binding to HCC and control cell line…….…… 24

Figure 1.13. Representative fluorescent labeling studies of HEPG2, HEP3B, and COS7 cells…….. 25

Figure 1.14. Designed and synthesized constrained analogs (**77, 78, 79** and **80**)……27

Figure 1.15. Sub-structure of sLex……. 31

Figure 1.16. Low energy conformations of 5-membered ring boronate compounds **29**, **22, 9** and **39**…….……33

Figure 1.17. Low energy conformations of compounds **77**, **78**, **79** and **80**……. 36

Figure 2.1. Photoinduced electron transfer (PET) mechanism proposed by the Shinkai group……67

Figure 2.2. Structures of intermolecular models studied by DFT methods. The structural units consist of phenyl and methyl boronic acids and esters. ……..……69

Figure 2.3. Structures of intramolecular models studied by DFT methods. ……70

Figure 2.4. Important conformational coordinates in the ground state potential energy surface of phenyl boronic glycol ester with a trimethyl amino group.……..……....78

Figure 3.1. Mechanism proposed by the Shinkai group of fluorescence intensity change of compound 1 upon binding with saccharides……....102

Figure 3.2. Fluorescence profile of compound **1** (2×10^{-5}M) in anhydrous DMSO decreased with the addition of *cis*-1, 2-cyclopentane diol ……..….107

Figure 3.3. Fluorescence profile of compound **1** (4×10^{-6}M) in chloroform decreased with the addition of *cis*-1, 2-cyclopentane diol ……...108

Figure 3.4**.** Fluorescence profile of compound **1** (2×10^{-5} M) in anhydrous acetonitrile decreased with the addition of *cis*-1, 2-cyclopentane diol ……108

Figure 3.5. Optimized geometry product of hydrolysis of **PBA-OTMA** and **PBA-OTME**.…….113

Figure 4.1. Equilibrium of phenyboronic acid binding with saccharides/diols……..121

Figure 4.2. Ionization states of p-nitrophenol…….122

Figure 4.3. Absorption of compound **7** at 2×10^{-4} M in pH=7.4, 0.1 M phosphate buffer with increasing concentration of fructose ……126

Figure 4.4. Titration curves of **7** (2×10^{-4} M) at λ = 373nm against sugars……...127

Figure 4.5. Absorption spectra of **8** (5×10^{-6} M) (4% methanol in water (v/v), 0.1M phosphate buffer, pH 7.4, by adding various concentration of D-fructose.……128

Figure 4.6. pH profile of compound **7**……...…….131

Figure 4.7. pH profile of compound **7** with 200 mM D-fructose ……..131

Figure 4.8. pKa test of **7** without and with sugar. …….132

Figure 4.9. pH profile of compound **11** …….133

Figure 4.10. pH profile of compound **11** with 200 mM D-fructose……...134

Figure 4.11. pKa of compound of **11** in the absence and presence of fructose……..134

Figure 4.12. ^{11}B NMR spectra of compound **7** and **7** with *cis*-1,2-cyclopentane diol (left) in pH 7.4 buffersolution.…….138

Figure 4.13. pH profile of **8** (initial concentration: 1×10^{-5} M in 4% methanol/96% water, and the ionic strength was initially fixed at 0.1 M NaCl)...…….140

Figure 4.14**.** pH profile of **8** (initial concentration: 1×10^{-5} M in 4% methanol/96% water, and the ionic strength was initially fixed at 0.1 M NaCl) with 200 mM fructose…….141

Figure 4.15. pKa profile of **8** with the presence and absence of fructose……...……141

List of Tables **Page**

Table 1.1. Comparison of the structures and binding results of diboronic acid compounds with sLex and the computational results for the conformation difference…… …….. 34

Table 1. 2. Comparison of the structures of diboronic acid compounds with sLex and the computational results for the conformation difference ...……. 37

Table 2.1. B-N bond lengths, energies and charges obtained from potential energy surface studies. ……...76

Table 2.2. Energies, charges and boron-nitrogen distances in the o-trimethylamino boronic acid/ester models **OTMA-PBA, OTMA-PBE** and **OTMA-PBP**……...78

Table 2.3. Effect of modification of the dihedral angle (O-C-C-O) in the boronate ring in compound **OTMA-PBE** on the energy and optimum B-N bond length in the adduct……..80

Table 2.4. Binding energy of the neutral and ionic form for various molecules that can act as donors or acceptors in an electron transfer quenching mechanism……..82

Table 2.5. Charge transfer energy for the respective donor-acceptor pair based on the calculation of the binding energies…….….82

Table 2.6. Reorganization energy for donors and acceptors involved in electron transfer quenching of the anthracene excited state fluorescence..……85

Table 2.7. Activation energies for the Franck-Condon factor of the electron transfer rate constant calculated according to eq 5.……...……..87

Table 3.1. Different aspects of comparing the mechanism of fluorescence change of B-N bond mechanism Shinkai proposed and hydrolysis mechanism we proposed.……...102

Table 3.2. Internal energy changes for the hydration and hydrolysis reactions of phenyl boronic acids (**PBE-OTMA**) and boronate esters (**PBE-OTME**)…….114

Table 3.3. Internal energy changes for the hydration and hydrolysis reactions of phenyl boronic acids (**PBA-OTMA**) and boronate esters (**PBA-OTME**) including a continuum model for solvation (COSMO, ε = 78.4)……..114

List of Schemes page

Scheme 1.1. The synthesis of the important intermediate amine **60**, methyl-(10-methylaminomethyl-anthracen-9-ylmethyl)-carbamic acid tert-butyl ester. ……...…….13

Scheme 1.2. Synthesis of dicarboxylic acids **70a**-**72a**. ……16

Scheme 1.3. Preparation of boronic acid moiety **76**…….17

Scheme 1.4. Preparation of diboronic acids (**17**-**21**, **48**-**54**)…….……18

Scheme 1.5. Preparation of anthracene compounds **83** and **85**…….……28

Scheme 1.5. Preparation of anthracene compounds **88** and **89**…….....30

Scheme 1.6. Preparation of constrained diboronic acids **77**, **78**, **79** and **80**……..…31

Scheme 3.1. Preparation of compound **1**.……...100

Scheme 3.2. Possible mechanisms for the fluorescence intensity changes.……...101

Scheme 3.3. Hydrolysis experiments calculation of **PBA-OTMA** and **PBE-OTME**....112

Scheme 4.1. Designed nitrophenol-based boronic acids **7** and **8**……..……..122

Scheme 4.2. Synthesis of *p*-nitrophenol-2-boronic acid (**7**)……..…….124

Scheme 4.3. Synthesis of 4, 6-dinitrophenol-2-boronic acid (**8**)……..……..124

Scheme 4.4. Equilibrium among different species of **7** and **8** in the presence and absence of D-fructose. ……..……..129

Scheme 4.5. Resonance structrues of deprotonated *p*-nitrophenol and some Species of compound **7**……...……136

List of Abbreviations

sLex: sialyl Lewis X

Lex: Lewis X

Ley: Lewis Y

sLea: sialyl Lewis a

HCC: hepatocellular carcinoma

MRI: magnetic resonance imaging

BNCT: boron neutron capture therapy

CD: circular dichroism

NMR: nuclear magnetic resonance

DMSO: dimethyl sulfoxide

TEA: trimethylamine

$(Boc)_2O$: di-tert-butyldicarbonate

NBS: n-bromosuccinimide

AIBN: 2,2'-aza-bis-isobutyryl nitrile

EDC·HCl: 1-(2-dimethylaminopropyl)-3-ethylcarbodiimide hydrochloride

TFA: trimfluoroacetic acid

DCM: dichloromethane

Kd: dissociation constant

Ka: association constant

Chapter 1. Development of Fluorescent Diboronic Acid Sensors for Cell Surface Carbohydrates

Abstract

Targeting on specific cell surface carbohydrate, such as sialyl Lewis X (sLex), Lewis X (Lex), Lewis Y (Ley) and sialyl Lewis a (sLea), which are biomarkers of certain cancers, a series of fluorescent diboronic acids was synthesized as potential sensors for these carbohydrates. The lead compound was found to show the strongest fluorescence enhancement upon binding with chemically synthesized sLex and has good selectivity over Lex, Ley and sLea. It was able to fluorescently label cells expressing high levels of sLex (HEPG2) within a concentration range of 0.5 to 10 μM. This compound did not label cells expressing Lewis Y (HEP3B), nor cells without fucosylated antigens (COS7). Starting from this lead compound for sensing sLex, conformationally restricted analogs were designed and synthesized. Low energy conformations of these analogs were compared to that of the lead compound using molecular mechanics method.

1.1. Contribution

The goal of this project was to develop a novel type of small molecule organic compound that can recognize cell-surface specific carbohydrate structures. By linking two boronic acid moieties with various spacers, the artificial receptors are complementary to the spatial arrangement of the diol structures of the carbohydrates, and could be used to sense the target carbohydrates. We sampled a series of dicarboxylic acid linkers with different lengths, rigidities, and spatial orientations. Around 50 compounds were synthesized, 26 of them have been examined for their binding to sialyl Lewis X and varying degrees of binding were observed. Among 50, I have synthesized 12 of these diboronic acid compounds. Dr. Wenqian Yang, Dr. Shouhai Gao, Dr. Xingming Gao and Dr. Vishnu Vardhan Reddy Karmati synthesized the others. The *in vitro* studies of the diboronic acid compounds on cells expressing the carbohydrates were performed by W. Borden Hooks and John Carson of the University of North Carolina at Chapel Hill. The results of the binding studies of diboronic acids with both chemically synthesized target carbohydrates and those expressed on cancer cells are included. For the synthetic part, only the experimental details for the compounds that I have synthesized are included.

1.2. Introduction

Cancer is one of the leading causes of death. Early detection and intervention is one of the most important factors in determining the success rate in the treatment of many types of cancers. Despite the tremendous progress made in recent years, there are still many challenging issues concerning the early diagnosis, localization, staging, and treatment of such diseases. The detection and diagnosis of the tumor is frequently many

years after the earliest stages of cancer development at the cellular and molecular levels. Early detection of the cellular changes at the molecular level relevant to cancer development represents a new and promising approach to the diagnosis and prognosis of this disease. So novel technologies as molecular recognition for the development of bio-molecular sensors should target on well-defined molecular changes associated with cancer development and eventually allow for the seamless interface between sensing/detection and intervention. We wanted to develop a novel type of small molecule organic compound that can recognize cell-surface specific carbohydrate structures. Such sensors are boron-containing compounds and could potentially be used for magnetic resonance imaging (MRI) detection,[1-4] fluorescent sensing, boron neutron capture therapy (BNCT), [4-9] and targeted delivery of therapeutic and imaging agents.

1.2.1. Targeting of Cell-Surface Saccharides

It is well known that cell surface carbohydrate structures as part of glycosylated proteins and peptides are characteristic biomarkers of different cell types.[10-13] The transformations of normal to cancerous cells are also often associated with the alteration of cell surface carbohydrates.[10,14,15] Altered cell surface carbohydrates, such as sialyl Lewis X (sLex), sialyl Lewis A (sLea), Lewis X (Lex) and Lewis Y (Ley), have been associated with the progression, invasiveness, and metastatic potential of many types of cancers.[16-26] Clinical correlates demonstrate that sLea/sLex expression on carcinoma cells is associated with advanced stage disease and poor prognosis.[27-31] So the expression or over-expression of many such carbohydrates in cancer compared with normal cells do offer an excellent chance for the profiling, identification, and targeting of certain cancers

based on changes at the molecular level. Monitoring the expressions of these carbohydrates could help the diagnosis and prognosis of the disease. The development of molecular analysis probes targeted on these pathologically relevant carbohydrates will undoubtedly aid the diagnosis, prognosis, staging and treatment of many cancers.

1.2.2. Boronic Acids and Carbohydrate Recognition Chemistry

To develop such sensors or molecular tags targeted on specific carbohydrates, it is desirable to use recognition moieties that can recognize unique structural features on carbohydrates with high affinities. It has been known since the 1940's that boronic acid moieties can bind with high affinity to compounds with a diol (dihydroxyl) structural motif resulting in the formation of boronates with 5- or 6-membered ring structures[32] (Figure 1.1) and such diol structures are commonly found in saccharides. Specifically in the cases of saccharides, *cis* vicinal diols form particularly tight complexes with boronic acids.[32-34] Similarly, hydroxyl groups on the side chain of a saccharide (e.g., sLex and sLea) can pair up with an adjacent hydroxyl group (either *cis* or *trans*) to form either a five- or six-membered boronate complex, although the five-membered complex forms more tightly.

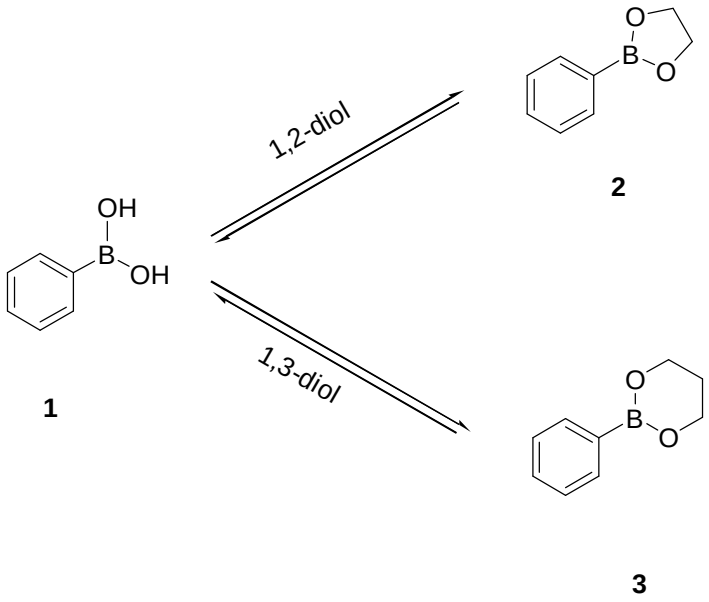

Figure 1.1. Boronic acid compounds bind with diols and form boronate.

Because of the unique properties of boronic acids in recognizing diol structures, boronic acid-based compounds are ideal recognition moieties for the construction of sensor for carbohydrates. In this application, we are interested in the construction of boronic acid-based sensors for oligosaccharides implicated in the development of cancer.

1.3. Design of Fluorescent Diboronic Acid Compounds

1.3.1. Fluorescence Monitoring System

There have been several methods developed to monitor the binding of boronic acids with carbohydrates, such as circular dichroism (CD), nuclear magnetic resonance (NMR) and fluorescence techniques. Among these methods, the fluorescence technique is the most sensitive, least expensive and most convenient way to monitor the binding event and can be used *in vivo*. Anthracene has been used frequently as a fluorophore in this field of research.[34-45] Shinkai and co-workers first developed a so-called

photoinduced electron-transfer (PET) fluorescence system with anthracene as a fluorophore, which was based on the boron-nitrogen interaction.[43,44] These sensors show increased fluorescence intensity when the anthracene boronic acid binds with saccharides (Figure 1.2).

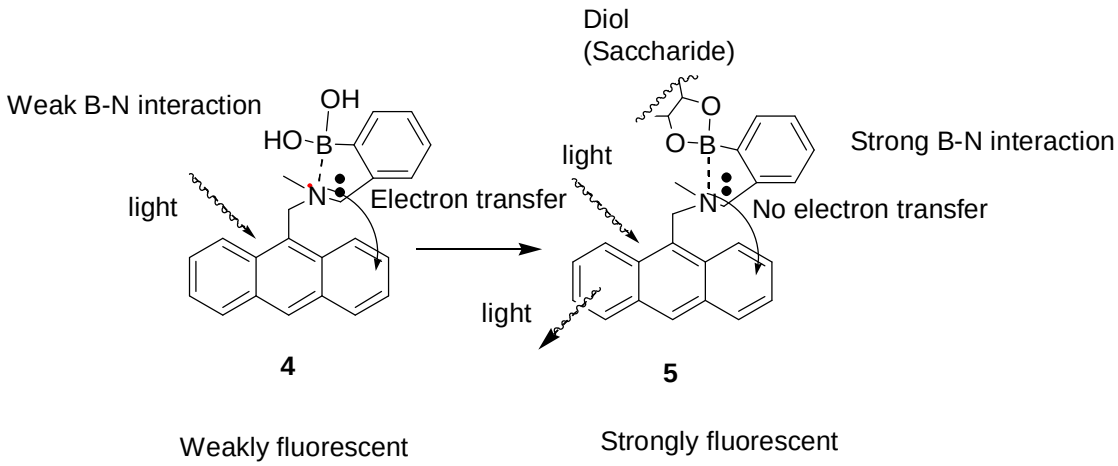

Figure 1.2. Mechanism[43] proposed by the Shinkai group of fluorescence intensity change of compound **4** upon binding with saccharides.

Anthracene is fluorescent, while in this system, it was widely believed that the lone pair nitrogen quenches (or decreases) the fluorescence intensity through photoinduced electron transfer to anthracene and makes compound **4** weakly fluorescent. Upon the binding of compound **4** with diol (or saccharide) to form boronate **5**, the Lewis acidity of boron will increase and it was proposed that the lone pair of amine will be involved in the boron-nitrogen bonding interaction but not participate in fluorescence quenching. As a result, compound **5** will be strongly fluorescent. In another word, the fluorescence intensity change is due to the suppression of the photo-induced electron transfer from nitrogen to the anthracene. Although the detailed mechanism may be a

matter subject to debate (See Chapter 2 and Chapter 3), the end result is that binding induces significant fluorescent intensity changes in protic solvents.

1.3.2. Structure Analysis of Cell Surface Carbohydrates

Figure 1.3 shows the structures of Ley, Lex, sLea, and sLex. With those hydroxyl groups that can interact tightly with boronic acid highlighted in bold with the paring indicated with circles. For sLex and sLea, either pair of the vicinal diols on the side chain could bind with boronic acid to form a boronate.

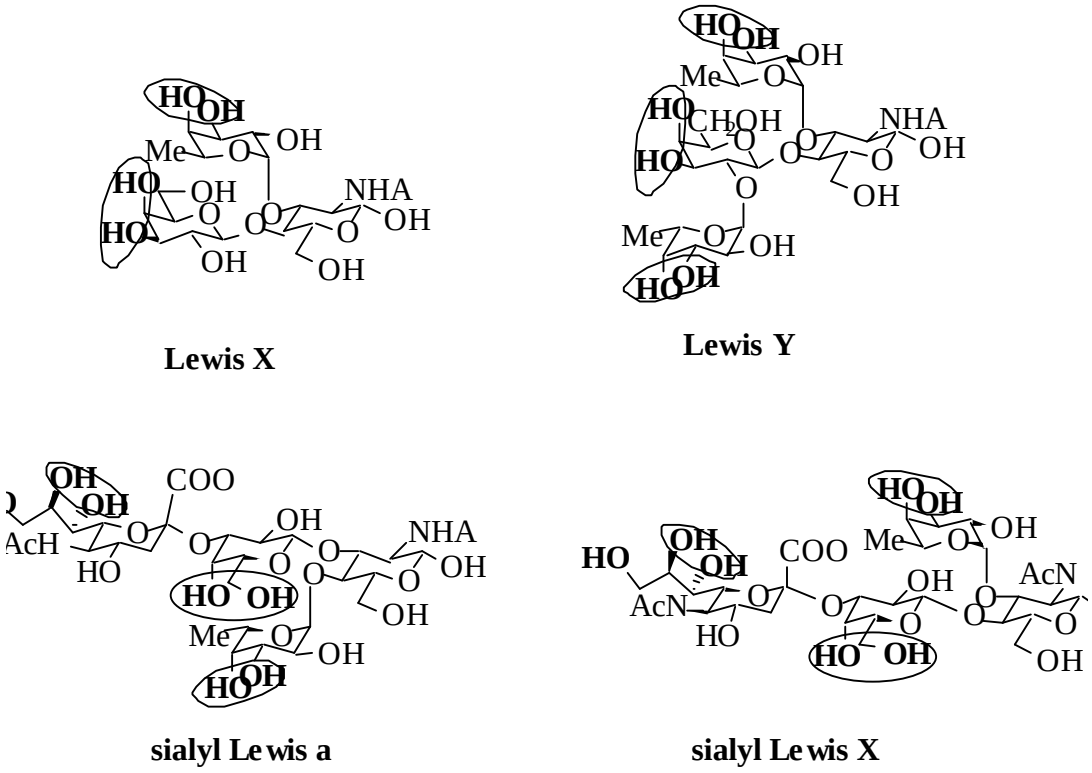

Figure 1.3. Sub-structures of Lewis X, Lewis Y, sialyl Lewis a, and sialyl Lewis X.

Although the drawing in Figure 1.3 does not specify the overall conformation and the spatial arrangement of each molecule, it is intuitive to expect that the spatial arrangements of these vicinal diol structural moieties are likely to be different among

these carbohydrates due to their grossly different primary (connectivity) structural features. It is understood that different cell surface carbohydrates will have different numbers and spatial orientations of vicinal diol moieties. For example, sLex, sLea, Lex, and Ley all have different numbers and/or different spatial orientations of vicinal diol structures. A number of boronic acid moieties arranged in a special three-dimensional orientation could bind the complementary carbohydrate moiety with high selectivity and affinity. Conceivably, artificial receptors with a special arrangement of two or more boronic acid moieties, which are complementary to the spatial arrangement of the vicinal diol structures of a particular carbohydrate, could be used as a selective and sensitive sensor for that particular carbohydrate.

1.3.3. Design of Fluorescent Diboronic Acids for Cell Surface Carbohydrates.

From the analysis of the structural characteristics above, diboronic acid compounds with different "linker" moieties as the scaffold have the chance to afford specific recognition of certain carbohydrates. Based on these principles, the sensors with two boronic acid moieties and various spacers were designed and synthesized (Figure 1.4).

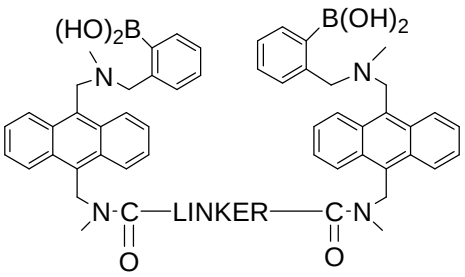

Figure 1.4. Designed fluorescent diboronic sensors for cell surface carbohydrates.

Such compounds are expected to have a possible correct spatial arrangements between two boronic acid moieties and complementary to the spatial arrangement of the vicinal diol structures of a particular carbohydrate, so that they may exhibit high affinity and specificity for the specific target carbohydrate. At first, the linkers were picked randomly and compounds synthesized were tested to find the lead compound, then based on the results, the structure of the lead compound was modified to increase the affinity and selectivity.

1.4. Project Objective

In summary, we are interested in the development of boron containing small-molecule sensor compounds that can recognize certain cell surface carbohydrates with high affinity and specificity. We tried to develop sensors that could target sLex, sLea, Lex, and Ley, because the expression of these carbohydrates has been correlated with the development and progression of many cancers.[16-26] We designed and synthesized fluorescent boronic acid compounds as molecule tags for sLex by linking two boronic acid moieties with various spacers that may make the two boronic acid moieties have correct spatial arrangements, so that they may exhibit high affinity and specificity for the target carbohydrate, sLex. These potential sensors will be screened using both chemically synthesized target carbohydrates as well as cancer cells over-expressing these carbohydrates. Their potential for MRI application will also be examined in the future. Such sensors could be used for both detection and targeted delivery of therapeutic agents (and imaging agents) and, therefore, have the potential to allow for the seamless interface of detection/sensing and treatment of certain cancers. Furthermore, because these

compounds are fluorescent, for accessible sites, such as colon, optical sensing is also feasible through optical fibers. If such sensors could recognize and bind certain cancer cells with high affinity and specificity, it could also be used for the delivery of high concentrations of boron specifically to a pathologically relevant site, which can subsequently be subjected to neutron radiation and be used in boron neutron capture therapy (BNCT).

These small molecule sensors may have the following advantages over antibody-based detection/delivery systems: (1) greater stability during storage and *in vivo*; (2) increased permeability through biological membranes and, therefore, enhanced target accessibility; (3) intrinsic properties allowing for magnetic resonance imaging (MRI) studies and boron neutron capture therapy; and (4) lower propensity to elicit undesirable immune responses. Similar methods, once developed, could also be used for the construction of sensors for other cell-surface carbohydrates implicated in human malignancies.

1.5. Synthesis

Figure 1.5 shows the synthesized fluorescent diboronic acid compounds.

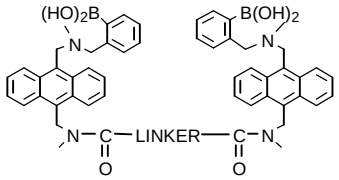

compounds	LINKER	compounds	LINKER	compounds	LINKER
7	10	**28**	5	**48**	
8	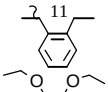 11	**29**			
9		**30**	8	**49**	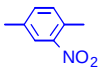
10	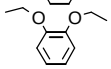	**31**	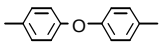		
11	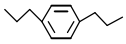	**32**		**50**	
12	3	**33**			
13	9	**34**	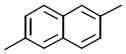	**51**	
14		**35**			
15	unsym[b]	**36**		**52**	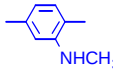
16		**37**	14		
17	2	**38**	-CH2OCH2-	**53**	
18	6	**39**	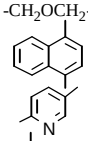	**54**	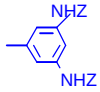
19	20	**40**			
20		**41**	H-Glu-Ala—		
21	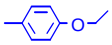	**42**	H-Ala-Ala—		
22	4	**43**	CO-Ala-		
23	12	**44**	CO-Ala-		
24	7	**45**	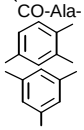		
25		**46**	-CH2CHCHCH2-		
26	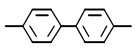	**47**	H-Glu-OH		
27	1		An-B(OH)2		

The number n on the LINKER column stands for $(CH_2)_n$.

The diboronic acids with LINKER in blue were what I prepared, others (in black) were made by other group members.

15

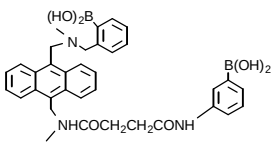

Figure 1.5. Designed and synthesized target diboronic acid compounds.

1.5.1. Retrosynthetic Route of Diboronic Acid Compounds

For the syntheses of diboronic acid compounds, the boronic acid moiety was put on at the last step. This was done due to the anticipated difficulty in the purification of boronic acids. The retrosynthetic route is outlined in Figure 1.6.

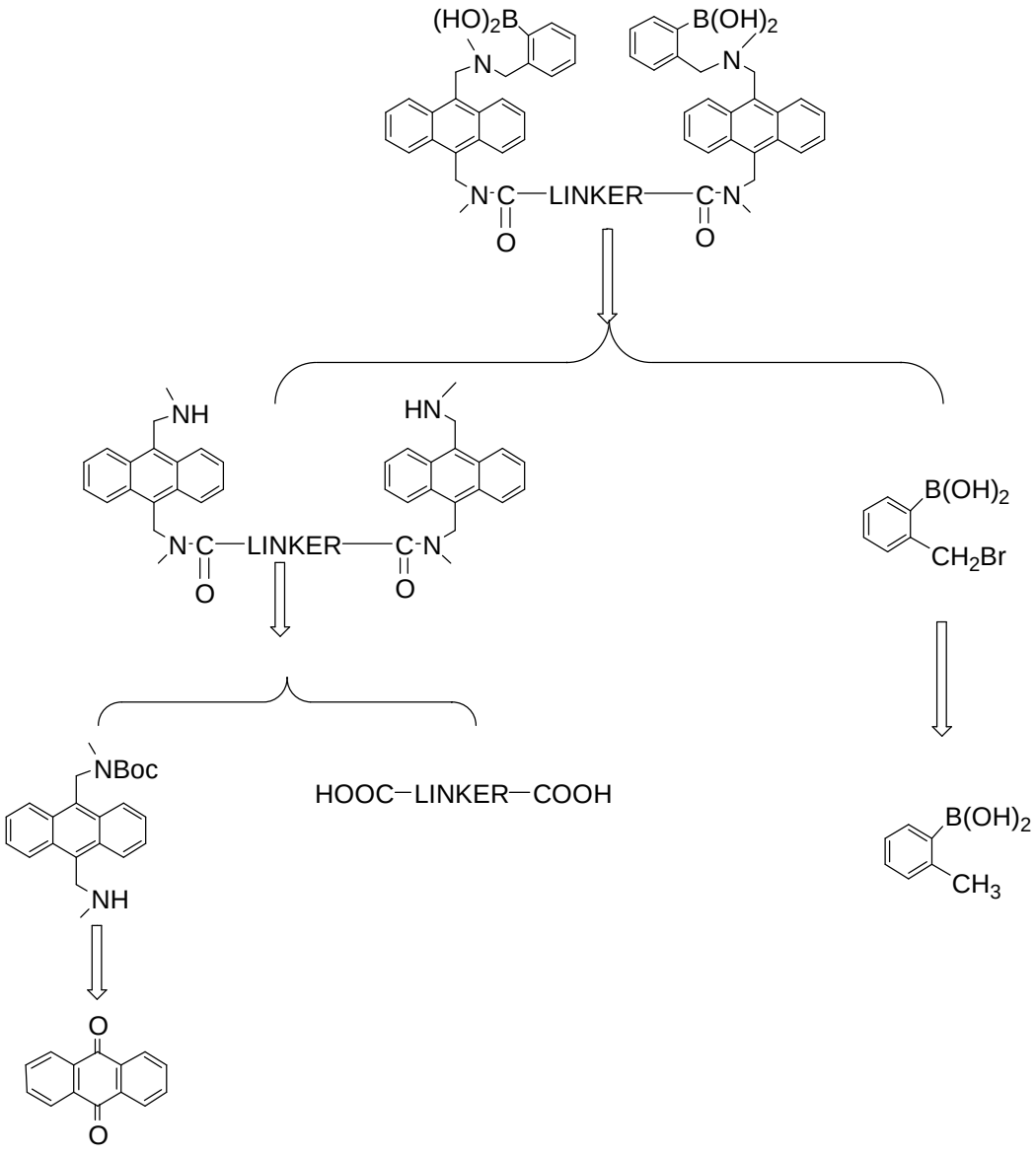

Figure 1.6. Retrosynthetic route of diboronic acid compounds.

1.5.2. Synthesis of Common Building Block Anthracene Amine 60

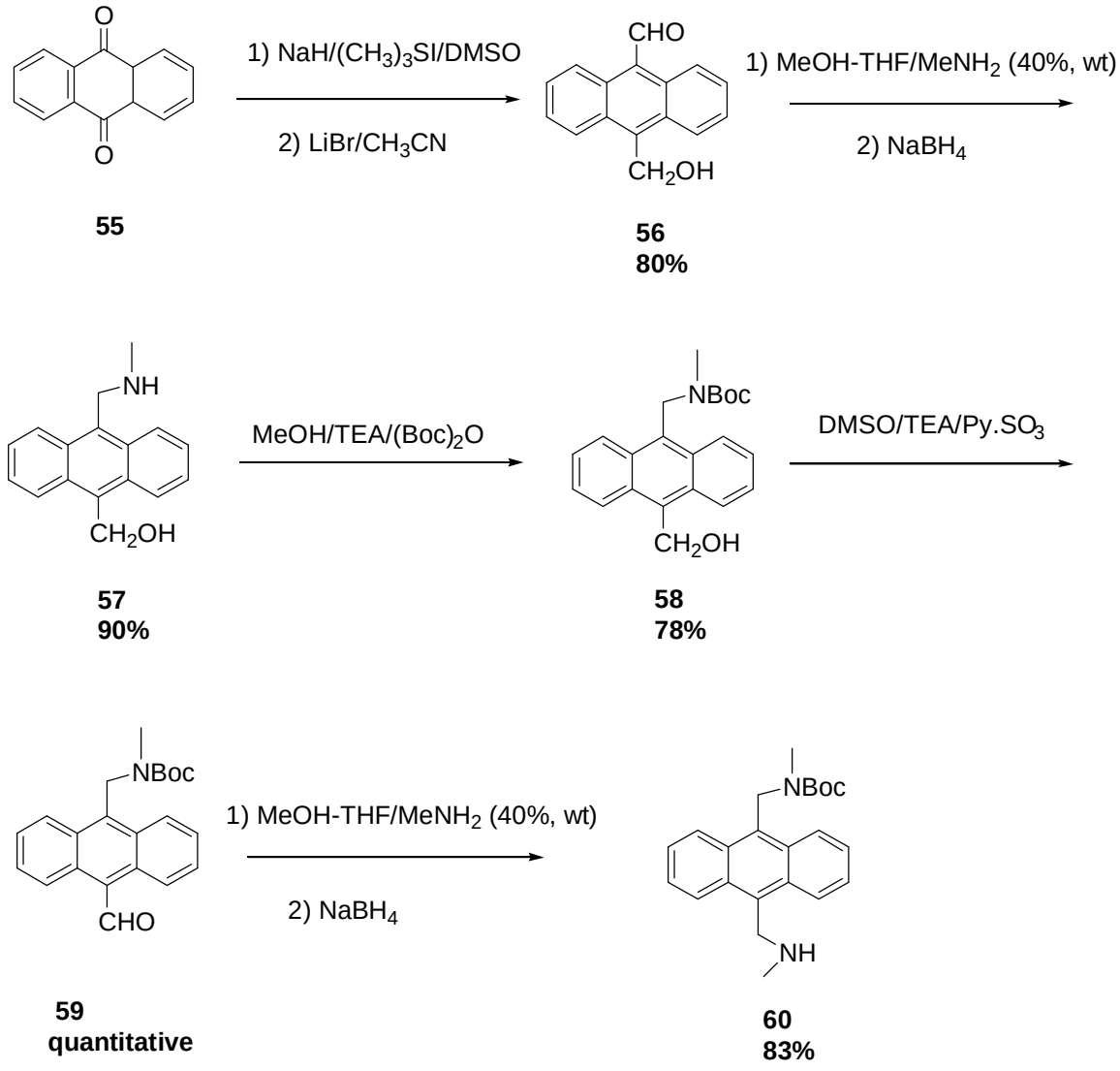

Scheme 1.1. The synthesis of the important intermediate amine **60**, methyl-(10-methylaminomethyl-anthracen-9-ylmethyl)-carbamic acid tert-butyl ester.

The synthesis of building block amine **60** started from the commercially available anthraquinone (**55**). Treatment of anthraquinone (**55**) with trimethylsulfonium iodide and sodium hydride in dimethyl sulfoxide (DMSO) to give corresponding bis(epoxide), which was then converted to hydroxyaldehyde **56** in 80% total yield in the presence of

lithium bromide in refluxing acetonitrile.[46] Hydroxyaldehyde **56**, upon reductive amination with methylamine in MeOH/THF and $NaBH_4$, gave amine **57** in 90% yield. The Boc-protected compound **58** was obtained in 78% yield by treatment of **57** with di-*tert*-butyldicarbonate in methanol in the presence of triethylamine (TEA). This was followed by oxidation with pyridine sulfur trioxide complex in DMSO in the presence of TEA to give aldehyde **59** in quantitative yield. The resulting aldehyde **59** was then converted to amine compound **60** in 83% yield through reductive amination.

1.5.3. Preparation of Linkers

In this project, we chose to use a spacer to link, through amide bond formation, two fluorescent boronic acid compounds for the construction of the potential sensors (Figure 1.5). In doing so, we sampled a series of dicarboxylic acid linkers with different length, rigidity, and spatial orientation in search of an optimal arrangement. Here only the syntheses of the compounds I prepared are reported. Figure 1.7 lists the dicarboxylic acids (compound **61a**-**72a**) I used. .

Dicarboxylic Acid

61 a		**67 a**	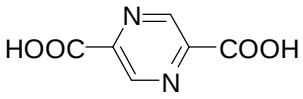
62 a		**68 a**	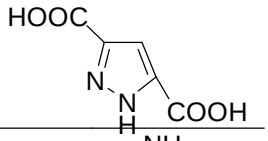
63 a		**69 a**	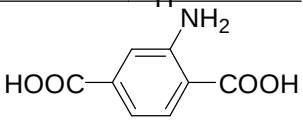
64 a	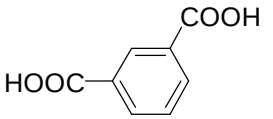	**70 a**	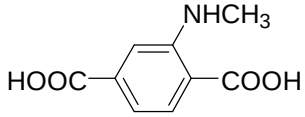
65 a	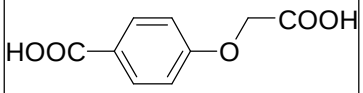	**71 a**	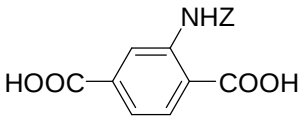
66 a	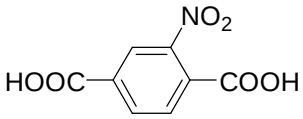	**72 a**	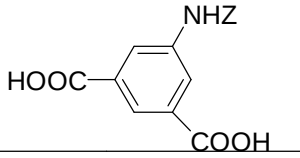

Z= 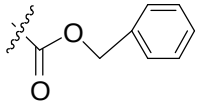

Figure 1.7. The dicarboxylic acids used as the linkers in the diboronic acid compounds I prepared.

Among the twelve acids, dicarboxylic acids **61a**-**69a** are commercially available. Compounds **70a**-**72a** were synthesized (Scheme 1.2), even though compound **70a** and **72a** are known compounds. Aminodicarboxylic acid **69a** was subjected to a reductive alkylation in ethanol and 37% formaldehyde with hydrogen in the presence of 5% Pt_2O to give 33% mono-methylation compound **70a**.[47] Treatment of 2-amino-terephthalic acid (**69a**) and 5-aminoisophthalic acid (**73a**) with benzyloxycarbonyl chloride in presence of

sodium hydroxide gave **71a** and **72a** in 40% and 80% yield respectively.[48]

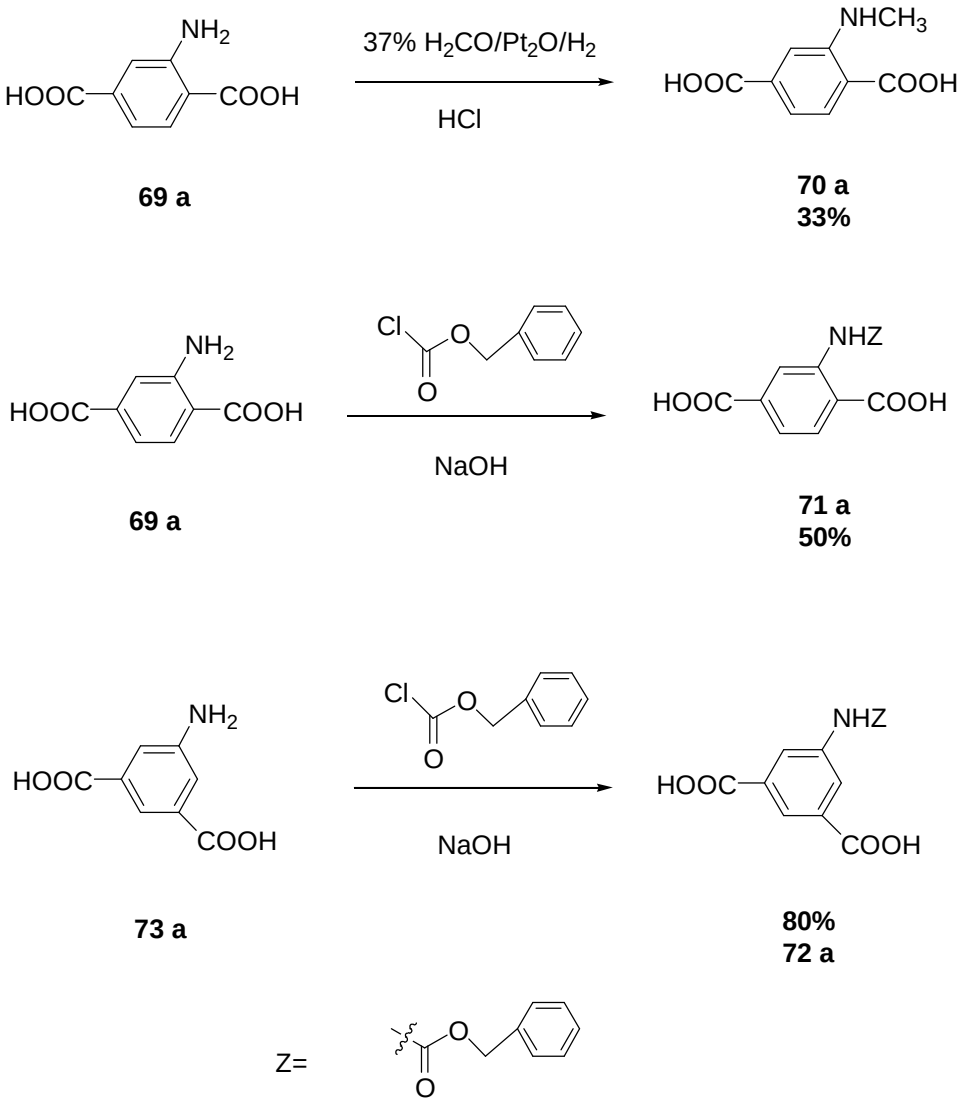

Scheme 1.2. Synthesis of dicarboxylic acids **70a**-**72a**.

1.5.4. Synthesis of Boronic Acid Moiety

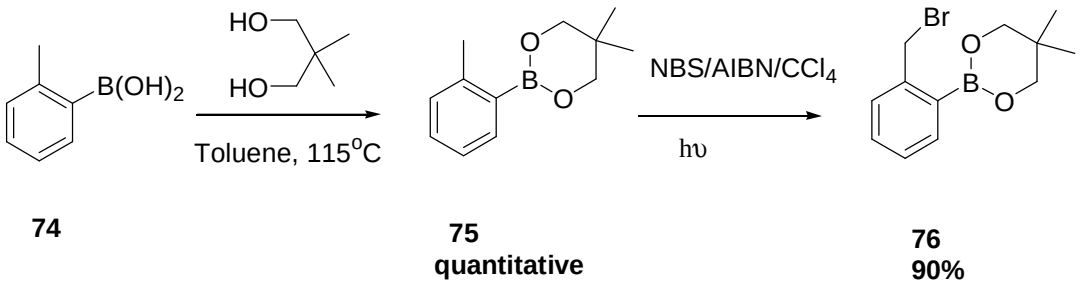

74 **75** **quantitative** **76** **90%**

Scheme 1.3. Preparation of boronic acid moiety **76**.

Boronate **76** was easily obtained (Scheme 1.3.) from a literature procedure.[44] Treatment of the commercially available compound *o*-toluneboronic acid **74** with 2-methyl-propane-1,3-diol in toluene gave boronate **75** in quantitative yield. Bromination of this boronate **75** using N-bromosuccinimide (NBS) in the presence of 2,2'-azo-bis-isobutyronitrile (AIBN) as initiator under 300 W tungsten light in carbon tetrachloride yielded 90% desired bromide compound **76**.

1.5.5. Synthesis of Diboronic Acid Compounds

Amine **60** was coupled with various diacids (compounds **61a**-**72a**, Figure 1.7) using 1-(2-dimethylaminopropyl)-3-ethylcarbodiimide hydrochloride (EDC • HCl) as the activating reagent to furnish compounds **61b**-**72b** in 30–90% yields. After deprotection of compounds **61b**-**72b** with trifluoroacetic acid (TFA), respectively, the free amines were then reacted with boronate **76** in the presence of potassium carbonate to give the diboronic acids **17**-**21**, **48**-**54** (Figure 1.5) in 30–80% yields. The synthesis is shown in Scheme 1.4.

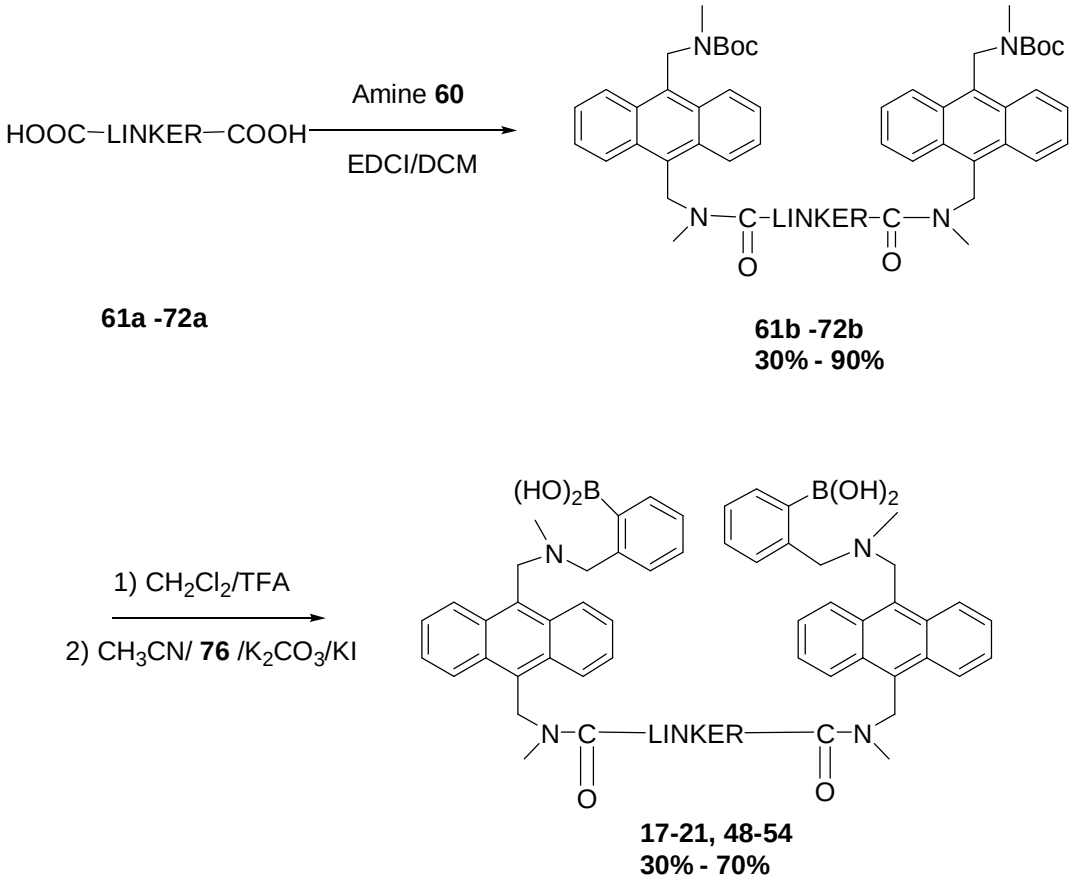

Scheme 1.4. Preparation of diboronic acids (**17**-**21**, **48**-**54**).

1.6. Binding Study

1.6.1. Binding Study Against Chemically Synthesized Carbohydrates in Solution.

These compounds (Figure 1.5) are designed to show significant fluorescence intensity changes upon binding with a complementary carbohydrate. In screening for their binding with the target carbohydrate, sLex, the fluorescence intensity changes of the sensor solutions upon addition of the carbohydrate were determined. Such experiments were conducted in a mixture of methanol and 0.1 M phosphate buffer (pH 7.4) (1:1, v/v). Methanol was used to improve the solubility of the sensor compounds. Concentration of

the sensors (Figure 1.5) was fixed at 1×10^{-6} M, and the concentration of sLex was set at 60 mM. The fluorescence intensity change profile for these diboronic acids is shown in Figure 1.8.

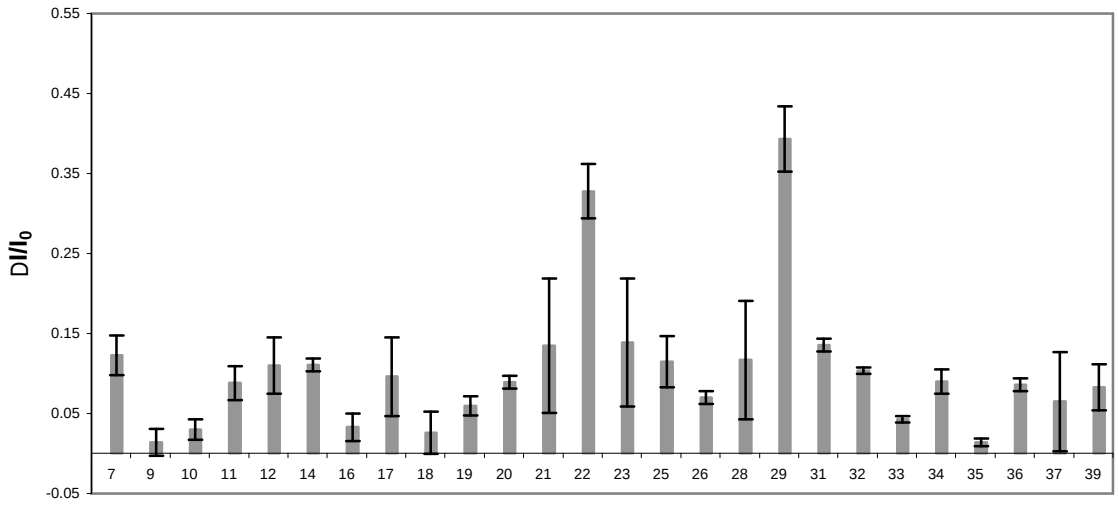

Figure 1.8. The fluorescence intensity change profile of the diboronic acids (compounds **7**, **9**, **10**, **11**, **12**, **14**, **16-23**, **25**, **26**, **28**, **29**, **31-36 and 39**, structure see Figure 1.5) (1×10^{-6} M) upon binding with cell surface carbohydrate sLex, [sLex] = 6×10^{-5} M, λ_{ex} = 370 nm, λ_{em} = 426 nm.

It can be seen that these compounds showed varying degrees of fluorescence intensity increase upon addition of sLex, indicating varying degrees of affinity for sLex. Among them, compound **29** (with 1,4–dicarboxylic acid as linker) shows the greatest fluorescence intensity change upon mixing with sLex (intensity increased 40% with addition of 60 mM sLex). However, the other diboronic acids with a 4-carbon linker but different spatial or geometric arrangements, such as a *trans* double bond (**16**), *trans* and *cis* cyclohexane rings (**32** and **33**) and naphthalene rings (**39**), showed smaller fluorescence enhancement, 3%, 11%, 5%, and 8% respectively. Most of the other diboronic acids also showed a small enhancement (<15%) of the fluorescence intensity

upon binding with sLex. These results indicate that the unique spatial relationship of the two boronic acid units allows for its more favorable interactions with sLex than the other diboronic acid compounds prepared (Figure 1.5 and Figure 1.8).

To see if compound **29** has good selectivity or not, the binding studies of compound **29** against Lex, Ley and sLea were also performed under the same condition. From the results shown in Figure 1.9, it is obvious that compound **29** has good selectivity with sLex over the others (Lex, Ley and sLea). Under the same test condition, **29** showed 40% fluorescence enhancement with sLex, while the fluorescence intensity was only increased around 5% with Ley, Lex and sLea (Figure 1.9), which is promising for our next step, *in vitro* tests on sLex.

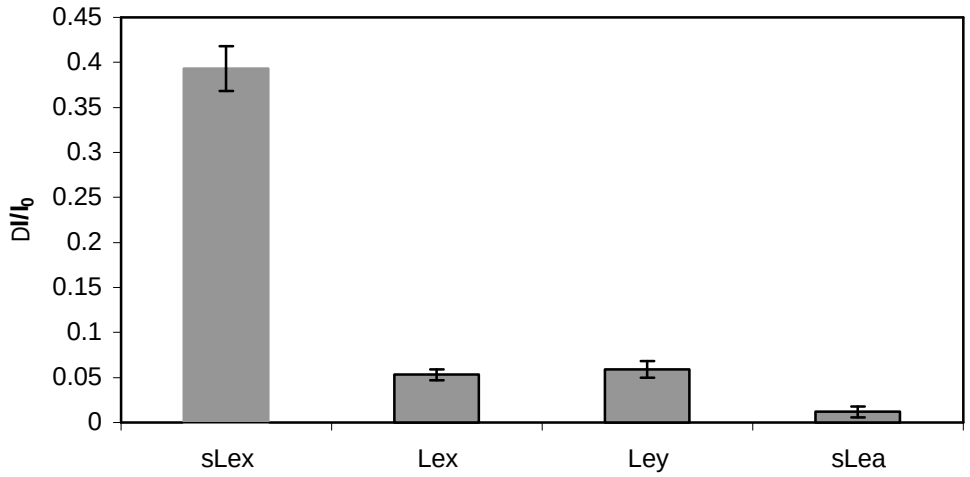

Figure 1.9. Comparison of the binding of the sensor **29** binding with sLex, Ley, sLea, and Lex. [**29**]=1 × 10^{-6} M in MeOH/phosphate buffer (pH 7.4) (1/1, v/v), [sLex] = [Ley] = [sLea] = 60 μM, [Lex] = 90 μM), λ_{ex} = 370 nm, λ_{em} = 426 nm.

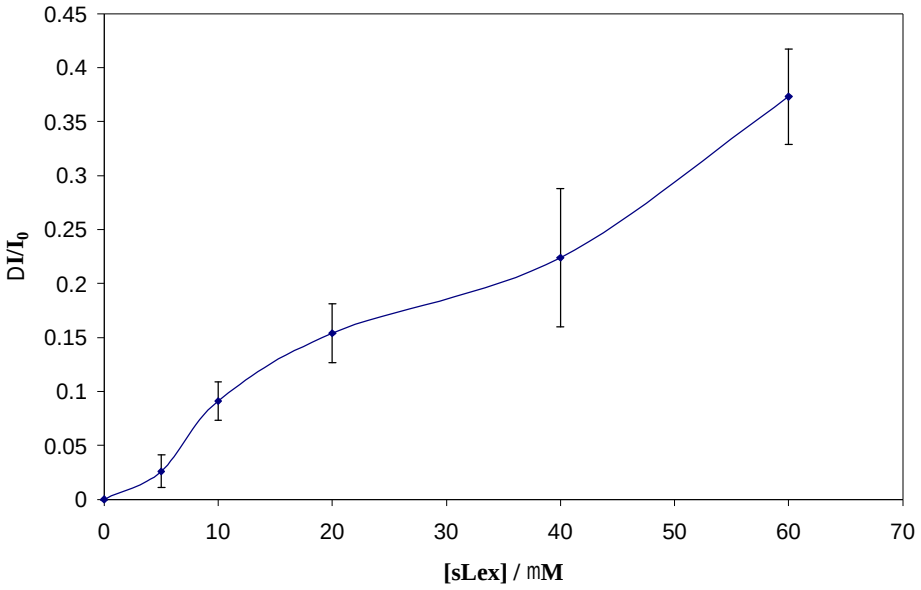

Figure 1.10. Titration curves of **29** (1×10^{-5} M, MeOH/phosphate buffer (pH 7.4) (1/1, v/v), λ_{ex} = 370 nm, λ_{em} = 426 nm) against sLex.

Further study of the fluorescence sensing behavior of compound **29** was conducted in a concentration effect against sLex (Figure 1.10). As a result, the dissociation constant (K_D) for **29** between this boronic acid and sLex was determined as 62 μ M (or with associate constant, Ka, 1.6×10^4 M^{-1}), which shows strong binding affinity.

1.6.2. *In Vitro* Binding Study

As discussed, our rationale for sensor design targets carbohydrate antigens associated with the development of cancer. Loss and gain of sLex expression in variously differentiated HCC specimens has been well described.[49,50] These observations have been linked to the development of cirrhosis, a frequent precursor of hepatocellular carcinoma (HCC). Such findings are comparable to chronic inflammatory states preceding development of colon carcinoma.[51] The specific role(s), if any, for sLex in transformation

and progression to HCC are not well understood. However, biosensors that could sensitively trace this development *in vitro* would likely further our understanding of hepatocarcinogenesis, in addition to providing new diagnostic and therapeutic approaches.

1.6.2.1. The Selection of Cells that Express sLex and Ley

After demonstration of binding of the sensors to sLex in solution, it was desirable to see whether **29**, the compound that showed the most significant fluorescence intensity increase upon addition of sLex, could bind the biomarker sLex on cell surfaces.[52,53] We therefore chose a cell line that selectively expresses sLex on the surface, HEPG2 (Figure 1.11).

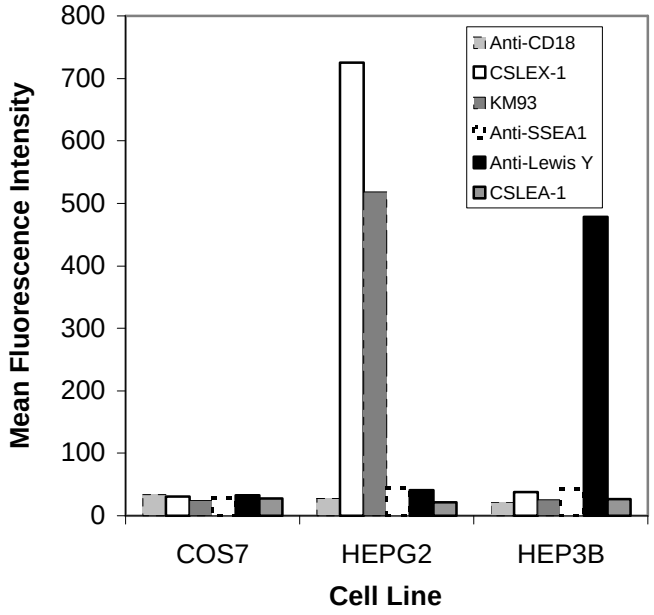

Figure 1.11. Flow cytometry analysis of surface antigens on HEPG2, HEP3B, and COS7 cells. Cells were harvested, stained with monoclonal antibodies, and subjected to flow cytometric analysis as described in experimental procedures. Anti-CD18 results are presented as negative controls. Monoclonal antibodies CSLEX-1 and KM93 both recognize sLex. Data presented here are the representative mean fluorescence intensity values from four experiments. The antigen-positive population of HEPG2 and HEP3B cells was gated at 1.5×10^1 units, and over 95% of stained cells were identified by these procedures with each primary antibody used.

To examine the selectivity of the sensor for cell surface sLex, HEP3B and COS7 cells were labeled in parallel. COS7 expresses none of the fucosylated antigens associated with carcinoma progression and HEP3B expresses only the Ley antigen.[54,55] Flow cytometry analysis of HCC lines with anti-carbohydrate monoclonal antibodies was performed to characterize surface glycan expression. Using two different monoclonal antibodies directed at sLex, HEPG2 cells were found to express high levels, while HEP3B cells expressed little or none (Figure 1.11). Anti-Ley monoclonal antibodies revealed the converse: high expression on HEP3B and little or no staining of HEPG2. None of the cell lines expressed Lex or sLea, related antigens expressed on other forms of carcinoma.[54-56] These cell lines were then used for the fluorescent labeling studies with the sensors.

1.6.2.2. Fluorescence Studies

HEPG2 and control cell lines were incubated with compound **29** (**S-23**) and three other diboronic acids (**9** (**S-3**), **11** and **22**, structures see Figure 1.5) selected as controls, examined under fluorescent microscopy, and photographed. Images were subjected to densitometry measurement as described in experimental procedures. As seen with sLex solution binding studies summarized in Figure 1.12, compound **29** was highest in mean gray value when binding HEPG2 cells expressing sLex. Compound **29** did not recognize Lewis Y on HEP3B cells. Compound **9** avidly bound Lewis Y-expressing HEP3B cells, and did not recognize sLex on HEPG2 cells at this concentration (1 μM),

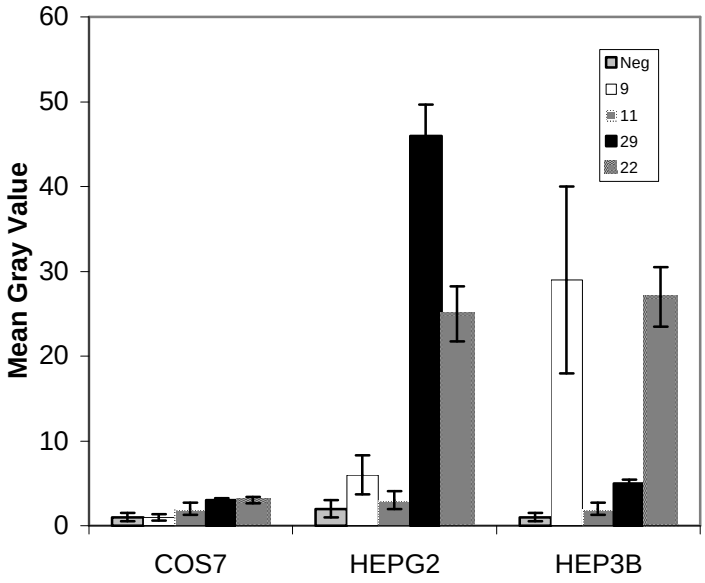

Figure 1.12. Densitometry quantification of fluorescent compounds binding to HCC and control cell line. Cells were labeled with 1 μM of sensors **9**, **11**, **22**, and **29** as described in experimental procedures. One well was incubated only in methanol/PBS without compound as a negative control ("neg"). Mean gray values (y-axis) were determined after subtraction of cell-free background. Results from five experiments are summarized.

Even at this relatively low concentration, compound **22** recognized surface sLex and Ley with equal avidity. Compound **11**, which had low affinity for sLex in solution, did not label HEPG2 or HEP3B. None of the compounds bound to COS7 cells at any of the concentrations tested. The above results showed that the cell labeling matched well with the solution binding studies using fluorimetry.

Images from a representative cell-labeling experiment are shown in Figure 1.13. HCC and control cell lines were incubated with compound **29**, examined under phase contrast and fluorescent microscopy, and digitally photographed. As expected, compound **29** labeled only HEPG2 cells, exhibiting dose-responsive fluorescence over the range of 0.5–10 μM. Even at higher concentrations, (e.g. 5 μM, Figure 1.13), **29** did not recognize Ley on HEP3B cells.

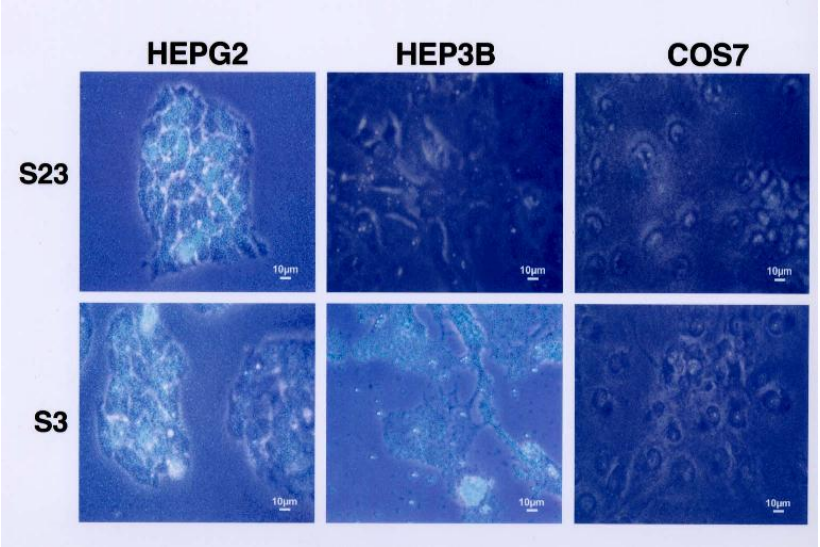

Figure 1.13. Representative fluorescent labeling studies of HEPG2, HEP3B, and COS7 cells. HEPG2 cells express only sLex, HEP3B cells express only Lewis Y, and COS7 cells do not express either antigen. Compounds **29** (S23) and **9** (S3) are used at 5 μM in the examples shown. λ_{ex} = 370 nm, λ_{em} = 426 nm. Scale in lower right corner indicates 10 micrometer length.

We also examined the selectivity of molecule **9** (**S3**). Compound **9** bound Lewis Y-expressing HEP3B cells at all concentrations tested (0.5–10 μM). At higher concentrations, **9** also labeled HEPG2 cells, suggesting cross-reactivity with sLex (e.g. 5 μM, Figure 1.12). Thus, sensor **29** alone appears to have both high sensitivity and specificity for sLex when compared to related compounds and carbohydrate antigens.

It is fortuitous that among this first group of diboronic compounds, **29** was able to label sLex-expressing cells at low concentrations (0.5 μM) without cross reactivity to Ley-expressing cells (HEP3B). This will serve as an excellent lead compound for further structural optimizations. However, much more work is needed to truly understand the structural features of **29** that led to this specific labeling activity. Such work will involve

extensive computational and conformational work and structure optimization of this lead compound and the constrained analogs synthesis will be discussed as below.

1.7. Design and Synthesis of Constrained Analogs of the Lead Compound for Sensing Sialyl Lewis X and Conformational Study

1.7.1. Design

As seen from above, after the syntheses of diboronic acids as sensors using randomly picked linkers for cell surface carbohydrates, these boronic acids were screened for their ability to bind both chemically synthesized carbohydrates in solution and carbohydrates expressed on cell surface. A lead compound **29** (sensor for sLex) was obtained, which showed high affinity labeling of cells expressing sLex. In order to design sensors with improved affinity and specificity, we were interested in exploring conformationally restricted analogs of **29**. As we can see from Figure 1.6, although **29** has a rigid linker, the overal structure of the compound is still somewhat flexible, due to the presence of many rotatable C-C and C-N single bonds. The initial design used crude approximation. We essentially maintained the same number of atoms in the linker moiety and constrained them in different fashions. Therefore, compounds **77, 78**, and **80** (Figure 1.14) were designed. In addition, we also designed a shortened conformationally restricted analog **79** (Figure 1.14). It was hard to know whether these newly designed analogs would have improved affinity and specificity for sLex due to the lack of understanding of the conformations of sLex and the binding mode. However, our initial intent was to gain some insight as to which direction the further modification should go.

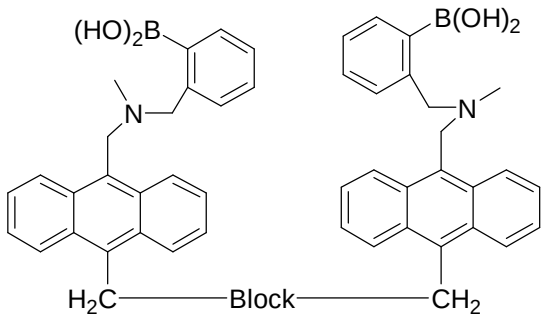

Diboronic Acid	Block
77	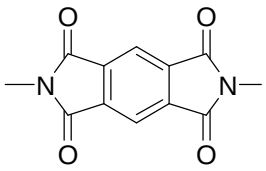
78	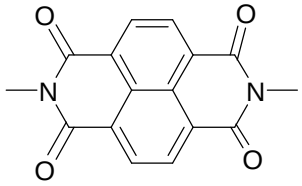
79	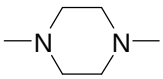
80	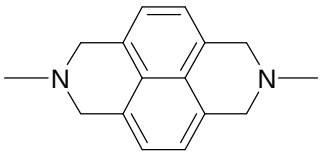

Figure 1.14. Designed and synthesized constrained analogs (**77, 78, 79** and **80**).

1.7.2. Synthesis of Constrained Analogs

The synthesis of these newly designed compounds followed similar strategies as described in the previous section. Again, the boronic acid moiety was attached last due to the anticipated difficulties in the purification of boronic acid compounds.

1.7.2.1. Synthesis of Two Constrained Building Blocks

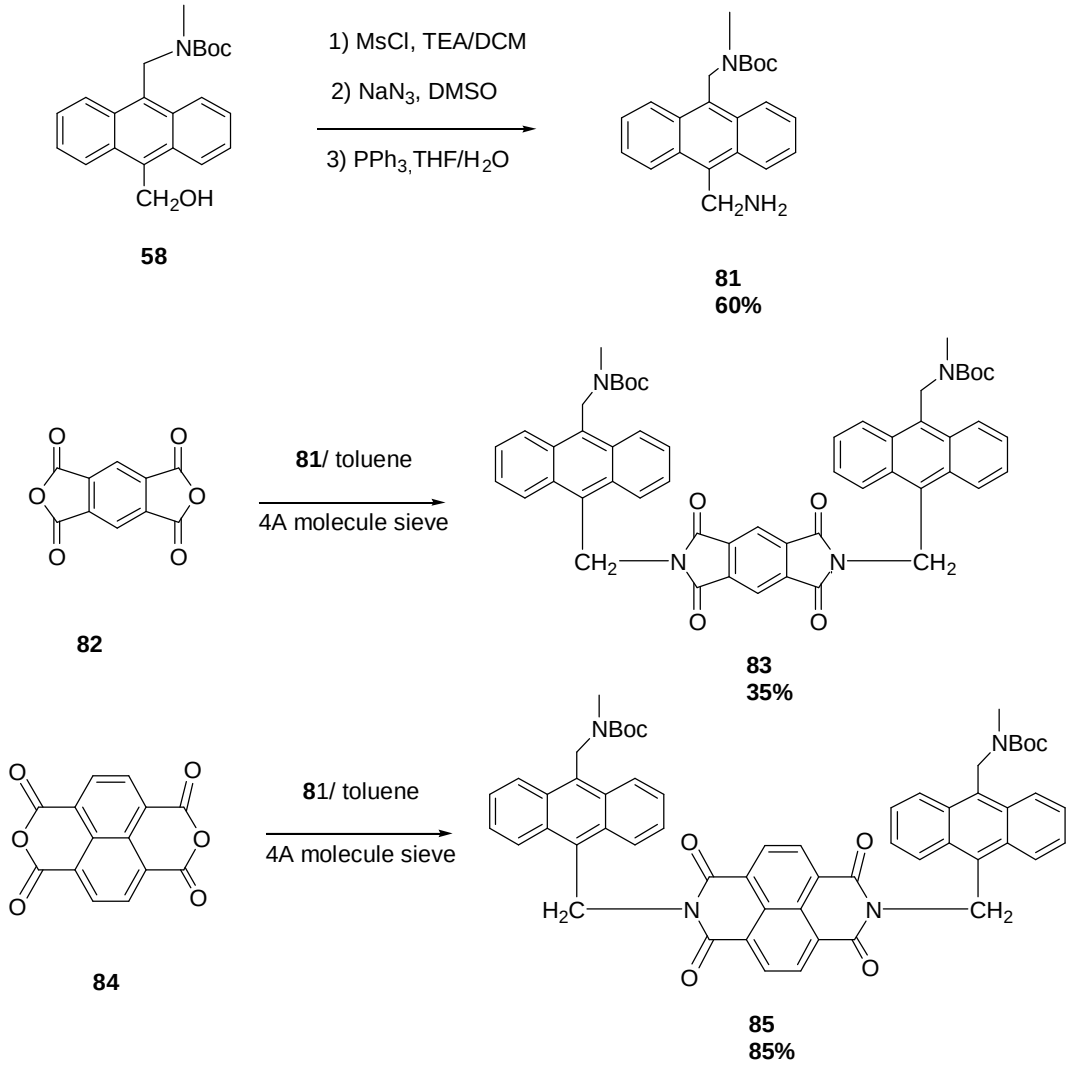

Scheme 1.5. Preparation of anthracene compounds **83** and **85**.

Two constrained analogs (**77** and **78**) have amide bonds as linkers, the syntheses of intermediates **83** and **85** are shown in Scheme 1.5. Compound **58** was first treated with methanesulfonyl chloride in the presence of TEA in dry CH_2Cl_2 solution in ice/water bath under nitrogen, which was followed by sodium azide in dry DMSO to yield desired azide compound. The resulting azide was then reduced by triphenyl phosphine to yield anthracene amine **81** in 60% yield. This amine **81** then was reacted with dianhydride **82** and **84** in toluene and gave diimide **83** and **85** in 35% and 85% yield, respectively.

One of the constrained analogs has a diamine **87** as linker, which was synthesized following a literature procedure[57] from commercially available 1,4,5,8-naphthalene tetracarboxylic dianhydride (**84)** (Scheme 1.5). Dianhydride compound **84** was treated with concentrated ammonium hydroxide solution to give 1,4,5,8-naphthalenetetracarboxylic diimide (**86**) in 60% yield. The reduction of diimide **86** by borane-tetrahydrofuran (BH_3-THF) gave 40% 1,2,3,6,7,8-hexahydro-2, 7-diazapyrene (**87**).

The anthracene alcohol **58** was treated by methanesulfonyl chloride in the presence of TEA in dry CH_2Cl_2 solution in ice/water bath under nitrogen, which was followed by the addition of diamine (piperizine or **87**) in dry DMF in the presence of potassium carbonate to yield constrained diboronic acid intermediates **88** (35%) and **89** (85%), respectively.

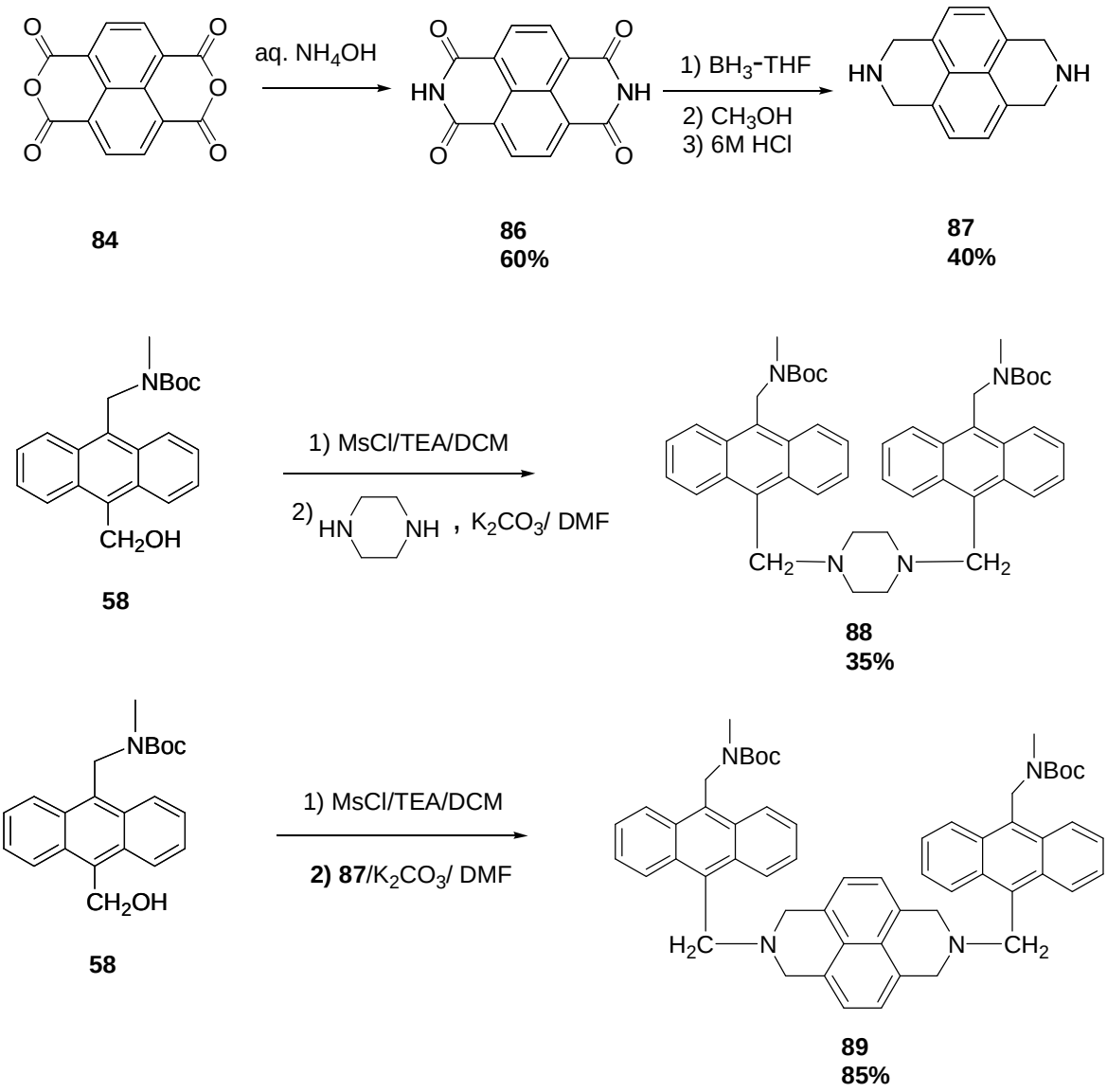

Scheme 1.5. Preparation of anthracene compounds **88** and **89**.

1.7.2.2. Synthesis of Constrained Analogs

The constrained boronic acid compounds **77**, **78**, **79** and **80**, were made from **83**, **85**, **88** and **89** following the same procedures for the synthesis of diboronic acid compounds in section 1.5.5 in 30–70% yields (Scheme 1.6).

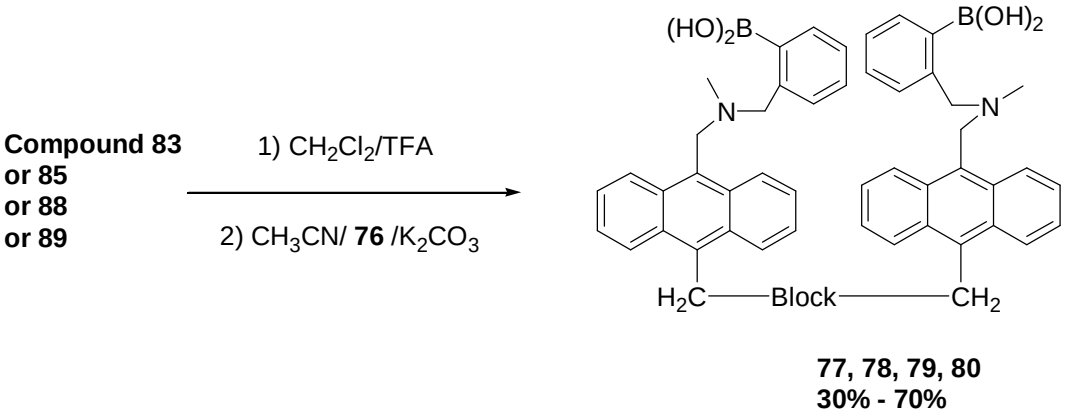

Scheme 1.6. Preparation of constrained diboronic acids **77**, **78**, **79** and **80**.

1.8. Conformational Study of the Constrained Analog Diboronic Acid Compounds Using Molecular Mechanics

1.8.1. Low Energy Conformation Study of the Non-constrained Compounds

In order to understand the structural features ideal for binding with sLex, we have also conducted computational studies of lead compound **29,** the compound with the best binding with sLex, and its constrained analogs (See previous section.). This study also included **39**, which has the same number of carbons in the "linker" region as **29**, but showed far less response in fluorescence upon sLex addition. As the first step, a conformational search using molecular mechanics was performed on lead **29** and a selected few analogs **9**, **22** and **39.**

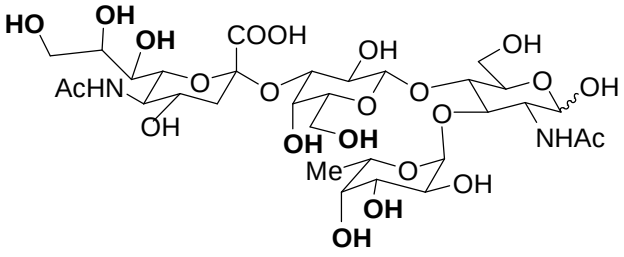

Figure 1.15. Sub-structure of sLex

.

From structure sLex above (Figure 1.15), it can be seen that when a diboronic acid binds with sLex, there two possibilities, the diboronic acid may bind with two sets of *cis*-diols and form two 5-membered ring boronate, or it may bind with one pair of *cis*-diols to form a 5-membered ring boronate and a pair of 1,3- diols to form a 6-membered ring boronate of diboronic acid compounds. To compare these modes of binding, we made two types of models, one is the simple 5-membered ring diboronate of the sensors and the other one is the diboronate of the sensor with one side 5-membered ring boronate and one 6-membered boronate. This comparison allows us to address two possible binding modes of the boronic acid with sLex. In addition, based on a literature report, the B-N was used in all these model calculations.[44]

It was expected that the diboronic acid co mpounds with different linkers (especially for those have different binding affinities for sLex) should have different lowest energy conformations. The low energy conformations of diborobonates with two 5-membered ring boronates, and one 5-membered and one 6-membered ring boronate of the diboronic acid compounds were studied. The figures of two kinds of boronates are very similar and here only the conformations of 5-membered ring boronates are listed in Figure 1.16. The distances of the two boron atoms vs. the linker are recorded for comparison in Table 1.1.

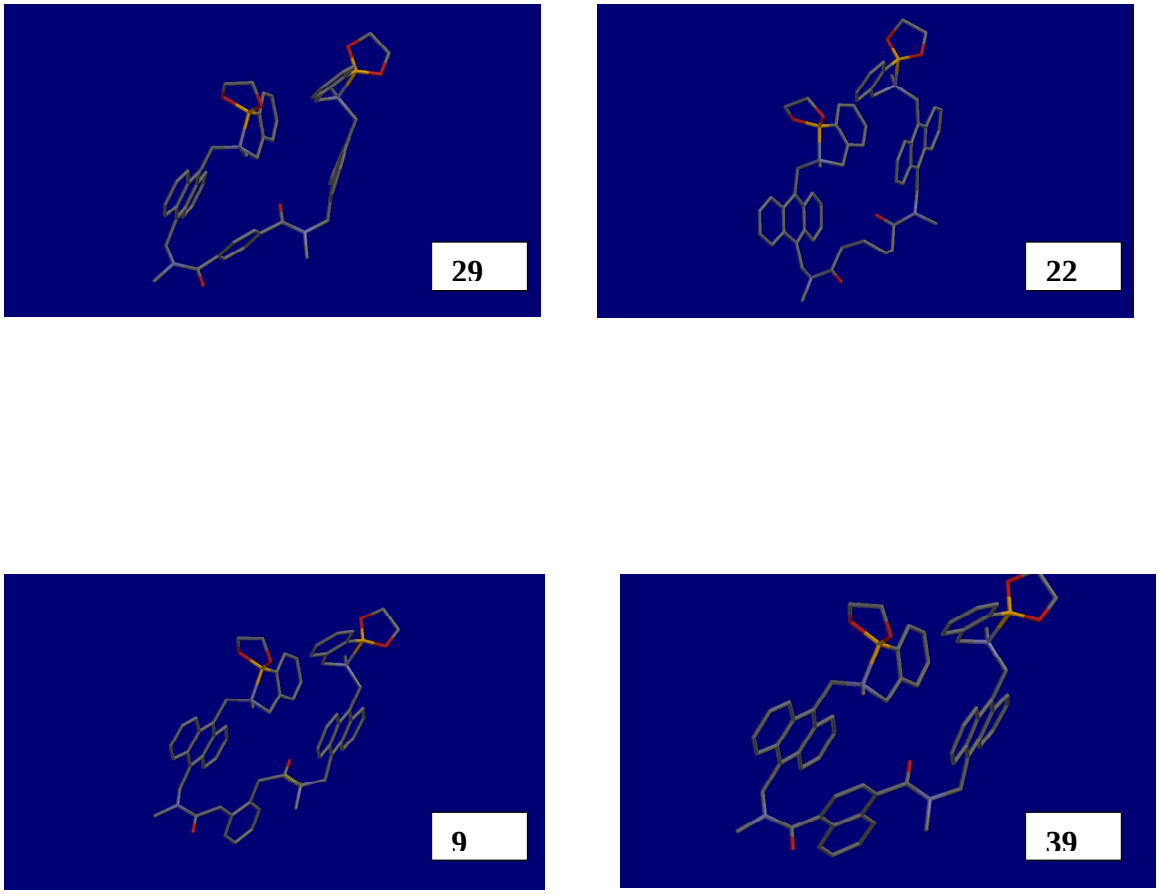

Figure 1.16. Low energy conformations of 5-membered ring boronate compounds **29**, **22, 9** and **39**.

Table 1.1. Comparison of the structures and binding results of diboronic acid compounds with sLex and the computational results for the conformation difference (recorded as the distance of two boron atoms).

A

two 5-membered ring boronate

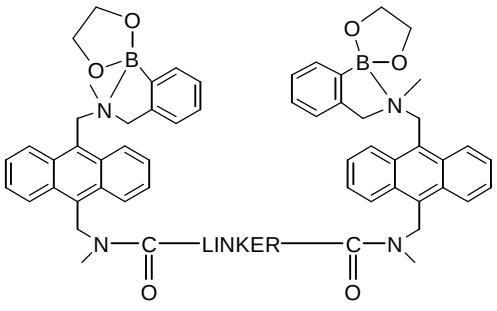

B

5, 6-membered ring boronate

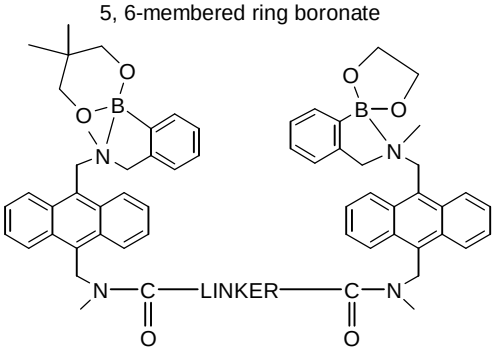

LINKER (Compound)	Distance of Boron Atoms/Å		Fluorescence Intensityl Increase with Addition of sLex $\Delta I/I_0$
	Type A	Type B	
 (**29**)	6.267	6.227	40%
—$(CH_2)_4$— (**22**)	6.325	6.363	32%
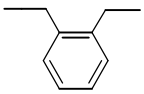 (**9**)	6.257	6.314	2%
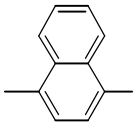 (**39**)	6.255	6.282	8%

From the conformations shown in Figure 1.6, it can be seen that the overall low energy conformations of these compounds are very similar, while the binding results vary with the structures. Mostly, the two anthracene rings are parallel with each other and the distance of two boron atoms varied from 6.1 Å to 6.4 Å for the both type A model (with two 5-membered boronate ring) and type B model (with one 5-membered ring and one 6-membered ring). These results apparently do not help to explain the experimental results. Several reasons could have contributed to this. First, the computations were conducted "in vacuum," while it is known that solvation could tremendously affect the computational outcome. Second, there are no reliable boron parameters published. Third, the assumption that B, N interaction is so strong that it actually forms a sigma bond is not necessarily correct (See Chapter 2 and Chapter 3). Our calculation at a higher level indicates that the B-N interaction, although present, may not necessarily play an important role in regulating the PET process and may have even less important role in affecting the conformations of the sensors (See Chapter 2 and Chapter 3). Fourth, it is not only the distance between the two boron atoms involved in the binding. The spatial orientation of these boronic acid moieties is also critical to the binding affinity and selectivity. Further computational studies will need to take all these into consideration before meaningful results can be obtained.

1.8.2. Low Energy Conformation Study of the Constrained Analogs

The low energy conformations of the constrained analogs were also studied using the same approach described in section 1.8.1. Figure 1.17 shows the low energy conformations of the 5-membered boronates of these constrained analogs. As can be

seen, the conformations of different linkers vary to some extent because of the rigidity of the linkers, though the two anthracene rings are still generally parallel to each other, but more separated than in **29**. As a result, the overall conformations of these constrained compounds are more "open," especially for compound **80** (with a large amine ring as the linker), the distance of two boron atoms reached 16.700 Å.

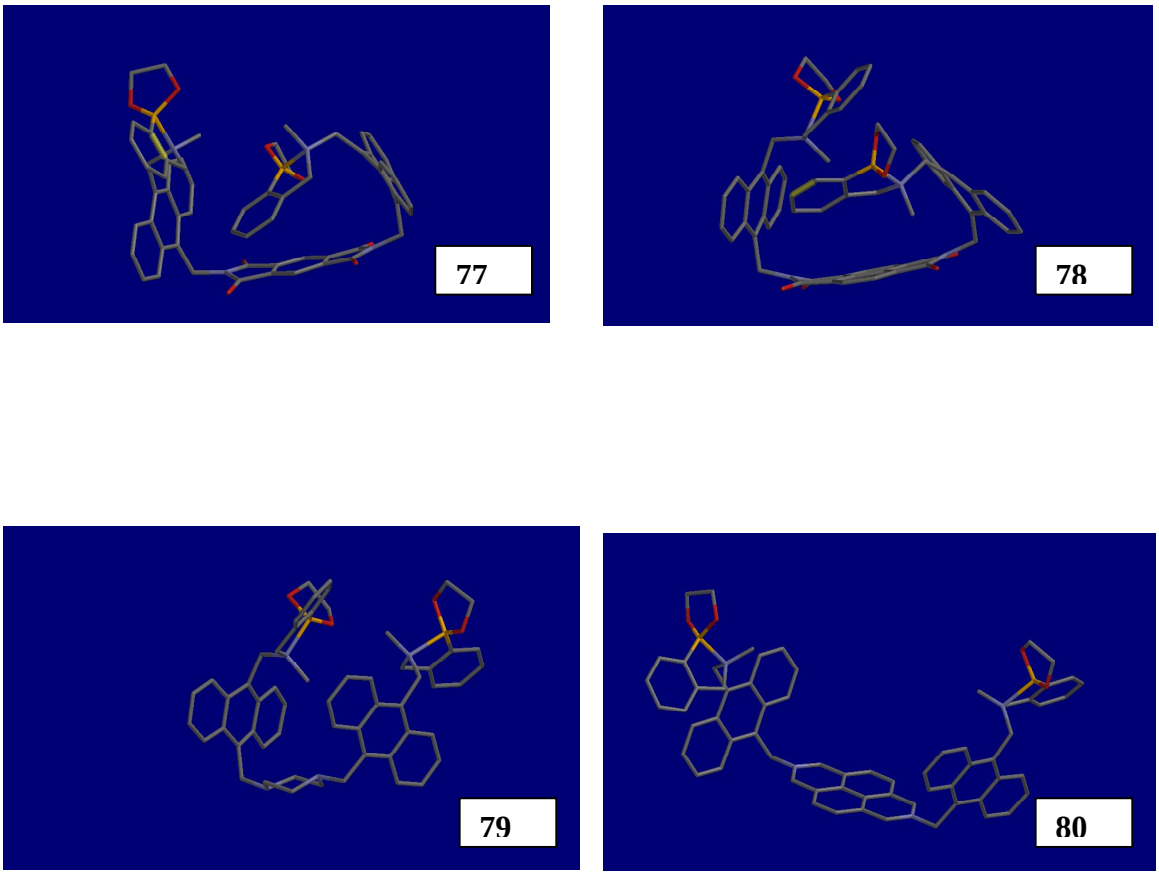

Figure 1.17. Low energy conformations of compounds **77**, **78**, **79** and **80**.

Table 1. 2. Comparison of the structures of diboronic acid compounds with sLex and the computational results for the conformation difference (recorded as the distance of two boron atoms of the 5-membered boronate compounds).

Type A

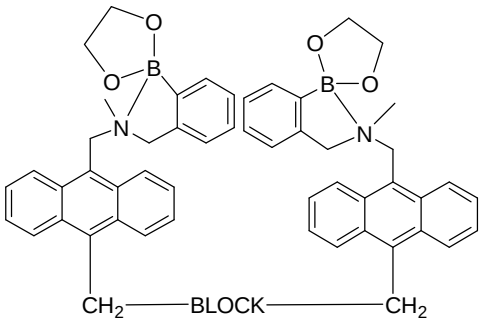

Type B

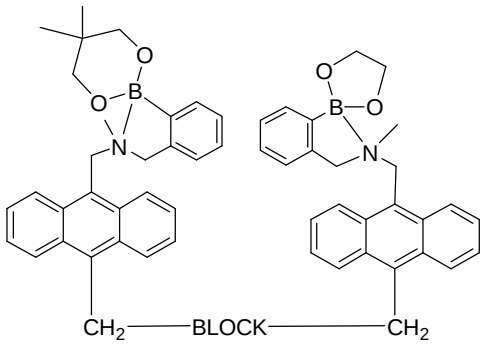

	Distance of Boron Atoms/ Å		Fluorescence Intensity Increase with Addition of sLex
	Type A	Type B	
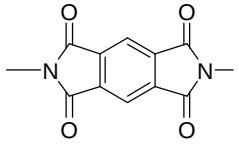 (**77**)	6.389	6.446	N/A
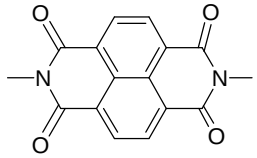 (**78**)	7.512	8.414	N/A
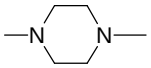 (**79**)	6.291	17.112	N/A
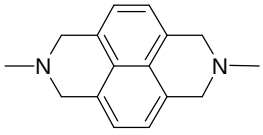 (**80**)	16.700	16.646	N/A

As can be seen from the Table 1.2, for the type B models, with one 5-membered ring boronate and one 6-membered ring boronate of these sensors, the distance between the two boron atoms of compound **79**, and **80** is very big, 17.112Å and 16.464 Å, respectively. One would not expect them to have good affinity and selectivity for sLex. It needs to be noted that these calculations suffer from the same problems as that described in the previous section. More rigorous calculations and parameterization will be needed to achieve more meaningful results. Especially, at this time the binding studies of these constrained diboronic acid compounds did not yield the desired improvement in binding with sLex.

1.9. Conclusion

Fluorescent diboronic acid compounds as sensors for sLex were designed and synthesized. The lead compound, having high binding affinity and good selectivity with sLex, was obtained through the screening by binding study against both chemically synthesized and cell expressed cell surface carbohydrates. The small fluorescent sensor developed here can be used for diagnostic purposes. Starting from the lead compound for sensing sLex, structural modification was performed and four constrained analogs were and synthesized. The binding studies of these compounds with sLex solution did not yield meaningful results. A molecular modeling study was used in an attempt to understand the relationship of structure and binding affinity. Low energy conformations of the constrained compounds and a few selected non-constrained diboronic compounds, which have been synthesized and tested against sLex, were searched using molecular mechanics methods. No direct correlations between the optimized conformations and

binding affinities were discovered. This could be due to the inherent flaws of the program and the computational approaches used. More rigorous approaches are needed in order to obtain meaningful results in this regard.

Experimental

General

All air- and/or water-sensitive reactions were performed under dry N_2 in flame-dried or oven-dried glassware. Most reagents were purchased from Aldrich or Fisher/Acros and used as received. SLex was purchased from Calbiochem and Aldrich. Tetrahydrofuran (THF) was distilled from Na/benzophenone prior to use. Acetonitrile (CH_3CN) and dichloromethane (CH_2Cl_2) were distilled from calcium hydride (CaH_2).

Analytical thin layer chromatography (TLC) was performed with Scientific Adsorbents plastic-backed TLC silica gel 60F hard layer plates. TLC plates were visualized with a 5% (w/v) solution of phosphomolybdic acid in ethanol or UV light (254 nm). Flash chromatography was performed with Scientific Adsorbents silica gel (flash, 32-63nm).

Mass spectral analyses were performed by the Mass Spectrometry Laboratories of North Carolina State University and the University of Kansas. Partial funding for the NCSU facility was obtained from the North Carolina Biotechnology Center and the National Science Foundation. ^{1}H and ^{13}C nuclear magnetic resonance (NMR) spectra were recorded on a Varian Gemini 300, Varian Mercury 300 and Varian Mercury 400 NMR spectrometer. NMR Chemical shifts (δ) for ^{1}H spectra are expressed in ppm relative to internal solvent peaks and coupling constants were measured in Hz. For ^{11}B NMR, $BF_3 \cdot Et_2O$ has been used as an external reference and the spectra were recorded on a GE Omega 300 spectrometer. All pH values were determined with an Accumet 1003 Handhold pH/mV/Ion Meter (Fisher Scientific). A Shimadzu RF-5301 PC fluoremeter

was used for the fluorescence studies. A Shimudzu UV-1601 spectrophotometer was used for the UV absorption studies.

10-Hydroxymethyl-anthacene-9-carbaldehyde (**56**). The preparation followed the literature procedure.[46] A stirred suspension of anthraquinone (10.4 g, 0.05mol) and sodium hydride (2.9, 0.1125 mol) in anhydrous DMSO (330 mL) was added dropwise a solution of trimethylsulfonium iodide (22.95 g, 0.1125 mol) in anhydrous DMSO (170 mL) at room temperature over a period of 30 min and stirred for another 3 h. The mixture was filtered and the filtrate was poured into 350 mL of ice water. The mixture was allowed to stand for 2 h, and then the precipitate was washed with water and dried under vacuum at 45 °C overnight giving the epoxide with no further purification. Then the epoxide compound (10.2 g, 0.043 mol) was added to a stirred solution of lithium bromide (20.0 g, 0.23 mol) in dry CH_3CN (500 mL), and the mixture was stirred at 60 °C in the dark for 16h and then was then cooled to – 40 °C in a dry ice-acetonitrile bath. The resulting product were collected by filtration, washed with water, and dried overnight under vacuum at room temperature. The yield for **56** (9.44 g) was 80%. The ^{1}H NMR spectrum (d6-DMSO, 11.50 (s, 2H), d 8.90 - 8.83 (m, 4H), 8.76 – 8.68 (m, 4H), 5.77 (s, 2H), was in agreement with the literature data.[46]

(10-Methylaminomethyl-anthacen-9-yl)-methanol (57). An aqueous solution of methylamine (40%, wt, 20 mL) was added to the solution of compound **56** (2.00 g, 8.47 mmol) in MeOH (100 mL) and THF (50 mL) and stirred at room temperature for 16 h. To this stirred mixture was added sodium boronhydride (0.90 g, 23.7 mmol). The

solution was stirred for another 30 min. After solvent evaporation, the resulting solid was dissolved in EtOAc (100 mL). The solution was washed with water (2 × 50 mL) and brine (40 mL), dried over $MgSO_4$ and concentrated. The resulting crude product was purified on silica gel column, eluting with MeOH/CH_2Cl_2 (1/50), to give compound **57** as a yellow solid (1.91 g, 90%). ^{1}H NMR ($CDCl_3$, 300 MHz) δ 8.45–8.42 (m, 2H), 8.37–8.34 (m, 2H), 7.55–7.52 (m, 4H), 5.64 (s, 2H), 4.65 (s, 2H), 2.65 (s, 3H). ^{13}C NMR ($CDCl_3$) δ 133.4, 131.7, 130.4, 130.3, 126.2, 126.1, 125.1, 124.8, 57.7, 48.2, 37.3. HRMS-FAB: Calcd for $C_{17}H_{18}NO$ (M^++H) 252.1388, found 252.1373. Anal. Calcd for $C_{17}H_{17}NO$: C, 81.24; H, 6.82; N, 5.57. Found: C, 80.96; H, 6.86; N, 5.53.

(10-Hydroxymethyl-anthacen-9-ylmethyl)-methyl-carbamic acid tert-butyl ester (58). Compound **57** (2.10 g, 8.37 mmol), di-*tert*-butyl dicarbonate (3.80 g, 17.4 mmol) and trimethylamine (20 mL) were mixed in MeOH (120 mL), and the mixture was stirred at room temperature for 30 min. After removal of the solvent, the resulting residue was dissolved in EtOAc (100 mL). The solution was washed with water (3 × 50 mL), 10% aqueous solution of sodium carbonate (30 mL), and saturated brine (50 mL), dried over $MgSO_4$ and concentrated. The resulting residue was purified on a silica gel column, eluting with EtOAc/hexanes (1/50–1/2), giving compound **58** as a yellow solid (2.30 g, 78%). ^{1}H NMR ($CDCl_3$) δ 8.51–8.43 (m, 4H), 7.60–7.55 (m, 4H), 5.71 (d, J = 5.6 Hz, 2H), 5.50 (s, 2H), 2.47 (s, 3H), 1.55 (s, 9H). ^{13}C NMR ($CDCl_3$) δ 156.0, 132.6, 131.3, 130.2, 129.9, 126.1, 125.8, 125.4, 125.0, 80.1, 57.6, 42.7, 31.8, 28.7. IR (cm^{-1}) 3413, 1681. HMRS-FAB Calcd. for $C_{22}H_{25}NO_3$ (M^+) 351.1834, found 351.1835. Anal. Calcd for $C_{22}H_{25}NO_3$: C, 75.19; H, 7.17; N, 3.99. Found: C, 75.21; H, 7.27; N, 3.97.

(10-Formyl-anthacen-9-ylmethyl)-methyl-carbamic acid tert-butyl ester (59). Compound **58** (2.30 g, 6.55 mmol) was dissolved in the mixture of dry DMSO (20 mL) and trimethylamine (20 mL). To the solution was added the solution of pyridine sulfur trioxide (7.30 g, 45.9 mmol) dissolved in dry DMSO (20 mL) over a period of 30 min. The reaction mixture was allowed to stir at room temperature for another 30 min, and then was poured into ice water (300 mL). The mixture was extracted with EtOAc (3 × 100 mL), dried over $MgSO_4$ and concentrated. The resulting yellow solid (2.30 g, 100%) was used without further purification. ^{1}H NMR ($CDCl_3$, 300 MHZ): d 11.51 (s, 1H), 8.90 (d, *J* = 8.5 Hz, 2H), 8.51 (d, *J* = 8.5 Hz, 2H), 7.70–7.61 (m, 4H), 5.56 (s, 2H), 2.48 (s, 3H), 1.56 (s, 9H).

Methyl-(10-methylaminomethyl-anthacen-9-ylmethyl)-carbamic acid tert-butyl ester (60). Compound **59** (2.29 g, 6.56 mmol) was dissolved in THF (50 mL) and MeOH (50 mL). To this solution was added an aqueous solution of methylamine (40%, wt, 20 mL), and the resulting reaction mixture was then stirred at room temperature under N_2 for 12 h. Sodium borohydride (1.00 g, 26.3 mmol) was added, and the reaction mixture was stirred for another 30 min. After concentration of the mixture, the resulting residue was dissolved in EtOAc (100 mL). The solution was washed with water (3 × 50 mL) and brine (30 mL), dried over $MgSO_4$ and concentrated. The resulting crude product was purified on silica gel column, eluting with MeOH/CH_2Cl_2 (1/5), giving compound **60** as a yellow solid (2.00 g, 83%). ^{1}H NMR ($CDCl_3$, 300 MHZ) d 8.44–8.39 (m, 4H), 7.56–7.53 (m, 4H), 5.51 (s, 2H), 4.71 (s, 2H), 2.69 (s, 3H), 2.46 (s, 3H), 1.55 (s, 9H). ^{13}C

NMR ($CDCl_3$) d 155.6, 132.5, 131.0, 130.0, 125.8, 125.7, 125.4, 125.3, 124.9, 79.7, 47.8, 42.6, 36.9, 31.6, 28.6. IR (cm^{-1}): 1686. HMRS-FAB: Calcd for $C_{23}H_{28}N_2O_2$ (M^+) 364.2151, found 364.2159. Anal. Calcd. for $C_{23}H_{28}N_2O_2$: C, 75.79; H, 7.74; N, 7.69. Found: C, 75.64; H, 7.71; N, 7.53.

2-Methylamino-terephthalic acid (70a). This is a known compound which was prepared by a literature procedure.[47] To a solution of 2-aminoterephthalic acid **69a** (0.1812g, 1 mmol) in THF (20 mL) and ethanol (20 mL) was added 2 N HCl (0.5 mL). The resulting mixture was cooled in an ice bath for 10 min and then transferred to a hydrogen reaction vessel with Pt_2O (10 mg). To this mixture was added formaldehyde (37%, 0.16 mL) and the mixture was hydrogenated at 45 psi for 2 h. The mixture was filtered through Celite. Evaporation removed most of the solvent, and the resulting residue was adjusted to pH 2 using concentrated hydrochloric acid. The crude product were collected by filtration, washed with water, and dried overnight under vacuum at room temperature. The product was purified on a flash silica gel (1/50 of MeOH/CH_2Cl_2) giving **70a** as light yellow powder (60mg, 33%). ^{1}H NMR ($CDCl_3$, 300 MHZ) d 7.96-7.93 (m, 1H), 7.34 (m, 1H), 7.18-7.15 (m, 1H), 2.94 (s, 3H).

2-Benzyloxycarbonylamino-terephthalic acid (71a).[48] Benzyloxycaronyl chloride (0.17 mL, 1.2 mmol) was added dropwise to a stirred solution of 2-aminophthalic acid (0.18g, 1.0 mmol) in 2 N NaOH (aq.) (1.0 mL, 2 mmol) at 0 °C over 0.5 h. The solution was allowed to warm to room temperature and was stirred for 6 h. The reaction mixture was diluted with Et_2O (3 × 2 mL), and the resulting mixture was

treated with concentrated HCl (aq.), adjusting to pH 2. The precipitated material was filtered, washed with Et_2O, and dried under vacuum for 5 h to yield **71a** as a light yellow solid (160 mg, 50%). ^{1}H NMR ($CDCl_3$, 300 MHz) d 9.05 (m, 1H), 8.15-8.12 (m, 1H), 7.70-7.66 (m, 1H), 7.45-7.34 (m, 1H), 5.22 (s, 2H). ^{13}C NMR (DMSO/CD_3OD): d 169.587, 167.023, 153.279, 141.571, 136.789, 132.034, 129.015, 128.700, 122.829, 119.623, 67.051. HMRS-FAB: Calcd for $C_{16}H_{13}NO_6$ (M^+) 315.0743, found 315.0736.

5-Benzyloxycarbonylamino-isophthalic acid (72a).[48] This compound was obtained as a light yellow solid following the same procedure for **71a** (above) from 5-aminoisophthalic acid (**73a**). ^{1}H NMR data (CD_3OD, 300 MHz) agreed with that of the literature.[48] d 8.35-8.30 (m, 2H), 7.42-7.30 (m, 6H), 5.21 (s, 2H).

General procedures for preparation of Boc-protected diamides (61b-72b). Compound **60** (100 mg, 0.275 mmol) was added to a solution of di-acid (**61a-72a**) (0.138 mmol) and 1-(2-dimethylaminopropyl)-3-ethylcarbodiimide hydrochloride (EDC·HCl, 210 mg, 1.10 mmol.) in dry CH_2Cl_2 (20 mL), and the mixture was stirred at room temperature under N_2 for 12 h. The mixture was diluted with CH_2Cl_2 (10 mL), washed with 10% citric acid (10 mL), and water (2 × 30 mL), and was dried over $MgSO_4$ and concentrated. The resulting residue was purified on silica gel column, eluting with MeOH/CH_2Cl_2 (1:100), to give the product.

[10-({[3-({10-[(tert-Butoxycarbonyl-methyl-amino)-methyl]-anthacen-9-ylmethyl}-methyl-carbamoyl)-propionyl]-methyl-amino}-methyl)-anthacen-9-

ylmethyl]-methyl-carbamic acid tert-butyl ester (61b). Yield 78%. ^{1}H NMR ($CDCl_3$, 300 MHz) d 8.48–8.41 (m, 8H), 7.60–7.55 (m, 8H), 5.77 (s, 4H), 5.56 (s, 4H), 2.86 (s, 4H), 2.79 (s, 6H), 2.50 (s, 6H), 1.53 (s, 18H). IR (cm^{-1}) 1685, 1643. HMRS-FAB: Calcd for $C_{50}H_{59}N_4O_6$ (M^+ +H) 811.4356, found 811.4412. Anal. Calcd for $C_{50}H_{58}N_4O_6$: C, 74.05; H, 7.21; N, 6.91. Found: C, 74.01; H, 7.34; N, 6.63.

[10-({[7-({10-[(tert-Butoxycarbonyl-methyl-amino)-methyl]-anthacen-9-ylmethyl}-methyl-carbamoyl)-heptanoyl]-methyl-amino}-methyl)-anthacen-9-ylmethyl]-methyl-carbamic acid tert-butyl ester (62b). Yield 75%. ^{1}H NMR ($CDCl_3$, 300 MHz) d 8.49–8.38 (m, 8H), 7.58–7.55 (m, 8H), 5.71 (s, 4H), 5.54 (s, 4H), 2.60 (s, 6H), 2.50 (s, 6H), 2.39 (t, *J* = 1.5 Hz, 4H), 1.90–1.40 (m, 8H), 1.58 (s, 18H). IR (cm^{-1}) 1684, 1636. HMRS-FAB: Calcd for $C_{54}H_{69}N_4O_6$ (M^+ +H) 867.4982, found 867.5229.

[10-({[21-({10-[(tert-Butoxycarbonyl-methyl-amino)-methyl]-anthacen-9-ylmethyl}-methyl-carbamoyl)-heneicosanoyl]-methyl-amino}-methyl)-anthacen-9-ylmethyl]-methyl-carbamic acid tert-butyl ester (63b). Yield 64%. ^{1}H NMR ($CDCl_3$, 300 MHz) d 8.49–8.38 (m, 8H), 7.59–7.56 (m, 8H), 5.72 (s, 4H), 5.55 (s, 4H), 2.60 (s, 6H), 2.50 (s, 6H), 2.40–2.34 (m, 4H), 1.90–1.20 (m, 54H). IR (cm^{-1}) 1692, 1643. HMRS-FAB: Calcd. for $C_{68}H_{95}N_4O_6$ (M^+ +H), 1063.7173, found 1063.5746. Anal. Calcd for $C_{54}H_{58}N_4O_6 \cdot 0.5H_2O$: C, 72.15; H, 8.92; N, 5.22. Found: C, 76.15; H, 8.92; N, 4.76.

[10-({[3-({10-[(tert-Butoxycarbonyl-methyl-amino)-methyl]-anthacen-9-ylmethyl}-methyl-carbamoyl)-benzoyl]-methyl-amino}-methyl)-anthacen-9-

ylmethyl]-methyl-carbamic acid tert-butyl ester *(64b)*. Yield 74%. ^{1}H NMR ($CDCl_3$, 300 MHz) d 8.52–8.45 (m, 8H), 7.60–7.56 (m, 8H), 7.50–7.40 (m, 4H), 5.85 (s, 4H), 5.58 (s, 4H), 2.53 (s, 12H), 1.59 (s, 18H). IR (cm^{-1}) 1688, 1632. HMRS-FAB: Calcd. for $C_{54}H_{59}N_4O_6$ (M^++H) 859.4435, found 859.4832. Anal. Calcd for $C_{54}H_{58}N_4O_6 \cdot 1.5H_2O$: C, 73.20; H, 6.88; N, 6.32. Found: C, 73.46; H, 6.93; N, 6.05.

{10-[({4-[({10-[(tert-Butoxycarbonyl-methyl-amino)-methyl]-anthacen-9-ylmethyl}-methyl-carbamoyl)-methoxy]-benzoyl}-methyl-amino)-methyl]-anthacen-9-ylmethyl}-methyl-carbamic acid tert-butyl ester *(65b)*. Yield 60%. ^{1}H NMR ($CDCl_3$) d 8.50–8.31 (m, 8H), 7.62–7.43 (m, 10H), 6.99–6.96 (m, 2H), 5.86 (s, 2H), 5.72 (s, 2H), 5.58–5.54 (m, 4H), 4.79 (s, 2H), 2.65 (s, 3H), 2.62 (s, 3H), 2.53 (s, 3H), 2.49 (s, 3H), 1.58 (s, 18H). IR (cm^{-1}) 1682, 1626. HMRS-FAB: Calcd for $C_{55}H_{61}N_4O_7$ ($M+H^+$) 889.4462, found 889.4086. Anal. Calcd for $C_{52}H_{60}N_4O_7 \cdot H_2O$: C, 73.56; H, 6.85; N, 6.23. Found: C, 73.31; H, 7.50; N, 5.35.

[10-({[4-({10-[(tert-Butoxycarbonyl-methyl-amino)-methyl]-anthacen-9-ylmethyl}-methyl-carbamoyl)-3-nitro-benzoyl]-methyl-amino}-methyl)-anthacen-9-ylmethyl]-methyl-carbamic acid tert-butyl ester (66b). Yield 24%. ^{1}H NMR (CDCl3, 300MHz) d 8.52-8.26 (m, 10H), 7.63-7.37 (m, 9H), 5.90 (s, 4H), 5.88(s, 4H), 2.55-2.43(m, 12H), 1.59 (s, 18H). IR: (cm^{-1}) 1715, 1669. MS-FAB: Calcd. for $C_{54}H_{58}N_5O_8$ ($M + H^+$) 904.6, found 904.4.

[10-({[5-({10-[(tert-Butoxycarbonyl-methyl-amino)-methyl]-anthacen-9-ylmethyl}-methyl-carbamoyl)-pyrazine-2-carbonyl]-methyl-amino}-methyl)-anthacen-9-ylmethyl]-methyl-carbamic acid tert-butyl ester (**67b**)**.** Yield 59%. ^{1}HNMR ($CDCl_3$, 300MHz) d 8.89 (s, 2H), 8.52-8.43 (m, 8H), 7.63-7.56 (m, 8H), 5.91 (s, 4H), 5.56 (s, 4H), 2.71 (s, 6H), 2.50 (s, 6H), 1.56 (s, 18H). IR (cm^{-1}): 1684, 1629. MS-FAB: Calcd. For $C_{54}H_{57}N_5O_8$ $(M + H)^+$ 861.4, found 861.5.

[10-({[5-({10-[(tert-Butoxycarbonyl-methyl-amino)-methyl]-anthacen-9-ylmethyl}-methyl-carbamoyl)-2H-pyrazole-3-carbonyl]-methyl-amino}-methyl)-anthacen-9-ylmethyl]-methyl-carbamic acid tert-butyl ester (**68b**)**.** Yield (54%). ^{1}HNMR ($CDCl_3$, 300 MHz) d 8.50-8.39 (m, 8H), 7.58-7.56 (m, 8H), 7.05 (s, 1H), 5.87 (s, 4H), 5.56 (s, 4H), 2.96 (s, 6H), 2.50(s, 6H), 1.59 (s, 18H). IR (cm^{-1}) 1686, 1622. HMRS-FAB Calcd for $C_{51}H_{57}N_6O_6$ $(M + H)^+$ 849.4261, found 849.5090. Anal. Calcd. for $C_{51}H_{56}N_6O_6 \bullet$ 0.5 H_2O: C, 71.39; H, 6.70; N, 9.79. Found: C, 71.13; H, 6.69; N, 9.45.

[10-({[3-Amino-4-({10-[(tert-butoxycarbonyl-methyl-amino)-methyl]-anthacen-9-ylmethyl}-methyl-carbamoyl)-benzoyl]-methyl-amino}-methyl)-anthacen-9-ylmethyl]-methyl-carbamic acid tert-butyl ester (**69b**)**.** Yield (60%). ^{1}HNMR ($CDCl_3$, 300MHz) d 8.51 (m, 8H), 7.59-7.57 (m, 8H), 7.04-6.56(m, 3H), 5.83 (s, 4H), 5.55 (s, 4H), 2.56-2.50 (m, 6H), 2.09(s, 6H), 1.58 (s, 18H). IR (cm^{-1}) 3380, 1728, 1685, 1627. HMRS-FAB: Calcd for $C_{54}H_{60}N_5O_6$ $(M+H)^+$ 874.4544, found 874.4517.

10-({[4-({10-[(tert-Butoxycarbonyl-methyl-$_{amino}$)-methyl]-anthacen-9-ylmethyl}-methyl-carbamoyl)-3-methylamino-benzoyl]-methyl-amino}-methyl)-anthacen-9-ylmethyl]-methyl-carbamic acid tert-butyl ester (**70b**)**.** Yield 52%. ^{1}HNMR ($CDCl_3$, 300MHz) d 8.43-8.40 (m, 8H), 7.57-7.56 (m, 8H), 6.98(m, 1H), 6.72-6.55 (m, 2H), 5.85 (s, 2H), 5.81 (s, 2H), 5.55(s, 4H), 2.78(s, 3H), 2.53 (s, 6H), 2.50 (s, 6H), 1.57 (s, 18H). IR (cm^{-1}) 3380, 1621, 1600. HMRS-FAB: Calcd for $C_{55}H_{61}N_5O_6$ $(M+H)^+$ 888.4700, found 888.4634.

[2,5-Bis-({10-[(tert-butoxycarbonyl-methyl-amino)-methyl]-anthacen-9-ylmethyl}-methyl-carbamoyl)-phenyl]-carbamic acid benzyl ester (**71b**)**.** Yield (40%). ^{1}H NMR ($CDCl_3$, 300MHz) d 8.49-8.28 (m, 10H), 7.72-7.41 (m, 12H), 7.10(m, 2H), 5.86 (s, 4H), 5.55 (s, 4H), 5.19(s, 2H), 2.54-2.50 (m, 12H), 1.57 (s, 18H). IR (cm^{-1}) 1728, 1686, 1627. HMRS-FAB: Calcd for $C_{62}H_{66}N_5O_8$ $(M+H)^+$ 1008.4833, found 1008.6684.

{3,5-Bis-[({10-[(tert-butoxycarbonyl-methyl-amino)-methyl]-anthacen-9-ylmethyl}-methyl-amino)-methyl]-phenyl}-carbamic acid benzyl ester (72b). Yield (70%). ^{1}H NMR ($CDCl_3$, 300MHz) d 8.47 (m, 8H), 7.54-7.22 (m, 16H), 5.78 (s, 4H), 5.44 (s, 4H), 5.09(s, 2H), 2.49 (s, 12H), 1.55 (s, 18H). IR (cm^{-1}) 1734, 1633, 1595. HMRS-FAB: Calcd for $C_{62}H_{66}N_5O_8$ $(M + H)^+$, 1008.5, found 1008.7. Anal. Calcd. for $C_{62}H_{65}N_5O_{8s}$• 0.5 H_2O: C, 73.21; H, 6.54; N, 6.88. Found: C, 73.30; H, 6.73; N, 6.57.

General procedures for preparation of diboronic acids (17-21, 48-54). The Boc-protected diamine [compound **61b-72b** (0.073 mmol)] was dissolved in dry CH_2Cl_2 (8mL). To this solution was added trifluoroacetic acid (3 mL). The reaction mixture was stirred at room temperature for 10 min. After concentration, the resulting residue was dried under vacuum for 3 h and then dissolved in dry acetonitrile (30 mL). To this solution was added compound **76** (85 mg, 0.30 mmol), potassium carbonate (100 mg, 0.73 mmol) and potassium iodide (2 mg), and the mixture was stirred at room temperature for 12 h. The insoluble materials were filtered off, and the filtrate was concentrated. The resulting residue was dissolved in CH_2Cl_2 (10 mL). Sodium bicarbonate (10% aq., 20 mL) was added, and the mixture was stirred at room temperature for 1 h. The reaction mixture was diluted with CH_2Cl_2 (20 mL), washed with water (2 × 30 mL) and brine (20 mL), and was dried over $MgSO_4$ and concentrated. The yielding crystal was precipitated from CH_2Cl_2/Et_2O.

Diboronic acid 17 from 61b. Yield 50%. ^{1}H NMR (CD_3OD+$CDCl_3$): d 8.49–8.46 (m, 4H), 8.24–8.22 (m, 4H), 7.80–7.60 (m, 2H), 7.57–7.54 (m, 8H), 7.36–7.28 (m, 6H), 5.70 (s, 4H), 4.96 (s, 4H), 4.33 (s, 4H), 2.78(s, 4H), 2.69 (s, 6H), 2.39 (s, 6H). IR (cm^{-1}): 1643, 1632. MS-ESI: $C_{54}H_{56}B_2N_4O_6$, Calcd. for $(M–H_2O+H)^+$ 861.4, found 861.5.

Diboronic acid 18 from 62b. Yield 49%. ^{1}H NMR (CD_3OD+$CDCl_3$) d 8.50–8.25 (m, 8H), 7.71–7.57 (m, 10H), 7.35–7.28 (m, 6H), 5.73 (s, 4H), 5.16 (s, 4H), 4.30 (s, 4H), 2.59 (s, 6H), 2.47 (s, 6H), 2.39 (t, *J* = 7.3 Hz, 4H), 1.80–1.60 (m, 4H),

1.50–1.35 (m, 4H). IR (cm^{-1}): 1632. MS-ESI: $C_{58}H_{64}B_2N_4O_6$, Calcd. for ($M–H_2O+H$) 917.5^+, found 917.5.

Diboronic acid 19 from 63b. Yield 30%. ^1H NMR ($CD_3OD+CDCl_3$) d 8.45–8.43(m, 4H), 8.28–8.26 (m, 4H), 7.67–7.59 (m, 10H), 7.38–7.36 (m, 6H), 5.70 (s, 4H), 5.11 (s, 4H), 4.39 (s, 4H), 2.59 (s, 6H), 2.50–2.38 (m, 10H), 1.66–1.61 (m, 4H), 1.40–1.18 (m, 32H). IR (cm^{-1}) 1649, 1632. MS-ESI: $C_{72}H_{92}B_2N_4O_6$, Calcd. for $(M–H_2O+H)^+$ 1130.7, found 1113.8.

Diboronic acid 20 from 64b. Yield 50%. ^1H NMR ($CD_3OD+CDCl_3$) d 8.50–8.34 (m, 8H), 7.71–7.61 (m, 12H), 7.45–7.34 (m, 8H), 5.86 (s, 4H), 5.06 (s, 4H), 4.24 (s, 4H), 2.57 (s, 6H), 2.42 (s, 6H). IR (cm^{-1}) 1631, 1620. MS-ESI: $C_{58}H_{56}B_2N_4O_6$, Calcd. for $(M–H_2O+H)^+$ 909.4, found 909.5.

Diboronic acid 21 from 65b. Yield 40%. ^1H NMR ($CD_3OD+CDCl_3$) d 8.46–8.30 (m, 8H), 8.29–7.56 (m, 10H), 7.28–7.26 (m, 8H), 7.10–6.90 (m, 2H), 5.89 (s, 2H), 5.76 (s, 2H), 5.16 (s, 2H), 5.12 (s, 2H), 4.90 (s, 2H), 4.38 (s, 2H), 4.35 (s, 2H), 2.68 (s, 3H), 2.63 (s, 3H), 2.46 (s, 3H), 2.42 (s, 3H). IR (cm^{-1}) 1632, 1608. MS-ESI: $C_{59}H_{58}B_2N_4O_7$, Calcd. for $(M–H_2O+H)^+$ 939.4, found 939.5 $(M–H_2O+H)^+$.

Diboronic acid 48 from 66b. Yield (70%). ^1H NMR (CD_3OD + $CDCl_3$): 8.55-8.36 (m, 8H), 7.76-7.65 (m, 8H), 7.34-7.42 (m, 9H), 5.95(s, 4H), 5.13 (s, 4H), 4.35 (s,

4H), 2.60 (s, 6H), 2.47 (s, 6H), IR (cm^{-1}): 1669.9, 1627. MS-ESI: $C_{55}H_{54}B_2N_4O_6$, Calcd. for $(M+Na)^+$ 939.4, found 939.8.

Diboronic acid 49 from 67b. Yield (80%). ^1H NMR (CD_3OD + $CDCl_3$):, 8.60-8.57 (m, 4H), 8.27 (m, 4H), 7.78-7.44(m, 11H), 7.61-7.33 (m, 8H), 5.91(s, 4H), 5.07 (s, 6H), 4.34 (s, 4H), 2.59 (s, 3H), 2.47 (s, 9H), IR (cm^{-1}): 1726, 1637. MS-ESI: $C_{58}H_{55}B_2N_5O_6$, Calcd. for $(M-H_2O+H)^+$ 954.43, found 954.75.

Diboronic acid 50 from 68b. Yield (50%). ^1H NMR (CD_3OD + $CDCl_3$) 8.88 (s, 2H), 8.50-8.20 (m, 8H), 7.83-7.47 (m, 14H), 7.30 (m, 2H), 5.90(s, 4H), 5.05 (s, 6H), 4.34 (s, 4H), 2.72 (s, 6H), 2.52 (s, 6H), IR (cm^{-1}): 1643, 1627. MS-ESI: $C_{56}H_{54}B_2N_6O_6$, Calcd for $(M-H_2O+H)^+$ 911.43, found 911.45.

Diboronic acid 51 from 69b. Yield (20%). ^1H NMR (CD_3OD + $CDCl_3$) 8.43-8.29 (m, 8H), 7.74-7.57 (m, 10H), 7.32 (m, 6H), 7.08(m, 1H), 6.76 (m, 1H), 6.60(m, 1H), 4.92 (s, 4H), 4.00(s, 4H), 2.52 (s, 6H), 2.29 (s, 6H), IR (cm^{-1}) 1616. MS-ESI: $C_{58}H_{57}B_2N_5O_6$, Calcd. for $(M-CH_3OH)^+$ 973.4, found 943.5.

Diboronic acid 52 from 70b. Yield (30%). ^1H NMR (CD_3OD + $CDCl_3$, 300 MHz) 8.53-8.36 (m, 8H), 7.62 (m, 8H), 7.33-7.30 (m, 8H), 7.10 (m, 1H), 6.68-6.60(m, 2H), 5.89(s, 4H), 5.10 (s, 4H), 4.27 (s, 4H), 2.79 (s, 3H), 2.56(s, 6H), 2.41 (s, 6H), IR (cm^{-1}) 1616. MS-ESI: $C_{59}H_{59}B_2N_5O_6$, Calcd for $(M-H_2O+H)^+$ 938.5, found 938.5.

Diboronic acid 53 from 71b. Yield (70%). ^{1}HNMR (CD_3OD + $CDCl_3$, 300 MHz) 8.40 (m, 8H), 7.59 (m, 8H), 7.37-7.08 (m, 16H), 5.85(s, 2H), 5.17 (s, 6H), 4.84 (s, 4H), 3.86(s, 4H), 2.56 (s, 6H), 2.26 (s, 6H), IR (cm^{-1}) 1622. HMRS-ESI: $C_{66}H_{63}B_2N_5O_6$, Calcd for $(M-H_2O+H)^+$ 1058.4835, found 1058.4839.

Diboronic acid 54 from 72b. Yield (70%). ^{1}HNMR (CD_3OD + $CDCl_3$) 8.48-8.29 (m, 8H), 7.70-7.57 (m, 8H), 7.36-7.28 (m, 16H), 5.81(s, 4H), 5.05 (s, 6H), 4.33 (s, 4H), 2.50 (s, 6H), 2.41 (s, 6H), IR (cm^{-1}) 1734, 1632. MS-ESI: $C_{66}H_{63}B_2N_5O_6$, Calcd. for $(M-H_2O+H)^+$ 1058.5, found 1058.5.

(10-Aminomethyl-anthacen-9-ylmethyl)-methyl-carbamic acid tert-butyl ester (81). Methanesulfonyl chloride (50 uL, 0.65 mmol) and TEA (0.2 mL) were added to a solution of compound **58** (100 mg, 0.28 mmol) in dry CH_2Cl_2 (5 mL) cooled in ice-water bath, and the mixture was stirred overnight. The reaction mixture was diluted with CH_2Cl_2 (20 mL), washed with water (2 × 20 mL) and brine (20 mL), and was dried over $MgSO_4$ and concentrated. The resulting residue was dried under vacuum and then was dissolved in 10 mL dry DMSO. To the solution under N_2 was added sodium azide (250 mg, 3.3 mmol), and the mixture was allowed to stir at 60 °C for 5 h and then poured to 20 mL of ice-water. The mixture was diluted with CH_2Cl_2 (30 mL), washed with water (2 × 20 mL) and brine (20 mL), and was dried over $MgSO_4$ and concentrated. The crude product was purified on silica gel column, eluting with MeOH/CH_2Cl_2 (1/300 ~ 1/50), to give the desired azide (50 mg, 50%). ^{1}H NMR ($CDCl_3$, 300 MHz) d 8.51-8.48 (m, 2H), 8.37-8.33(m, 2H), 7.64-7.56 (m, 4H), 5.54 (s, 2H), 5.35(s, 2H), 2.49 (s, 3H), 1.57 (s, 9H).

The mixture of this azide (50 mg, 0.14 mmol), triphenyl phosphine (100 mg, 0.44 mmol) and H_2O (20 uL) in THF (15 mL) was refluxed under N_2 and darkness overnight. After concentration, the resulting residue was dissolved in CH_2Cl_2 (20 mL), washed with water (2×20 mL) and brine (20 mL), and was dried over $MgSO_4$ and concentrated. The crude product was purified on silica gel column, eluting with MeOH/CH_2Cl_2 (1:100 ~1:5), to give a yellow solid (30 mg, 60%). ^{1}H NMR ($CDCl_3$, 300 MHz): d 8.46-8.44 (m, 4H), 7.59-7.54 (m, 4H), 5.50 (s, 2H), 4.85(s, 2H), 2.47 (s, 3H), 1.55 (s, 9H). IR: 3386, 1652. MS-FAB: Calcd. for $C_{22}H_{26}N_2O_2$ 350.20, found 350.19. Anal. Calcd. for $C_{22}H_{26}N_2O_6 \cdot 1/6H_2O$: C,74.12; H, 7.48; N, 7.85. Found: C, 74.72; H, 7.44; N, 7.34.

[10-(6-{10-[(tert-Butoxycarbonyl-methyl-amino)-methyl]-anthacen-9-ylmethyl}-1,3,5,7-tetraoxo-3,5,6,7-tetrahydro-1H-pyrrolo[3,4-f]isoindol-2-ylmethyl)-anthacen-9-ylmethyl]-methyl-carbamic acid tert-butyl ester (**83**)**:** To the mixture of amine **81** (100 mg, 0.28 mmol) and benzo[1,2-c;4,5-c']difuran-1,3,5,7-tetraone (31 mg, 0.14 mmol) in toluene (50mL) was added TEA (60 uL) . The mixture was refluxed for 6 h with a Dean-Stark trap. The solvent was removed and the resulting residue was dissolved in CH_2Cl_2 (50 mL). The solution was washed with 1 N HCl (30 mL), water (2×20 mL) and brine (20 mL), and was dried over $MgSO_4$ and concentrated. The crude product was purified on silica gel column, eluting with MeOH/CH_2Cl_2 (1:300 ~1:100), giving a yellow solid (30 mg, 60%). ^{1}H NMR ($CDCl_3$, 300 MHz) d 8.60-8.58 (m, 4H), 8.44 (m, 4H), 8.06(s, 2H), 7.60-7.54(m, 8H), 5.91 (s, 4H), 5.50 (s, 4H), 2.46 (s, 6H), 1.53 (s, 18H). IR 1722, 1693. HMRS-FAB: Calcd. for $C_{54}H_{50}N_4O_8$ 882.3629, found 882.3618.

(10-{2-[7-(2-{10-[(tert-Butoxycarbonyl-methyl-amino)-methyl]-anthacen-9-yl}-ethyl)-1,3,6,8-tetraoxo-3,6,7,8-tetrahydro-1H-benzo[lmn][3,8]phenantholin-2-yl]-ethyl}-anthacen-9-ylmethyl)-methyl-carbamic acid tert-butyl ester (**85**)**.** The procedure was same as above (**83**), except using anhydride isochomeno [6,5,4-def] isochomene-1,3,6,8-tetraone (**84**), and the yield was 80%. ^{1}H NMR ($CDCl_3$, 300 MHz) d 8.62-8.56 (m, 8H), 8.45 (m, 4H), 7.53-7.52(m, 8H), 6.40 (s, 4H), 5.50 (s, 4H), 2.47 (s, 6H), 1.53 (s, 18H). IR 1728, 1693. HMRS-FAB: Calcd for $C_{58}H_{52}N_4O_8$ 932.3785, found 932.3754. Anal. Calcd. for $C_{58}H_{52}N_4O_8 \cdot 1/6H_2O$: C,71.88; H, 5.78; N, 5.82. Found: C, 71.72; H, 5.49; N, 5.64.

1,4,5,8-Naphthalenetetracarboxylic Diimide (**86**). 1,4,5,8-Naphthalenetetracarboxylic dianhydride **84** (0.5 g, 1.87 mmol) was added to a stirred concentrated aqueous solution of ammonium hydroxide (25ml, 29.9% w/w) and stirred at room temperature for 7 h. During that time, analytically pure diimide **86** precipitated as a pale yellow solid, which was filtered, washed with distilled water, and dried under vacuum at 60 °C overnight (0.3g, 60%). ^{1}H NMR data (d_6-DMSO, 300 MHz) d 8.62(s, 4H) agreed with that of the literature.[57]

1,2,3,6,7,8-Hexahydro-2,7-diazapyrene (**87**). This is a known compound which was made following a literature procedure.[57] An oven-dried, three-neck flask equipped with a magnetic stirrer, reflux condensor, addition funnel, inlet, and a gas vent, was flushed with N_2, and then was charged with diimide **86** (0.3g, 1mmol) and anhydrous

THF (6 mL) . To this suspension was added slowly by syringe, a 1 M solution of BH_3-THF (15 mL) at room temperature. The reaction mixture was then refluxed for 60 h. During that time there was hydrogen evolution and the color of the reaction mixture turned to orange. After cooling to 0°C, the reaction mixture was quenched by addition of 2 mL of MeOH. After stirring for 30 min at room temperature, HCl (5 M 10 mL) was added and the mixture was refluxed for 3 h. The liquid was then evaporated under reduced pressure. The residue was cooled to 0°C and aqueous saturated potassium carbonate solution was added with stirring until the pH was basic (>10). All of the liquid was evaporated under reduced pressure and the solid was dried completely under vacuum at 40 °C. The dry solid was extracted with refluxing benzene in a Soxhlet extractor for four days. After this period, the benzene was removed under vacuum to yield of pure diamine **88**. ^{1}H NMR ($CDCl_3$, 300 MHz) d 7.11 (s, 4H), 4.28 (s, 8H), 1.68 (s, 2H) agreed with that of the literature.[101]

[10-(4-{10-[(tert-Butoxycarbonyl-methyl-amino)-methyl]-anthacen-9-ylmethyl}-piperazin-1-ylmethyl)-anthacen-9-ylmethyl]-methyl-carbamic acid tert-butyl ester (**88**). To a solution of compound **58** (203.2 mg, 0.59 mmol) in dry CH_2Cl_2 (20 mL) cooled in ice-water bath was added methanesulfonyl chloride (90 uL, 1.2 mmol) and 0.4 mL TEA under N_2. The mixture was stirred at room temperature overnight. Then the solvent was removed and the resulting residue was dissolved in CH_2Cl_2 (20 mL). The solution was washed with water (2 × 20 mL) and brine (20 mL), and was dried over $MgSO_4$ and concentrated. The residue was dried under vacuum and then was dissolved in anhydrous DMF (2 mL) and 30 mL dry acetonitrile. To the solution under

N_2 protection was added potassium carbonate (0.2 g, 14 mmol) and a solution of piperazine (18.6 mg, 0.216 mmol) in anhydrous DMF (1.5 mL). The resulting mixture was stirred at 45 °C for 4 h and then the solvent was evaporated. The residue was dissolved with CH_2Cl_2 (30 mL). The solution was washed with water (2 × 20 mL) and brine (20 mL), and was dried over $MgSO_4$ and concentrated. The crude product was purified on silica gel column, eluting with EtoAc/CH_2Cl_2 (1/100 ~ 1/10), to give a yellow solid (100 mg, 50%). ^{1}H NMR ($CDCl_3$, 300 MHz): d 8.57~8.41(m, 8H), 7.56-7.48 (m, 8H), 5.52(s, 4H), 4.42(s, 4H), 2.60(s, 8H), 2.49(s, 6H), 1.57(s, 18H). ^{13}C NMR ($CDCl_3$), 156.0, 131.4, 131.3, 131.1, 128.9, 126.2, 125.9, 125.3, 124.9, 79.9, 54.5, 53.6, 43.5, 42.8, 32.0, 28.7. IR (cm^{-1}): 1688. HMRS-FAB. Calcd. for $C_{48}H_{57}N_4O_4$ $(M+H)^+$, 753.4380, found 753.4407. Anal. $C_{48}H_{56}N_4O_4$, Calcd. for (M+1/3 H_2O): C, 75.95; H, 7.48; N, 7.35. Found: C, 75.96; H, 7.50; N, 7.29.

[10-(7-{10-[(tert-Butoxycarbonyl-methyl-amino)-methyl]-anthacen-9-ylmethyl}-3,6,7,8-tetrahydro-1H-benzo[lmn][3,8]phenantholin-2-ylmethyl)-anthacen-9-ylmethyl]-methyl-carbamic acid tert-butyl ester (**89**). This product was obtained as a yellow solid in 20% yield. ^{1}H NMR ($CDCl_3$, 300 MHz) d 8.51-8.43 (m, 8H), 7.54-7.47 (m, 8H), 7.04 (s, 4H), 5.54 (s, 4H), 4.72 (s, 4H), 4.18 (s, 8H), 2.51 (s, 6H), 1.56 (s, 18H). ^{13}C NMR ($CDCl_3$) 131.6, 131.4, 131.2, 127.9, 126.0, 125.6, 124.9, 122.3, 68.3, 56.4, 52.8, 43.4, 42.8, 28.7. IR (cm^{-1}) 1695. HMRS-FAB: Calcd. for $C_{58}H_{61}N_4O_4$ $(M+H)^+$, 877.4693, found 877.4689.

The synthetic procedures for constrained diboronic acids **77**, **78**, **79** and **80** were same as those non-constrained diboronic acids. The spectral data are shown below.

Constrained diboronic acid 77 from **83**: ^{1}H NMR ($CD_3OD/CDCl_3$, 300 MHz) d 8.56-8.53 (m, 4H), 8.14-7.86 (m, 8H), 7.58-7.32(m, 14H), 5.85(s, 4H), 4.60 (s, 4H), 3.93 (s, 4H), 2.26(s, 3H), 2.24 (s, 3H). IR(cm^{-1}) 1727. HMRS-FAB: Calcd. for $(C_{58}H_{48}B_2N_4O_8 +2H)^+/2$: 476.1907, found 476.1901.

Constrained diboronic acid 78 from **85**: ^{1}H NMR ($CDCl_3$, 300MHz) d 9.02(s, 2H), 8.55-8.50 (m, 6H), 8.25-8.19(m, 4H), 7.96-7.82 (m, 2H), 7.49-7.36 (m, 14H), 6.28 (s, 4H), 4.56 (s, 4H), 3.92 (s, 4H), 2.13 (s, 6H). IR (cm^{-1}) 1707. HMRS-FAB: Calcd. for $(C_{62}H_{50}B_2N_4O_8 +2H)^+/2$: 501.1986, found 501.1972. .

Constrained diboronic acid 79 from **88**: ^{1}H NMR ($CD_3OD/CDCl_3$, 300 MHz) d 8.57 (m, 4H), 8.20 (m, 4H), 7.70-7.28 (m, 16H), 5.07 (s, 4H), 4.49 (s, 4H), 4.34 (s, 4H), 2.63 (s, 8H), 2.41 (s, 6H). ^{13}C NMR ($CD_3OD/CDCl_3$) 135.3, 132.2, 127.7, 127.0, 126.6, 125.3, 64.3, 54.1, 40.5. IR(cm^{-1}) 2953, 2860. ESI-MS: $C_{52}H_{54}B_2N_4O_4$, Calcd. for $(M-H_2O+H)^+$ 803.4, found 803.7.

Constrained diboronic acid 80 from **89**: ^{1}H NMR ($CD_3OD/CDCl_3$, 300 MHz) d 8.43 (m, 4H), 8.17 (m, 4H), 7.48 (m, 16H), 7.08 (s, 4H), 4.72 (s, 4H), 4.20 (s, 8H), 2.29 (s, 6H). IR (cm^{-1}) 2920. ESI-MS: $C_{62}H_{58}B_2N_4O_4$, Calcd. For $(M-H_2O+H)^+$ 927.5, found 927.7.

Biology

Cell culture. HEPG2 and COS7 cells were maintained in RPMI with 10% FBS (GIBCO). HEP3B cells were maintained in RPMI with 10% FBS and 1X sodium pyruvate and 1X non-essential amino acids (GIBCO).

Flow cytometry analysis. Cell lines HEPG2, HEP3B, and COS7 were prepared and stained with monoclonal anti-carbohydrate antibodies at saturating concentrations as described [134,135]. Anti-SSEA-1 (anti-Lewis X) was used at a dilution of 1:1000, anti-Lewis Y (clone F3, Calbiochem, and clone A70-C/C8, NeoMarkers) at a dilution of 1:20, anti-sialyl Lewis X (CSLEX-1 and KM93) at 10 μg/ml, and anti-sialyl Lewis a (CSLEA-1) at 1:500. Cells were then stained with fluorescein isothiocyanate-conjugated goat anti-mouse IgM or anti-mouse IgG. FITC-conjugated murine IgG1/IgG2 and anti-CD18 antibodies (negative controls thoughout) were used according to the manufacturer's instructions. Cells were analyzed on a Becton-Dickinson FACScan.

Fluorescent labeling studies. 6-well plates were seeded with 1 x 10^6 cells per well and incubated at 37 ºC and 5% CO_2 for 48 h. The media was removed and cells were washed twice with 1X PBS. The cells were fixed with 1.5 mL of 1:1 MeOH/PBS and incubated 20 min at 4 ºC. After incubation, the MeOH/PBS solution was removed and cells were washed twice with PBS.

Diboronic acid compounds were resuspended in 1:1 MeOH/PBS and added to wells at 0.5 to 10 μM concentrations. One well was incubated only in MeOH/PBS without compound as a negative control. The plates were then incubated in darkness at 4

ºC for 45 min. Plates were examined with phase contrast microscopy followed by fluorescent microscopy (blue cube wavelengths 370 nm excitation, 426 nm emission; 20X lens). Plates were photographed using a Nikon DXM1200 digital camera and images captured with the Nikon ACT-1 program (v 2.10). The phase contrast and fluorescent images were then overlaid, organized and labeled using Adobe Photoshop 6.0. The images were quantified with NIH ImageJ 1.28. The units (mean gray value) were subtracted from background, where there are no cells. The fluorescent signal was stable for at least 96 h when cells were maintained in darkness.

References

(1) Bendel, P.; Frantz, A.; Zilberstein, J.; Kabalka, G. W.; Salomon, Y. *Medicine* **1998**, *39*, 439-477.

(2) Huang, L. R.; Straubinger, R. M.; Kahl, S. B.; Koo, M. S.; Alletto, J. J.; Mazurchuk, R.; Chau, R. I.; Thamer, S. L.; Fiel, R. J. *Imaging* **1993**, *3*, 351-356.

(3) Kabalka, G. W.; Cheng, G. Q.; Bendel, P.; Micca, P. L.; Slatkin, D. N. *J. Magnetic Res. Imaging* **1991**, *9*, 969-973.

(4) Kabalka, G. W.; Tang, C.; Bendel, P. *J. Neuro-Oncol.* **1997**, *33*, 153-161.

(5) Gabel, D.; Moss, R. *Boron Neutron Capture Therapy. Toward Clinical Trials of Glioma Treatment*; Plenum Press: New York, 1992.

(6) Shelly, K.; Feakes, D. A.; Hawthorne, M. F. *The Royal Society of Chemistry: Cambridge* **1993**, 165-168.

(7) Arlinghaus, H. F.; Spaar, M. T.; Switzer, R. C.; Kabalka, G. W. *Anal. Chem.* **1997**, *69*, 3169-3176.

(8) Kabalka, G. W.; Smith, G. T.; Dyke, J. P.; Reid, W. S.; Desmond-Longford, C. P.; Roberts, T. G.; Reddy, N. K.; Buonocore, E.; Hübner, K. F. *J. Nuclear Med.* **1997**, *38*, 1762-1767.

(9) Kabalka, G. W. *Expert Opin. on Ther. Pat.* **1998**, *8*, 545-551.

(10) Fukuda, M. *Cell Surface Carbohydrates in Hematopoietic Cell Differentiation and Malignancy*; CRC Press: Boca Raton, 1992.

(11) Fukuda, M. In *Molecular Glycobiology*; Fukuda, M., Hindsgaul, O., Eds.; Oxford University Press: New York, 1994, p 1-52.

(12) Fukuda, M. *Cancer Research* **1996**, *56*, 2237-2244.

(13) Alavi, A.; Axford, J. S. *Glycoimmunology. Adv. Exp. Med. Biol.*; Plenum Press: New York, 1995; Vol. 376.

(14) Musser, J. H.; Fugedi, P.; Anderson, M. B. *Carbohydrate-based Therapeutics*; John Wiley & Sons: New York, 1995.

(15) Dennis, J. W. *Changes in Glycosylation Associated with Malignant Transformation and Tumor Progression*; CRC press: Boca Raton, 1992.

(16) Jorgensen, T.; Kanagasingam, Y.; Kaalhus, O.; Tveter, K. J.; Bryne, M.; Skjorten, F.; Berner, A.; Danielsen, H. E. *J. Urol.* **1997**, *158*, 164-170.

(17) Idikio, H. A. *Glycoconj. J.* **1997**, *14*, 875-877.

(18) Satoh, H. A.; Ishikawa, H.; Kamma, H.; Yamashita, Y. T.; Takahashi, H.; Ohtsuka, M.; Hasegawa, S. *Cancer Research* **1997**, *3*, 495-499.

(19) Fujiwara, M.; Satoh, H. A.; Fujimoto, M.; Yazawa, T.; Ishikawa, H.; Horiguchi, H.; Ogata, T.; Matsui, M.; Kamma, H. *Anticancer Research* **1998**, *18*, 1043-1046.

(20) Hosona, J.; Narita, N.; Kimura, N.; Sato, M.; Nakashio, T.; Kasai, Y.; Nonami, T.; Nakao, A.; Takagi, H.; Kannagin, R. *J. Surg. Oncol.* **1998**, *67*, 77-84.

(21) Farmer, R. W.; Richtsmeier, W. J.; Scher, R. L. *Head Neck* **1998**, *20*, 726-731.

(22) Martensson, S.; Bigler, S. A.; Brown, M.; Lange, P. H.; Brawer, M. K.; Hakomori, S. *Hum. Pathol.* **1995**, *26*, 735-739.

(23) Culig, Z.; Hittmair, A.; Hobisch, A.; Bartsch, G.; Klocker, H.; Pai, L. H.; Pastan, I. *Prostate* **1998**, *1998*, 162-167.

(24) Myers, R. B.; Grizzle, W. E. *Eur. Urol.* **1996**, *30*, 153-166.

(25) Zhang, S.; Zhang, H. S.; Cordon-Cardo, C.; Reuter, V. E.; Singhal, A. K.; Lloyd, K. O.; livingston, P. O. *Int. J. Cancer.* **1997**, *73*, 50-56.

(26) Kannagi, R. *Glycoconj. J.* **1997**, *14*, 577-584.

(27) Nakamori, S.; Kameyama, M.; Imaoka, S.; Furukawa, H.; Ishikawa, O.; Sasaki, Y.; Izumi, Y.; Irimura, T. *Dis. Colon Rectum* **1997**, *40*, 420-431.

(28) Nakamori, S.; Kameyama, M.; Imaoka, S.; Furukawa, H.; Ishikawa, O.; Salomon, Y.; Kabuto, T.; Iwanaga, T.; Matsushita, Y.; Irimura, T. *Cancer Res.* **1993**, *53*, 3632-3637.

(29) Kuusela, P.; Jalanko, H.; Roberts, P.; Sipponen, P.; Mecklin, J. P.; Pitkanen, R.; Makela, O. *Britian J. Cancer* **1984**, *49*, 135-139.

(30) Hoff, S.; Irimura, T.; Matsushita, Y.; Ota, D.; Cleary, K.; Hakamori, S. *Arch. Surg* **1990**, *125*, 206-209.

(31) Herlyn, M.; Sears, H. F.; Verrill, H.; Koprowski, H. *J. Immunol. Methods* **1984**, *1984*, 15-21.

(32) Böeseken, J. *Adv. Carbohydr. Chem.* **1949**, *4*, 189.

(33) Lorand, J. P.; Edwards, J. O. *J. Org. Chem.* **1959**, *24*, 769-774.

(34) Sugihara, J. M.; Bowman, C. M. *J. Am. Chem. Soc.* **1958**, *80*, 2443.

(35) Ward, C. J. *J. Chem. Soc., Perkin Trans. 1* **2000**, 963-969.

(36) Wang, W.; Gao, S.; Wang, B. *Org. Lett.* **1999**, *1*, 1209-1212.

(37) Ward, C. J.; James, T. D. *SPIE Conference in Advances in Fluorescence Sensing Techanology IV* **1999**, 194-201.

(38) Kijima, H.; Robertson, A. R.; Shinkai, S.; Cooper, C.; James, T. D. *Chem. Commun* **1999**, 2011-2012.

(39) Tamamoto, M.; M., T.; Shinkai, S. *Tetrohedron* **1998**, *54*, 3125-3140.

(40) Bielecki, M.; Eggert, H.; Norrid, J. C. *J. Chem. Soc., Perkin Trans. 2* **1999**, 449-455.

(41) James, T. D.; Shinmori, H.; Shinkai, S. *Chem. Commun.* **1997**, 71-71.

(42) James, T. D.; Linnane, P.; Shinkai, S. *Chem. Commun.* **1996**, 281-288.

(43) James, T. D.; Sandanayake, K. R. A. S.; Shinkai, S. *Nature (London)* **1995**, *374*, 345-347.

(44) James, T. D.; Samankumara, K. R. A.; Iguchi, R.; Shinkai, S. *J. Am. Chem. Soc.* **1995**, *117*, 8982-8987.

(45) Sandanayake, K. R. A. S.; Nakashima, K.; Shinkai, S. *Chem. Commun.* **1994**, 1621-1622.

(46) Lin, Y.-I.; Lang, S. A.; Seifert, C. M.; Child, R. G.; Morton, G. O.; Fabio, P. F. *J. Org. Chem.* **1979**, *44*, 4701-4703.

(47) Pearson, D. E.; Bruton, J. D. *J. Am. Chem. Soc.* **1951**, *73*, 864.

(48) Hayash, T.; Hitomi, Y.; Ogoshi, H. *J. Am. Chem. Soc.* **1998**, *120*, 4910-4915.

(49) Fujiwara, Y.; Shimada, M.; Takenaka, K.; Kajiyama, K.; Shirabe, K.; Sugimachi, K. *Hepatogastroenterology* **2002**, *49*, 213-217.

(50) Okada, Y.; Jin-no, K.; Ikeda, H.; Sakai, N.; Sotozono, M.; Yonei, T.; Nakanishi, S.; Moriwaki, S.; Tsuji, T. *Cancer Res.* **1994**, *73*, 1811-1816.

(51) Shacter, E.; Weitzman, S. A. *Oncology* **2002**, *16*, 217-223.

(52) Weston, B. W.; Hiller, K. M.; Mayben, J. P.; Manousos, G. A.; Bendt, K. M.; Liu, R.; Cusack, J. C. J. *Cancer Research* **1999**, *59*, 2127-2135.

(53) Hiller, K. M.; Mayben, J. P.; Bendt, K. M.; Manousos, G. A.; Singer, K.; Cameron, H. S.; Weston, B. W. *Mol. Carcinog.* **2000**, *27*, 280-288.

(54) Weston, B. W.; Smith, P. L.; Kelly, R. J.; Lowe, J. B. *J. Biol. Chem.* **1992**, *267*, 24575-24584.

(55) Weston, B. W.; Nair, R. P.; Larsen, R. D.; Lowe, J. B. *J. Biol. Chem.* **1992**, *267*, 4152-4160.

(56) Yago, K.; Zenita, K.; Ginya, H.; Sawada, M.; Ohmori, K.; Minoru, O.; Kannagi, R.; Lowe, J. *Cancer Research* **1993**, *53*, 5559-5565.

(57) Leventis, C. S.; Mao, Z. *J. Heterocyclic Chem.* **2000**, *37*, 1665-1667.

Chapter 2. Study of the Mechanism of Electron-Transfer Quenching by Boron-Nitrogen Adducts in Fluorescent Sensors

Abstract

The mechanism of the change in fluorescence quenching by the amine in boronic acid-based carbohydrate sensor molecules has been explored using density functional theory (DFT). The geometric constraints of the system have been studied in both intra- and intermolecular model systems of the boron-nitrogen (B-N) bonding interaction. The effect of the B-N bonding on the rate of electron transfer (ET) quenching of the anthracene acceptor by an amine donor is considered using a theoretical model. The results suggest a new mechanism other than B-N bond strength change for fluorescent switching in biosensors that involves interaction of boron and nitrogen affected by boronate ester formation.

2.1. Introduction

Due to its unique high affinity and reversible interactions with diols,[1-3] the boronic acid functional group is routinely incorporated into synthetic receptors for the complexation of saccharides and other guests that possess 1,2- and 1,3-diol group.[4-17] This is particularly true in the design of fluorescent sensors for saccharides. However, in a sensor design, high affinity and specificity binding alone are not sufficient. There needs to be a reporting event that signals the binding.

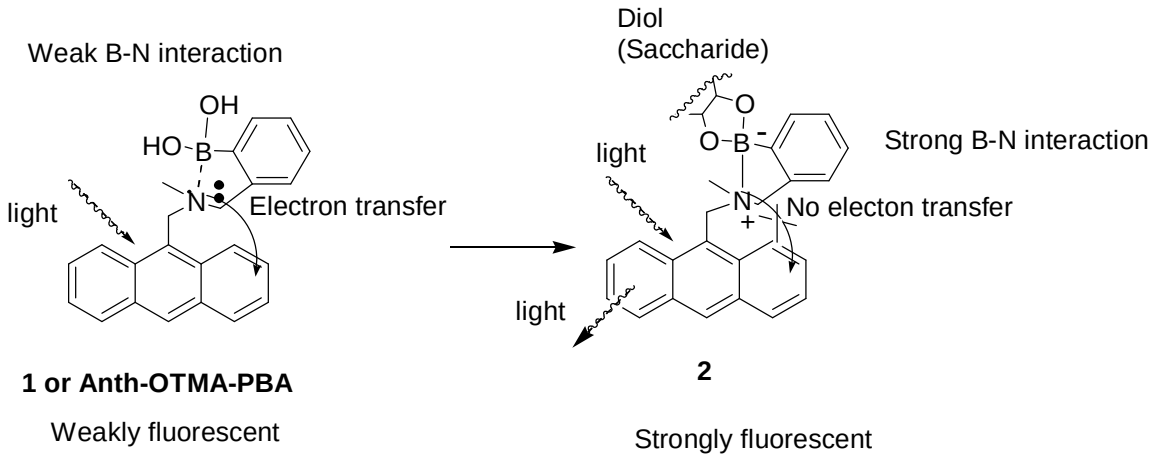

Figure 2.1. Photoinduced electron transfer (PET) mechanism proposed by the Shinkai group.[18] The formation of boron-nitrogen bond upon binding of boronic acid **1** with diol containing compounds causes the fluorescent change.

Among the boronic acid-based fluorescent reporter compounds reported during the last decades, Shinkai's anthracene-based reporter compound **1** (Figure 2.1) occupies a special place due to its large fluorescence intensity changes upon binding with a diol-containing compound.[18] Our laboratories have studied modifications of **1** both theoretically and experimentally as fluorescent sensors for various saccharides.[13,14,16,19] In the design of **1**, the anthracence moiety is the fluorophore. However, the lone pair electrons of the benzylic amine is known to quench the anthracene fluorescence through a

photoelectron transfer mechanism, which makes compound **1** only weakly fluorescent. It is known that binding of most saccharides to a boronic acid increases the acidity of the boron atom. Therefore, upon binding of a saccharide to the boronic acid group, the increased acidity of the boron promotes the formation of the B-N bond (**2**) via a five-membered ring. Such B-N bond formation was thought to mask the lone pair electrons and therefore diminish the ability of the lone pair electrons to quench the anthracene fluorescence. Consequently, binding of a saccharide to **1** causes a significant fluorescence intensity increase.[8]

2.1.1. Boron-Nitrogen Bond Chemistry

The nature of the boron nitrogen bond and the details of the quenching mechanism are still subject to intense investigation. There is relatively little structural data on B-N adducts of the type shown in Figure 2.2 and Figure 2.3, despite the burgeoning interest in this field. In fact, the current literature presents a contradiction since the bond lengths of the ester[20] and acid[15] determined by X-ray crystallography are 1.754 Å and 1.669 Å, respectively. This trend is opposite to what is expected based on the increased Lewis acidity in the ester form. Another study that seems to contradict the B-N bond role in regulating the fluorescence intensity of such a system (**1**) upon binding with a saccharide is fluorescence recovery studies with various monosaccharides conducted by James and co-workers.[21] In this study, it was found that the most of the monosaccharides tested gave essentially the same fluorescence intensity recovery at saturating concentration. For example, the fluorescence intensity of **1** in the presence of fructose and glucose were about the same, while the boronic esters of these two saccharides are known to be very different.[2] For example, the pKa of the ester of

phenylboronic acid with fructose is about 4.6 and with glucose the pKa is about 6.8. If the B-N bond strength were the only reason for the fluorescence intensity changes upon binding, it would be hard to explain the same fluorescence intensity recovery with these two saccharides. It is because of these unanswered questions, we set out to examine the details of the B-N bond interaction in this boronic acid fluorescent system (**1**) using computational chemistry.

The interaction between boron and nitrogen has fascinated chemists for many years.[22-31] The boron-nitrogen bond is isoelectronic with a carbon-carbon bond. Due to the difference in the electronegativity of boron and nitrogen, the bonding tends to be weaker in the B-N than in the corresponding C-C compounds. We approached an understanding of the interaction of boronic esters with the tertiary amine by calculating the potential energy surfaces for a variety of intermolecular models (Figure 2.2) and intramolecular models (Figure 2.3) that will lead up to the systems of interest.

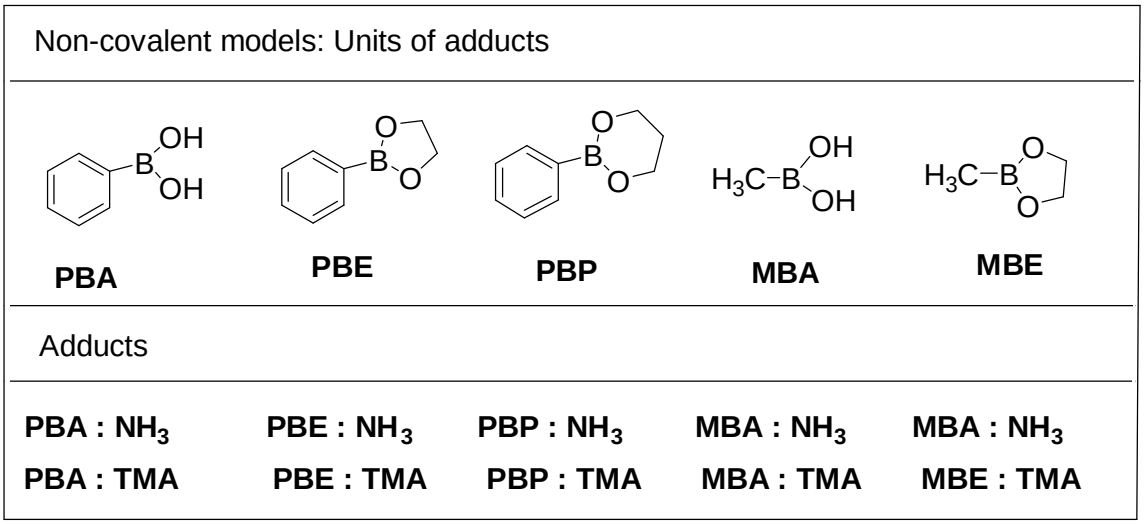

Figure 2.2. Structures of intermolecular models studied by DFT methods. The structural units consist of phenyl and methyl boronic acids and esters. The adducts of these molecules with ammonia and trimethylamine (TMA) were studied to determine the strength of the boron-nitrogen bond and conformation of the boronic acid/ester relative to the phenyl ring.

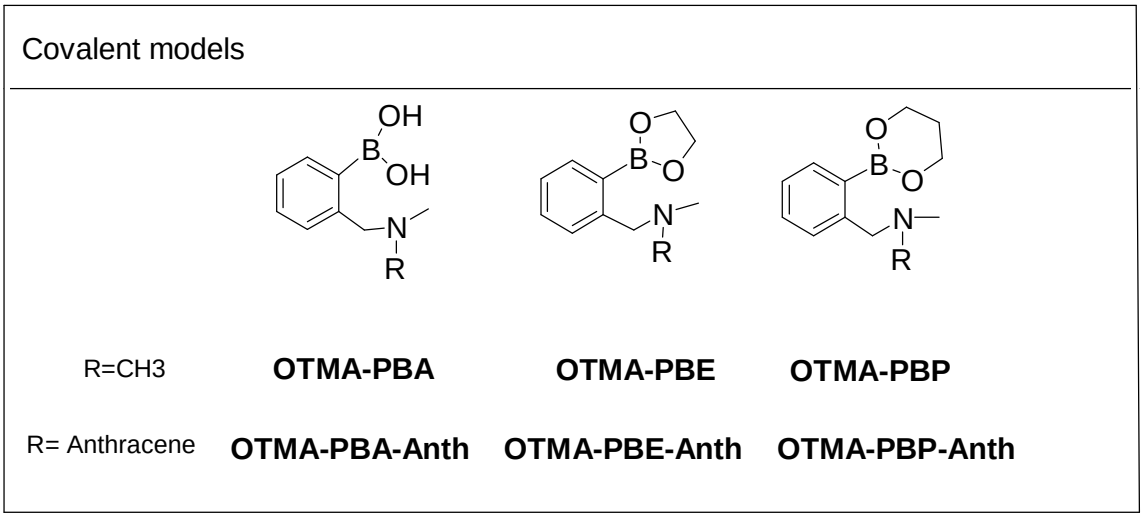

Figure 2.3. Structures of intramolecular models studied by DFT methods. The biosensor models include both boronic acid/ester moiety and a trimethyl amine base covalently attached to a phenyl ring.

These studies show that B-N bonding is surprisingly weak in both intermolecular boron-nitrogen adducts shown in Figure 2.2 and intramolecular models in Figure 2.3. Although weak B-N bonds that have the strength of typical hydrogen bonds are found, it is the difference in bond strength upon boronate ester formation that must account for the change in fluorescence quenching observed experimentally.

2.1.2. Charge Transfer Theory Involved in this Fluorescence Change Mechanism

The effect of a B-N bonding interaction on the quenching of anthracene fluorescence can be considered in terms of the effect it has on the electron transfer process that competes with fluorescence. Two possible charge transfer reactions can compete with fluorescence from ^{1}A back to the ground state. The electron transfer rate constant is:

$$k_{ET} = \frac{\hbar^2}{2\pi}|V^2|FC \qquad (1)$$

where V is the electronic coupling and FC is the Franck-Condon factor. V is an electronic factor that can be expressed in terms of the electronic wave functions.

$$V = \left\langle \Psi\ {}^{1}ANB|H|\Psi_{A^{-}N^{+}B} \right\rangle \tag{2}$$

where Ψ represents the electronic wave function. The subscripts indicate that photoexcited state and one of the possible charge separated states, respectively. The effect of formation of the B-N bond can alter the FC factor by changing the energy of the charge transfer state. This will affect the nuclear overlap factors. The FC factor is given by:

$$FC = \sum_{v,v'=0}^{\infty} \left\langle \chi_{v}\ {}^{1}ANB|\chi_{v'}^{A^{-}N^{+}B} \right\rangle^{2} \rho \tag{3}$$

where χ_v and $\chi_{v'}$ are the nuclear wave functions for the reactant and product states, respectively. The term ρ is the density of states term. This can be represented by a line shape function (Gaussian, Lorentzian or delta function) that represents the energy matching condition. In the high temperature limit or in polar solvents the FC factor is reduces to the Marcus theory expression,

$$FC = \frac{1}{\sqrt{4\pi\lambda kT}} \exp\left\{ -\frac{\left(\lambda - \varepsilon\right)^{2}}{4\lambda kT} \right\} \tag{4}$$

In this expression it is clear that the barrier for charge-separation is:

$$E^{*} = \frac{\left(\lambda - \varepsilon\right)^{2}}{4\lambda} \tag{5}$$

where ε is the energy gap between the reactant and product states and λ is the reorganization energy. In molecular terms the reorganization energy can be represented as:

$$\lambda = \sum_{i=1}^{N} S_i \hbar\omega_i \qquad (6)$$

where S is the electron phonon coupling parameter. For each vibrational mode, S_i is related to the displacement Δ_i by $S_i = \Delta_i^2/2$. The inner sphere reorganization energy includes changes in the bond length on the donor and acceptor that give rise to displacements, Δ_i. In Marcus theory, the low frequency modes are usually treated in a dielectric continuum approximation. In other words, there is a significant contribution from reorientation of solvent dipoles to accommodate the charge separation that is usually calculated as a polarization contribution. A major segment of the present study involves the calculation of λ including both inner sphere (molecular) and outer sphere (solvent) contributions.

The present study presents a critical view of the role of electron transfer quenching in boron-nitrogen based sensors. Density functional theory is adapted to the calculation of the parameters (V^2, ε and λ) useful in Marcus theory calculation of the rate constant. The study begins by addressing the calculation of the conformational energies of different possible B-N bonding adducts that could be involved in a conformational switch mechanism. The interplay of torsional coordinates in the molecule with the weak B-N bonding interaction is studied. Then the structures consistent with the strongest B-N interaction are studied as both vacuum (isolated molecule) and solvated (explicit solvent or dielectric continuum) systems. These factors are used to determine the activation energy and estimate the relative magnitude of the rate constant required for quenching. Finally, the comparison of phenyl boronic acids (**PBA**) and the corresponding boronate esters (**PBE** or **PBP**) is made to determine the role that these factors play in the switching mechanism for the boron-nitrogen based biosensor.

The main conclusion of the study is that the weak B-N interaction and small change in B-N bond strength upon formation of a boronate ester of <4kJ/mol cannot account for the observed change in fluorescence. The effects of B-N bond formation on the energy of ET, reorganization energy, and electronic coupling are considered systematically. The inner sphere (molecular) and outer sphere (molecule + solvent) reorganization energies are calculated using models that include a dielectric continuum method and explicit solvent molecules. According to the DFT calculations, neither the driving force nor the reorganization for electron transfer is strongly affected by the formation of a boronate ester. The net change in activation energy for the electron-transfer process actually favors fluorescence quenching in the phenylboronate ester. Since the calculations are carried out using a dielectric continuum, the results would correspond to the observation in an aprotic solvent. The present calculations make a prediction that the fluorescence quantum yield will show the opposite behavior in aprotic solvents from the observed in aqueous buffer (see Chapter 3). This prediction of DFT theory was tested and confirmed in experimental fluorescence studies of phenylboronate ester formation in acetonitrile. The results of this study suggest that protonation rather than B-N bond formation is the mechanism for the switching of the boronic acid biosensors from a nonfluorescent to a fluorescent state upon boronate ester formation (Details see Chapter 3).

2.2. Method

Density function theory (DFT) calculations were carried out for various intermolecular models (BXY_2:NZ_3) in Figure 2.2 and intramolecular models the given in

Figure 2.3. The calculations have been carried out using DMol3[32] with the generalized gradient approximation (GGA) using the DNP basis set. The calculations were carried out at the North Carolina Supercomputer Center on the IBM SP and SGI/Cray Origin 2000. DFT has been shown to give excellent geometries, dipole moments and vibrational frequencies for dative bond adducts. The interaction energies of adducts were calculated by calculation a potential energy surface (PES) or thermodynamic equilibria. The energies used for comparing conformations of charge-separated states are the total energies or binding energies of the molecules. The difference in the energies of two conformers and the difference in the energies of charge-separated state are identical whether the total energy or binding energy is used for the comparison. The PES was obtained by plotting single point energy at displacements of the donor, NZ_3 and acceptor, BXY_2 along the B-N bond from 1 Å to 10 Å (BXY_2 ß R(Å) à NZ_3). Such a potential energy surface approach uses the calculation of the donor and acceptor at 10 Å as the reference state. The energy of the reference state is used as the zero of energy to determine the relative interaction energy of the adduct. Energies were also calculated using thermodynamic equilibria of the type shown below:

$BXY_2{:}NZ_3$ à $BXY_2 + NZ_3$

The energy of adduct formation is calculated as $E(BXY_2) + E(NZ_3) - E(BXY_2{:}NZ_3)$, where the energies E are the binding energies determined by DFT. For boronate ester formation with ethylene glycol the hydrolysis equilibrium was considered.

$BXC_2H_4O_2{:}NZ_3 + 2\ H_2O$ à $BX(OH)_2{:}NZ_3 + C_2H_6O_2$

where X = OH, CH_3 or C_6H_5, $Y_2 = (OH)_2$, $C_2H_4O_2$ or $C_3H_6O_2$ and Z = H or CH_3. Each molecule was geometry optimized separately in these calculations leading to possible

artifacts in the energy calculation. The calculated B-N bonding interaction was not identical for the two methods. We have generally regarded the PES as the more reliable method for determining the magnitude of binding interactions. The values obtained from PES calculations are reported in the Results section.

Solvation is an important factor in the stabilization of charge transfer states. Solvation energies were calculated using a dielectric continuum model (COSMO)[33,34] and using explicit water molecules as described in the Results section.

2.3. Results

2.3.1. B-N interaction

We have performed density function theory (DFT) calculations of the potential energy of interaction for various models given in Table 2.1. The Lewis acids considered include borane, boric acid (**BA**), methyl boronic acid (**MBA**), phenylboronic acid (**PBA**) and the corresponding esters **BE**, **MBE** and **PBE**. The Lewis bases considered are NH_3 and $N(CH_3)_3$ (**TMA**). The bond length BH_3-NH_3 is 1.66 Å compared to 1.52 Å for CH_3-CH_3 as determined from a DFT in good agreement with literature values.[26,29,34-37] The experimental bond energies for BH_3-NH_3 and BH_3-$N(CH_3)_3$ are –195.4 and –190.0 kJ/mol, which can be compared to calculated values of –141.0 kJ/mol and –172.8 kJ/mol, [36] respectively. The calculated bond energy for CH_3-CH_3 is –496.6 kJ/mol. The B-N bond is significantly weaker than the C-C bond due to poorer overlap in the asymmetric B-N structure. Nonetheless, the B-N bonds in BH_3-NH_3 and BH_3-$N(CH_3)_3$ are much stronger than those for any boronic acid or boronate ester in Table 2.1.

Table 2.1. B-N bond lengths, energies and charges obtained from potential energy surface studies.

Model	d(B-N) (Å)	Bond energy (kJ/mol)	ESP Charge Boron	ESP Charge Nitrogen
BH_3: NH_3	1.66	195.4	0.22	-0.44
BH_3: TMA	1.52	190.0	0.32	-0.44
BA:NH_3	1.79	14.9	0.82	-0.64
BE:NH_3	3.24	14.0	0.80	-0.76
MBA:NH_3	3.27	13.4	0.77	-0.94
MBE:NH_3	3.18	14.6	0.88	-0.93
PBA:$NH_3$0	3.40	18.7	0.49	-0.82
PBE:$NH_3$0	2.80	22.2	0.70	-0.68
PBP:$NH_3$0	3.25	25.0	0.71	-0.73
PBA:$NH_3$90	3.35	14.2	0.77	-0.88
PBE:$NH_3$90	2.73	14.2	0.87	-0.81
PBP:$NH_3$90	3.20	13.8	0.84	-0.86
BA:TMA	1.81	22.2	0.69	0.32
BE:TMA	4.65	20.3	0.82	-0.06
MBA:TMA	2.66	28.3	0.77	0.21
MBE:TMA	2.57	30.3	0.88	0.22
PBA:TMA0	3.86	17.1	0.49	0.20
PBE:TMA0	2.70	29.7	0.70	0.16
PBP:TMA0	3.98	16.8	0.73	0.12
PBA:TMA90	3.70	15.5	0.60	0.11
PBE:TMA90	3.85	15.9	0.71	0.12
PBP:TMA90	4.00	16.4	0.81	0.22

To understand the effect of boronate ester formation on boron-nitrogen bonding, we have considered both non-covalent and covalent models shown in Figure 2.2 and Figure 2.3. The study of intermolecular adducts shows that boron-nitrogen bonding is very weak (<30 KJ/mol) for all boronic acid and boronate ester adducts (Table 2.1). The intrinsic weakness of the B-N bond in acids and esters presents the fundamental challenge to understanding the origin of the effects in biosensors that involve the interaction of boronic acids and amines in intramolecular adducts such as those shown in

Figure 2.3. The intermolecular models have the strongest B-N interactions for an in-plane conformation of the phenylboronic acid and esters (for example **PBE:TMA0 > PBE:TMA90).** Non-covalent Lewis acid:base complexes include the various alkyl (**MBA**, **MBE**) and phenyl boronic acids (**PBA**, **PBE**, **PBP**) with **NH_3** or $(CH_3)_3N$ (**TMA**). The non-covalent adducts can be indicated as **TMA:PBA** etc. where the boron-nitrogen interaction is the only covalent interaction between the amine donor and boron Lewis acid acceptor. The covalent models are denoted **OTMA-PBA** etc. to indicate that the trimethylamino group is in the ortho position to the boronic acid moiety (Figure 2.3). The designation for phenyl boronic acid is **PBA** and that for the glycol and 1,3-propanediol ester are **PBE** and **PBP**, respectively.

2.3.2. Phenyl Boronic Ester Formation Requires a Cp-Cp-B-O Dihedral Angle ($t_{C-C-B-O}$) of 90°

The nature of the B-N interaction is sufficiently weak that there is a competition between the torsional coordinate $t_{C-C-B-O}$ and the B-N interaction for the intramolecular models relevant to the biosensor **4**. The intermolecular models discussed in section 2.4.2 have the strongest B-N interactions (see Table 2.1) for an in-plane conformation of the boronic acid or boronate ester group. However, for intramolecular adducts of type shown in Figures 2.3 and 2.4, the in-plane geometry has the weakest B-N bond formation.

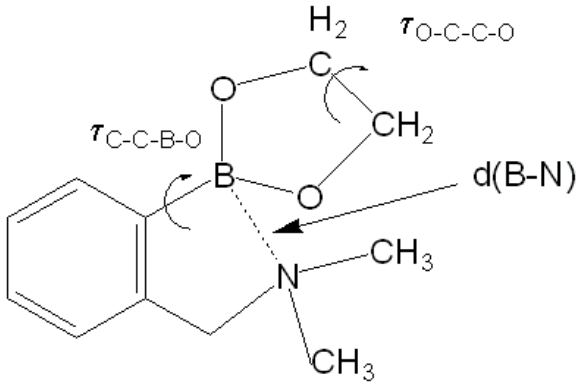

Figure 2.4. Important conformational coordinates in the ground state potential energy surface of phenyl boronic glycol ester with a trimethyl amino group.

Table 2.2. Energies, charges and boron-nitrogen distances in the o-trimethylamino boronic acid/ester models **OTMA-PBA, OTMA-PBE** and **OTMA-PBP.**

Model	Cp-Cp-B-O Dihedral	d(B-N) (Å)	Energy (kJ/mol)	ESP Charge Boron	ESP Charge Nitrogen
OTMA-PBA0	0	3.13	-12628.1	0.50	-0.01
OTMA-PBA45	45	2.99	-12629.8	0.55	0.004
OTMA-PBA90	90	1.98	-12636.9	0.51	0.17
OTMA-PBE0	0	3.23	-14582.1	0.77	-0.023
OTMA-PBE90	90	1.85	-14592.5	0.85	0.16
OTMA-PBP0	0	3.40	-15856.9	0.68	0.009
OTMA-PBP90	90	2.26	-15867.0	0.61	-0.46

Table 2.2 shows the energy and B-N bond length for three different geometries of the covalent adducts **OTMA-PBA**, **OTMA-PBE** and **OTMA-PBP.** The three geometries correspond to Cp-Cp-B-O dihedral angles of $\tau_{C\text{-}C\text{-}B\text{-}O} = 0^o$ (**OTMA-PBA0**), $\tau_{C\text{-}C\text{-}B\text{-}O} = 45^o$ (**OTMA-PBA45***)* or $\tau_{C\text{-}C\text{-}B\text{-}O} = 90^o$ (**OTMA-PBA90**) with corresponding

nomenclature for **OTMA-PBE** and **OTMA-PBP**. Geometry optimizations were carried out from each of the starting geometries. While the angle changes slight, the structures observed are each in distinct local minima. In **OTMA-PBA0** the Cp-Cp-B-O dihedral angle is 0^o and thus the boronic acid moiety lies in the plane of the benzene ring. For this geometry the boron-nitrogen interaction is extremely weak due to steric interactions. For the **OTMA-PBA90** structure, which has a Cp-Cp-B-O dihedral angle of 90^o, the B-N bond length is significantly shorter (1.98 Å) than for **OTMA-PBA0** (3.13 Å). The geometry in **OTMA-PBA45** is intermediate with a Cp-Cp-B-O dihedral angle of 45^o, but the B-N bond is still quite long (2.86 Å) for this geometry. These calculations show that B-N bonding does not occur in the covalent adducts unless the boronic acid plane is nearly perpendicular to that of the benzene ring. Given that the opposite is true for the non-covalent Lewis base:acid adducts **OTMA:PBA**, **OTMA:PBE**, and **OTMA:PBP**, it appears that conformational strain reduces the B-N bond strength for $\tau_{C\text{-}C\text{-}B\text{-}O} = 0^o$ in the intramolecular adducts.

The covalent adducts provide an indication of a specific B-N interaction. The difference in energy between adducts **OTMA-PBA90** and **OTMA-PBE90** is not readily described in terms of bond strength, since the difference is subtle and is part of relatively large molecule. For the intramolecular adducts, we consider the bond length as a measure of the strength of the bonding interaction. Table 2.2 shows that for $\tau_{C\text{-}C\text{-}B\text{-}O} = 90^o$ **OTMA-PBE90** has a B-N bond length of 1.85 Å, which can be considered a bonding interaction. The B-N bond length is significantly longer (1.98 Å) in **OTMA-PBA90** presumably due to the decreased Lewis acidity on the boronic acid compared to the boronate ester. Table 2.2 shows further that a B-N bond length is longer (2.26 Å) for

the ester of 1,3-propandiol (**OTMA-PBP90**) than for the glycol ester or the acid.

2.3.3. The Minimum Energy Structure is Found for O-C-C-O Dihedral Angle $t_{O\text{-}C\text{-}C\text{-}O} = 30^{o}$

The O-C-C-O dihedral angle shown in Figure 2.4 is the angle of the diol in a boronate ester. Molecules of the phenyl boronic acid class (**PBA**) recognize cis-diols. Based on this observation, we can surmise that the optimal dihedral angle will be relatively small. Since the specificity of binding is a crucial aspect of the function of a biosensor it is of interest to identify the optimal structure for molecular recognition. Molecular recognition of particular oligosaccharides will arise because of preferred dihedral angles for formation of boronic esters. The propensity for a particular dihedral angle was investigated by a systematic study of the **OTMA-PBE** molecule as a function of the O-C-C-O dihedral angle ($\tau_{O\text{-}C\text{-}C\text{-}O}$) as shown in Figure 2.4 and tabulated in Table 2.2. Optimal binding is found for a dihedral angle of $\tau_{O\text{-}C\text{-}C\text{-}O} \sim 30^{o}$. There is a competition between ester formation and B-N bond strength. The optimal B-N bond length decreases as the O-C-C-O dihedral angle increases; however, the overall energy of the molecule also begins to increase sharply as the O-C-C-O dihedral angle increases to greater than 30^{o} (see Table 2.3).

Table 2.3. Effect of modification of the dihedral angle (O-C-C-O) in the boronate ring in compound **OTMA-PBE** on the energy and optimum B-N bond length in the adduct.

	Neutral	Neutral	Cation	Cation
O-C-C-O	d(B-N) (Å)	E (kJ/mol)	d(B-N) (Å)	E (kJ/mol)
10	1.98	-14623	1.74	-13818
20	1.92	-14628	1.75	-13820
30	1.84	-14629	1.72	-13821
40	1.82	-14623	1.71	-13815
50	1.80	-14614	1.70	-13806

2.3.4. Energy of charge transfer states

Fluorescence quenching involves competing pathways for deactivation of the excited state. Quenching by charge transfer is a common mechanism. To understand the factors that govern the competition between charge transfer and fluorescence in biosensors (**OTMA-PBA-Anth**) of the type shown in Figures 2.2 and 2.3, using DFT calculations, the energy of the charge transfer state was studied as a function of the solvation. The excited state of anthracene can serve either as an electron acceptor for donation by trimethylamine or as a donor with the boron center acting as an acceptor. Both of these possibilities are considered. The ground state is written as BNA to indicate the presence of neutral boron (B), nitrogen (N) and anthracene (A) moieties. In general we can write two alternate electron transfer schemes:

$$A\cdots N\cdots B \xrightarrow{h\nu} {}^1A\cdots N\cdots B \rightarrow A^-\cdots N^+\cdots B \rightarrow A\cdots N\cdots B$$

$$A\cdots N\cdots B \rightarrow {}^1A\cdots N\cdots B \rightarrow A^+\cdots N\cdots B^- \rightarrow A\cdots N\cdots B$$

The relative energy of a charge transfer state BN^+A^- or B^-NA^+ state relative to the BNA ground state can be obtained from calculations of the energy of the individual cations and anions of the donor and acceptor molecules. The energy of the charge transfer state was obtained from the sum of the anthracene anion (A-) or cation (A^+) with the cation or anion of **OTMA-PBA, OTMA-PBE** and **OTMA-PBP**, respectively. The reference for these calculations was the **TMA$^+$anth$^-$PBE** charge transfer state for an anthracene acceptor and the **TMA anth$^+$ PBE$^-$** charge transfer state for an anthracene donor relative to the energy of neutral **TMA$^-$anthPBE**.

Table 2.4. Binding energy of the neutral and ionic form for various molecules that can act as donors or acceptors in an electron transfer quenching mechanism.

	Neutral (kJ/mol)		Anion (kJ/mol)		Cation (kJ/mol)	
Solvation à	Cosmo	None	Cosmo	None	Cosmo	None
Anthracene	-15616	-15595	-15839	-15639	-15164	-14989
TMA	-4970	-4960	NA	NA	-4515	-4219
OTMA-PBA	-12691	-12637	-12794	-12582	-12224	-12014
OTMA-PBE	-14633	-14592	-14763	-14538	-14161	-13969
OTMA-PBP	-15906	-15867	-16030	-15809	-15440	-15256
PBA	-8153.4	-8104.4	-8138.6	-8030.3	NA	NA
PBE	-10101	-10080	-10263	-10026	NA	NA
PBP	-11390	-11363	-11535	-11301	NA	NA

Table 2.4 presents the binding energies of individual molecules. The ionization potentials (IPs) were calculated using one half electron occupancy of the HOMO, as indicated for DFT theory by Slater.[35] The calculated (and experimental) IPs for anthracene and **TMA** are 6.6 (7.4) eV and 8.8 (7.8) eV, respectively.[36]

Table 2.5. Charge transfer energy for the respective donor-acceptor pair based on the calculation of the binding energies (see Table 2.4). All of the values given in the table are higher in energy than the lowest singlet excited state, which is 337 kJ/mol above the ground state.

Electron-ransfer process	COSMO (kJ/mol)	None (kJ/mol)
TMA + Anth à TMA^+ + $anth^-$	232.5	696.1
OTMAPBA + anth à $OTMAPBA^+$ + $anth^-$	244.3	579.1
OTMAPBE + anth à $OTMAPBE^+$ + $anth^-$	250.4	579.2
OTMAPBP + anth à $OTMAPBP^+$ + $anth^-$	243.5	567.1
OTMAPBA + anth à $OTMAPBA^-$ + $anth^+$	351.2	794.6
OTMAPBE + anth à $OTMAPBE^-$ + $anth^+$	325.6	794.5
OTMAPBP + anth à $OTMAPBP^-$ + $anth^+$	330.9	798.5

.

Table 2.5 shows the calculated energy difference between the charge transfer state and the ground state. The calculated electronic transition energy for the absorption of a photon A à ^{1}A is 28172 cm^{-1} or 337 kJ/mol. The predicted wavelength for the singlet absorption is 354 nm compared to the observed 0-0 transition at 370 nm.[38] The energies of states such as B^-NA^+ (boron acceptor) were calculated to significantly (~130 kJ/mol) higher than BN^+A^- (nitrogen donor). The boron acceptor states are reported in Table 2.5, but not considered further for this reason. In the absence of solvation, even the reference charge transfer state **TMA$^+$Anth$^-$** is significantly higher in energy than the anthracene singlet excited state making the electron transfer endothermic. The relative energies of the charge transfer states are lowered substantially if solvation is included. This calculated result corresponds to the observation that many charge transfer processes that result in fluorescence quenching occur only in polar solvents. Solvent polarity results in solvation of the charge separated state and screening of the charges. The latter effect reduces the magnitude of the Coulomb term. We use a point charge approximation rather than a DFT calculation for the Coulomb term for two reasons. First, the Coulomb term should have approximately the same magnitude for charge separation distance is quite similar in both. Second, the Coulomb term is small in polar solvents and we are concerned with a charge separation process in water.

2.3.5. Calculation of Solvation Effects

To account for the effect of solvation, the energies of cation and anionic forms of molecules were calculated using the dielectric continuum model provided by COSMO.[33,34] The dielectric constant used for the calculation was ε_s = 78.4 corresponding

to an aqueous solution. These calculations show that solvation by water lowers the energy of the charge transfer state to a range that permits an exothermic electron transfer reaction as required for any mechanism that involves quenching of anthracene fluorescence. The presence of boronic acid (**OTMA-PBA**) or boronate (**OTMA-PBE**) also lowers the energy of the amino oxidation reaction **TMA** à **TMA**$^{+}$ + **e**$^{-}$. Table 2.4 shows that the amine in **OTMA-PBA** is particularly easy to ionize resulting a special role for this species that may a play a role in the switching mechanism required for a boronic acid-based biosensor. A solvation calculation was also carried out using explicit water. A model with 14 H_2O molecules surrounding **TMA** and 20 H_2O molecules surrounding **anth** was geometry optimized. The energy of the process **TMA anth** à **TMA**$^{+}$ **anth**$^{-}$ is essentially the same as that obtained using the dielectric continuum approach known as COSMO (see Supporting Information). Calculations were carried out for different numbers of explicit water molecules. The trend was towards lower energy for the charge-separated state as the number of waters increased. A detailed quantitation of the effect of explicit solvent water would require calculation for a significantly larger number of waters. This was deemed prohibitive and was not pursued.

The inclusion of solvation places the energy of the charge-transfer quenching states below that of the excited singlet state of anthracene, in agreement with experiment with experimental observation of the quenching of anthracene fluorescence by TMA in polar solvents. Table 2.5 shows that for the series **OTMA-PBA**$^{+}$**-anth**$^{-}$, **OTMA**$^{-}$**PBE**$^{+}$**-anth**$^{-}$, and **OTMA-PBP**$^{+}$**-anth**$^{-}$ the energy gaps, ε, are 93, 87, and 93 kJ/mol, respectively.

2.3.6. Calculation of the Reorganization Energy

The reorganization energy is the energy required for distortion along the product potential energy surface until the equilibrium geometry of the reactant is reached. The reorganization energy can be divided conceptually into inner sphere (molecular) and outer sphere (solvent) contributions. The reorganization energy can be calculated by comparing the energy of a geometry optimized neutral molecule calculated as a cation or anion with the energy of the geometry optimized cation or anion. The energy differences that account for the inner sphere reorganization energy arise from the elongation of bonds that accompanies the removal of an electron from the HOMO (cation) or addition of an electron to the LUMO (anion). Calculations of the inner sphere reorganization energy (λ_{inner}) are presented in the second column of Table 2.6.

Table 2.6. Reorganization energy for donors and acceptors involved in electron transfer quenching of the anthracene excited state fluorescence.

Electron Transfer Process	λ_{inner}	$\Delta\Delta G_{solv}$	λ_{total}
TMA + anth à TMA^+ + $anth^-$	144	465	497
OTMAPBA + anth à $OTMAPBA^+$ + $anth^-$	36	335	259
OTMAPBE + anth à $OTMAPBE^+$ + $anth^-$	7	330	225
OTMAPBP + anth à $OTMAPBP^+$ + $anth^-$	8	324	220

The outer sphere reorganization energy arises from the adjustment of solvent dipoles to accommodate the change in charge distribution on the molecule that occurs in an electron-transfer process. It is given by:

$$\lambda_{outer} = \frac{e^2}{4\pi\varepsilon_0}\left(\frac{1}{\varepsilon_\infty} - \frac{1}{\varepsilon_s}\right)\left(\frac{1}{R_D} + \frac{1}{R_A} - \frac{1}{R_{DA}}\right) \quad (7)$$

Where e is the charge of an electrsson, ε_0 is the permittivity of vacuum, ε_∞ is the high frequency dielectric constant (equal to the square of the index of refraction), ε_s is the state dielectric constant (78.4 for H_2O at room temperature). The symbols R_D, R_A and R_{DA} are the radii of the donor, acceptor and the donor-acceptor distance, respectively. The terms in $1/R_D$ and $1/R_A$ are closely related to the Born solvation energy, ΔG_{solv} of the respective ions D^+ and A^-. We estimate this difference solvation energy by calculation of the difference solvation energy of the neutral D and A and the Born solvation energy of the ions D^+ and A^-. We will call this difference free energy $\Delta\Delta G_{solv}$ in Table 2.6. The term in $-1/R_{DA}$ is the Coulombic attraction of the ions D^+ and A^-. The comparison of a vacuum calculation and COSMO calculation can be used to estimate the difference Born solvation energy $\Delta\Delta G_{solv}$. This is done by subtracting the binding energy from a vacuum calculation from the binding energy obtained from a COSMO calculation. For **Anth** and **TMA** these difference Born solvation energies are 179 kJ./mol and 286 kJ/mol, respectively. Since the factor $e^2/4\pi\varepsilon_0$ corresponds to 1422 kJ/mol we can estimate the difference Born solvation energy using Eqn. 7. If we use 1.33 for the index of refraction of water we have $\varepsilon_\infty = 1.77$ and $\varepsilon_s = 78.4$. Thus, the values of $\Delta\Delta G_{solv}$ for **anth** and **TMA** calculated by the DFT theory correspond to effective ionic radii of ~4.4 Å and ~2.6 Å, respectively, using Eqn. 7. The entries in column 3 of Table 2.6 are the sum of $\Delta\Delta G_{solv}$ for the cation and anion in reaction given in column 1 of Table 2.6. Assuming R_{DA} ~ 7 Å the calculated Coulomb energy using eq 7 is -112 kJ/mol. It is not readily apparent how

the Coulomb term would be calculated using DFT, so the estimate obtained from eq 7 was used for all of the reactions given in Table 2.6. The total reorganization given in column 4 of Table 2.6 is the sum of the inner sphere (column 1), the difference Born solvation energy (column 2) and a negative Coulomb term (-112 kJ/mol) assumed to be the same for all of the systems. The comparison presented in Table 2.6 shows that the reorganization energy for charge transfer from an amine to anthracene decreases in the order **TMA > OTMA-PBA** > **OTMA-PBE > OTMA-PBP**.

2.3.7. Calculation of the Activation Energy for Electron Transfer

The use of DFT to calculate the energies of solvated charge-seperated states requires a number of approximations discussed in the foregoing sections. Nonetheless, we can use the energy gap, ε and reorganization energy, λ, to calculate the activation energy using eq 5. The important point here is that we are comparing the activation energies of boronic acid and boronate ester to see whether there is a profound difference that can explain the fluorescence quenching observed in biosensors of the type shown in Figure 2.1. Table 2.7 reveals that the difference in activation energy favors electron-transfer quenching in the ester (**OTMA-PBE** or **OTMA-PBP**) over that in the acid (**OTMA-PBA**).

Table 2.7. Activation energies for the Franck-Condon factor of the electron transfer rate constant calculated according to eq 5.

Electron Transfer Process	COSMO (kJ/mol)
TMA + Anth à TMA$^+$ + Anth$^\bullet$	77.2
OTMAPBA + Anth à OTMAPBA$^+$ + Anth$^\bullet$	26.6
OTMAPBE + Anth à OTMAPBE$^+$ + Anth$^\bullet$	21.2
OTMAPBP + Anth à OTMAPBP$^+$ + Anth$^\bullet$	18.3

This is opposite to the normally observed trend in aqueous buffers. The calculations make the prediction that a *cis*-diol ester will be more quenched than the corresponding acid if the measurement is carried out in an aprotic polar solvent. This prediction has been confirmed by measurements in acetonitrile and dimethyl sulfoxide as discussed below.

2.4. Discussion

The classic experiments on biosensor molecule **1** indicate that the electron-transfer quenching of anthracene fluorescence is reduced by boronate ester formation in molecules of the type **OTMA-PBE-anth** in aqueous buffer. The origin of the change in fluorescence quenching has been attributed to an increased boron-nitrogen bonding interaction in the boronate ester form. However, the calculations show that the assumption that the nitrogen lone pair electrons are simply "tied up" in a strong boron-nitrogen bond is a simplified view. In fact, the boron-nitrogen bond is quite weak, being roughly equivalent to that of a typical hydrogen bond in both the trigonal boronic acid and tetrahedral boronate ester forms. Moreover, the *difference* in bond energy for the adducts **OTMA:PBA0** and **OTMA:PBE0** is only ~13 kJ/mol and, in fact, the energy difference for **OTMA:PBA90** and **OTMA:PBE90** is only 0.4 kJ/mol (see section 2.4.1). The results presented above suggest that the mechanism of action for molecules of type 4 may involve specific interactions with solvent water. The present study does not specific interactions with solvent water. The present study does not specifically address the new

mechanism but does address problems with the original mechanism based on B-N bond formation.

The calculations agree with experimental trends in terms of both structure and energies. The geometry shows a bond length for the intramolecular B-N bond in the phenyl boronic ester (**OTMA-PBE90**) of 1.85 Å, while the bond length in **OTMA-PBA90** is 1.98Å. These results are in agreement with observed structures that show a 90^{o} geometry for the boronic acid moiety.[15,20] The calculated bond length is 1.85 Å, which is approximately 9% larger than the experimentally observed bond lengths. [15,20]

DFT calculations obtain the correct trends for bond strengths of interest where experimental data are available. For example the bond strengths for *d*(C-C) in ethane and *d*(B-N) in borane and BH_3-$N(CH_3)_3$ differ from experiment by 28%, 9% and 23%, respectively. Although these are the largest relative errors in our study, it is the *difference* in bond strength that is of interest here. For example, how is the B-N bond length and bond strength affected by boronate ester formation? The conclusions concerning the conformational effects are based as much on structure (changes in bond length) as on energetics. The bond lengths and frequencies calculated by GGA differ from experiment by <10% in all cases and are often within 5% of the experimental values.[38-41] The ordering of the ionization potentials for anthracene and TMA is correct, and both deviate from experiment by ~11 %. The transition energy for anthracene of 337 kJ/mol is within 5% of the experimental value.

Solvation in a dielectric continuum model lowers the energy of the dipolar charge separated state nearly to the correct range for quenching by nitrogen to generate a charge-separated state $BN^{+}A^{-}$. For example, trimethylamine (**TMA**) is known to quench

anthracene fluorescence and both the explicit solvent model and the COSMO calculation indicate that the energy of **TMA^{+}-anth$^{\bullet}$** is ca. 100 kJ/mol (~ 1 eV) lower than the singlet excited state of anthracene (337 kJ/mol or ~3.5 eV), see section 2.4.4. Thus, the computation approach suggests a driving force of approximately 1 eV for electron transfer. Such a value is consistent with the wavelength of exciplex emission at around 500 nm (i.e. 20,000 cm^{-1} or 2.5 eV) from systems such as dimethylaniline and anthracene.[42]

The rate constant for electron transfer will affect the fluorescence quantum yield by providing a quenching mechanism. The quantum yield of anthracene is:

$$\Phi_F = \frac{k_F}{k_F + k_{NR} + k_{ET}}$$

where k_F and k_{NR} are the intrinsic fluorescence and nonradiative decay rate constants, respectively. For example, the fluorescence quantum yield[37] and lifetime[43] for anthracene in ethanol are 0.27 and 5.3 ns, respectively. If no quenching is present, then the observed fluorescence lifetime is $k_{obs} = k_F + k_{NR}$ where $k_F = \bullet_F k_{obs}$. Using the fact that $k_{OBS} = 1/\tau_{obs,}$ we have $k_{obs} = 1.9 \times 10^8\ s^{-1}$, $k_F = 5.1 \times 10^7\ s^{-1}$, and $k_{NR} = 1.4 \times 10^8\ s^{-1}$, in the absence of quenching. k_{ET} depends on distance in the electronic coupling factor V^2 and the energetics in the FC factor through the activation energy $E^* = (\lambda - \bullet)^2/4\lambda$. We consider each of these factors to attempt to understand how the fluorescent switch functions in boron-nitrogen biosensors.

Quenching of the anthracene excited state requires efficient charge transfer by the process k_{ET}. The fluorescent biosensor is triggered by formation of a boronate ester that reduces the yield of charge transfer quenching thereby increasing the fluorescence quantum yield. The FC factor for the electron-transfer reaction could be reduced because

of two possible effects. First, the energy level of the charge-separated state could be increased thereby reducing the energy gap • in the boronate ester form. Second, the reorganization energy • could be increased in the boronate ester form. Either of these would raise the barrier, E^* for the photoexcited electron transfer process, $k_{ET,}$ as indicated in eqs. 4 and 5. The role of • and • was obtained by the calculations in Tables 2.5 and 2.6, respectively. The results for the barrier presented in Table 3.8 show the opposite trend from that required for an increase in fluorescence upon formation of a boronate ester. The reduction in the barrier presented in Table 2.7 for formation **OTMA-PBE$^+$-anth$^-$** and **OTMA-PBP$^+$-anth$^-$** compared to **OTMA-PBA$^+$-anth$^-$** would suggest that fluorescence should actually decrease for formation of a the ester contrary to literature precedents in water and alcohol solutions. To test this hypothesis we have conducted experiments in anhydrous acetonitrile and DMSO that verify such a behavior. In acetonitrile or DMSO solution, fluorescence is quenched upon boronate ester formation. However, if one drop of methanol is added to the acetonitrile solution the normally observed trend is observed, in which fluorescence increases for boronate ester formation.

2.5. Conclusion

An electron transfer mechanism for the trigger that gives rise to a fluorescent biosensor triggered by boronic ester formation has been explored by DFT calculations of a range of structures in neutral, cationic and anionic forms. The driving force for electron transfer is not significantly reduced in a phenyl boronate ester (**OTMA-PBE** or **OTMA-PBP**) relative to boronic acid (**OTMA-PBA**). The electron transfer mechanism for fluorescence quenching does not adequately explain the data in aqueous solutions

because the mechanism for the switch in fluorescence quenching likely involves protonation rather than a B-N bond strength change. The B-N bond in all species considered is so weak that it is altered significantly by displacement along either of two torsions: the O-C-C-O dihedral angle, the Cp-Cp-B-O dihedral angle, and the **anth-TMA** distance. The O-C-C-O dihedral angle has an optimum value of 30 - 40^{o}. Distortion of this dihedral towards 60^{o} increases the energy of the **OTMA-PBE** molecule by an amount greater than the B-N bond energy. A stable intramolecular B-N bond in **OTMA-PBE** is formed only for a Cp-Cp-B-O dihedral angle of nearly 90^{o}. Thus, there are significant conformational constraints on the formation of the B-N bond.

This study has illustrated general principles for the calculation of parameters relevant to electron transfer reactions. Solvation still presents the greatest problem for the accurate calculation of charge-separated states. The comparison of charge-separated states using a dielectric continuum approach (COSMO) is favorable in that the energies of those states are much closer to the experimental values. The approach was further verified by comparison with explicit solvent for the anthracene and trimethylamine. Solvation and molecular geometry changes in charge-separated states were used to calculate reorganization energies and activation energies. These quantities in turn determined the relative magnitude of the electron transfer rate constant. The calculations make a significant prediction that can be tested experimentally, namely, that the fluorescence quenching trend for boronate ester formation formation will be reversed in aprotic polar solvents (e.g. acetonitrile and dimethyl sulfoxide) compared to the trend in polar protic solvents (e.g. methanol or water). In other words, the calculation indicates that boronate ester formation will have a lower fluorescence quantum yield than that of

the corresponding acid in aprotic polar solvents. This trend has been experimentally verified. The calculations indicate that the next task will be the inclusion of explicit solvent molecules in the model of the full sensor (i.e. **OTMA-PBA and OTMA-PBE**), since the role of solvent interaction with the phenylboronic acid biosensor cannot be neglected.

References

(1) Lorand, J. P.; Edwards, J. O. *J. Org. Chem.* **1959**, *24*, 769-774.

(2) Springsteen, G.; Wang, B. *Tetrahedron* **2002**, *58*, 5291-5300.

(3) Sugihara, J. M.; Bowman, C. M. *J. Am. Chem. Soc.* **1958**, *80*, 2443.

(4) Arimori, S.; Bosch, L. I.; Ward, C. J.; James, T. D. *Tetrahedron Lett.* **2001**, *42*, 4553-4555.

(5) Adhikiri, D. P.; Heagy, M. D. *Tetrahedron Lett.* **1999**, *40*, 7893-7896.

(6) Cao, H.; Diaz, D. I.; DiCesare, N.; Lakowicz, J. R.; Heagy, M. D. *Org. Lett.* **2002**, *4*, 1503-1505.

(7) Eggert, H.; Frederiksen, J.; Morin, C.; Norrid, J. C. *J. Org. Chem.* **1999**, *64*, 3846-3852.

(8) James, T. D.; Samankumara, K. R. A.; Iguchi, R.; Shinkai, S. *J. Am. Chem. Soc.* **1995**, *117*, 8982-8987.

(9) James, T. D.; Linnane, P.; Shinkai, S. *Chem. Commun* **1996**, 281-288.

(10) James, T. D.; Sandanayake, K. R. A. S.; Shinkai, S. *Chem. Commun* **1994**, 477 -478.

(11) Norrild, J. C.; Eggert, H. *J. Am. Chem. Soc.* **1995**, *117*, 1479-1484.

(12) Lavigne, J. J.; Anslyn, E. V. *Angew. Chem. Int. Ed. Engl.* **1999**, *38*, 3666-3669.

(13) Wang, B. *Curr. Org. Chem.* **2002**, *6*, 1285-1317.

(14) Wang, W.; Gao, S.; Wang, B. *Org. Lett.* **1999**, *1*, 1209-1212.

(15) Wiskur, S.; Lavigne, J. J.; Ait-Haddou, H.; Lynch, V.; Chiu, Y. H.; Canary, J. W.; Anslyn, E. V. *Org. Lett.* **2001**, *3*, 1311-1314.

(16) Yang, W.; Gao, S.; Gao, X.; Karnati, V. R.; Ni, W.; Wang, B.; Hooks, W. B.; Carson, J.; Weston, B. W. *Bioorg. Med. Chem. Lett* **2002**, *12*, 2175-2177.

(17) Yang, W.; He, H.; Drueckhammer, D. G. *Angew. Chem. Int. Ed. Engl.* **2001**, *40*, 1714-1718.

(18) James, T. D.; Sandanayake, K. R. A. S.; Shinkai, S. *Nature (London)* **1995**, *374*, 345-347.

(19) Gao, S.; Wang, W.; Wang, B. *Bioorg. Chem.* **2001**, *29*, 308-320.

(20) Toyota, S.; Oki, M. *Bull. Chem. Soc. Jpn* **1992**, *65*, 1832-1840.

(21) Cooper, C.; Spencer, N.; James, T. D. *Chem. Commun* **1998**, 1365-1366.

(22) Leboeuf, M.; Russo, N.; Salahub, D. R.; Toscano, M. *J. Chem. Phys.* **1995**, *103*, 7408-7413.

(23) Glendening, E. D.; Streitweiser, A. *J. Chem. Phys.* **1994**, *100*, 2900-2909.

(24) Anane, H.; Jarid, A.; Boutalib, A.; Nebot-Gil, I.; Tomas, F. *Chem. Phys. Lett.* **2000**, *324*, 156-160.

(25) Anane, H.; Boutalib, A.; Tomas, F. *J. Phys. Chem. A* **1997**, *101*, 7879-7884.

(26) Anane, H.; Jarid, A.; Boutalib, A.; Nebot-Gil, I.; Tomas, F. *Chem. Phys. Lett.* **1998**, *287*, 575-578.

(27) Anane, H.; Jarid, A.; Boutalib, A.; Nebot-Gil, I.; Tomas, F. *Theochem - J. Mol. Struct.* **1998**, *455*, 51-57.

(28) Rablen, P. R.; Hartwig, J. F. *J. Am. Chem. Soc.* **1996**, *118*, 4648-4653.

(29) Umeyama, H.; Morokuma, K. *J. Am. Chem. Soc.* **1976**, *98*, 7208-7220.

(30) Jonas, V.; Frenking, G.; Reetz, M. T. *J. Am. Chem. Soc.* **1995**, *117*, 8741-8753.

(31) Brint, P.; Sangchakr, B.; Fowler, P. W. *J. Chem. Soc. - Faraday Trans. II* **1989**, *85*, 29-37.

(32) Delley, B. *J. Phys. Chem.* **2000**, *113*, 7756-7764.

(33) Klamt, A.; Schuurmann, G. *J. Chem. Soc. - Perkin Trans. 2* **1993**, 799-805.

(34) Andzelm, J.; Kolmel, C.; Klamt, A. *J. Chem. Phys.* **1995**, *103*, 9312-9320.

(35) Slater, J. C. *Quantum Theory of Molecules and Solids, Volume 4, The self-consistent field for molecules and solids*; McGraw-Hill: New York, 1974.

(36) Cockett, M. C. R.; Kimura, K. *J. Chem Phys.* **1994**, *100*, 3429-3441.

(37) Dawson, W. R.; Windsor, M. W. *J. Phys. Chem.* **1968**, *72*, 3251-3260.

(38) Franzen, S. *Proc. Natl. Acad. Sci. U.S.A.* **2002**, *99*, 16754-16759.

(39) Franzen, S. *J. Am. Chem. Soc.* **2001**, *123*, 12578-12589.

(40) Franzen, S. *J. Am. Chem. Soc.* **2002**, *124*, 13271-13281.

(41) Franzen, S.; Fritsch, K.; Brewer, S. H. *J. Phys. Chem. B* **2002**, *106*, 11641-11646.

(42) Vaidyanathan, S.; Ramakrishnan, V. *Indian J. of Chem.* **1975**, *13*, 257-260.

(43) Greiner, G. *J. Photochem. Photobiol. A* **2000**, *137*, 1-7.

Chapter 3. A Study of the Hydrolysis Mechanism for a Photoinduced Electron Transfer (PET) Sensor System for Diol and Saccharides

Abstract

A widely used photo-induced electron transfer (PET) fluorescent sensor system (**1**) for saccharides was originally proposed to go through the B-N bond formation mechanism. However, our own fluorescence studies suggest an alternative mechanism for the fluorescence change upon the formation of boronic acid (**1**) complex with diols. In this new mechanism, complex formation induces solvolysis if the reactions are carried out in a protic solvent such as methanol or water, which results in the protonation of the amine nitrogen. Consequently, electron transfer is significantly reduced due to the masking of the amine lone pair electrons, resulting in reduced PET quenching and increased fluorescence intensity. A series of experiments examining the effect of solvent, diol structures, and trivalent binding as well as the correlation between fluorescence intensity change and the pKa of **1** all support the solvolysis mechanism. Computational studies also support hydrolysis being the most likely possible mechanism of this PET system (**1**).

3.1. Introduction

Among the developed fluorescent boronic acid sensors for saccharides, the Shinkai photoelectron transfer (PET) system (Figure 3.1) using B-N bond strength to modulate the fluorescence quenching process and therefore the fluorescent intensity changes,[1-3] occupied the most prominent position. We also applied this system in our fluorescence sensors to monitor the binding event with cell surface carbohydrates (Chapter 1). These sensors showed increased fluorescence intensity when the anthracene boronic acid binds with saccharides.

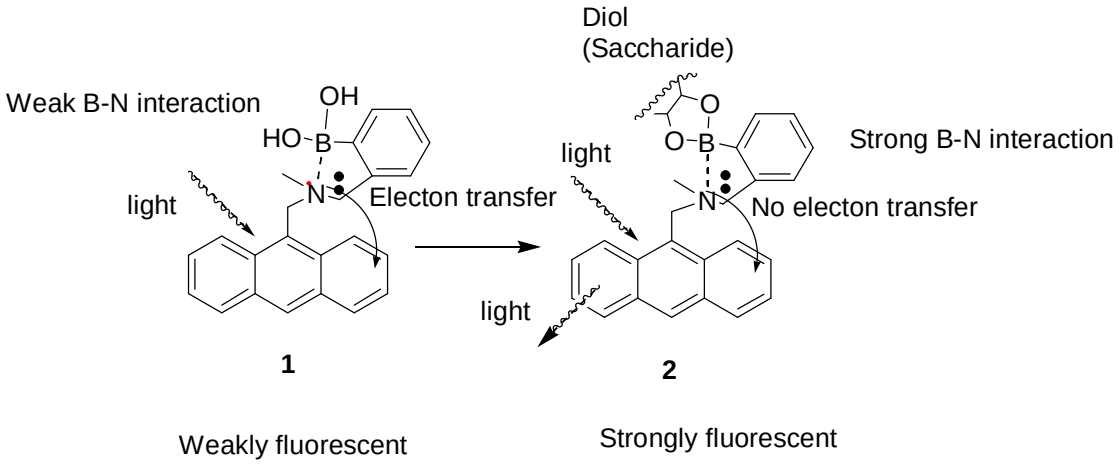

Figure 3.1. Mechanism[4] proposed by the Shinkai group of fluorescence intensity change of compound **1** upon binding with saccharides.

According to this PET mechanism, the boron-nitrogen interaction is the central element triggering the fluorescence change. For compound **1**, the lone pair electrons of the tertiary amine quench the fluorescence of anthracene through photoelectron transfer. Therefore, compound **1** is only weakly fluorescent. It was proposed that due to the proximity of the amine to the boron atom, a B-N bond can form leading to a five-membered ring (**2**). Because diol binding, most of the time, increases the Lewis acidity of the boron atom, carbohydrate binding results in the strengthening of the B-N bond in

2, which makes the lone pair electrons less "available" for fluorescence quenching through PET. This results in decreased fluorescence quenching and increased fluorescence intensities in **2**.

Although this system (**1**) has worked very well in functioning as a fluorescent reporter compound, there are tell tale signs that the mechanism through which such a system works may not be as what was originally proposed. For example, this B-N bond formation mechanism has been explored by calculation using density functional theory (DFT) theory (see details in Chapter 2). In Chapter 2, the geometric constraints of the system have been studied in both intra- and intermolecular model systems of the boron-nitrogen (B-N) bonding interaction. The results suggest a new mechanism other than B-N bond strength change for fluorescent switching in biosensors that involve interaction of boron and nitrogen affected by boronate ester formation. Because of the enormous role this design has played in the field of boronic acid-based sensor design, there is the need to understand better the mechanism through which the fluorescence intensity change occurs.

3.2. Synthesis

Fluorescent boronic acid **1** was synthesized following literature procedure[1] from commercially available compound **3**.

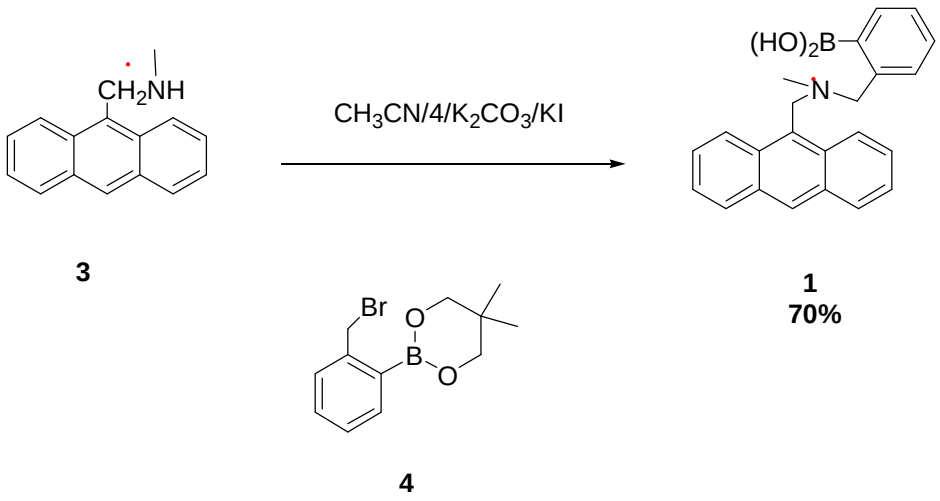

Scheme 3.1. Preparation of compound **1**.

3.3. Results and Discussion

3.3.1. The Proposal of a New Hydrolysis Mechanism

To analyze the possible mechanism through which fluorescence intensity changes can occur, one can first write the different possible forms that the boronic acid and the boronic acid-diol complex can exist (Scheme 3.2). For boronic acid itself, it can exist in the protonated form when the pH is below its first pKa (**1a**). With increasing pKa, there are ample literature results proving that it is the deportonation of the amine and formation of a B-N bond (**1b**) that constitutes the first pKa. This results in a very significant fluorescence intensity decrease despite the formation of the B-N bond. Such results indicate that B-N bond formation itself is not sufficient to "tie up" the lone pair electrons to prevent PET. With the further increase of the pH, the hydroxide comes in to displace the amino group to give **1c**, which no longer has a B-N bond.

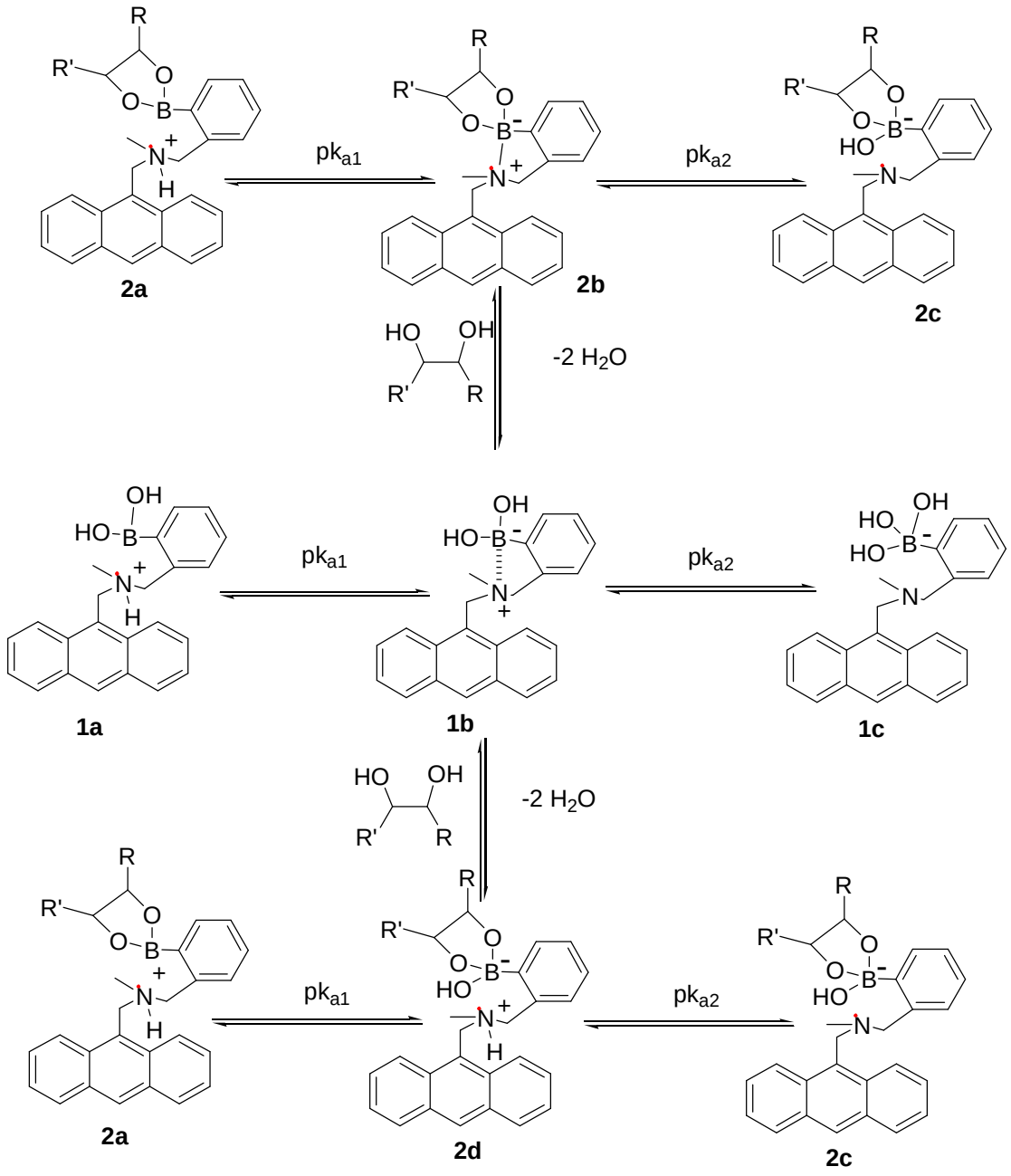

Scheme 3.2. Possible mechanisms for the fluorescence intensity changes.

With the addition of the diol, there are two possible scenarios, none of which has been experimentally proven or excluded yet. In the first scenario, the first pKa of the ester (**2a**) is still the deprotonation of the amino group and the formation of the B-N bond

(**2b,** or see Figure 3.1, from **1** to **2**) as originally proposed by Shinkai and co-workers. The second pKa is the replacement of the B-N bond by a B-O bond leading to the formation of **2c**. In the second scenario, the first pKa is the addition of the hydroxide to the boron atom leading to the formation of **2d.** The second pKa is still the same leading to the formation of **2c**. The key difference between these two mechanisms is that under neutral conditions, addition of a diol will lead to the formation of **2b** with increased B-N bond strength in one mechanism (referred to as the B-N bond mechanism) and **2d** in the other. The latter is referred to as hydrolysis mechanism since going from **1b** to **2d** is similar to a hydrolysis of the B-N bond with the exception that boron is complexed to a diol in **2d**.

Table 3.1. Different aspects of comparing the mechanism of fluorescence change of B-N bond mechanism Shinkai proposed and hydrolysis mechanism we proposed.

Phenomenon	Expected results for the B-N bond mechanism	Expected results for the hydrolysis mechanism	Results observed
Fluorescence intensity change associated with the first pKa	Should be observable for both the acid (**1**) and the ester (**2**).	Should be observable only for the acid (**1**), not the ester (**2**).	Observable only for the acid (**1**)
Fluorescence intensity change associated with the second pKa	Should be observable for both the acid (**1**) and the ester (**2**).	Should be observable only for the ester (**2**), not the acid (**1**).	Observable only for the ester (**2**)
Results from aprotic and protic solvents	Should be similar or the same	Should be completely different	Completely different
Magnitude of fluorescence recovery with different sugars	Should be different	Should be the same	The same
B-N bond strength difference between the acid (**1**) and the ester (**2**)	Should be very large	Small	Small*
The effect of carbohydrates engaged in trivalent binding	Should not induce fluorescence intensity changes	Should induce fluorescence intensity changes	Did cause fluorescence intensity changes

*Not experimental results, but computational results.

In order to design experiments that can help to elucidate the mechanism, one has to analyze the possible experimental outcome under different experimental conditions. In Table 3.1, we have listed situations where we expected that different results would be expected for these two possible mechanisms.

First, for the B-N bond formation mechanism (going from **2a** to **2b** to **2c**) one would expect to see a significant fluorescence intensity decrease associated with both the first and second pKa's since the deprotonation of the amino group and breaking the B-N bond are both expected to affect the availability of the lone pair electrons. This is particularly true considering there is a significant fluorescence intensity change going from **1a** to **1b.** However, in the hydrolysis mechanism (going from **2a** to **2d** to **2c**) one would only expect to see a significant fluorescence intensity change associated with the second pKa since the first pKa does not affect the protonation state of the amino group, and therefore does not affect the "availability" of the nitrogen lone pair electrons in the PET process.

Second, the B-N bond formation is a Lewis acid-Lewis base reaction. One would expect competition from other Lewis base such as water and methanol for the boron open shell. Therefore, one would expect that the B-N bond being stronger in a solvent that does not have readily available lone pair electrons for interaction with the boron or at least has diminished Lewis basicity. With this assumption, one would expect that the fluorescence intensity increase associated with diol addition being greater in aprotic solvents such as chloroform, acetonitrile, and DMSO if the B-N formation mechanism is at work.

Third, since binding with different diols may result in the lowering of the boron pKa to different degrees, one would expect that the B-N bond strength being different in the boronic acid complexes with different sugars. This difference in B-N strength should be reflected in the fluorescence intensity changes observed with addition of sugars if the B-N bond formation mechanism is at work. However, if the hydrolysis mechanism were at work, one would not expect to see difference in the magnitude of the maximal fluorescence recovery.

Fourth, there are some sugars that are known to bind to boronic acid in a trivalent fashion. If the B-N bond formation mechanism is the reason for the observed fluorescence intensity change, one would not expect these trivalent sugars to cause a fluorescence intensity increase because the trivalency prevents the B-N bond formation in the sugar-boronic acid complex (**2**).

Fifth, if the strengthening of the B-N bond is the reason for the observed fluorescence intensity changes with this system, one would expect that the B-N bond in the boronic acid-diol complex (**2b**) is much stronger than in the free boronic acid (**1b**).

With these expected difference in mind, we examined these factors one by one, some through experiments and others through the examination of literature results.

3.3.2. Examination of the Hydrolysis Mechanism

3.3.2.1. pH Profiles of the Acid 1 and Various Complexes.

We have recently conducted theoretical calculations of the B-N bond strength under various conditions and found that the B-N bond strength is in the general range of about 10 kJ/mol. More importantly, the difference in B-N bond strength between the free

boronic acid and an ester is most likely less than 3 kJ (details see Chapter 2). Give some room for deviation in calculation from that in an experimental situation, we can still say with confidence that the difference in B-N bond strength upon ester formation is small compared with the B-N bond itself. This has direct implications in the pH titration profile of **1** and **2**. We can first examine the pH profile of **1**. It has been reported that there is a very significant decrease in fluorescence intensity associated with the first pKa of the boronic acid (**1**).[2] This makes sense since it has been experimentally proven using a similar system that the first pKa is the deprotonation of the amino group accompanied by B-N bond formation.[5] The deprotonation unmasks the nitrogen lone pair electrons and make them available for PET. It should be noted that the "affinity" a proton for an amine group has been estimated to be in the range of 200 kcal/mol.[6] It is understood that the specific number may be significantly different depending on salvation and the pKa of a specific amine, but even if this "protonation affinity" is half of that number, it is still very strong, comparable to a sigma covalent bond, and higher than the energy required to remove an n electron in an amine nitrogen. On the other hand, the B-N strength is only about 10 kcal/mol (see chapter 2), which would not be able to "tie up" the nitrogen lone pair electrons nearly as effectively as protonation does in order to prevent PET. Such reasoning directly contradicts the B-N bond mechanism.

Along this line, it becomes easy to understand why there was no fluorescence decrease associated with the second pKa in the case of the free acid (**1**) because breaking of a 10 kJ/mol) B-N bond does not make much of a difference in the PET process. With the addition of fructose, the pH profile of the complex became very different.[3] The first pKa of the complex (**2**) was not associated with a decrease in fluorescence intensity. This

observations would not have been expected if the B-N bond mechanism is at work since one would able to see a fluorescence intensity decrease when it the amine nitrogen goes from the protonated form to the B-N bond. However, if the hydrolysis mechanism is at work, the observations can be very easily explained. In the boronic acid-diol complex, going from **2a** to **2d** does not involve the deprotonation of the amino group. Therefore, one would not expect to see any fluorescence intensity change associated with the first pKa in the complex (**2**) in the hydrolysis mechanism. With the second pKa, it is deprotonation of the amino group that is the reason for the decrease in fluorescence intensity. Such a mechanism is also in agreement with the different results observed between the acid (**1**) and complex (**2**). This means that the B-N bond, whether it is 10 or 13 kcal, is not sufficient to "tie up" the lone pair electrons to prevent the PET, which is why the fluorescence intensity changes were observed for the first pKa of the acid (**1**), but not the ester (**2**). These observations also agree with DFT calculations that indicate that fluorescence quenching will occur in the neutral B-N forms. The hydrolysis hypothesis also explains why fluorescence intensity changes were observed for the second pKa of the ester (**2**) and the first pKa of the acid (**1**) because again it is the deprotonation step that gives rise to fluorescence intensity changes.

3.3.2.2. The Solvent Effect

Since B-N bond formation is a Lewis acid-Lewis base reaction, one would expect competition from other Lewis bases such as water and methanol for the boron open shell. Therefore, one would expect the B-N bond to be stronger in a solvent that does not have readily available lone pair electrons for interaction with the boron or at least has diminished Lewis basicity. With this assumption in mind, we tested the fluorescence of **1**

with the addition of *cis*-1, 2-cyclopentanediol. This cyclopentanediol was used in the initial studies because of its high solubility in aprotic organic solvents such as chloroform, acetonitrile, and DMSO. The first set of experiments was conducted in anhydrous DMSO. When *cis*-1, 2-cyclopentanediol was added to the DMSO solution of **1** (2×10^{-5} M), a significant decrease of the fluorescence intensity was observed (Figure 3.2). Such results are in contradiction of the B-N bond mechanism.

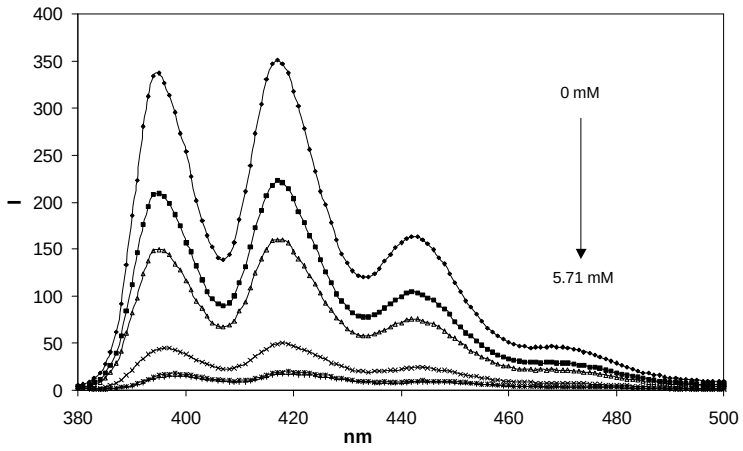

Figure 3.2. Fluorescence profile of compound **1** (2×10^{-5}M) in anhydrous DMSO decreased with the addition of *cis*-1, 2-cyclopentane diol (0, 0.09, 0.15, 0.19, 0.57 and 5.71 mM), λ_{ex} = 370 nm. The fluorescence intensity stops decrease when the concentration of diol reaches 0.57mM.

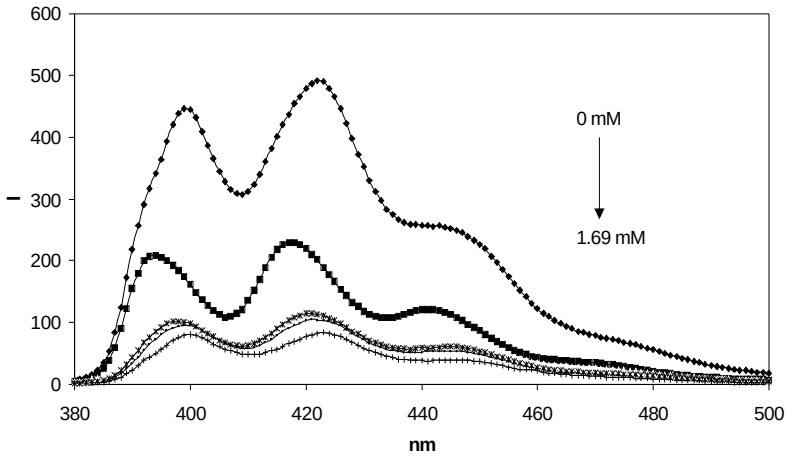

Figure 3.3. Fluorescence profile of compound **1** (4×10^{-6}M) in chloroform decreased with the addition of *cis*-1, 2-cyclopentane diol (0, 0.02, 0.05, 0.10, 0.33, 0.68 and 1.69 mM), λ_{ex} = 370 nm.

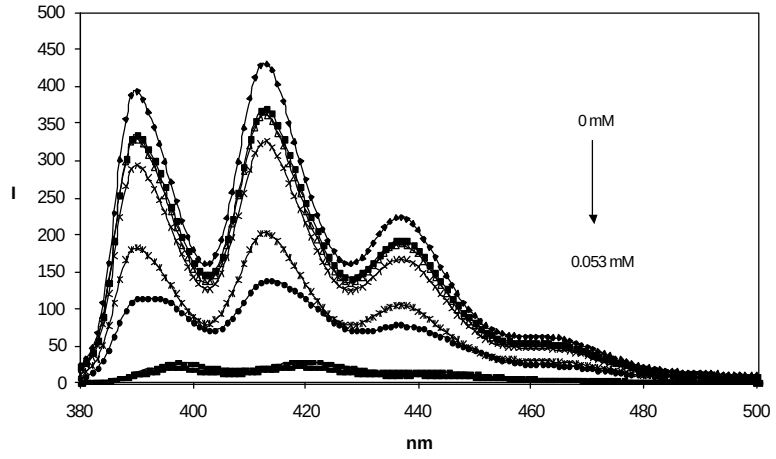

Figure 3.4. Fluorescence profile of compound **1** (2×10^{-5} M) in anhydrous acetonitrile decreased with the addition of *cis*-1, 2-cyclopentane diol (0, 0.0037, 0.0038, 0.060, 0.011, 0.016, 0.28 and 0.053 mM), λ_{ex} = 370 nm.

Aimed at seeing whether this is a general phenomenon, the same experiments were done in chloroform (Figure 3.3) and anhydrous acetonitrile (Figure 3.4) and the same results were obtained. The associate constants, Ka's for *cis*-1, 2-cyclopentanediol

in DMSO, chloroform, and acetonitrile were determined as 2621, 140000, and 3560 M^{-1} respectively.

3.3.2.3. The Effect of Different Sugars on the Fluorescence Intensity Changes of 1

It has been known for a long time that ester formation (**2**) lowers the pKa of the boron species to different degrees depending on the sugar/diol used. We have recently determined the apparent pKa's of the phenylboronic acid-diol complexes with various sugars/diols and found that the apparent pKa drop to be in the range of 2-4 pKa units.[7] For example, the apparent pKa of phenylboronic acid is about 8.8. The pKa's (or more precisely the apparent pKa's under the experimental conditions) of its esters fructose and glucose are 4.5 and 6.8 respectively. If the B-N bond mechanism is at work, one would expect that the fluorescence intensity of the boronic acid-diol complex to be dependent on the pKa of the boron. One would also expect to see as much change in fluorescence intensity when adding glucose to the free boronic acid as when replacing the glucose with fructose because their pKa separations (ΔpKa) are about the same. In other words, the fluorescence intensity of the glucose complex should be much lower than that of the fructose complex because of their pKa difference. The same is true with the complex with other sugars. Aimed at testing the correlation between the B-N bond strength and the fluorescence intensity of various sugar complexes, James and co-workers[8] have examined the fluorescence recovery by addition different sugars to **1** until the fluorescence intensity levels off. It was a surprise to see that most of the sugars tested, except those that do not bind well, gave the same fluorescence recovery. Such results cannot be explained by the B-N bond mechanism, but are consistent with the hydrolysis

mechanism since the amine is in the same (protonated) state (**2d**) no matter which sugar/diol is added.

3.3.2.4. The B-N Bond Strength

As has been elucidated to in the pH profile studies, in order for the B-N to play a role in regulating the PET process two things have to happen.

First, the B-N bond needs to be so strong that it can "tie up" the lone pair electrons. This would mean that the B-N bond strength in the ester (**2**) is on the same scale as the energy required to transfer one electron of nitrogen lone pair electrons. The effect of protonation on the PET process serves as a good reference point. Using mass spectrometry, it has been determined that the proton affinity of an aniline amine is on the order of 215 kcal/mol.[6] However the B-N bond strength has been estimated to be at about 15 kJ/mol using density Functional Theory, which is far smaller than what is required to "tie up" the nitrogen lone pair electrons to prevent PET (See DFT calculation Section) and than the effect of protonation. Second, the B-N bond strength difference upon diol binding should be large compared to the B-N strength of the free acid (**1**) in order to act as an on-off switch. Again, our theoretical calculation indicates that the B-N bond in an ester (**2**) is not much different from in the free acid (**1**) form and more importantly the change in bond strength upon ester formation is probably no more than 3 kJ/mol. The first point would directly contradict a B-N bond mechanism. Even if there is an increase in B-N bond strength upon ester formation, such a small change is not expected to function as an on-off switch as described in a B-N bond mechanism. On the other hand, the computational results and the "proton affinity" experiments are all consistent with the hydrolysis mechanism.

3.3.2.5. DFT Calculation Study

We have conducted DFT calculations of the B-N bond strength under various conditions and found that the B-N bond strength is in the general range ~15 kJ/mol for geometry observed experimentally (details see Chapter 2). The B-N interaction energy was calculated for an intermolecular model with a C-C-B-O torsion angle of 90^{o}. Due to its small magnitude the intramolecular binding strength is difficult to disentangle from conformational energies. More importantly, the difference in B-N bond strength between the free boronic acid and an ester is calculated to be less than 1 kJ/mol. The DFT calculations further show that the change in B-N interaction in an aprotic solvent environment does not provide an off-switch for PET. This conclusion was based on studies of the possible factors in the electron transfer rate constant, the electronic coupling (amine-anthracene distance), the reorganization energy and driving force in both the boronic acid and boronate ester forms. The calculated result in that study predicted that the fluorescence yield should increase for boronate ester formation in an aprotic solvent, if the B-N bond formation mechanism was true. Another issue that was examined computationally was whether electron transfer is allowed in the presence of a B-N bond. For this, we calculated the PET rate constants, which indicate that electron transfer is allowed from all neutral B-N. Analysis of the relative quenching by the hydrolysis mechanism is straightforward since the protonated form of the amine is incapable of electron donation to the anthracene-excited state. Thus, the relative amounts of the protonated form can be estimated directly from the acid-base equilibrium.

An alternative mechanism for switching consists of solvolysis. If H_2O hydrolysis were favored in the boronate ester form, then electron transfer would be significantly

reduced due to protonation of the amine group. The present study tests such a hypothesis by examining the energy of model compounds with and without H_2O.

The hydrolysis calculation was performed by putting a H_2O molecule onto the optimized structures of **PBA-OTMA** and **PBE-OTMA** next to the atoms of boron and nitrogen (Scheme 3.3), and then the models of were optimized using DFT method. The results were shown in Figure 3.5.

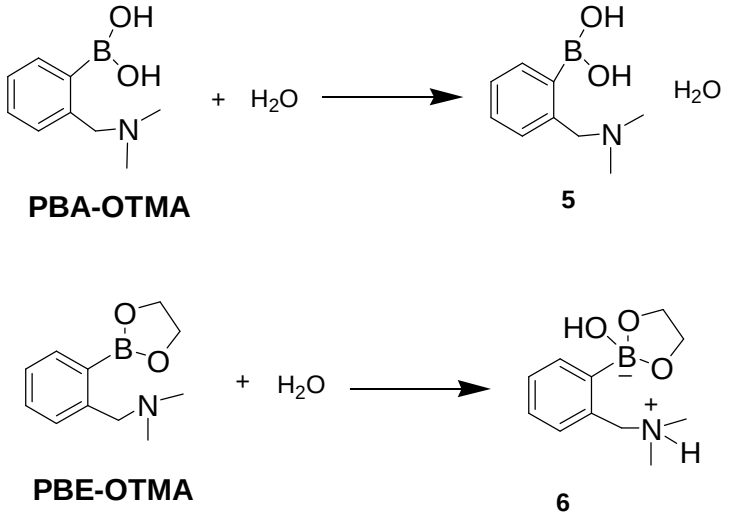

Scheme 3.3. Hydrolysis experiments calculation of **PBA-OTMA and PBE-OTME.**

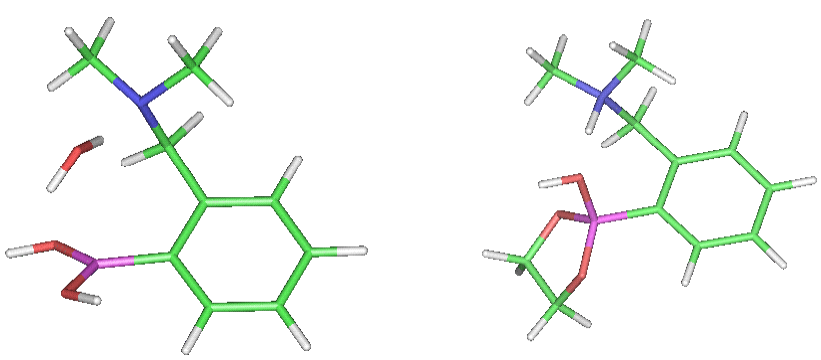

5 **6**

Figure 3.5. Optimized geometry product of hydrolysis of **PBA-OTMA** and **PBA-OTME.**

As we can see that in Figure 3.5, the geometry optimized structures for **PBA-OTMA** and one nearby water molecule led to a separate H_2O molecule (**5**), however, the geometry optimized structures for **PBE-OTMA** and nearby water molecule led to the split of H_2O and formed a new molecule **6**, with protonated amine and OH added to boron atom. In other words hydrolysis is predicted to occur in the ethylene glycol boronate ester, but not in the phenyl boronic acid.

We can further test the hydrolysis in the case of **PBE-OTMA-H-OH** (Figure 3.5, geometry **6**) by creating models where the boronic acid or boronate ester moiety is hydrated (i.e. one H_2O molecule is placed near the boron and nitrogen of the molecule) or hydrolyzed (i.e. OH- and H+ are explicitly added to the boron and nitrogen, respectively). The geometry optimization of these models leads to an energy trajectory for the system that can then be compared. Using this approach the energies for the hydrated (H_2O) and hydrolyzed (H-OH) systems were compared in Table 3.2. The energy for hydration and hydrolysis in the **PBE-OTMA** model was quite similar and, in fact, this analysis predicts that hydrolysis is lower in energy than hydration by 10 kJ/mol. Moreover, both processes

are uphill in energy according to this analysis. Hydration and hydrolysis were both significantly less favorable energetically for **PBA-OTMA**. When water is replaced by methanol, the trend is similar.

Table 3.2. Internal energy changes for the hydration and hydrolysis reactions of phenyl boronic acids (**PBE-OTMA**) and boronate esters (**PBE-OTME**).

Reaction	Energy (kJ/mol)
PBA-OTMA + H_2O à PBA-OTMA-H-OH	-133.9
PBA-OTMA + H_2O à PBA-OTMA-H_2O	-148.2
PBE-OTMA + H_2O à PBE-OTMA-H-OH	-13.0
PBE-OTMA + H_2O à PBE-OTMA-H_2O	-24.5
PBA-OTMA + CH_3OH à PBA-OTMAH-CH_3O	-121.2
PBA-OTMA + CH_3OH à PBA-OTMA-CH_3OH	-144.4
PBE-OTMA + CH_3OH à PBE-OTMA-H-CH_3O	-3.1
PBE-OTMA + CH_3OH à PBE-OTMA-CH_3OH	-27.4

The role of solvation was probed using the dielectric continuum model provided by COSMO. Table 3.3 gives the energies for the hydration and hydrolysis processes in the presence of solvation. The hydration and hydrolysis processes for **PBE-OTMA** are exothermic when solvation is included. Moreover, they are nearly identical in energy. On the other hand, the hydration and hydrolysis reactions are endothermic for **PBA-OTMA**.

Table 3.3. Internal energy changes for the hydration and hydrolysis reactions of phenyl boronic acids (**PBA-OTMA**) and boronate esters (**PBE-OTME**) including a continuum model for solvation (COSMO, $\varepsilon = 78.4$).

Reaction	Energy (kJ/mol)
PBA-OTMA + H_2O à PBA-OTMA-H-OH	-124.6
PBA-OTMA + H_2O à PBA-OTMA-H_2O	-105.9
PBE-OTMA + H_2O à PBE-OTMA-H-OH	-18.0
PBE-OTMA + H_2O à PBE-OTMA-H_2O	+1.3
PBA-OTMA + CH_3OH à PBA-OTMA-H-CH_3O	-120.4
PBA-OTMA + CH_3OH à PBA-OTMA-CH_3OH	-109.1
PBE-OTMA + CH_3OH à PBE-OTMA-H-CH_3O	-13.3
PBE-OTMA + CH_3OH à PBE-OTMA-CH_3OH	+2.3

As the results shown above, hydrolysis is a possible mechanism for fluorescence quenching. The energetics of hydrolysis is clearly different for the phenyl boronic acid (**PBA-OTMA**) as compared to the boronate ester (**PBE-OTMA**). Moreover, the energetics for hydrolysis is calculated to favorable when dielectric continuum solvation is included in the model. Further study using explicit water is warranted.

3.4. Conclusion

In this chapter, the mechanism of fluorescence change of PET system **1** with addition of diol/sugar was extensively studied. A new mechanism, hydrolysis mechanism, was proposed and explored by DFT calculation and fluorescence studies. Compared to the B-N bond formation mechanism, which was believed widely, this hydrolysis mechanism is much more reasonable.

Experimental

Most reagents were purchased from Aldrich or Fisher/Acros and used as received. Anhydrous tetrahydrofuran (THF) was distilled from Na/benzophenone prior to use. Acetonitrile (CH_3CN) and dichloromethane (CH_2Cl_2) were distilled from CaH_2.

All pH values were determined with an Accumet 1003 Handhold pH/mV/Ion Meter (Fisher Scientific). A Shimadzu RF-5301 PC fluoremeter was used for the fluorescence studies. The excitation wavelength was set at 370 nm. A Shimudzu UV-1601 spectrophotometer was used for the UV absorption studies.

Synthesis of model Compound **1** followed the literature procedure.[1] The mixture of amine **3** (110 mg, 0.5 mmol), compound **4** (225 mg, 0.80 mmol), potassium carbonate (276 mg, 2 mmol) and potassium iodide (20 mg) in dry acetonitrile (30 mL), was stirred at RT for 12 hr. The insoluble materials were filtered off, and then the solvent was evaporated under vacuum. The resulting residue was dissolved in CH_2Cl_2 and 10% aqueous solution of sodium bicarbonate (20 mL), and the mixture was stirred at room temperature for 1 hr. The organic phase was washed with water (2×30 mL), and dried over $MgSO_4$. . Solvent evaporation gave a crude product, which was purified on a silica gel column [silica gel, MeOH/DCM] afforded the model compound **1** (70%).

References

(1) James, T. D.; Samankumara, K. R. A.; Iguchi, R.; Shinkai, S. *J. Am. Chem. Soc.* **1995**, *117*, 8982-8987.

(2) James, T. D.; Sandanayake, K. R. A. S.; Shinkai, S. *Chem. Commun.* **1994**, 477-478.

(3) Sandanayake, K. R. A. S.; Nakashima, K.; Shinkai, S. *Chem. Commun.* **1994**, 1621-1622.

(4) James, T. D.; Sandanayake, K. R. A. S.; Shinkai, S. *Nature (London)* **1995**, *374*, 345-347.

(5) Wiskur, S.; Lavigne, J. J.; Ait-Haddou, H.; Lynch, V.; Chiu, Y. H.; Canary, J. W.; Anslyn, E. V. *Org. Lett.* **2001**, *3*, 1311-1314.

(6) Hahn, I. S.; Wesdemiotis, C. *Int. J. Mass Spectrom.* **2003**, *222*, 465-479.

(7) Springsteen, G.; Wang, B. *Tetrahedron* **2002**, *58*, 5291-5300.

(8) Cooper, C.; James, T. D. *Chem. Lett.* **1998**, 883-884.

(9) Norrild, J. C. *J. Chem. Soc. Perkin Trans. 2* **2001**, 719-726.

(10) Norrild, J. C.; Eggert, H. *J. Chem. Soc., Perkin Trans. 2* **1996**, 2583-2588.

(11) Lorand, J. P.; Edwards, J. O. *J. Org. Chem.* **1959**, *24*, 769-774.

Chapter 4. Development of Nitrophenol-Based Boronic Acid Compounds for Color Sensing of Diols

Abstract

The complex that forms between a boronic acid and a diol is often much more acidic than the starting boronic acid. In conditions where the solution pH is between the two pKa values, the boron atom will convert from a neutral trigonal form to a anionic tetrahedral form upon complexation. Such a change is likely to dramatically alter the electron density of neighboring groups. Utilizing this effect, we have designed and synthesized two nitrophenol-based boronic acid reporter compounds that change ionization states and therefore spectroscopic properties upon diol binding. Both compounds show significant UV changes upon addition of saccharides. For example, a blue shift of the absorption max from 373 nm to 332 nm was observed with the addition of D-fructose to 2-hydroxy-5-nitrophenylboronic *acd*at neutral pH. Such a reporter compound can be used as a recognition and signaling unit for the construction of polyboronic acid sensors for the selective and specific recognitions of saccharides of biological significance.

4.1. Introduction

Due to the unique strong interactions between boronic acids and diols through reversible ester formation, there has been a great deal of interest in using a boronic acid as the recognition moiety for the development of fluorescent and color sensors,[1-11] carbohydrate transporters,[12-18] and chromatographic stationary materials.[19-24] Recently, our group for the first time showed that boronic acid-based fluorescent sensors for cell surface carbohydrate sialyl Lewis X (sLex) can be used for the fluorescent labeling of HEPG2 cells that are engineered to over express sLex[25] (also see details in Chapter 1). Parallel with our sensor development effort, we have also examined systematically the binding between boronic acid with various iols.[26,27] Such studies allowed us to correct many literature mistakes[28] including the strength of the binding between phenylboronic acid and various sugars.

Critical to the sensor development effort is the availability of reporter compounds that can generate a detectable signal upon binding with the target molecules. Along this line, Czarnik,[29] Shinkai,[30,31] Lakowicz,[32-35] James,[36-39] and Heagy[40,41] have developed various fluorescent boronic acid compounds that show fluorescent intensity/wavelength changes upon binding with diols to varying degrees. The most prominent one is the Shinkai photoelectron transfer (PET) system using B-N bond strength to modulate the fluorescence quenching process and therefore the fluorescent intensity changes.[9,30,42,43] However, many aspects of these available reporters need to be improved. This includes water solubility, the magnitude of fluorescence intensity changes, and photo- and chemical stabilities of these compounds. There has also been a great deal of interest in developing colorimetric sensors for sugars using boronic acid compounds. Along this line, Strongin,[44] James,[45] Lakowicz,[46] and Shinkai[47] have reported several compounds

that upon addition of sugar change colors. Most of these designs are based on the modulation of the electronic properties of the chromophores through B-N bond formation or inductive effects. The mechanism of action for the Strongin system, however, is not clear[44]. The Anslyn group has reported several systems that use a reporter compound to form an ensemble for sugar and other diol detection.[3,4] Herein we report the design, synthesis, and evaluation of nitrophenol-based boronic acid reporter compounds that show significant spectroscopic changes upon addition of sugars at neutral pH in aqueous solution. Our design took advantage of the ability of a boronic acid functional group to modulate the pKa and/or the electron density of a neighboring group upon addition of a diol, through both a proximity effect as well as an inductive effect. Such a spectroscopic reporter compound can be used for the construction of diboronic acid sensors for the specific recognition of various carbohydrates.

4.2. Design of UV Boronic Acid Sensors for Saccharides

4.2.1. pKa Differences between Boronic Acid and Ester

It has long been recognized that the pKa of a boronic ester is, most of the time, lower than that of the corresponding boronic acid[27,28] (Figure 4.1). For example, the pKa of phenylboronic acid is about 8.8 and the pKa's of its glucose and fructose esters are 6.8 and 4.5 respectively.[27] Such significant changes in pKa upon ester formation has one major implication that can be taken advantage of in designing boronic acid-based fluorescent and color sensors. This is particularly important for sensors that have a desirable functional pH close to neutral. We have recently examined a series of about 30 phenylboronic acid compounds with varying substituents and found that the highest pKa

was about 9.0 when the substitutent was a methoxy group. If binding to a sugar lowers its pKa by 2-4 units, this would mean that at pH 7.4 the boronic acid would exist in the neutral form and addition of a sugar would change it to the anionic tetrahedral form.

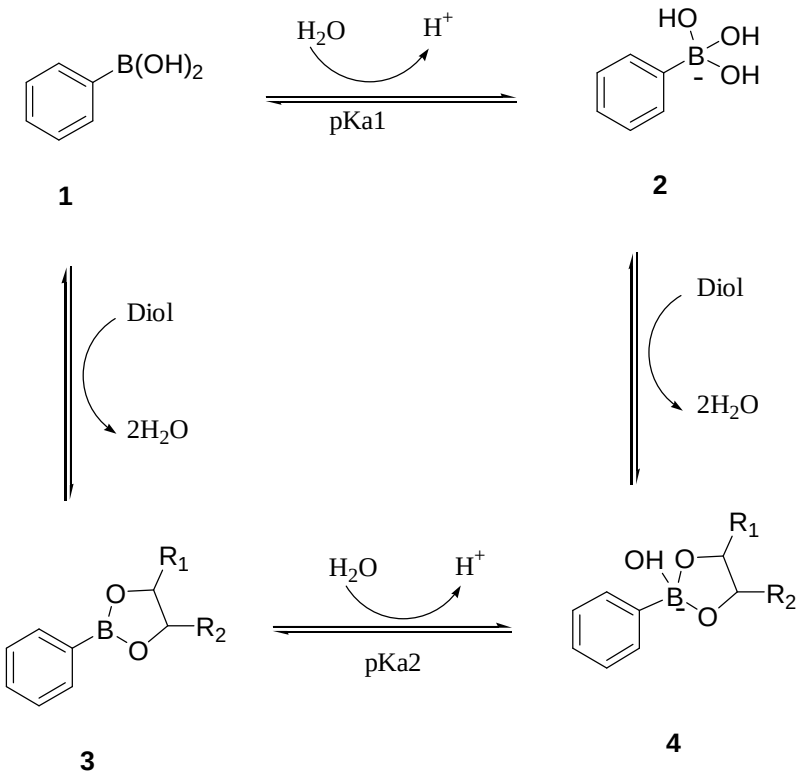

pKa2 < pKa1 in most conditions

Figure 4.1. Equilibrium of phenyboronic acid binding with saccharides/diols.

This change in charge states can be used to modulate the electron density of the neighboring group through either proximity or inductive effects. There is also the possibility that the protonation state of a neighboring group that is either an acid or base can be affected by the ionization state change of the boronic acid. Both of these factors are known to affect the spectroscopic properties of a chromophore.

4.2.2. p-Nitrophenol Chemistry

p-Nitrophenol (PNP) is known to change its ionization states depending on the pH and such a change causes tremendous shifts in its spectroscopic properties (Figure 4.2).[48] Therefore, nitrophenol-based compounds have been widely used for the development of substrates for enzyme assays among other things.[49]

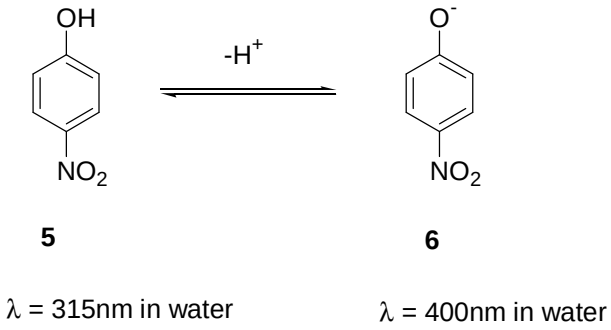

Figure 4.2. Ionization states of p-nitrophenol.

4.2.3. Design of Nitrophenol Boronic Acid

We envisioned that if a boronic acid is positioned next to the phenol group of *p*-nitrophenol or its analogs, the ionization state changes of the boronic acid moiety upon binding with a diol would likely affect the pKa and/or the electron density of the phenol group through either proximity or inductive effect. If this change straddles at the neutral pH range, we would be able to develop a spectroscopic reporter compound functional at physiological pH. For this purpose, we designed (Scheme 4.1) 2-hydroxy-5-nitrophenylboronic acid (**7**) and, and for comparison, 4, 6-dinitrophenol-2-boronic acid (**8**).

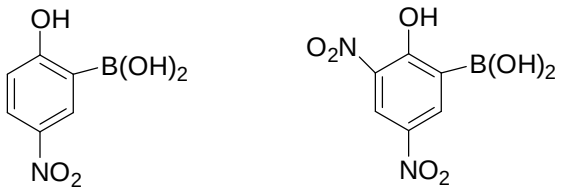

7 **8**

Scheme 4.1. Designed nitrophenol-based boronic acids **7** and **8**.

4.3. Synthesis

4.3.1. Synthesis of 2-hydroxy-5-nitrophenylboronic acid(7)

The synthesis of compound **7**, 2-hydroxy-5-nitrophenylboronic acid, started with commercially available 2-bromo-4-nitroanisole. Borylation of this bromide **9** with bis(pinacolato)diboron using $Pd(dppf)Cl_2$ as the catalyst in the presence of potassium acetate furnished pinacolboronate **10** in 20% yield.[50] The oxidative deprotection of pinacolboronate ester **10** by sodium periodate[51] yielded 70% of methoxy phenylboronic acid **11**. Then, the treatment of this methoxy nitrated phenylboronic **11** by 1 M boron tribromide in methylene chloride yielded 2-hydroxy-5-nitro phenylboronic acid **7** in 90% yield (Scheme 4.2).

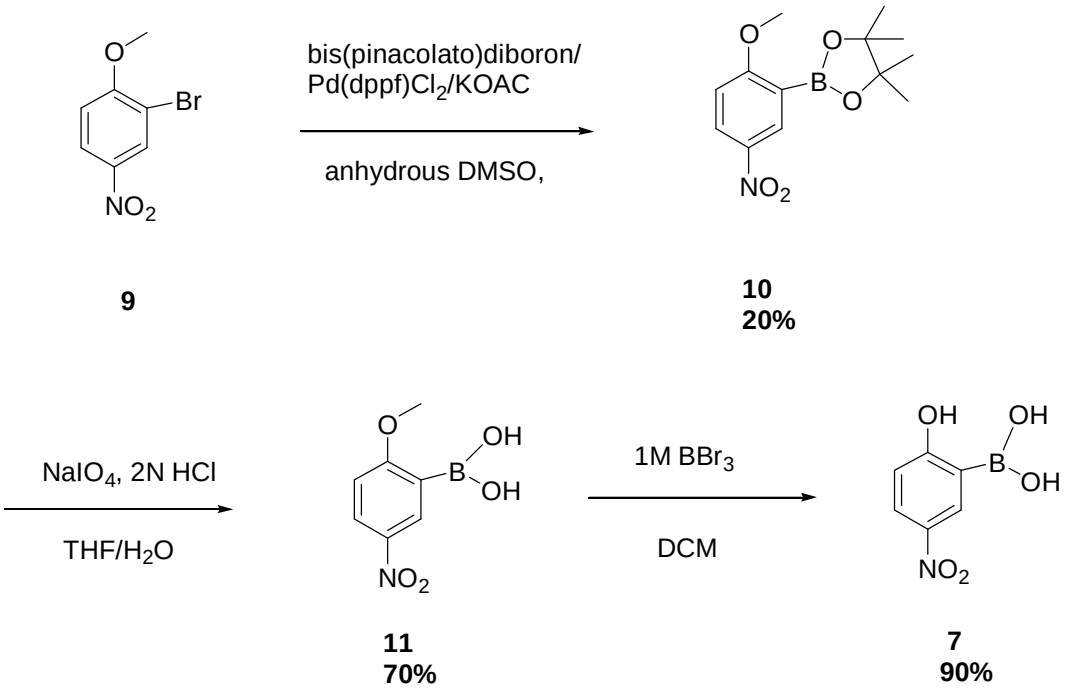

Scheme 4.2. Synthesis of 2-hydroxy-5-nitrophenylboronic acid (**7**).

4.3.2. Synthesis of 4, 6-Dinitrophenol-2-Boronic Acid (8)

The synthesis of 4, 6-dinitrophenol-2-boronic acid (**8**) started with commercially available compound 2-methoxyphenylboronic acid (**12**). The nitration of this boronic acid using a mixture of nitric acid and sulfuric acid at -10 °C gave the desired di-nitrated product **12** in 50% yield, and 10% side product 1-methoxy-2, 4-dinitro-benzene. There are literature precedents showing that nitration reactions can cause the cleavage of the C-B bond.[52] Then, the treatment of this boronic acid **13** by 1 M boron tribromide in methylene chloride yielded compound **8**, 4,6-dinitrophenol-2-boronic acid in 90% yield (Scheme 4.3). Boronic acid compounds sometimes exhibit poor NMR spectra due to the possible formation of dimers or polymers. Therefore, for the full characterization of these compounds, boronic acids **13** and **8** were protected by reacting with 2,2-dimethyl-propane-1, 3-diol to give boronates **14** and **15**.

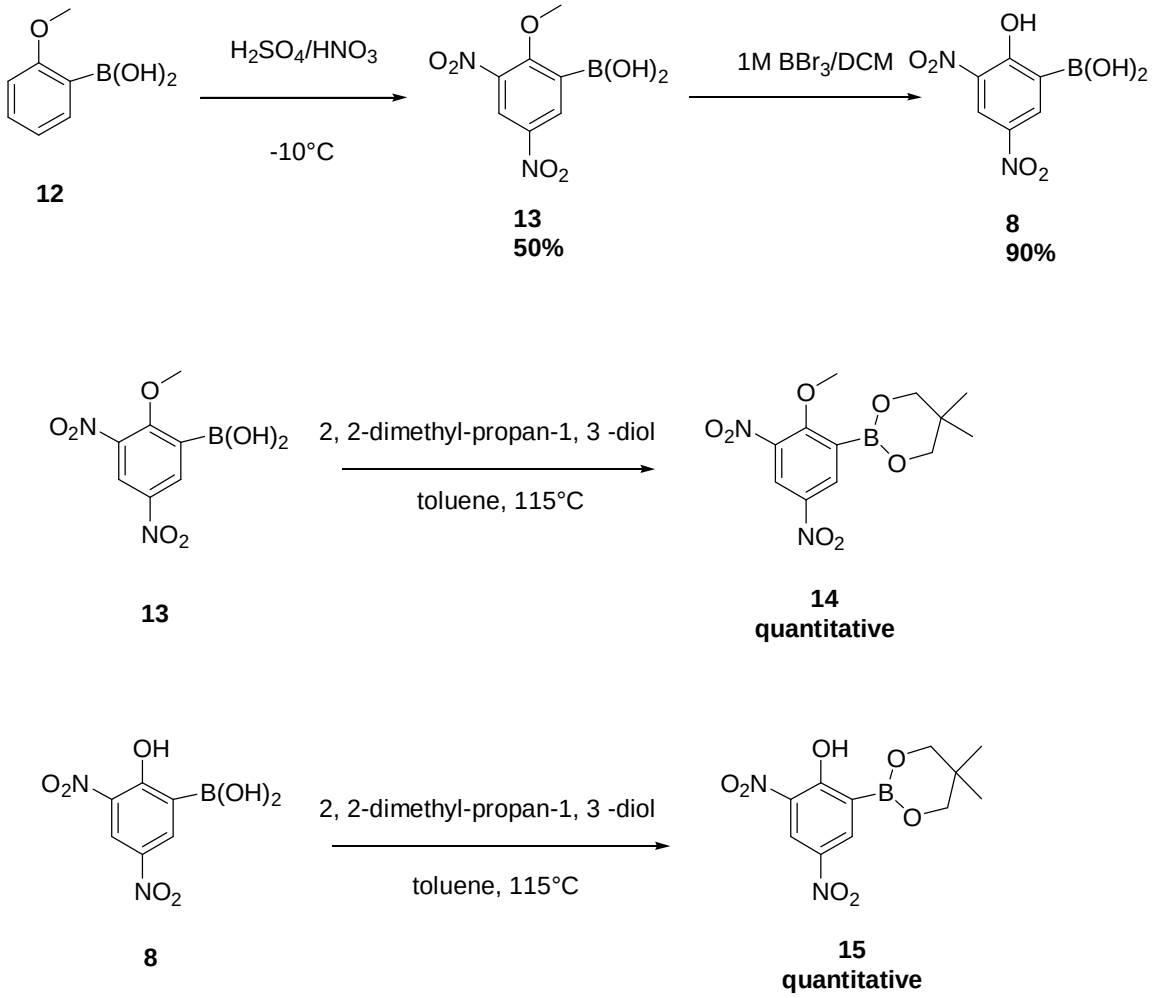

Scheme 4.3. Synthesis of 4, 6-dinitrophenol-2-boronic acid (**8**).

4.4. Results and Discussions

4.4.1 Binding Studies of 2-Hydroxy-5-nitrophenylboronic Acid (7) with Diol-containing Compounds

In order to see whether our design works or not, the effect of fructose on the absorption of compound **7** was examined (Figure 4.3). Without specification, the studies were carried out at concentration of 2×10^{-4} M (4% methanol: 96% pH 7.4, 0.1M phosphate buffer).

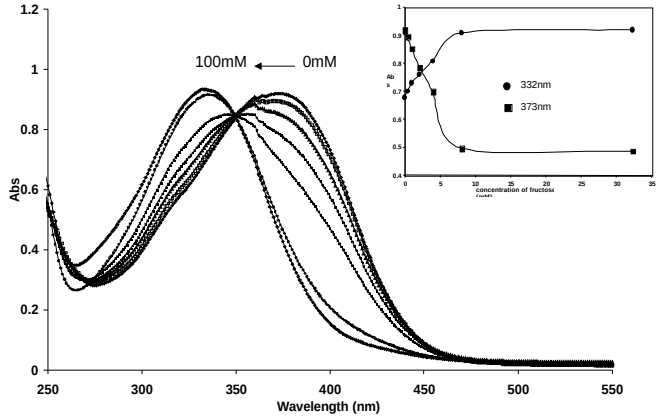

Figure 4.3. Absorption of compound **7** at 2×10^{-4} M in pH=7.4, 0.1 M phosphate buffer with increasing concentration of fructose (0, 0.4, 1.0, 2.1, 4.0, 16.0, 100 mM). Inset — absorption increase (λ = 332nm) and absorption decrease (λ = 373nm) of **7** in the presence of fructose.

As can be seen from Figure 4.3, the spectroscopic properties of 2-hydroxy-5-nitrophenylboronic acidchanged tremendously at pH 7.4 with the addition of fructose. Millimolar concentrations of fructose were sufficient to cause a significant blue shift of the absorption λ_{max} (from 373 nm to 332 nm). With increasing concentrations of fructose, the UV intensity decreased at 373 nm and increased at 332 nm. This essentially forms a ratiometric system with large λ_{max} shifts (51 nm). The response seems to reach a plateau at 16 mM. An isosbestic point is observed at 350 nm showing the equilibrium of two species.

To further examine the detailed effect of these sugars on the spectroscopic properties of **7**, we studied the concentration effect of fructose, glucose, galactose and 1,2-*cis*-cyclopentanediol on this compound (Figure 4.4).

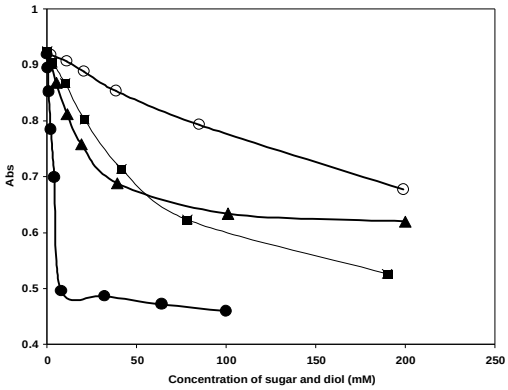

Figure 4.4. Titration curves of **7** (2×10^{-4} M) at λ = 373nm against sugars: μ — glucose (Ka = 8.0 M^{-1}), g — galactose (Ka = 44.0 M^{-1}), • — 1, 2-*cis*-cyclopentanediol (Ka = 34.7 M^{-1}), n — fructose (Ka = 245 M^{-1}). All studies were studies in 4% methanol / 96% 0.1 M pH 7.4 phosphate buffer (v/v).

Spectroscopic changes were observed with the addition of all three sugars and *cis*-1, 2-cyclopentanediol. At the same time compound **7** has good selectivity with fructose over the others, as expected with monoboronic acids.[27] The binding constants between this boronic acid and fructose, glucose, galactose and 1,2-*cis*-cyclopentanediol were determined as 245, 8.0, 44.0 and 34.7 M^{-1} respectively.

4.4.2. Binding Studies of 4, 6-Dinitrophenol-2-boronic Acid with Diol-containing Compounds

For comparison, we also studied the binding of 4, 6-dinitrophenol-2-boronic acid (compound **8**) with fructose, glucose and galactose. The studies were also carried out at a concentration of 5×10^{-6} M for **8** (4% methanol/96% 0.1M pH = 7.4 phosphate buffer). Spectroscopic changes were observed with the addition of all three sugars, with binding constants of 13.5, 1.2, 0.7 M^{-1} for fructose, galactose and glucose, respectively. Figure 4.5 shows the spectroscopic changes of **8** with the addition of fructose. It can be seen

that such spectroscopic changes at physiological pH are also significant with a pattern similar to that of **7**. With increasing fructose concentrations, the UV intensity decreased at 361 nm and increased at 272 nm. The presence of fructose also results in the appearance of a new peak at 369 nm. Two isosbestic points were observed at 323 nm and 423 nm, indicative of two equilibria of three species.

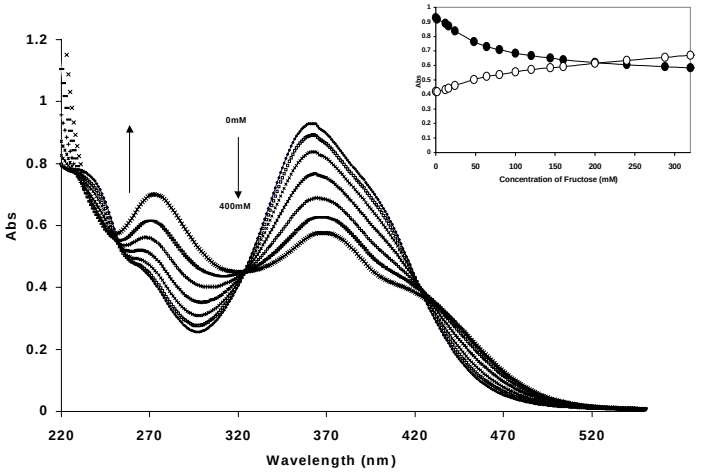

Figure 4.5. Absorption spectra of **8** (5×10^{-6} M) (4% methanol in water (v/v), 0.1M phosphate buffer, pH 7.4, by adding various concentration of D-fructose (0, 12 mM, 24 mM, 48 mM, 100 mM, 200 mM, 400 mM). Inset — absorption change of **2** at 361 nm (●) 272 nm (○) respectively upon addition of fructose.

It is very interesting to see that the binding constants for **8** with various sugars are smaller than that of **7**. This contradicts the conventional notion that boronic acids with lower pKa's bind more tightly to diols. Our group has also generated other data that indicate that boronic acid pKa's are not directly proportional to the binding constants.[27]

4.5. Mechanistic Studies

Since compounds **7** and **8** work very well for signaling sugar binding, especially for compound **7**, it is very important to examine the mechanism. As we mentioned above, the design was based on the idea that the charge state changes of the boronic acid group upon ester formation may affect the charge state or density of a neighboring group, it is important to examine the possible ionization species existing in the reaction solution.

4.5.1. Ionization States Study

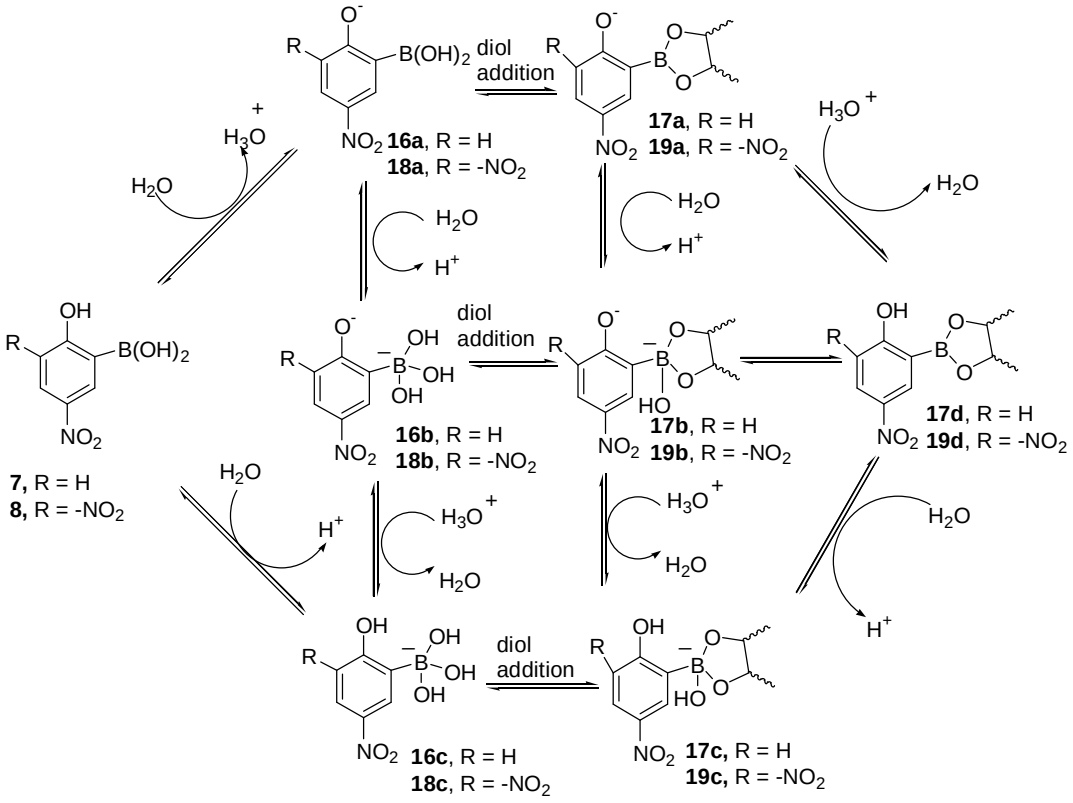

Scheme 4.4. Equilibrium among different species of **7** and **8** in the presence and absence of D-fructose.

Both compounds **7** and **8** may exist in different ionization states at different pH, because of the presence of two ionizable functional groups, the phenol hydroxyl group and the boronic acid group. So do the boronate esters of **7** and **8** with diols. Scheme 4.4

shows the equilibrium among different species of **7** and **8** in the presence and absence of D-fructose.

4.5.1.1. Analyzation of the Ionization States through pH profiles of 7 the Absence and Presence of Diols

In evaluating the likelihood for the formation of different ionization species, one needs to analyze the pKa of each functional group present (Scheme 4.4). For compound **7** at neutral pH, if the hydroxyl group has a lower pKa, it would favor species **16a**, and if the boronic acid has a lower pKa, it would favor the formation of **16c**. If these two groups have comparable pKa, both species may exist simultaneously in different ratios depending on the conditions. *p*-Nitrophenol has a pKa of about 7.2. Since boronic acid is considered an electron-withdrawing functional group, it is most likely that the pKa of the hydroxyl group of compound **7** is lower than 7.2. 2-Methoxy-5-nitrophenylboronic acid has a pKa of about 7.1 (data see below). This should be comparable to the boronic acid moiety pKa of compound **7**. Therefore, it is possible that the pKa's of these two functional groups are so close that both **16a** and **16c** exist at the same time at physiological pH. Upon ester formation, there are four possible species, **17a-d**. Since binding with a diol most of the time lowers the pKa of the boron by 2-4 pKa units, we expect that species **17c** will be predominant upon ester formation, which would lower the ratio of hydroxyl ionized species **17a**. This shift in the concentration of the species with the hydroxyl group ionized should result in a change in the spectroscopic properties of the solution.

To understand the ionization state changes upon ester formation, it is also important to examine the spectroscopic properties of the different species existing in

solution. The pH titration profiles of compound **7** in the absence of any diols (Figure 4.6) and that of **7** in the presence of 200 mM fructose (Figure 4.7) were performed, and in both of the situations, only one pKa was obtained, the pKa of **7** is 6.0 and **7** with fructose is 4.7, respectively (Figure 4.8).

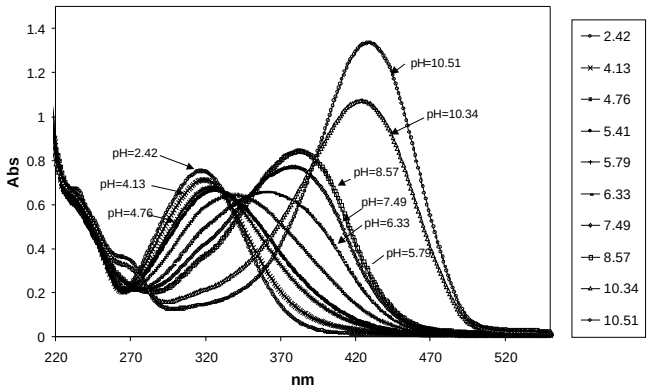

Figure 4.6. pH profile of compound **7** (initial concentration of **7** is set 2×10^{-4} M in 4% methanol/96% water, and the ionic strength was initially fixed at 0.1 M NaCl).

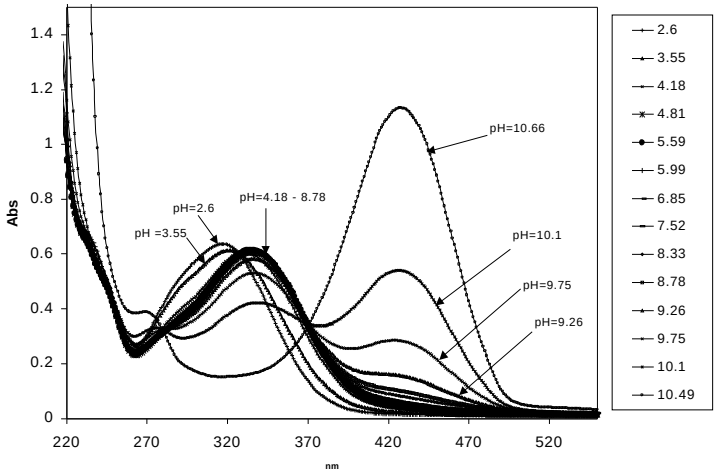

Figure 4.7. pH profile of compound **7** with 200 mM D-fructose (initial concentration of 1 is set 2×10^{-4} M in 4% methanol/96% water, and the ionic strength was initially fixed at 0.1 M NaCl).

From Figure 4.6, one can readily see that there are three absorption maxima at 315, 380, and 427 nm. These three λ_{max}'s represent three different ionization stages. At low pH (pH < 4), the absorption λ_{max} is at 315 nm corresponding to the non-ionized form of **7** (Scheme 4.5). The absorption peak at 380 nm represents the first ionization (first pKa), which can be either the deprotonation of the hydroxyl group (**16a**) or the ionization of the boron (**16c**) or a combination of these two since their pKa's are very close. The third peak at 427 nm represents the fully ionized form with two anions on the same molecule (**16b**). Figure 4.7 shows the pH titration profile of **7** in the presence of D-fructose (200 mM). In this case, there also seems to be three ionization stages corresponding to λ_{max}'s of 315, 325, and 427 nm. The first λ_{max} is the same as that of **7** in the absence of any diol. This is understandable since at low pH little binding is expected[27] and the species present should be the free sensor **7** with no ionization. The last λ_{max} (427 nm) is also the same as that of **7** in the absence of any diol. It is known that the binding affinity of boronic acid with diols increases with increasing pH, and at high pH one would expect that, essentially all the boronic acid has been converted to its ester. This would indicate that at pH 10.5, the species is also the di-anion species (**17b**), which has the same spectroscopic properties as that of **16b**. This further indicates that forming an ester alone does not change the electronic properties of the complex enough to affect their spectroscopic properties. The major difference between the system with a diol (fructose) and without a diol (Scheme 4.4) is in the neutral pH region, which is ideal (and by design) for the sensing of diol compounds near physiological conditions.

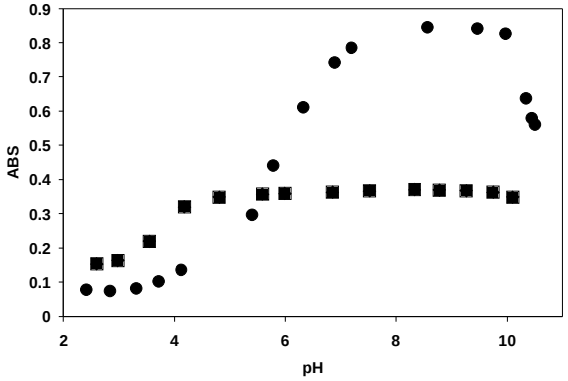

Figure 4.8. pKa test of **7** without and with sugar. This figure is from the data of Figure 5.6 and 5.7. (n) — pH titration of the absorption of **7** (2×10^{-4} M) at 380 nm; pKa1=6.0. (g) — **7** (2×10^{-4} M) in the presence of 0.2 M fructose at 368 nm; pKa1=3.8. (data from Figure 4.6 and Figure 4.7)

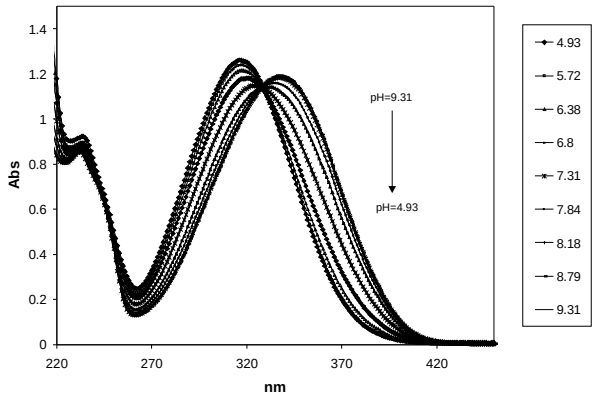

Figure 4.9. pH profile of compound **11** (initial concentration of **11** is set 2×10^{-4} M in 4% methanol/96% water, and the ionic strength was initially fixed at 0.1 M NaCl).

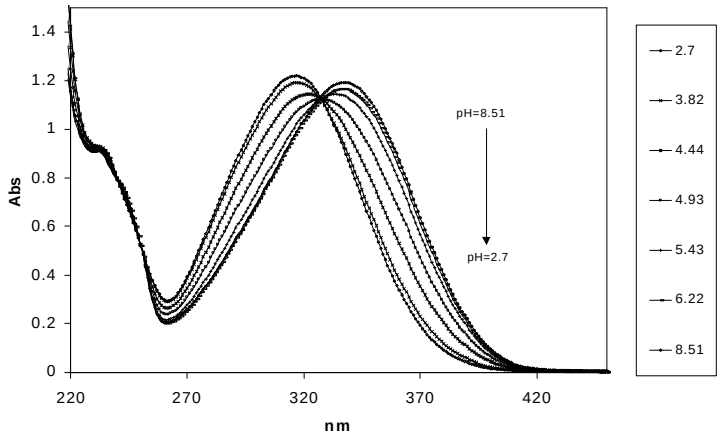

Figure 4.10. pH profile of compound **11** with 200 mM D-fructose (initial concentration of 5 is set 2×10^{-4} M in 4% methanol/96% water, and the ionic strength was initially fixed at 0.1 M NaCl).

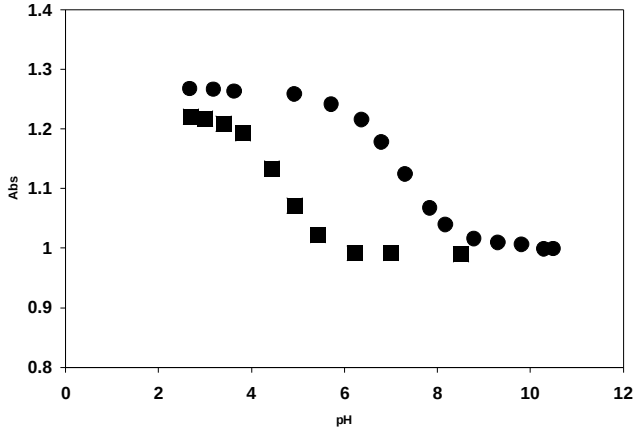

Figure 4.11. pKa of compound of **11** in the absence and presence of fructose. n — pH titration of the absorption of **11** (2×10^{-4} M) at 318 nm, pKa=7.0 g — **11** (2×10^{-4} M) in the presence of 0.2 M fructose at 317 nm, pKa=4.7. (data from Figure 4.8 and Figure 4.9).

In the presence of fructose, there are two possible species at neutral pH, **17a** and **17c**. In order to see which the dominant species is, we also examined the spectroscopic

changes of the methylated version of **7**, compound **11**, in the presence (Figure 4.9) and absence (Figure 4.8) of fructose. As expected, the pH titration curve of **11** shows two species (Figure 4.8), one with a λ_{max} of 315 nm and the other at 337 nm. It is easy to understand that the peak at 315 nm corresponds to the un-ionized form and the peak at 337 nm corresponds to the anionic tetrahedral boron species. It needs to be noted that the first λ_{max} is about the same as that of the un-ionized **7**, which indicates that methylation did not change the electronic properties of the molecules sufficiently to affect its UV properties. This would also suggest that **17c** should have about the same λ_{max} as the ionized form of **11**. If we compare the UV spectrum of **7** in the presence of fructose at around neutral pH, it is easy to see that the λ_{max} is about the same as that the ionized **11**. This would suggest that upon addition of fructose to **7**, the lowered pKa of the boron in the ester makes **17c** the predominant species.

Now if we can go back to analyze the situation of **7** in the absence of fructose. A detailed examination of the spectral set with **7** in the absence of any sugar reveals a "shifting" λ_{max} for the middle peak (380 nm, Figure 4.6). The lack of an isosbestic point transitioning from the first to the second "ionization state" indicates the formation of more than one "intermediate." This could only mean that both **16a** and **16c** were formed in the pH range of 5.79 and 8.57. The shifting of the λ_{max} from 339 to 380 nm in this region indicates the formation of a species with a shorter λ_{max} wavelength at low pH and a species with a longer λ_{max} wavelength at high pH. Intuitively, it is reasonable to assign **16a** as the species with a longer wavelength, and **16c** as the one with a shorter wavelength. Such an assumption is also consistent with experimental data. For example, **17c** and the ionized form of **11** all have λ_{max}'s around 325 nm, and they are structurally

analogous to **16c**. Therefore, it is logical to assign the species with an approximate λ_{max} of 339 nm (Please note that at this point, it is already a mixture of more than one species. Therefore, it may not reflect the λ_{max} of a single species.), not 380 nm. Furthermore, the ionization of the hydroxyl group in a *p*-nitrophenol type of structure is known to significantly increase its λ_{max}. For example, the ionized form *p*-nitrophenol itself has a λ_{max} of about 425 nm, which is similar to **16b** and **17b**.

One might ask if the hydroxyl group deprotonated form of *p*-nirophenol, **6** and **16b** and **17b** all have similar λ_{max}'s, why should the λ_{max} of **16a** be very different if it also has the hydroxyl group deprotonated.

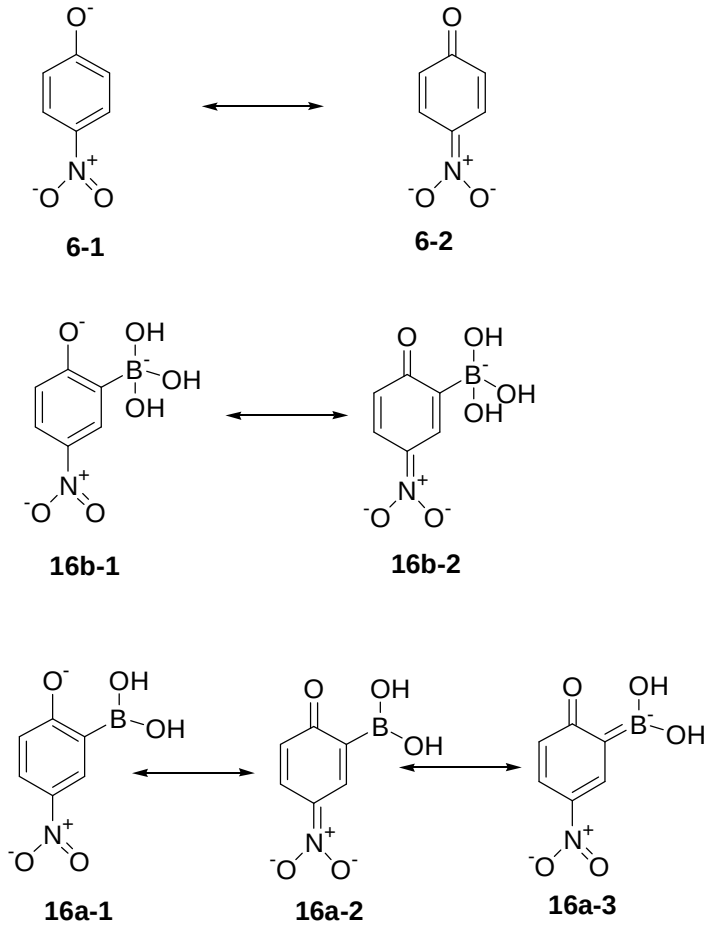

Scheme 4.5. Resonance structrues of deprotonated *p*-nitrophenol and some species of compound **7**.

This can be explained by examining the resonance structures of these different species (Scheme 4.5). For *p*-nitrophenol, there are two resonance structures, **6-1** and **6-2**, with **6-2** being the species contributing most to the long wavelength UV absorption properties. For **16b**, the situation is similar; there are only two analogous resonance forms. Therefore, it is reasonable to expect that *p*-nitrophenol and **16b** have similar λ_{max}'s. Since **17b** should behave similarly to **16b**, its resonant forms are not shown. For **16a**, the situation is very different. Because the boron open shell is not occupied, it is resonantly electron-withdrawing. One can write a third resonance structure, **16a-3**. Therefore, the UV absorption of **16a** can be expected to be quite different from that of *p*-nitrophenol, **16b-1**, and **16b-2.**

Overall, the pH titration (Figure 4.6) of **7** in the absence of any sugar can be interpreted as follows. At low pH, there is no ionization, and free **7** is the only species (Scheme 4.4). With increasing pH, the first ionization occurs to generate **16c**, which has a λ_{max} of around 330 nm. With increasing pH, **16a** starts to appear. Since **16a** has a longer λ_{max}, the UV spectra shift to longer wavelength. Because the transition from free **7** to the species with one ionized functional group involves two "products," no isosbestic point was observed.

4.5.1.2. ^{11}B NMR Studies of Compound 7 and its Ester

As discussed earlier, ^{11}B NMR is known to indicate the electronic and ionization state of the boron atom. For example, ^{11}B NMR chemical shift for of the neutral and trigonal form (such as **16a**) is about 30 ppm and for the anion tetrahedral form (such as **16b**) it is 10 ppm.[53]

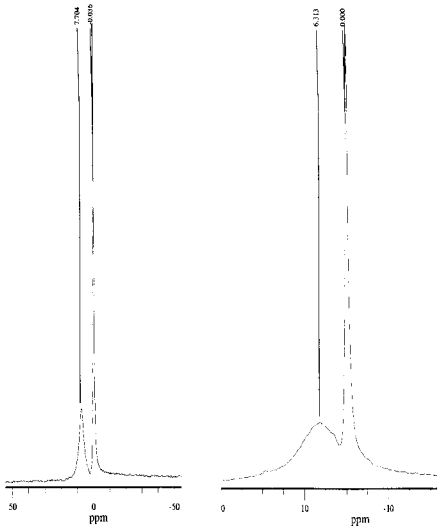

Figure 4.12. ^{11}B NMR spectra of compound **7** and **7** with *cis*-1,2-cyclopentane diol (left) in pH 7.4 buffer solution.

As can be seen from Figure 4.12, at pH 7.4 (phosphate buffer), the ^{11}B NMR of compound **7** in the presence of excess *cis*-1, 2-cyclopentanediol was a fairly sharp peak at about 7.7 ppm, indicative of anionic species consistent with either **17b** or **17c** (Scheme 4.4). However, it is unlikely that at neutral pH, it can be doubly ionized. Therefore, the NMR results are consistent with the formation of **17c** upon addition of a diol to the solution of **7** at neutral pH. It should be noted that *cis*-1, 2-cyclopentanediol was used in the NMR experiments to reduce the complexity of the NMR spectrum. Because fructose

can bind to a boronic acid in several fashions, the ^{11}B NMR would be expected to reflect the presence of several species, which would complicate the interpretation. When the ^{11}B NMR spectrum of **7** in the absence of any diol was determined at pH 7.4, a broad peak center around 6.3 ppm was observed, an indication that the boron also is in the anionic state (Figure 4.12). There are two things that need to be noted. First, the broad peak is an indication that there is more than one species in the solution, which is consistent with the earlier proposal that it was a mixture of **16a** and **16c**. Second, the chemical shift is consistent with the boron being more shielded than in the trigonal neutral form. However, much more work will be needed to understand exactly what the composition is for all the different species.

4.5.2. Mechanism of the Spectroscopic Change of 7 with the Addition of D-Fructose at Neutral pH

At pH 7.4, the λ_{max} for the solution of **7** is at about 373 nm in the absence of any sugar and 325 nm in the presence of fructose, which forms the basis for the sugar sensing at physiological pH in aqueous solution. The mechanism responsible for this sensing is that the addition of fructose shifted the UV absorption of the solution from that of **16a** to that of **17c**. This was the direct result of the pKa-lowering effect of fructose addition. Because the ratio of **17a** over **17c** (and **16a** over **16c**) is directly related to the relative pKa of these two species and these two species are mutually exclusive, the lowered boron pKa of the ester relative to the hydroxyl group would result in a shift in the acid-base equilibrium by lowering the percentage of the hydroxyl-ionized species (**17a**). Consequently, addition of fructose to the solution of **7** results in a shift of the UV absorption of the solution from that of **16a** to that of **17c**.

4.5.3. Mechanism of the Spectroscopic Change of 8 with the Addition of D-fructose at Neutral pH

To help understand the mechanism of the spectroscopic change of the binding of compound **8** with sugar, the pKa's of the compound **8** only (Figure 4.13) and **8** with fructose (Figure 4.14) were determined. The pKa profile from the data of Figure 4.13 and Figure 4.14 is shown in Figure 4.15. From Figure 4.15, it can be seen that in the absence of any sugar the first pKa (the ionization of only one functional group which can be either the boronic acid or the hydroxyl group) of compound **8** is at about 3.3 and the second pKa (the ionization of two functional groups) is at about 9.2. With the addition fructose (200 mM), the first pKa remained essentially the same (pKa 3.2) and the second one was lowered to about 7.2.

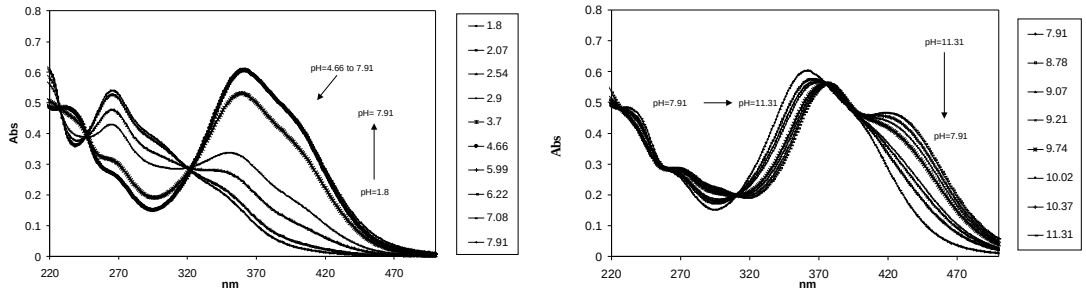

Figure 4.13. pH profile of **8** (initial concentration: 1×10^{-5} M in 4% methanol/96% water, and the ionic strength was initially fixed at 0.1 M NaCl). pH 1.8~7.9 (Left), pH 7.9~13.1 (Right).

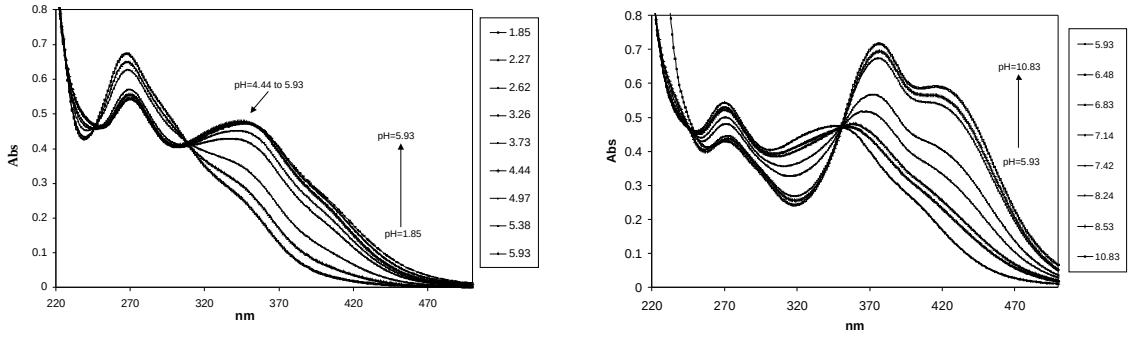

Figure 4.14. pH profile of **8** (initial concentration: 1×10^{-5} M in 4% methanol/96% water, and the ionic strength was initially fixed at 0.1 M NaCl) with 200 mM fructose. pH 1.8~5.9 (Left), pH 5.9~10.8 (Right).

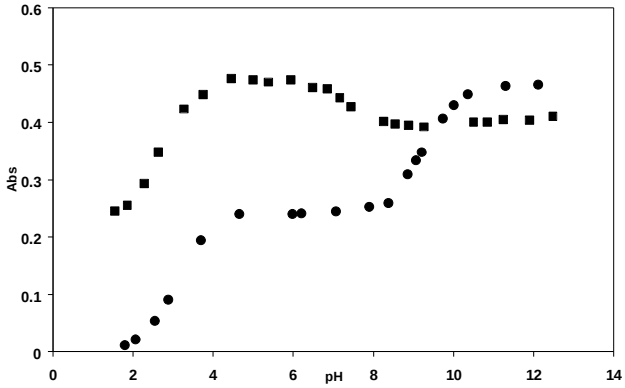

Figure 4.15. pKa profile of **8** with the presence and absence of fructose. (n) — pKa profile of the absorption of **8** (1×10^{-5} M) at 424nm, (g) — **8** (1×10^{-5} M) with the presence of 0.2 M fructose at 345nm (data from Figure 4.13 and Figure 4.14).

One can assume a similar mechanism in operation for **8** as it is for **7**. In the absence of any sugar, the peak at 369 nm is attributed to species **18a**. However, upon addition of a sugar and the lowering of the boronic pKa,[27] the concentration of **18a** decreased with increasing concentration of **19c**, which contributed to the decrease in

absorption at 369 nm and increase in absorption at 323 nm. The major difference between **8** and **7** is that the second pKa with the addition of fructose is much lower (7.2). This means that at physiological pH, addition of fructose can also result in the formation of the di-ionized species **19b**, which is responsible for the peak at 425 nm.

4.6. Conclusion

We have designed and synthesized two nitrophenolboronic acids (**7** and **8**). Binding of sugars to these compounds results in very significant spectroscopic changes both in intensity and wavelength. The mechanism for the changes is through the manipulation of the pKa of the boronic acid, which affect the equilibrium among different chromophoric species. Such compounds can be used as colorimetric reporters as both the recognition and signaling unit for the construction of polyboronic acid spectroscopic sensors for mono- and complex carbohydrates, many of which are biomarkers for important biological and pathological events.

Experimental

General

All air- and/or water-sensitive reactions were performed under dry N_2 in flame-dried or oven-dried glassware. Most reagents were purchased from Aldrich or Fisher/Acros and used as received. SLex was purchased from Calbiochem and Aldrich. Tetrahydrofuran (THF) was distilled from Na/benzophenone prior to use. Acetonitrile (CH_3CN) and dichloromethane (CH_2Cl_2) were distilled from calcium hydride (CaH_2).

Analytical thin layer chromatography (TLC) was performed with Scientific Adsorbents plastic-backed TLC silica gel 60F hard layer plates. TLC plates were visualized with a 5% (w/v) solution of phosphomolybdic acid in ethanol or UV light (254 nm). Flash chromatography was performed with Scientific Adsorbents silica gel (flash, 32-63nm). Column chromatography was followed by combining appropriate fractions, rotary evaporating, and drying under oil pump vacuum.

Mass spectral analyses were performed by the Mass Spectrometry Laboratories of North Carolina State University and the University of Kansas. Partial funding for the NCSU facility was obtained from the North Carolina Biotechnology Center and the National Science Foundation. ^{1}H and ^{13}C nuclear magnetic resonance (NMR) spectra were recorded on a Varian Gemini 300, Varian Mercury 300 and Varian Mercury 400 NMR spectrometer. NMR Chemical shifts (δ) for ^{1}H spectra are expressed in ppm relative to internal solvent peaks and coupling constants were measured in Hz. For ^{11}B NMR, $BF_3 \cdot Et_2O$ has been used as an external reference and the spectra were recorded at GE Omega 300 spectrometer. All pH values were determined with an Accumet 1003 Handhold pH/mV/Ion Meter (Fisher Scientific). A Shimudzu UV-1601 spectrophotometer was used for the UV absorption studies.

2-(2-Methoxy-5-nitro-phenyl)-4,4,5,5-tetramethyl-[1,3,2]dioxaborolane (10).[50] Potassium acetate (360 mg, 3.7 mmol) in a three-necked flask (25 mL) was flame-dried under N_2. To this flask was added 2-bromo-4-nitroanisole (360 mg, 1.56 mmol), bis(pinacolato)diborane (360 mg, 1.41 mmol), and [1,1'-bis(diphenylphosphino)ferrocene] dichloropalladium (II) (pd(dppf)Cl_2 , 32 mg, 0.04 mmol). To this mixture was added anhydrous DMSO (10 mL). The reaction mixture was stirred at 85 ^oC under N_2 for 5 h and then was poured to 20 mL of ice-cold water. The mixture was extracted with EtOAc (2 × 30 mL), and the combined organic extracts were washed with water (30 mL) and brine (30 mL), dried over $MgSO_4$ and concentrated. Column chromatography of the residue [silica gel, EtOAc/CH_2Cl_2] afforded the boronate **10** (20%). ^1H NMR ($CDCl_3$, 300 MHz) δ 8.56 (1H, d, *J* = 3Hz), 8.30-8.26 (1H, dd, *J* = 3, 9 Hz), 6.91 (1H, d, *J* = 9 Hz), 3.92 (3H, s), 1.36 (12H, s). ^{13}C NMR ($CDCl_3$) δ 168.9, 141.3, 132.9, 128.7, 110.3, 84.4, 56.6, 25.0. Anal. Calcd. for $C_{13}H_{18}BNO_5 \cdot 0.5\ H_2O$, C, 54.19; H, 6.65; N, 4.86. Found: C, 54.52; H, 6.41; N, 4.64. ESI-MS $C_{13}H_{18}BNO_5$, Calcd. 279.1, Found 279.0.

2-Methoxy-5-nitrophenylboronic Acid (11). To the solution of pinacolboronate ester **10** (133.7 mg, 0.48 mmol) in THF/H_2O (4:1, 4 mL) was added sodium periodate (320 mg, 1.50 mmol) at room temperature. The mixture was allowed to stir for 30 min, and then 2 N HCl (0.5 mL) was added. The resulting solution was stirred overnight. The reaction mixture was extracted with EtOAc (2 × 30 mL), and the combined organic extracts were washed with water (2 × 20 mL) and brine (20 mL), dried over $MgSO_4$ and

concentrated. The crude product was purified on silica gel column, eluting with EtOAc/CH_2Cl_2 (1/20) afforded the boronic acid (70%). ^{1}H NMR (CD_3OD, 300 MHz) δ 8.29-8.26 (1H, dd, J = 2.8 Hz, 9 Hz), 8.13 (d, 1H, *J* = 2.8Hz), 7.12 (1H, d, J = 9.2Hz), 3.95 (s, 3H). ^{13}C NMR (CDCl3) δ 132.9, 130.00 129.1, 128.1, 111.3, 56.9. ESI-MS: $C_7H_8BNO_5$, Calcd. for ($M+CH_3OH–H_2O+H^+$), 212.1, Found 212.1.

2-Hydroxy-5-nitrophenylboronic acid (7). General Procedure for the Deprotection of the Methoxy Group. To the solution of the methoxy-phenylboronic acid (**11**) in dry CH_2Cl_2 cooled with an acetone/dry ice bath was added dropwise 3 eq of 1.0 M boron triboromide in methylene choloride solution. The reaction solution was allowed to stir for 1 h. The mixture was warmed to room temperature and stirred for another 3 h. The mixture was concentrated and extracted with Et_2O, and the extract was washed with water. The organic layer was washed with 2N sodium hydroxide solution and the resulting basic solution was neutralized with 2N HCl aq. solution. Then the product was obtained by extraction with CH_2Cl_2. ^{1}H NMR (CD_3OD, 300 MHz) δ 8.31 (1H), 8.14 (1H, dd, *J* = 2.7, 9 Hz), 6.86 (1H, d, *J* = 9.2 Hz). ^{13}C NMR (CD_3OD) 142.0, 132.9, 128.6, 116.5, 103.0. ESI-MS: $C_6H_6BNO_5$, Calcd. for 3M-1, 548.1, Found 548.1.

2-Methoxy-3, 5-nitro-phenylboronic acid (13). To the stirring mixture of nitric acid (1.5 mL) and sulfuric acid (1.5 mL) cooled in acetonitrile-dry ice bath was added slowly *o*-methoxyphenylboronic acid **12** (0.1 g, 6.6 mmol) over 20 min and stirred for 3 h in a salt-ice solution while the temperature was kept below –10 °C. A brown solid was seen during the reaction. The reaction mixture was poured onto 5 g of ice and kept in

ice-water bath for 3 h. The brown solid precipitated. The solid was filtered and washed with ice-cold water and dried under vacuum. The crude product was purified by silica gel column, eluting with EtOAc/CH_2Cl_2 (1:20), to afford the boronic acid **7** (30%). ^{1}H NMR (d_6-DMSO, 400MHz) δ 8.53 (1H, d, *J* = 3.0 Hz), 7.60 (1H, d, *J* = 3.0 Hz), 4.08 (3H, s). ^{13}C NMR (d_6-DMSO): 156.6, 139.6, 138.4, 129.4, 121.1, 115.1, 58.0.

2-(2-Methoxy-3, 5-dinitro-phenyl)-5,5-dimethyl-[1,3,2]dioxaborinane (14). The mixture of compound **13** (240 mg, 1.22 mmol) and 2, 2-dimethyl-propan-1, 3 –diol (145.4 mg, 1.23 mmol) was refluxed in toluene (20 mL) using a Dean-Stark trap to remove water overnight. The toluene was evaporated and the solid residue was extracted with CH_2Cl_2 (20 mL). The combined organic extracts were washed with water (2 × 30 mL) and brine (20 mL), dried over $MgSO_4$, concentrated and dried under vacuum. ^{1}H NMR ($CDCl_3$, 300 MHz) 8.94 (1H, d, *J* = 2.4 Hz), 8.63 (1H, d, *J* = 2.4 Hz), 4.05 (3H, s), 3.85 (4H, s), 1.09 (6H, s). Anal Calcd for $C_{12}H_{15}BN_2O_9$: C, 46.48; H, 4.88; N, 9.03. Found: C, 46.40, H, 4.90, N, 8.89.

.

2-(5,5-Dimethyl-[1,3,2]dioxaborinan-2-yl)-4,6-dinitro-phenol (15). The procedure was the same as the preparation of **14** from **13**. ^{1}H NMR ($CDCl_3$, 400 MHz) δ 10.80 (1H, s), 8.95 (1H, d *J* = 2.4 Hz,), 8.77 (1H, d, *J* = 2.4 Hz), 3.89 (4H, s), 1.09 (6H, s). ^{13}C NMR (CD_3OD) 162.2, 139.8, 136.6, 124.6, 73.1, 32.3, 21.9. Anal Calcd for $C_{11}H_{13}BN_2O_7$: C, 44.63; H, 4.43; N, 9.46. Found: C, 44.56; H, 4.47; N, 9.46.

References

(1) Dennis, J. W. Changes in Glycosylation Associated with Malignant Transformation and Tumor Progression; CRC press: Boca Raton, 1992.

(2) Eggert, H.; Frederiksen, J.; Morin, C.; Norrid, J. C. *J. Org. Chem.* **1999**, *64*, 3846-3852.

(3) Cabell, L. A.; Monahan, M.-K.; Anslyn, E. V. *Tetrahedron Lett.* **1999**, *40*, 7753-7756.

(4) Lavigne, J. J.; Anslyn, E. V. Angew. *Chem. Int. Ed. Engl.* **1999**, *38*, 3666-3669.

(5) Norrild, J. C.; Eggert, H. *J. Am. Chem. Soc.* **1995**, *117*, 1479-1484.

(6) Norrild, J. C.; Eggert, H. *J. Chem. Soc., Perkin Trans. 2* **1996**, 2583-2588.

(7) James, T. D.; Sandanayake, K. R. A. S.; Shinkai, S. *Nature (London)* **1995**, *374*, 345-347.

(8) James, T. D.; Shinmori, H.; Shinkai, S. *Chem. Commun.* **1997**, 71-72.

(9) Sandanayake, K. R. A. S.; Nakashima, K.; Shinkai, S. *Chem. Commun.* **1994**, 1621-1622.

(10) Wiskur, S.; Lavigne, J. J.; Ait-Haddou, H.; Lynch, V.; Chiu, Y. H.; Canary, J. W.; Anslyn, E. V. *Org. Lett*. **2001**, *3*, 1311-1314.

(11) Wang, B. *Curr. Org. Chem.* **2002**, *6*, 1285-1317.

(12) Paugam, M.-F.; Bien, J. T.; Smith, B. D.; Chrisstoffels, L. A. J.; de Jong, F.; Reinhoudt, D. N. *J. Am. Chem. Soc.* **1996**, *118*, 9820-9825.

(13) Westmark, P. R.; Gardiner, S. J.; Smith, B. D. *J. Am. Chem. Soc.* **1996**, *118*, 11093-11100.

(14) Westmark, P. R.; Gardiner, S. J.; Smith, B. D.; Karpa, M. J.; Griffin, G.; Duggan, P. J. *Tetrahedron Lett.* **1996**, *37*, 6303-6306.

(15) Smith, B. D.; Gardiner, S. J.; Munro, T. A.; Paugam, M.-F.; Riggs, J. A. *J. Incl. Phenom. Mol. Recogn. Chem.* **1998**, *32*, 121-131.

(16) Gardiner, S. J.; Smith, B. D.; Duggan, P. J.; Karpa, M. J.; Griffin, G. *Tetrahedron* **1999**, *55*, 2857-2864.

(17) Draffin, S. P.; Duggan, P. J.; Duggan, S. A. M. *Org. Lett.* **2001**, *3*, 917-920.

(18) Riggs, J. A.; Hossler, K. A.; Smith, B. D. *Tetrahedron Lett.* **1996**, *37*, 6303-6306.

(19) Soundararajan, S.; Badawi, M.; Kohlrust, C. M.; Hageman, J. H. *Anal. Biochem.* **1989**, *178*, 125-134.

(20) Singhal, R. P.; Ramamurthy, B.; Govindraj, N.; Sarwar, Y. J. *Chromatography* **1991**, *543*, 17-38.

(21) Psotova, J.; Janiczek, O. Chem. Listy **1995**, 89, 641-648.

(22) Liu, X. C.; Hubbard, J. L.; Scouten, W. H. *Organomet. Chem.* **1995**, *493*, 91-94.

(23) Wulff, G.; Poll, H.; Minarik, M. J. *Liq. Chromatography* **1986**, *9*, 385-405.

(24) Wulff, G.; Vesper, W. J. *Chromatography* **1978**, *167*, 171-186.

(25) Yang, W.; Gao, S.; Gao, X.; Karnati, V. R.; Ni, W.; Wang, B.; Hooks, W. B.; Carson, J.; Weston, B. W. *Bioorg. Med. Chem. Lett* **2002**, *12*, 2175-2177.

(26) Springsteen, G.; Wang, B. *Chem. Commun* **2001**, 1608-1609.

(27) Springsteen, G.; Wang, B. *Tetrahedron* **2002**, *58*, 5291-5300.

(28) Lorand, J. P.; Edwards, J. O. *J. Org. Chem.* **1959**, *24*, 769-774.

(29) Yoon, J.; Czarnik, A. W. *J. Am. Chem. Soc.* **1992**, *114*, 5874-5875.

(30) James, T. D.; Linnane, P.; Shinkai, S. *Chem. Commun* **1996**, 281-288.

(31) Yamamoto, M.; Takeuchi, M.; Shinkai, S. *Tetrahedron* **1998**, *54*, 3125-3140.

(32) DiCesare, N.; Lakowicz, J. R. *Chem. Commun* **2001**, 2022-2023.

(33) DiCesare, N.; Lakowicz, J. R. *Tetrahedron Lett.* **2001**, *42*, 9105-9108.

(34) DiCesare, N.; Lakowicz, J. R. *Anal. Biochem.* **2002**, *301*, 111-116.

(35) DiCesare, N.; Lakowicz, J. R. *Tetrahedron Lett.* **2002**, *43*, 2615-2618.

(36) Ward, C. J.; Patel, P.; James, T. D. *J. Chem. Soc., Perkin Trans. 1* **2002**, 462-470.

(37) Cooper, C.; Spencer, N.; James, T. D. *Chem. Commun* **1998**, 1365-1366.

(38) Cooper, C.; James, T. D. *Chem. Lett.* **1998**, 883-884.

(39) Arimori, S.; Bosch, L. I.; Ward, C. J.; James, T. D. *Tetrahedron Lett.* **2001**, *42*, 4553-4555.

(40) Cao, H.; Diaz, D. I.; DiCesare, N.; Lakowicz, J. R.; Heagy, M. D. *Org. Lett.* **2002**, *4*, 1503-1505.

(41) Adhikiri, D. P.; Heagy, M. D. *Tetrahedron Lett.* **1999**, *40*, 7893-7896.

(42) James, T. D.; Samankumara, K. R. A.; Iguchi, R.; Shinkai, S. *J. Am. Chem. Soc.* **1995**, *117*, 8982-8987.

(43) James, T. D.; Sandanayake, K. R. A. S.; Shinkai, S. *Chem. Commun* **1994**, 477-478.

(44) Davis, C. J.; Lewis, P. T.; McCarroll, M. E.; Read, M. W.; Cueto, R.; Strongin, R. M. *Org. Lett.* **1999**, *1*, 331

(45) Ward, C. J.; Patel, P.; James, T. D. *Org. Lett.* **2002**, *4*, 477-479.

(46) DiCesare, N.; Lakowicz, J. R. *Org. Lett.* **2001**, *3*, 3891-3893.

(47) Kirmura, T.; Takeuchi, M.; Nagasaki, T.; Shinkai, S. *Tetrahedron Lett.* **1994**, *53*, 444-451.

(48) Dodgson, C.; Rose, A.; Spencer, B. *Biochem. J.* **1953**, *53*, 444-451.

(49) Nistor, C.; Rose, A.; Wollenberger, U.; Pfeiffer, D.; Emneus, J. *Analyst* **2002**, *127*, 1076-1081.

(50) Ishiyama, T.; Murata, M.; Miyaura, N. *J. Org. Chem*. **1995**, *60*, 7508-7510.

(51) Falck, J. R.; Bondlela, M.; Venkataraman, S. K.; Srinivas, D. *J. Org. Chem.* **2001**, *66*, 7148-7150.

(52) Salzbrunn, S.; Simon, J.; Prakash, G. K. S.; Petasis, N. A.; Olah, G. A. *Synlett* **2000**, *10*, 1485-1487.

(53) Nöth, H.; Wrackmeyer, B. In NMR Basic Principles and Progress Series 14; Diehl, P., Fluck, E., Kosfeld, R., Eds.; Springer-Verlag: Berlin, 1978, p 5-14, 287.

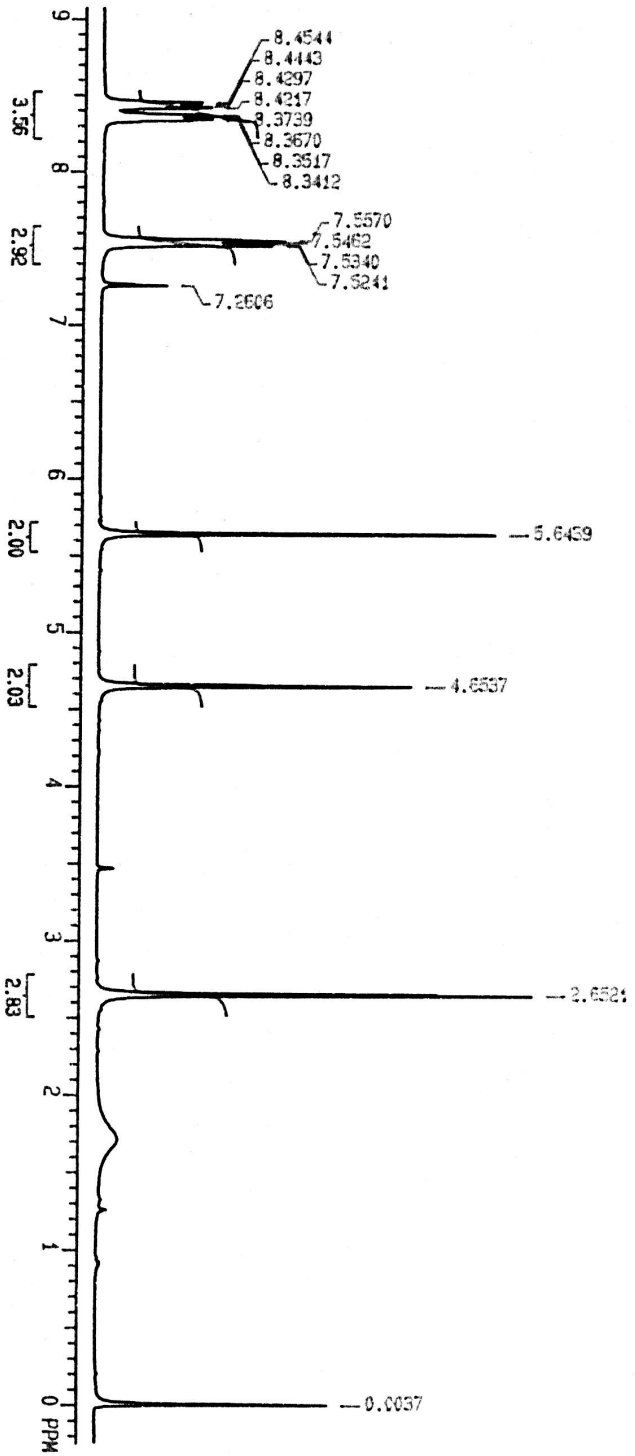

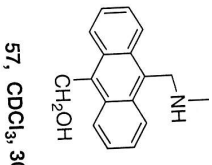

57, $CDCl_3$, 300 MHz

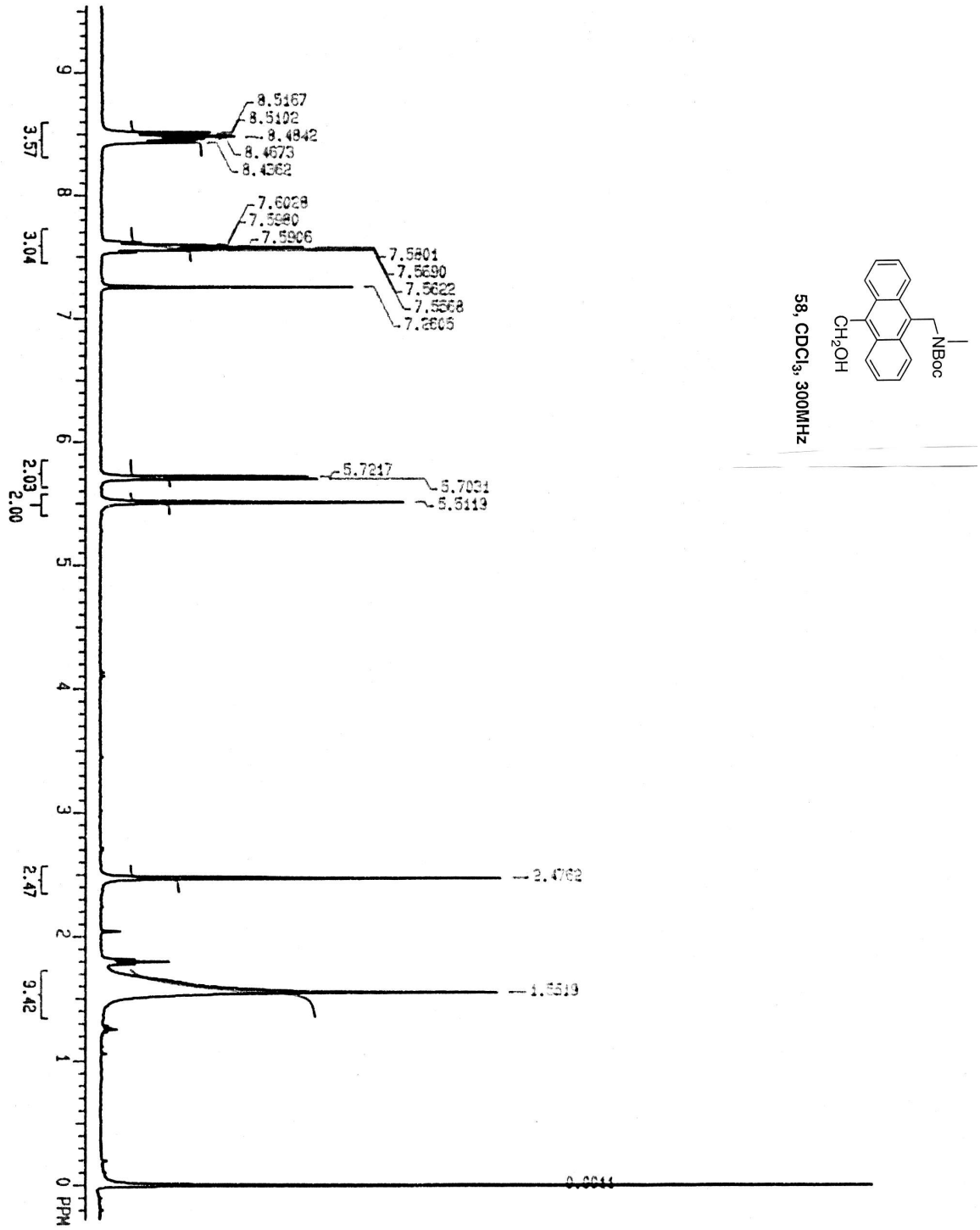
8.5167
8.5102
8.4842
8.4673
8.4362
7.6028
7.5980
7.5906
7.5801
7.5690
7.5622
7.5568
7.2605
5.7217
5.7031
5.5119
2.4762
1.5619
0.0011
3.57
3.04
2.03
2.00
2.47
9.42
0 PPM
58, CDCl3, 300MHz
CH2OH
NBoc

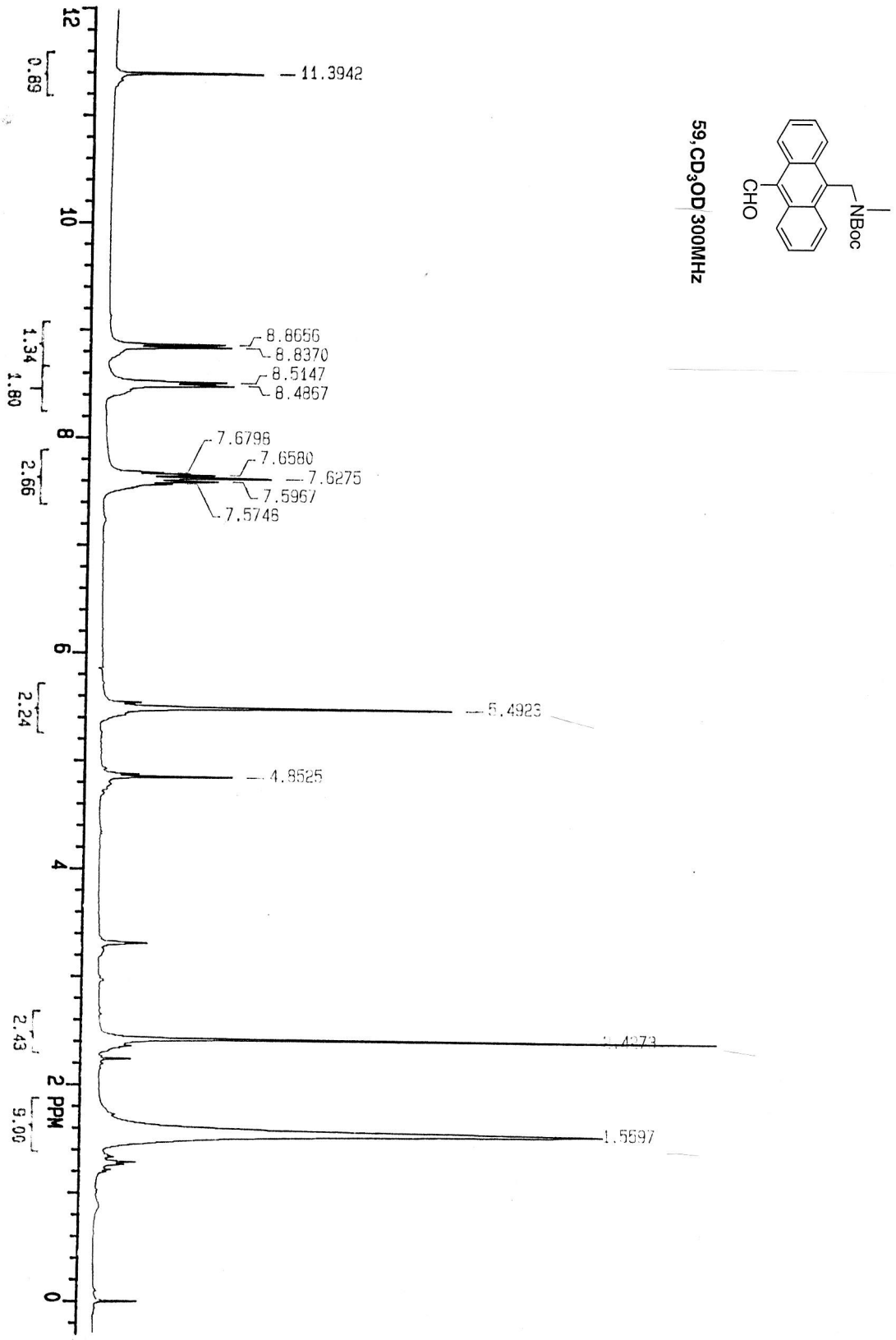
59,CD3OD 300MHz
CHO
NBoc
11.3942
8.8656
8.8370
8.5147
8.4867
7.6798
7.6580
7.6275
7.5967
7.5746
5.4923
4.8525
1.5597
PPM

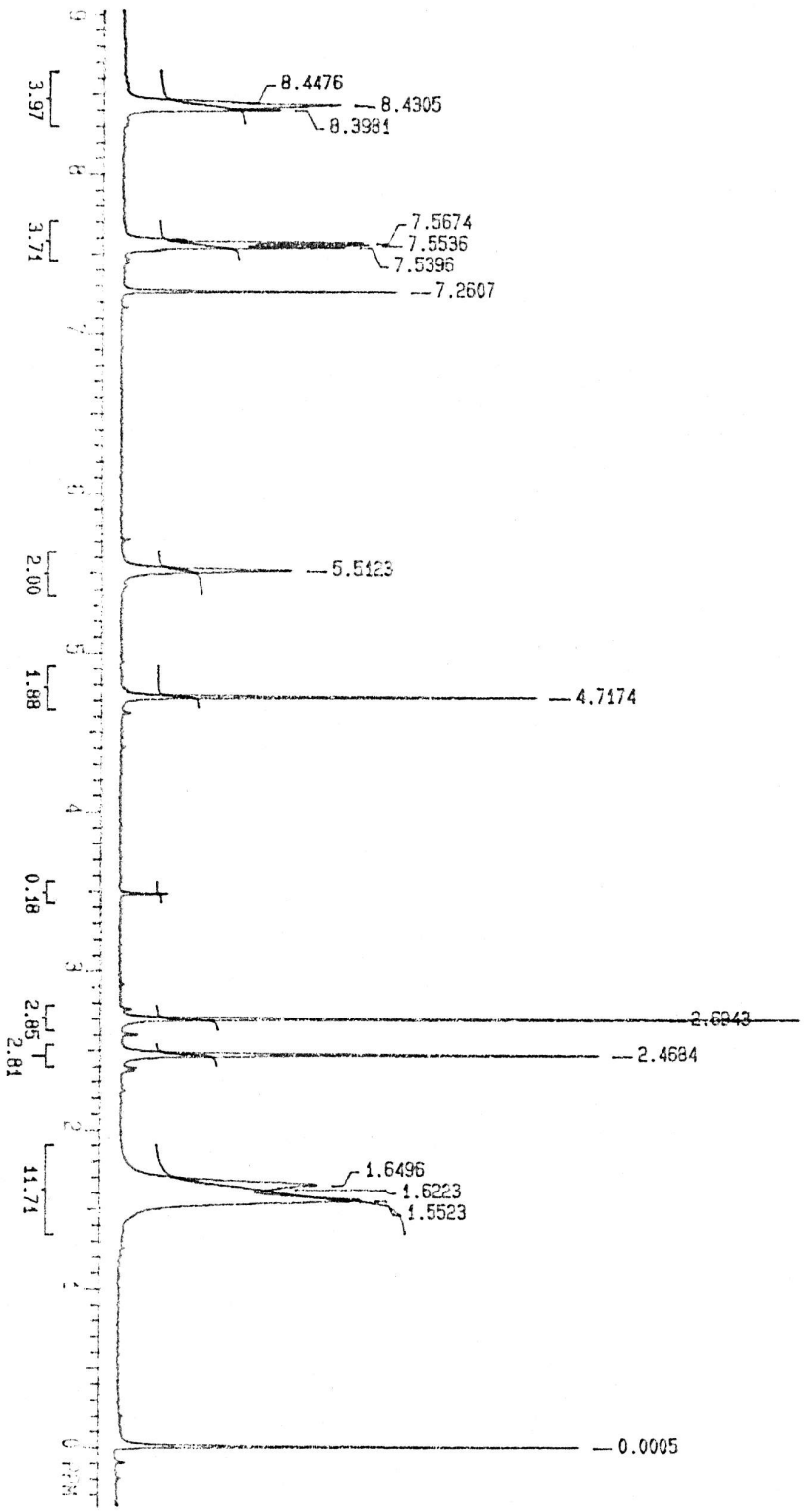

60, $CDCl_3$, 300MHz

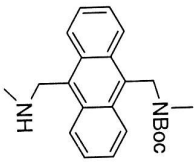

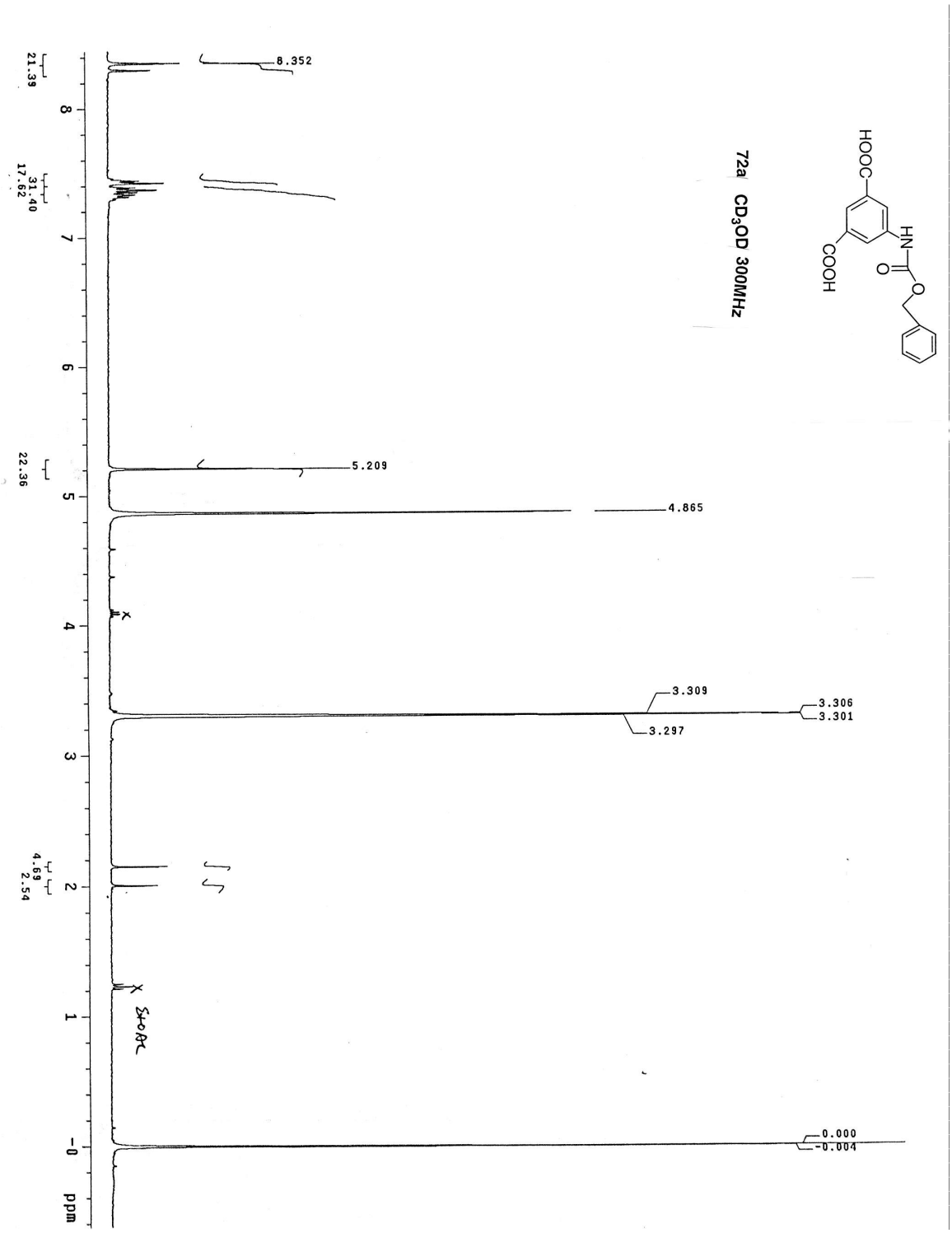
72a CD3OD 300MHz
HOOC
COOH
HN
O
O
8.352
5.209
4.865
3.309
3.306
3.301
3.297
0.000
-0.004
21.39
31.40
17.62
22.36
4.69
2.54
ppm

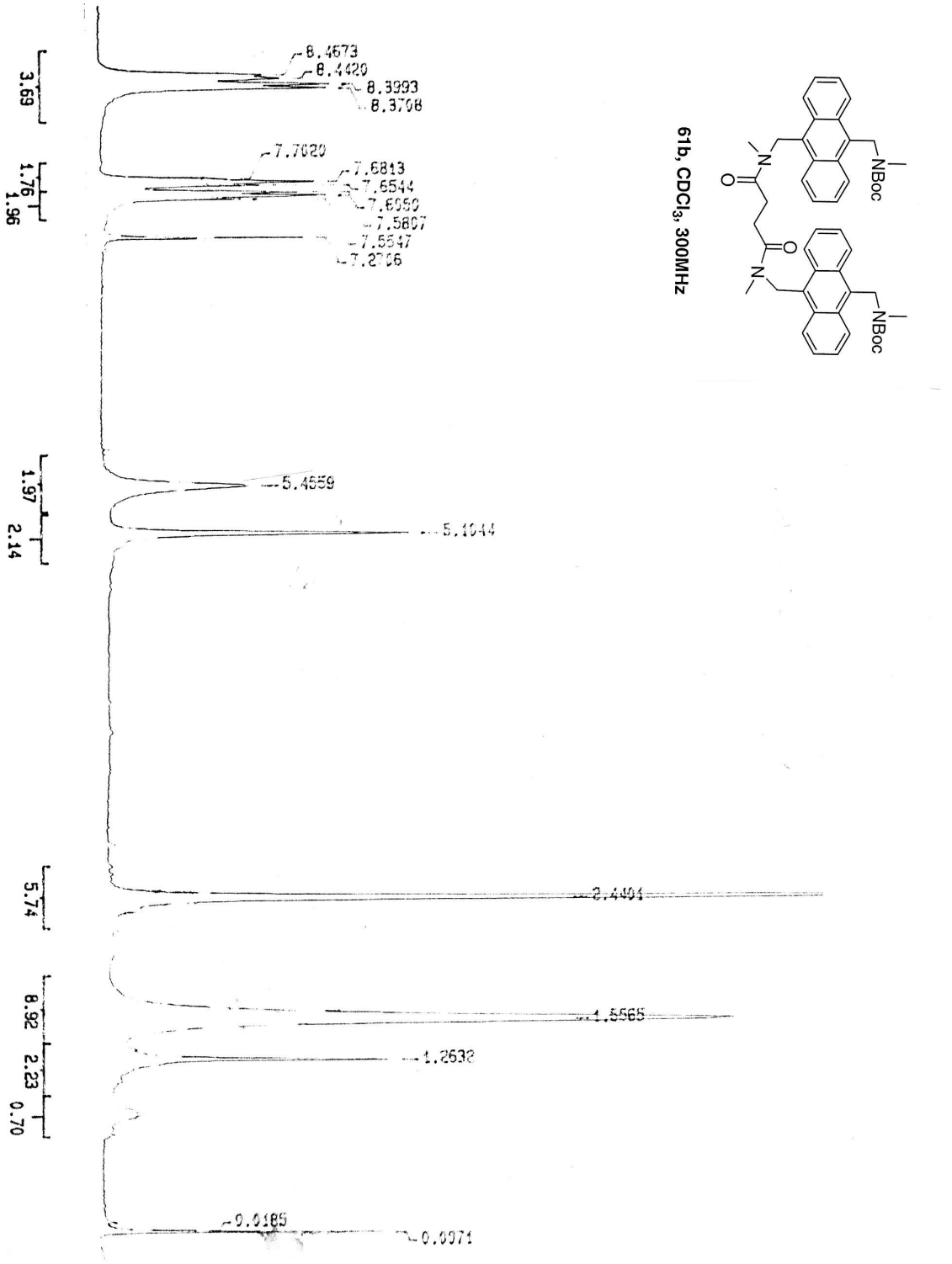
61b, CDCl3, 300MHz
NBoc
NBoc
8.4673
8.4420
8.3993
8.3798
7.7020
7.6813
7.6544
7.6059
7.5807
7.5547
7.2706
5.4659
5.1044
2.4491
1.5565
1.2638
0.0185
0.0071
3.69
1.76
1.96
1.97
2.14
5.74
8.92
2.23
0.70

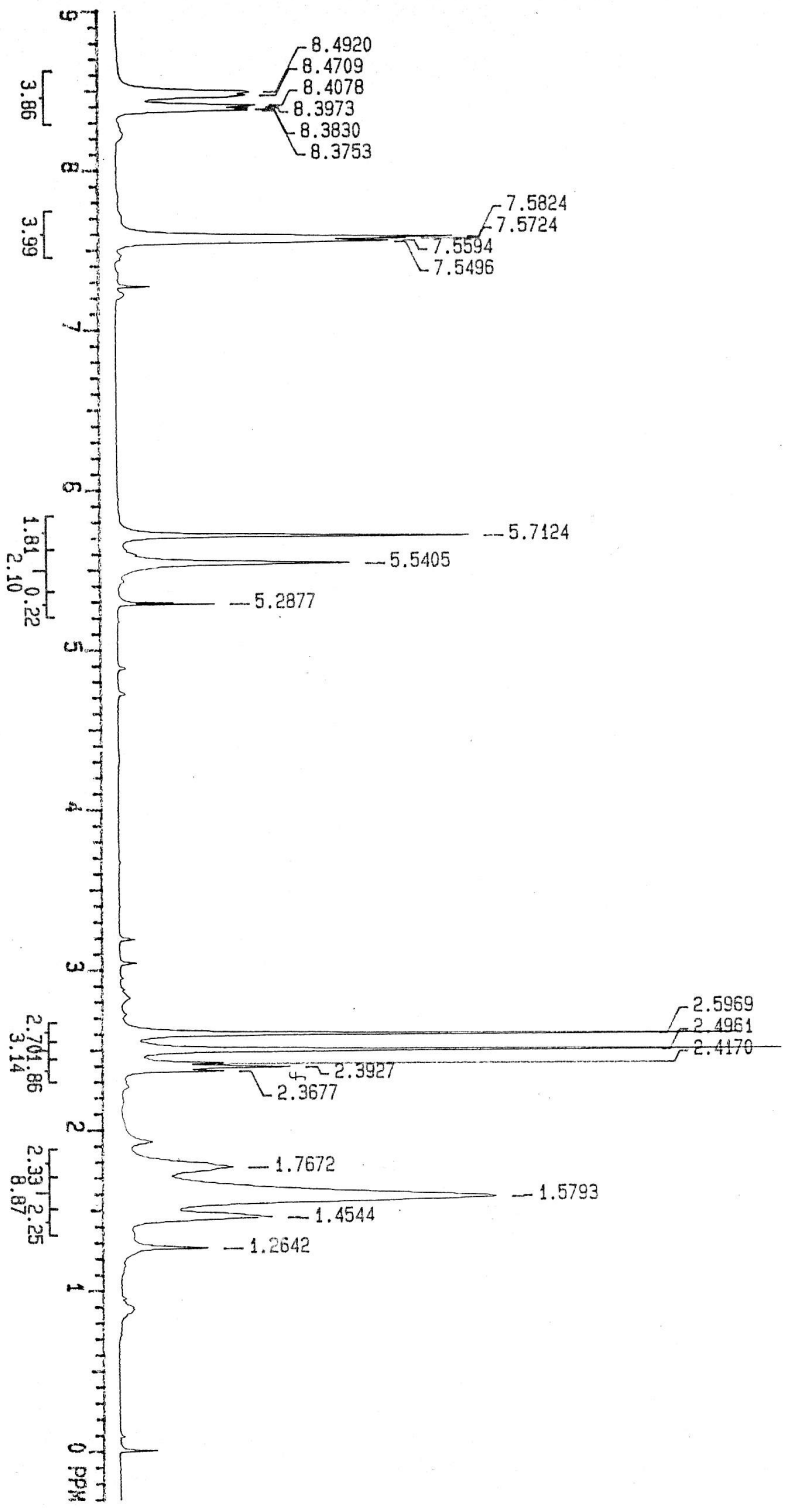

62b, $CDCl_3$, 300MHz

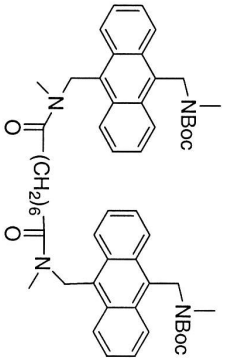

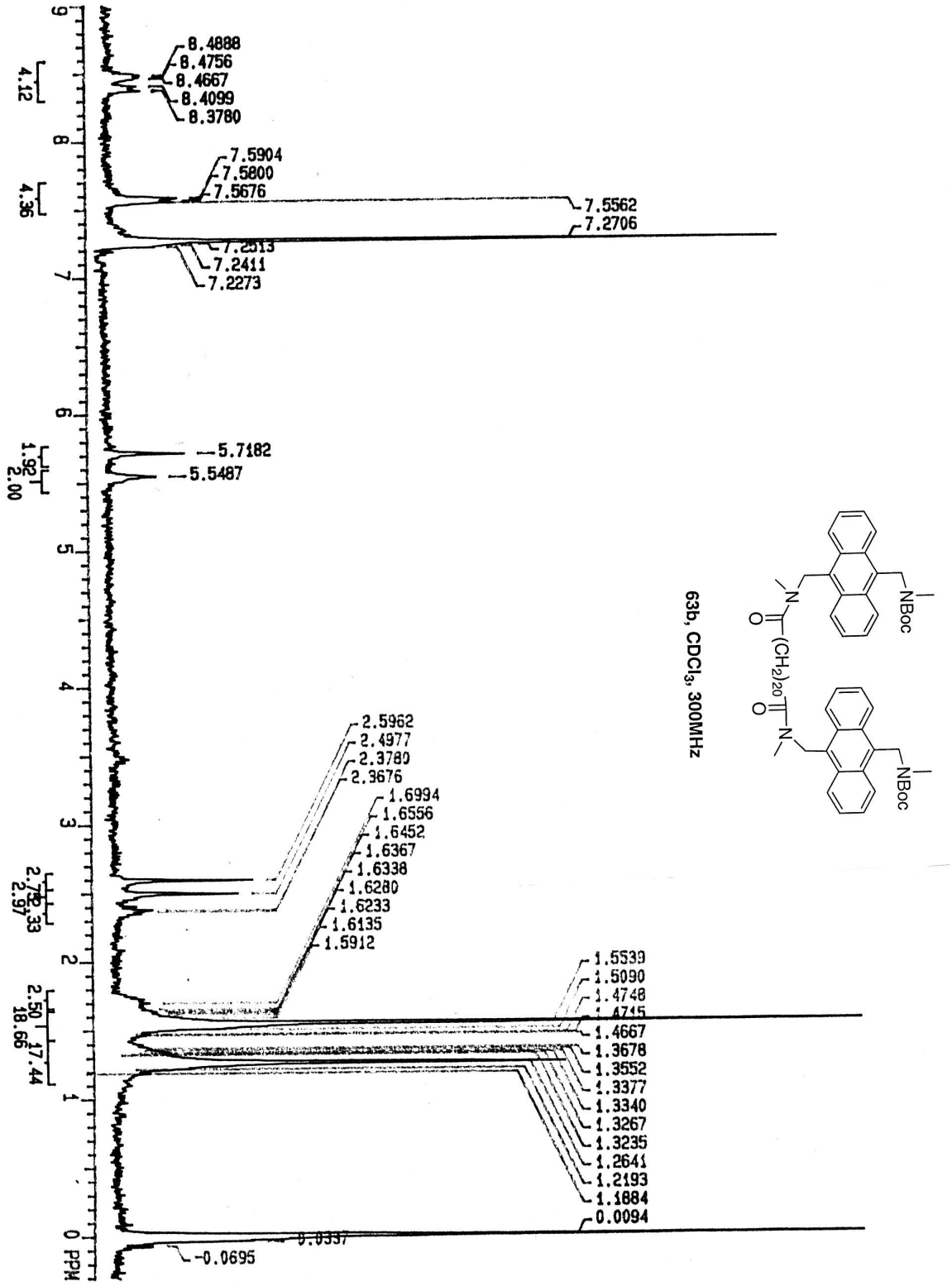
8.4888
8.4756
8.4667
8.4099
8.3780
7.5904
7.5800
7.5676
7.5562
7.2706
7.2513
7.2411
7.2273
5.7182
5.5487
2.5962
2.4977
2.3780
2.3676
1.6994
1.6556
1.6452
1.6367
1.6338
1.6280
1.6233
1.6135
1.5912
1.5539
1.5090
1.4748
1.4667
1.3678
1.3552
1.3377
1.3340
1.3267
1.3235
1.2641
1.2193
1.1884
0.0094
0.0337
-0.0695
4.12
4.36
1.92
2.00
2.78
2.97
2.33
2.50
18.66
17.44
PPM
63b, CDCl3, 300MHz
NBoc
(CH2)20
NBoc

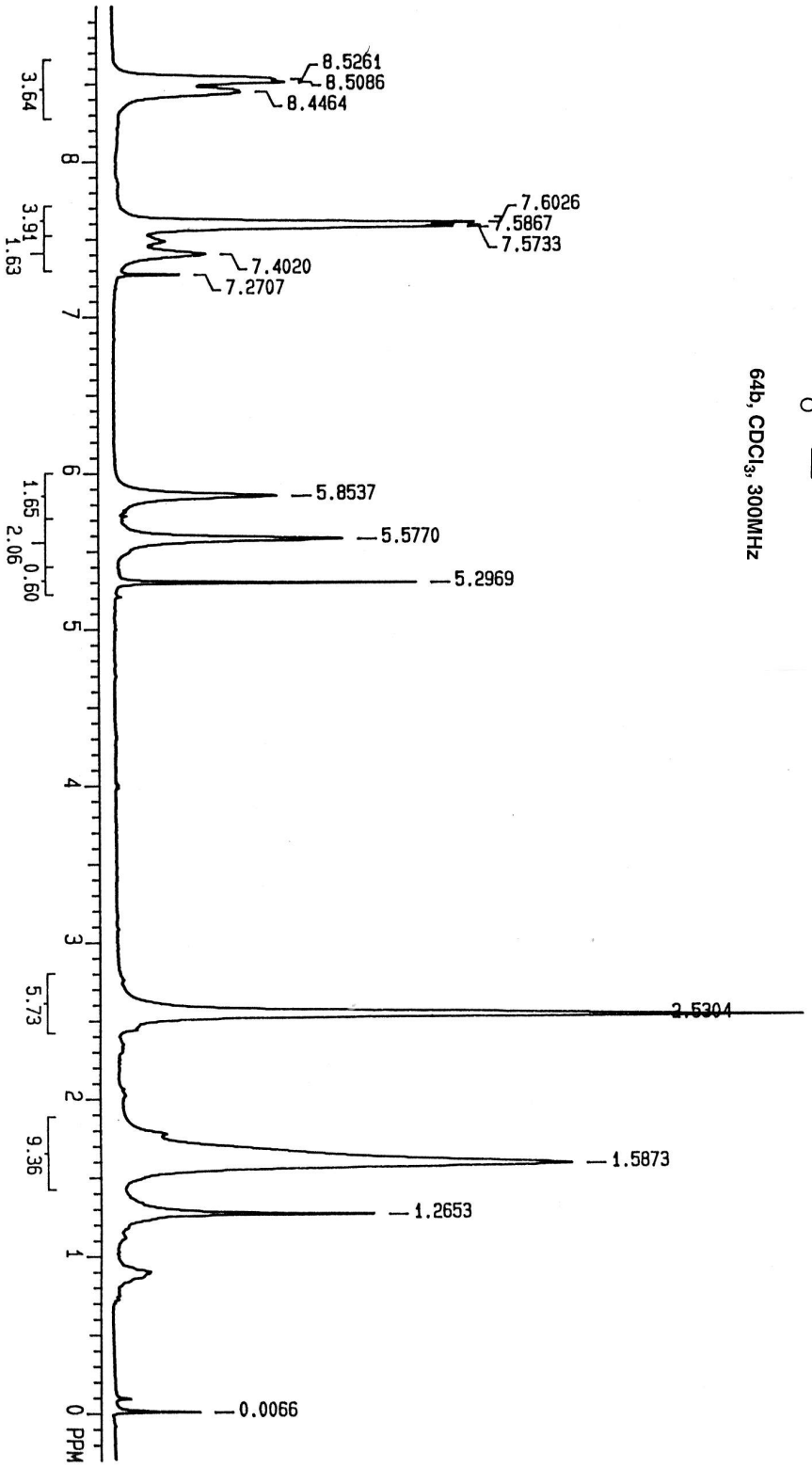
8.5261
8.5086
8.4464
7.6026
7.5867
7.5733
7.4020
7.2707
5.8537
5.5770
5.2969
2.5304
1.5873
1.2653
0.0066
PPM
3.64
3.91
1.63
1.65
2.06
0.60
5.73
9.36
64b, CDCl3, 300MHz
NBoc
NBoc

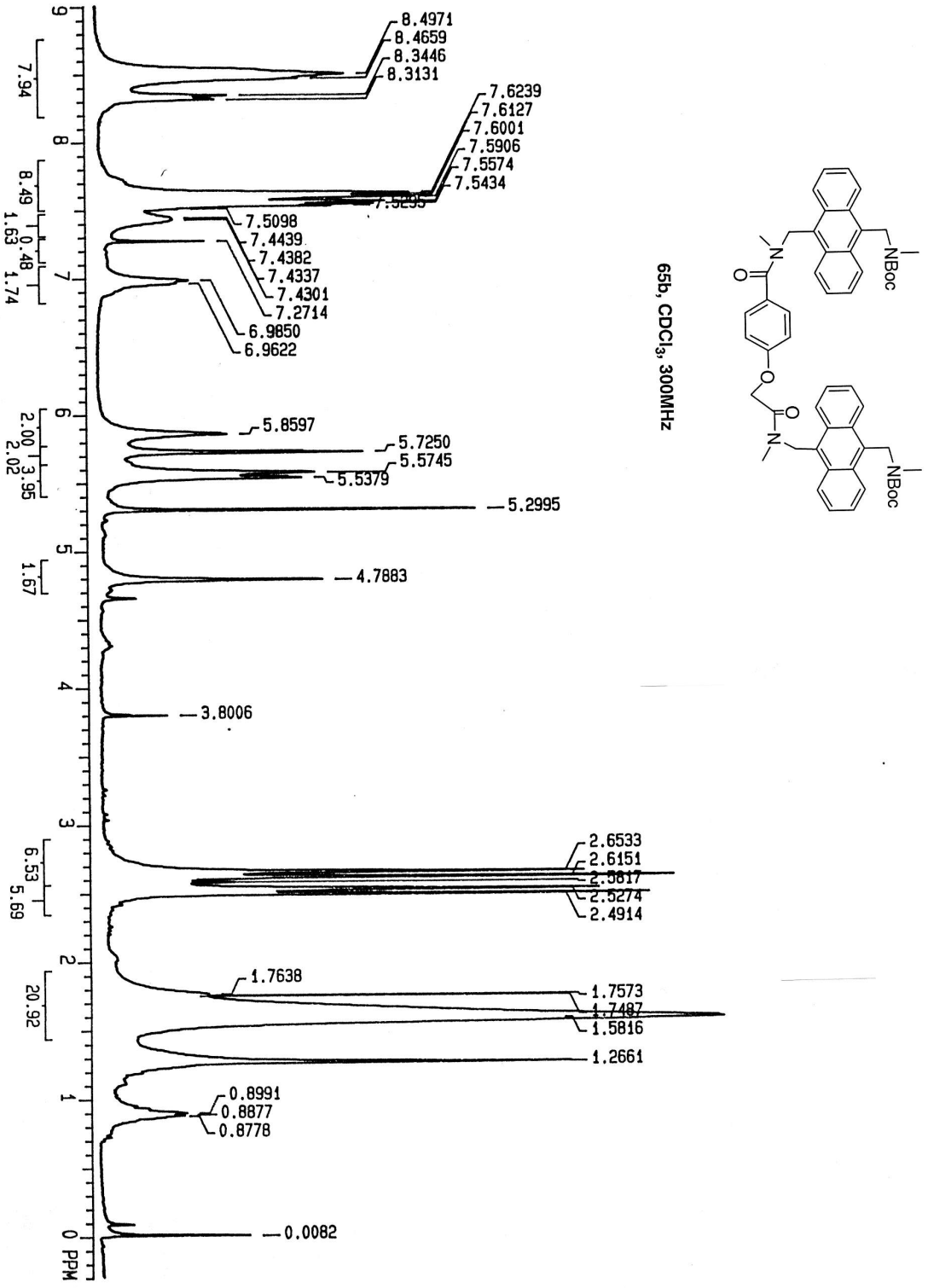
8.4971
8.4659
8.3446
8.3131
7.6239
7.6127
7.6001
7.5906
7.5574
7.5434
7.5295
7.5098
7.4439
7.4382
7.4337
7.4301
7.2714
6.9850
6.9622
5.8597
5.7250
5.5745
5.5379
5.2995
4.7883
3.8006
2.6533
2.6151
2.5817
2.5274
2.4914
1.7638
1.7573
1.7487
1.5816
1.2661
0.8991
0.8877
0.8778
0.0082
7.94
8.49
1.63
0.48
1.74
2.00
2.02
3.95
1.67
6.53
5.69
20.92
PPM
65b, CDCl3, 300MHz
NBoc
NBoc

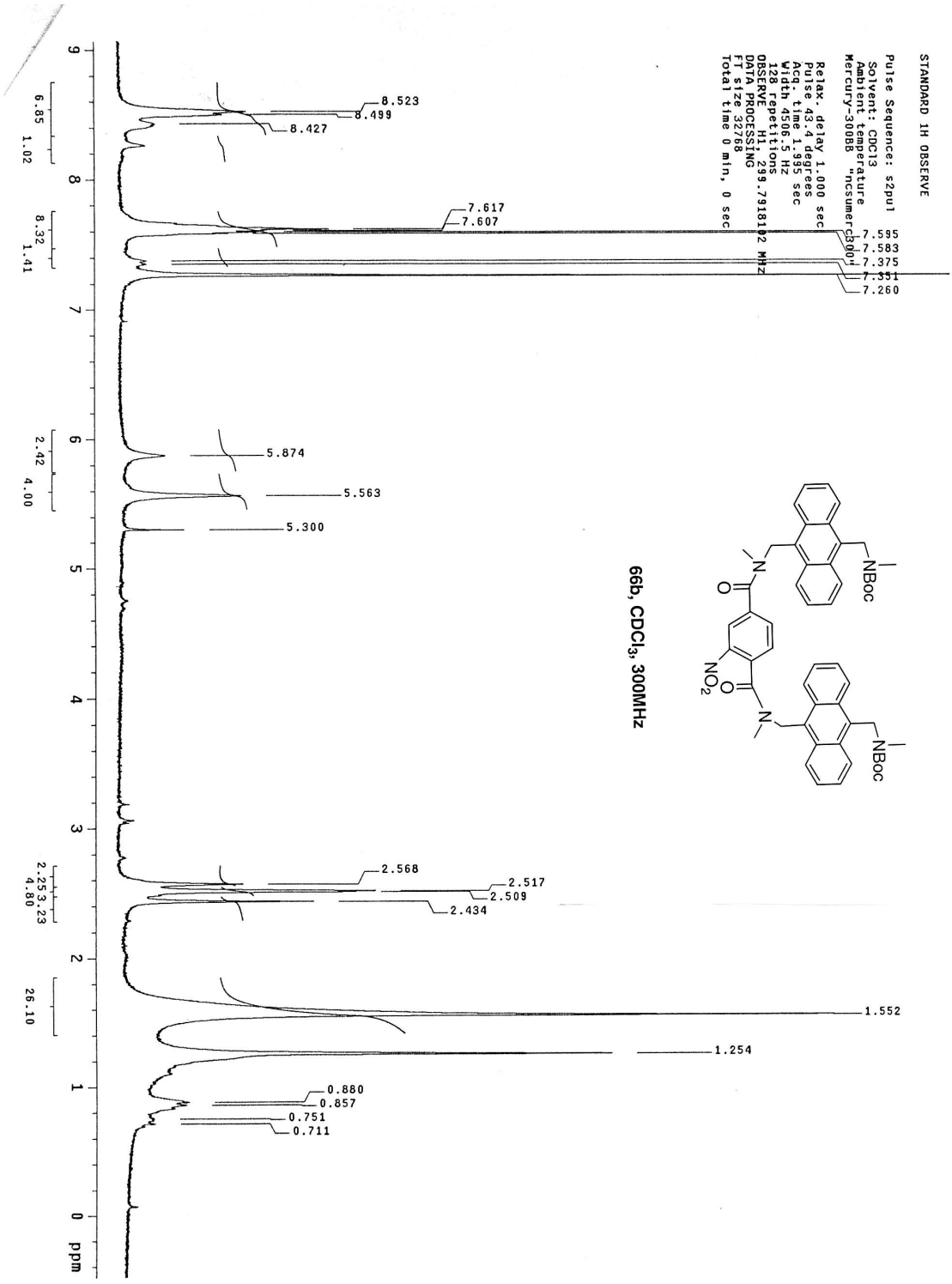
STANDARD 1H OBSERVE
Pulse Sequence: s2pul
Solvent: CDCl3
Ambient temperature
Mercury-300BB "ncsumerc300"
Relax. delay 1.000 sec
Pulse 43.4 degrees
Acq. time 1.995 sec
Width 4506.5 Hz
128 repetitions
OBSERVE H1, 299.7918102 MHz
DATA PROCESSING
FT size 32768
Total time 0 min, 0 sec
8.523
8.499
8.427
7.617
7.607
7.595
7.583
7.375
7.351
7.260
5.874
5.563
5.300
2.568
2.517
2.509
2.434
1.552
1.254
0.880
0.857
0.751
0.711
6.85
1.02
8.32
1.41
2.42
4.00
2.25
3.23
4.80
26.10
ppm
66b, CDCl3, 300MHz
NBoc
NBoc
NO2

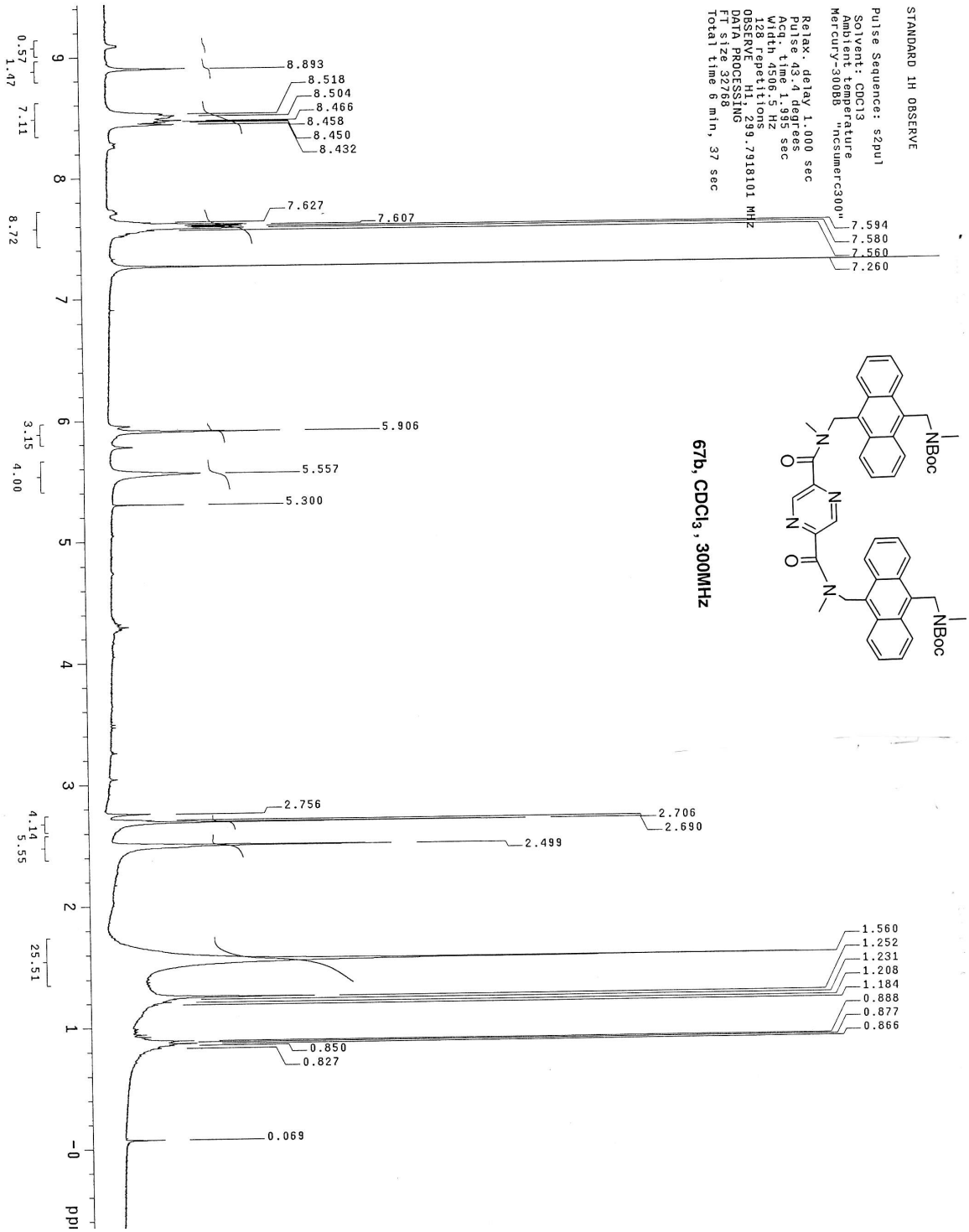
STANDARD 1H OBSERVE
Pulse Sequence: s2pul
Solvent: CDCl3
Ambient temperature
Mercury-300BB "ncsumerc300"
Relax. delay 1.000 sec
Pulse 43.4 degrees
Acq. time 1.995 sec
Width 4506.5 Hz
128 repetitions
OBSERVE H1, 299.7918101 MHz
DATA PROCESSING
FT size 32768
Total time 6 min, 37 sec
67b, CDCl3, 300MHz
NBoc
NBoc
8.893
8.518
8.504
8.466
8.458
8.450
8.432
7.627
7.607
7.594
7.580
7.560
7.260
5.906
5.557
5.300
2.756
2.706
2.690
2.499
1.560
1.252
1.231
1.208
1.184
0.888
0.877
0.866
0.850
0.827
0.069
0.57
1.47
7.11
8.72
3.15
4.00
4.14
5.55
25.51
ppm

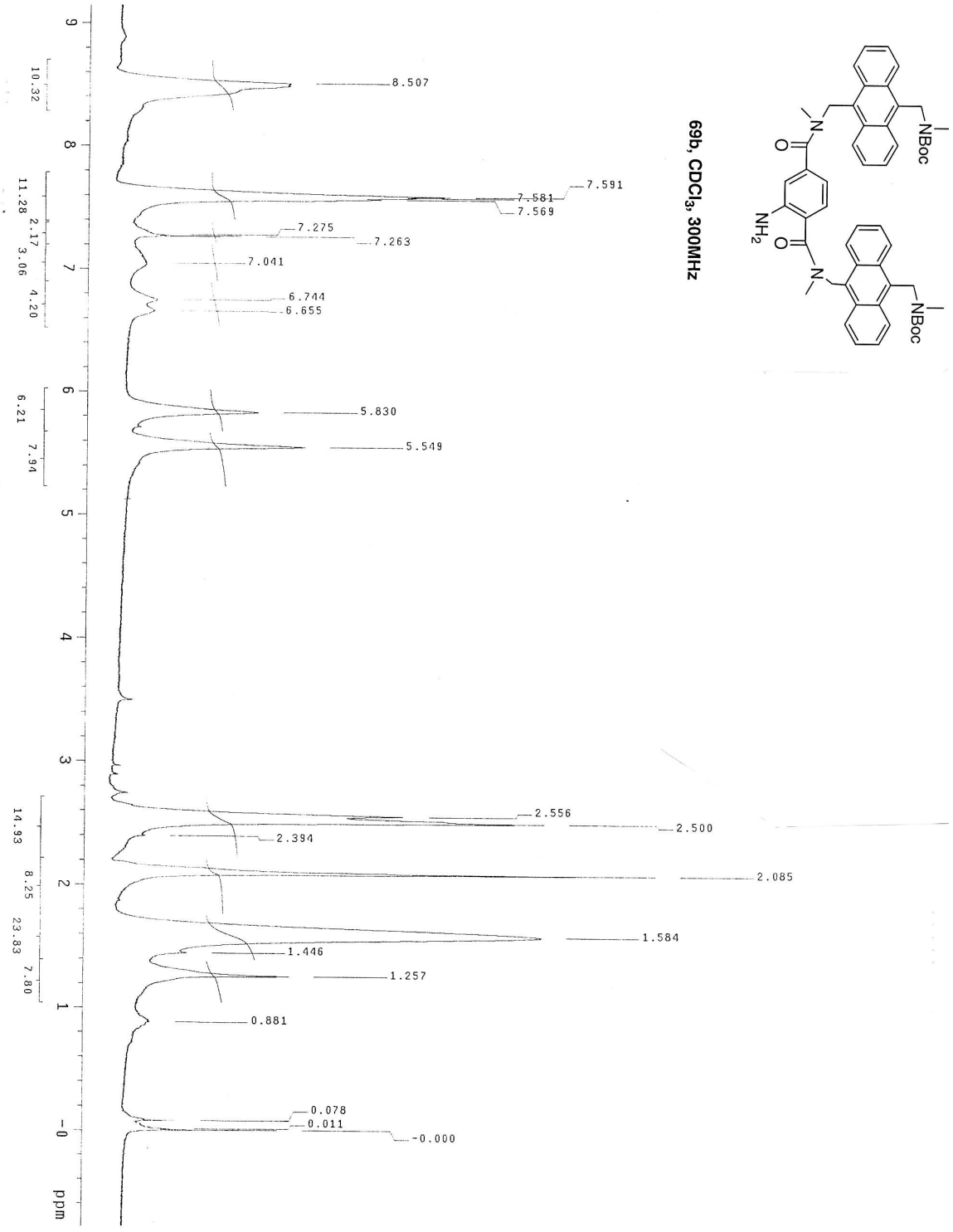
69b, CDCl3, 300MHz
NBoc
NH2
O
N
8.507
7.591
7.581
7.569
7.275
7.263
7.041
6.744
6.655
5.830
5.549
2.556
2.500
2.394
2.085
1.584
1.446
1.257
0.881
0.078
0.011
-0.000
10.32
11.28
2.17
3.06
4.20
6.21
7.94
14.93
8.25
23.83
7.80
ppm

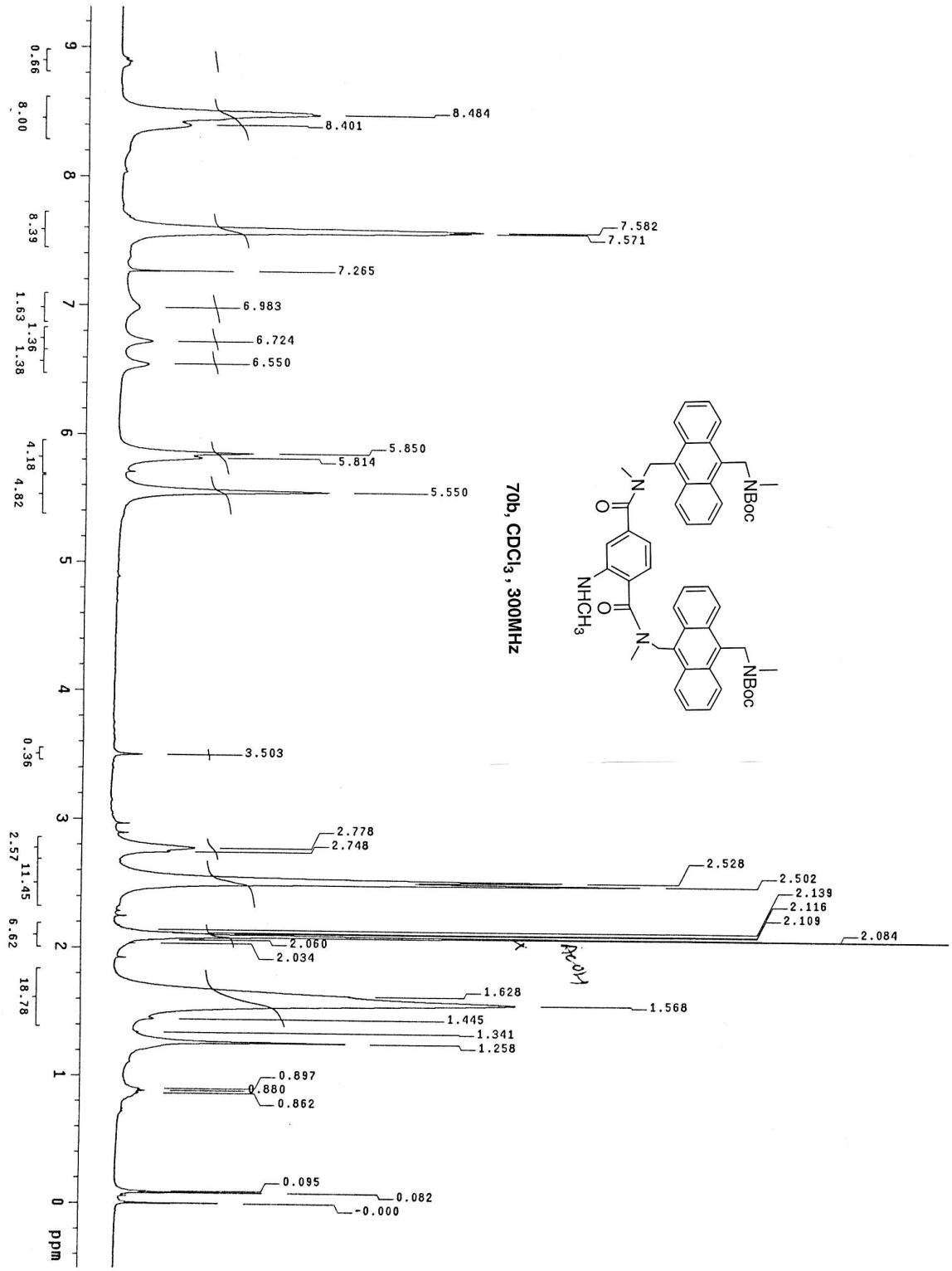
8.484
8.401
7.582
7.571
7.265
6.983
6.724
6.550
5.850
5.814
5.550
3.503
2.778
2.748
2.528
2.502
2.139
2.116
2.109
2.084
2.060
2.034
1.628
1.568
1.445
1.341
1.258
0.897
0.880
0.862
0.095
0.082
-0.000
ppm
0.66
8.00
8.39
1.63
1.36
1.38
4.18
4.82
0.36
2.57
11.45
6.62
18.78
70b, CDCl3, 300MHz
NHCH3
NBoc
NBoc

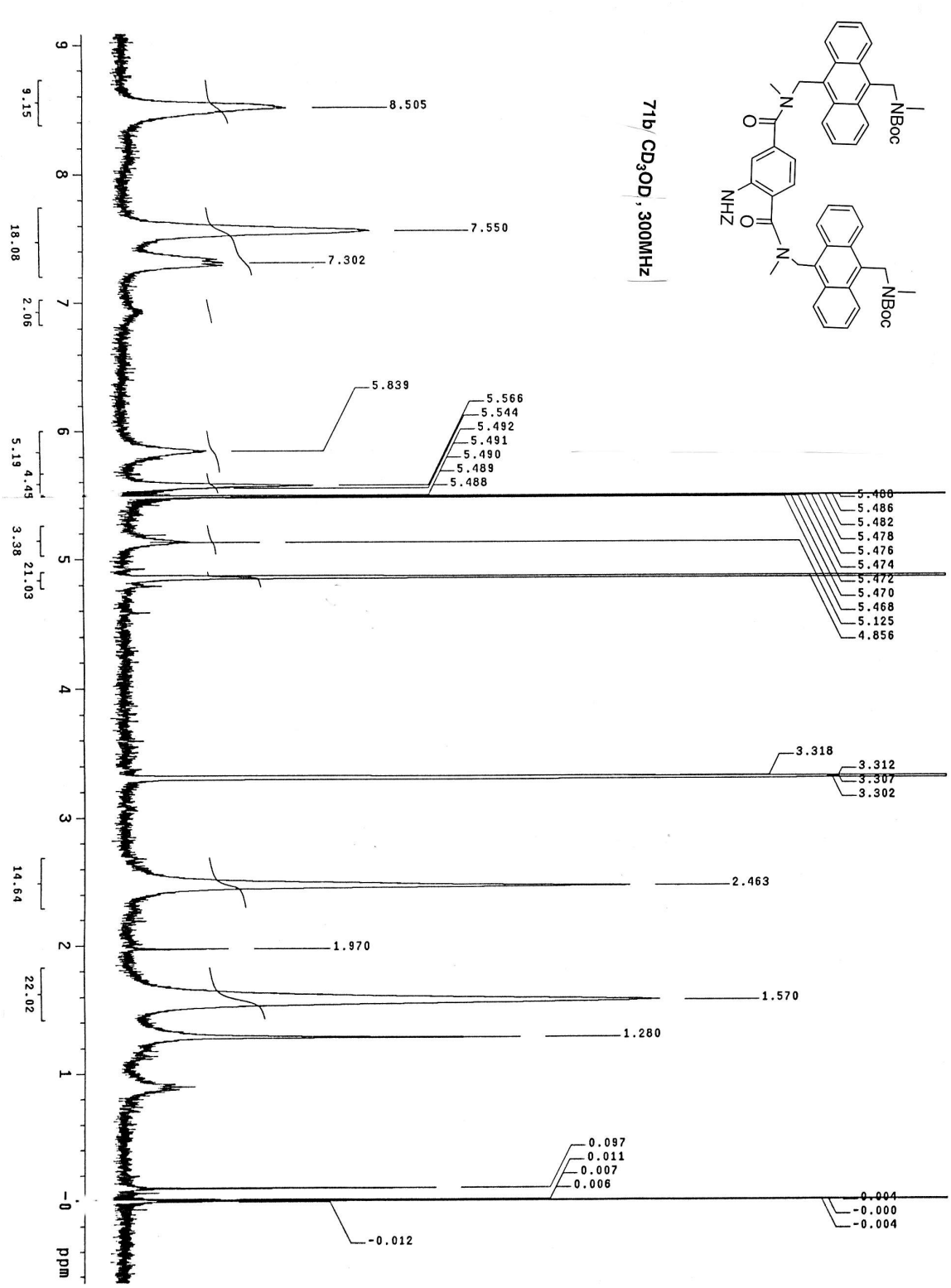
71b/ CD3OD, 300MHz
NHZ
NBoc
NBoc
8.505
7.550
7.302
5.839
5.566
5.544
5.492
5.491
5.490
5.489
5.488
5.486
5.482
5.478
5.476
5.474
5.472
5.470
5.468
5.125
4.856
3.318
3.312
3.307
3.302
2.463
1.970
1.570
1.280
0.097
0.011
0.007
0.006
-0.000
-0.004
-0.012
9.15
18.08
2.06
5.19
4.45
3.38
21.03
14.64
22.02
ppm

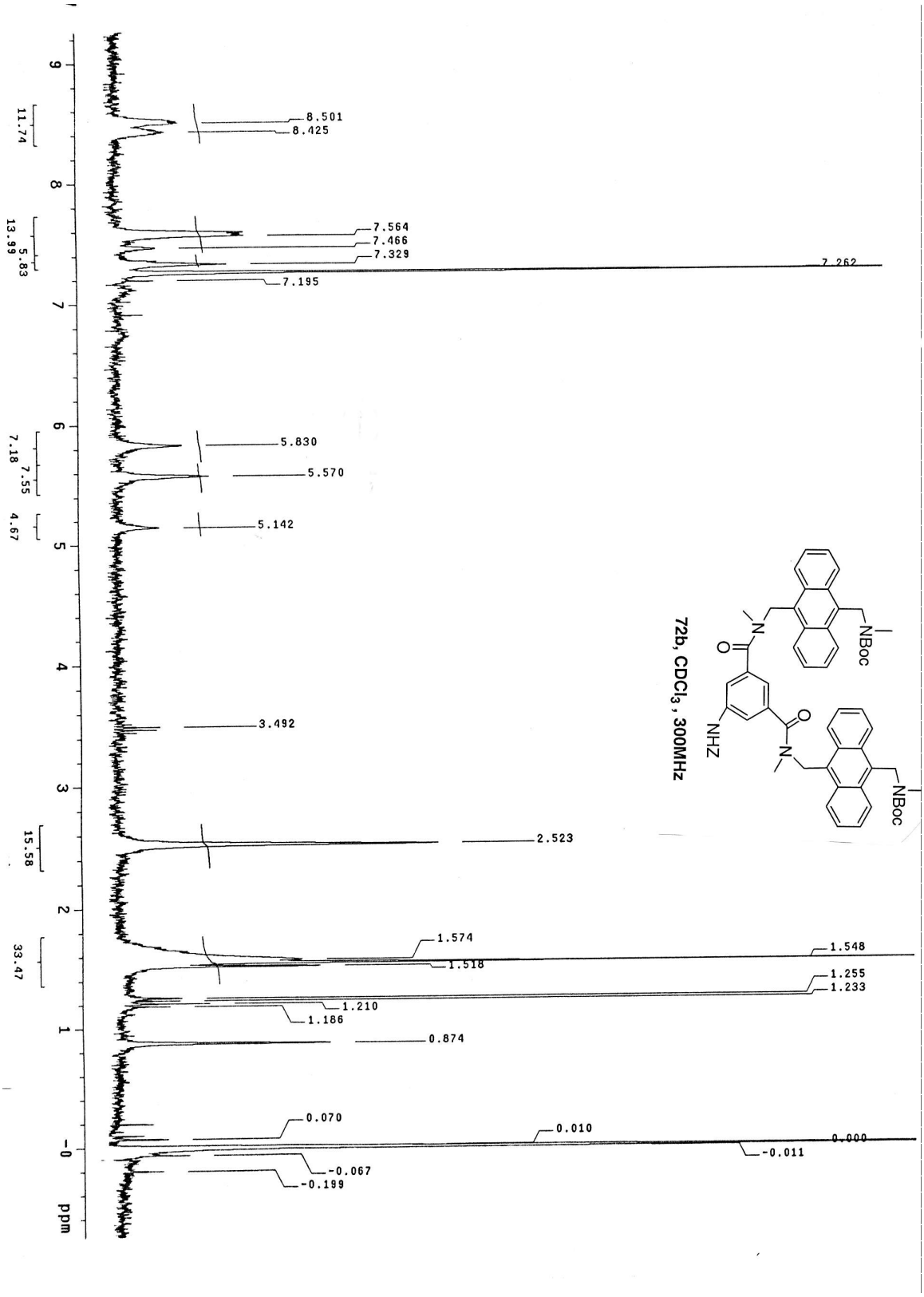
8.501
8.425
7.564
7.466
7.329
7.262
7.195
5.830
5.570
5.142
3.492
2.523
1.574
1.548
1.518
1.255
1.233
1.210
1.186
0.874
0.070
0.010
0.000
-0.011
-0.067
-0.199
11.74
13.99
5.83
7.18
7.55
4.67
15.58
33.47
ppm
72b, CDCl3, 300MHz
NBoc
NHZ
NBoc

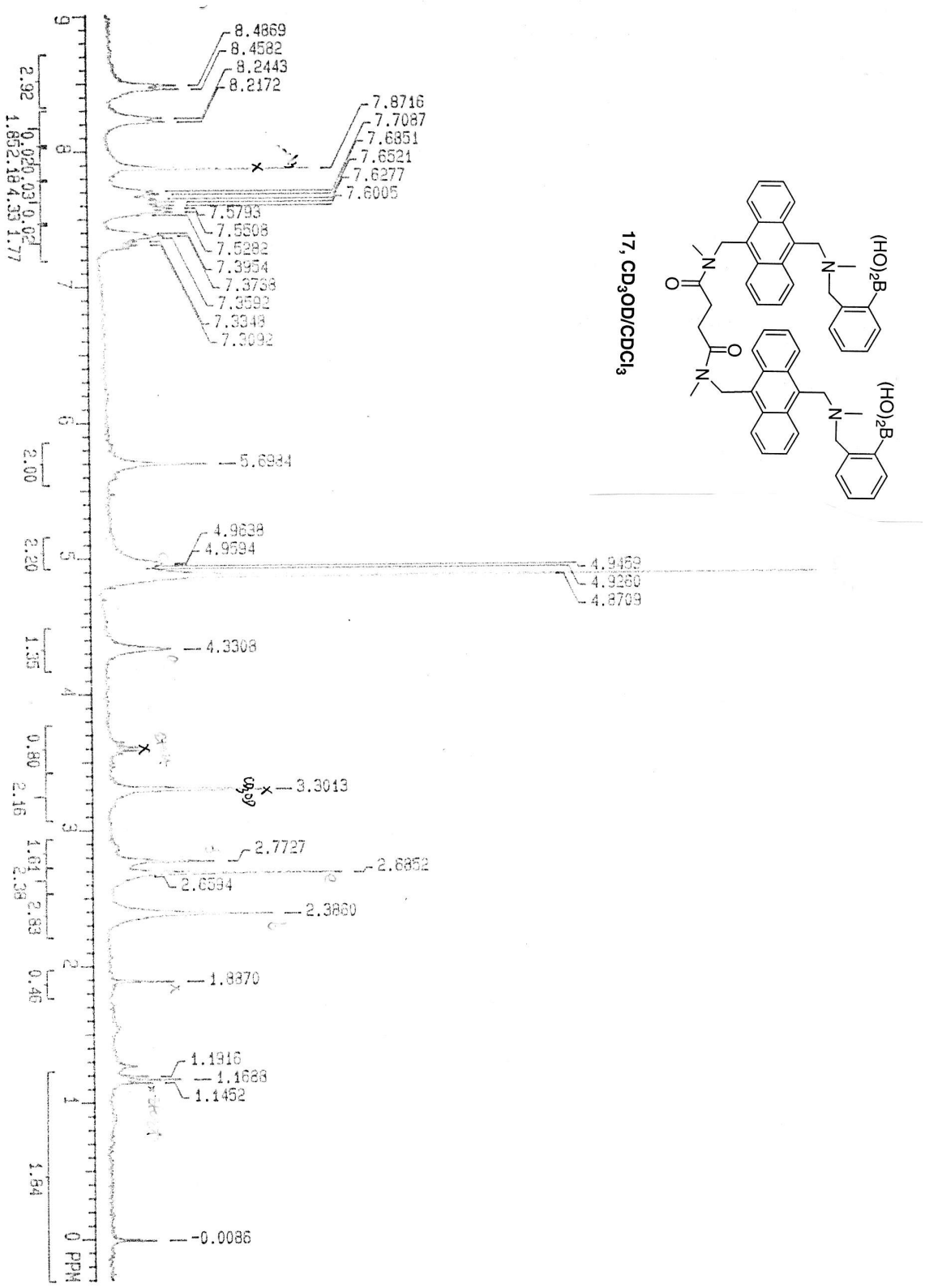
17, CD3OD/CDCl3
(HO)2B
(HO)2B
8.4869
8.4582
8.2443
8.2172
7.8716
7.7087
7.6851
7.6521
7.6277
7.6005
7.5793
7.5508
7.5282
7.3954
7.3738
7.3592
7.3348
7.3092
5.6984
4.9638
4.9594
4.9469
4.9280
4.8709
4.3308
3.3013
2.7727
2.6852
2.6594
2.3860
1.8870
1.1916
1.1688
1.1452
-0.0086
PPM

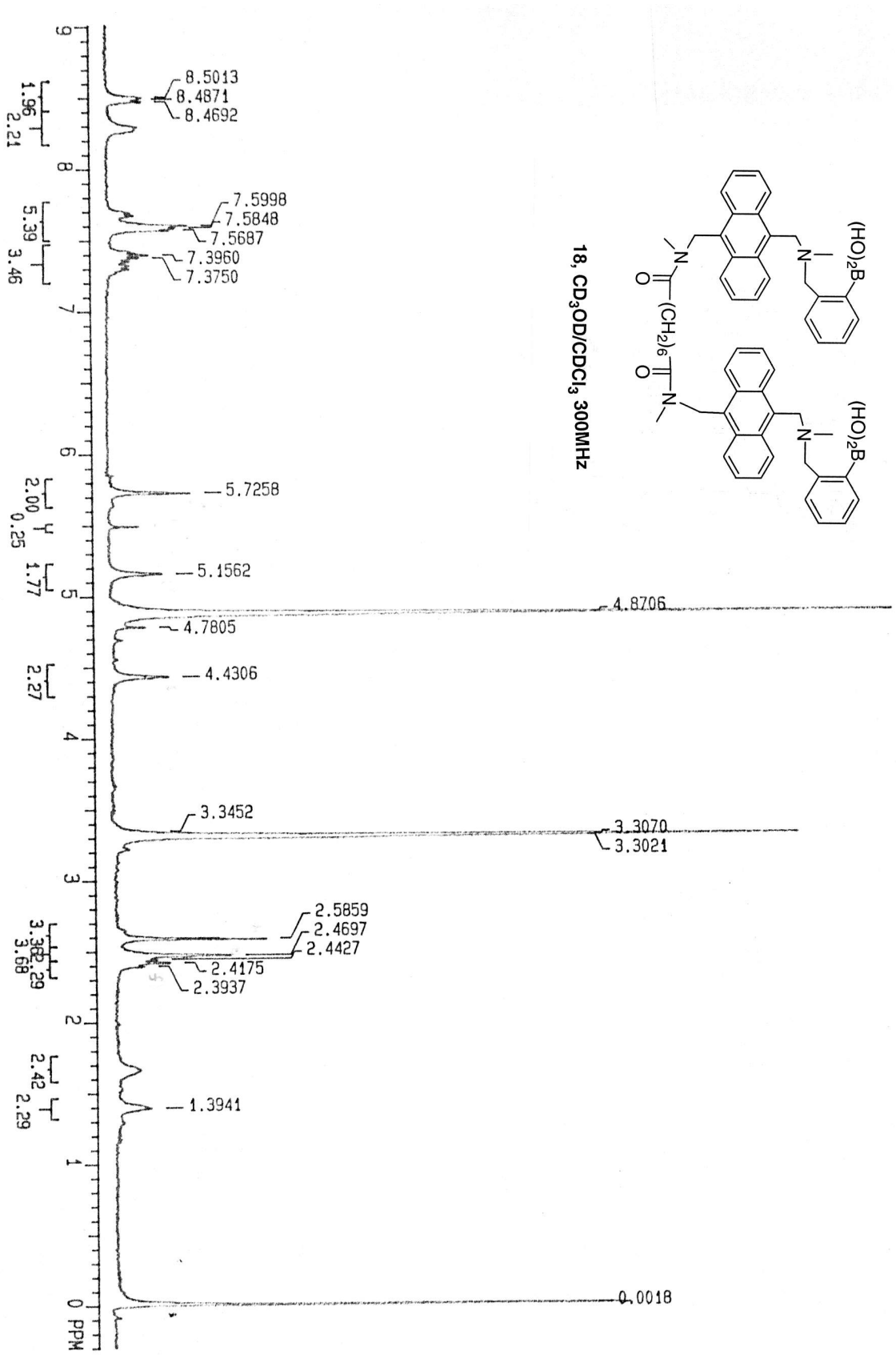
18, CD3OD/CDCl3 300MHz
(HO)2B
(CH2)6
8.5013
8.4871
8.4692
7.5998
7.5848
7.5687
7.3960
7.3750
5.7258
5.1562
4.8706
4.7805
4.4306
3.3452
3.3070
3.3021
2.5859
2.4697
2.4427
2.4175
2.3937
1.3941
0.0018
PPM

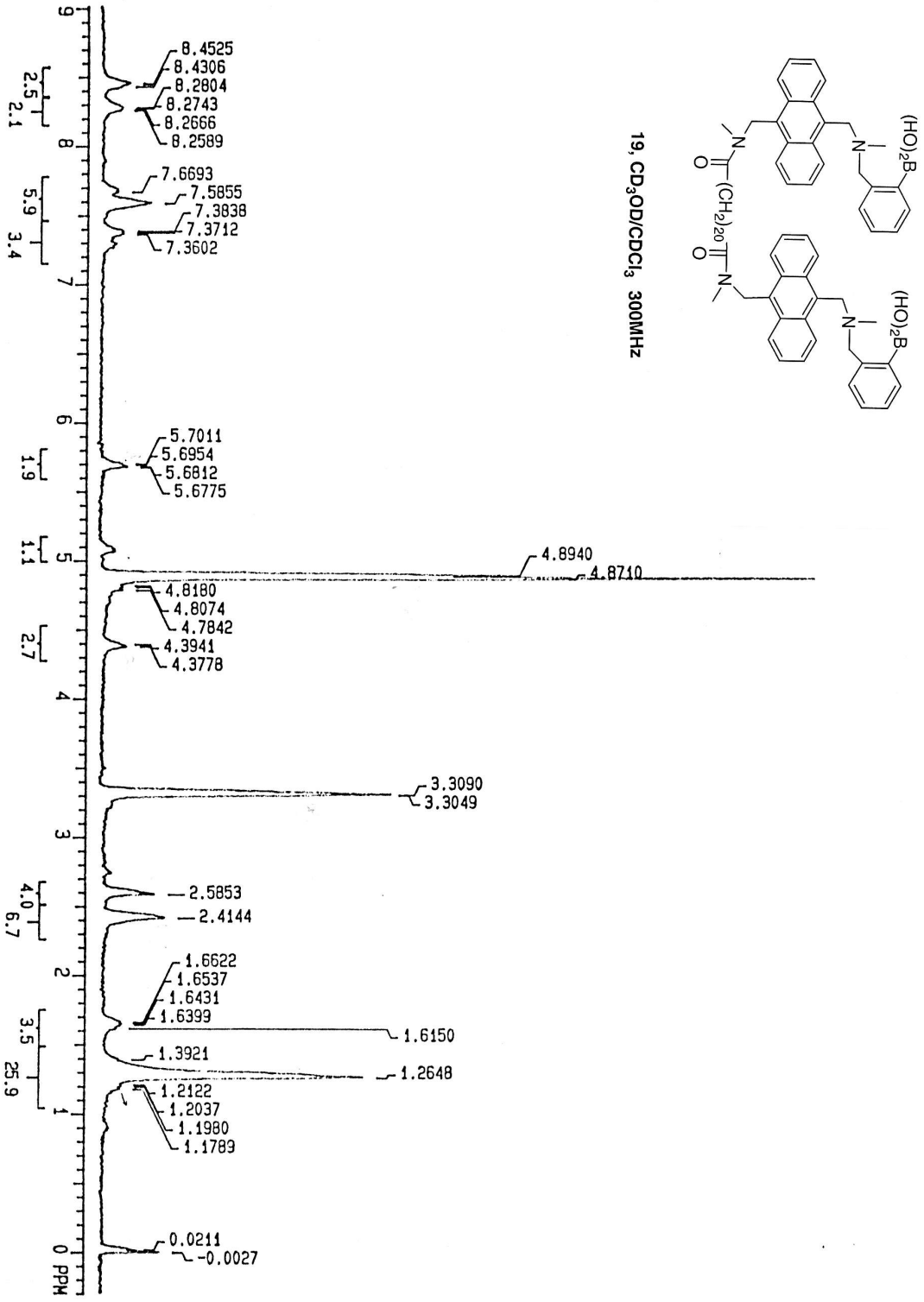
19, CD3OD/CDCl3 300MHz
(HO)2B
(CH2)20
(HO)2B
8.4525
8.4306
8.2804
8.2743
8.2666
8.2589
7.6693
7.5855
7.3838
7.3712
7.3602
5.7011
5.6954
5.6812
5.6775
4.8940
4.8710
4.8180
4.8074
4.7842
4.3941
4.3778
3.3090
3.3049
2.5853
2.4144
1.6622
1.6537
1.6431
1.6399
1.6150
1.3921
1.2648
1.2122
1.2037
1.1980
1.1789
0.0211
-0.0027
ppm

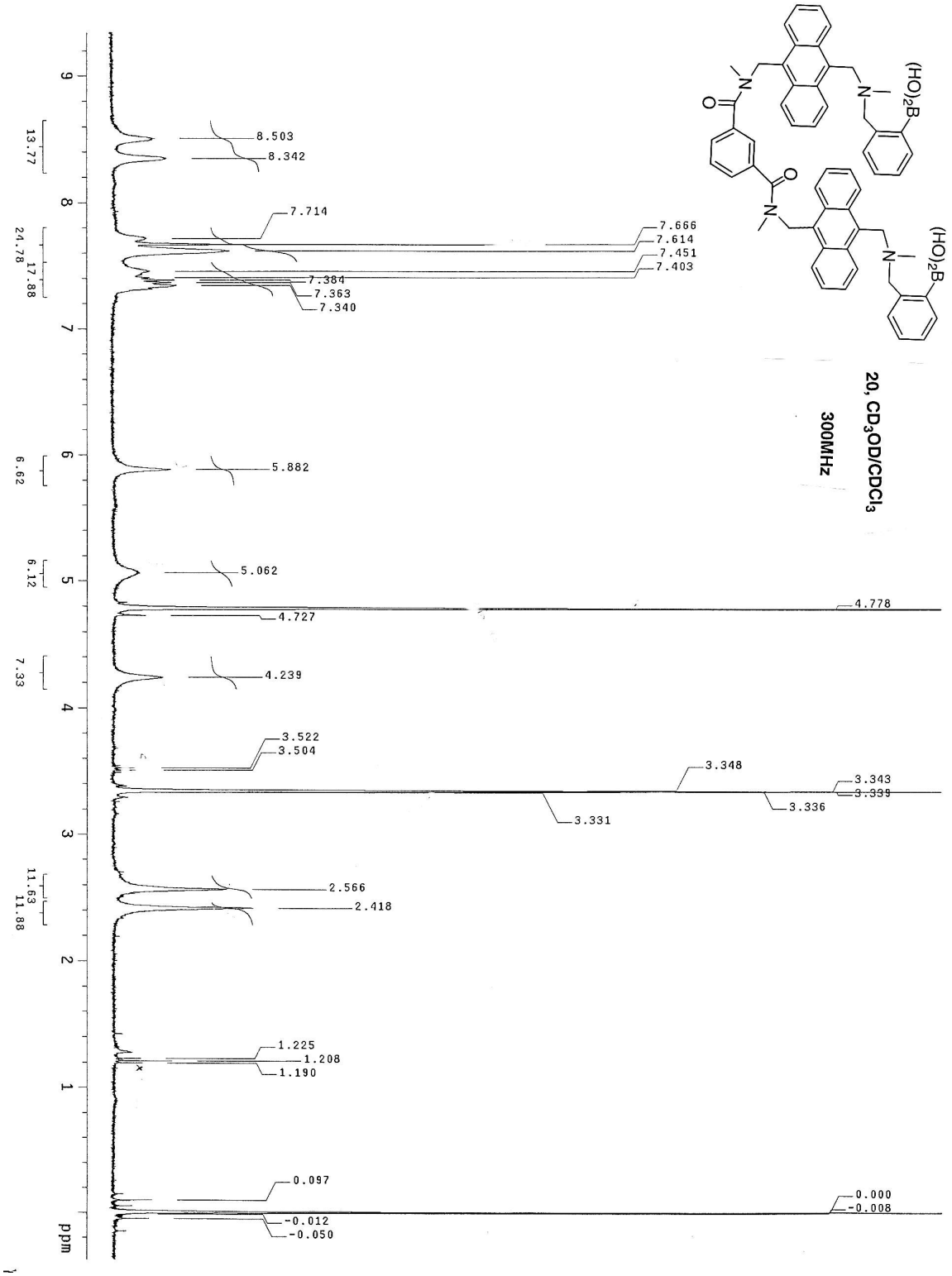
20, CD3OD/CDCl3
300MHz
(HO)2B
(HO)2B
8.503
8.342
7.714
7.666
7.614
7.451
7.403
7.384
7.363
7.340
5.882
5.062
4.778
4.727
4.239
3.522
3.504
3.348
3.343
3.339
3.336
3.331
2.566
2.418
1.225
1.208
1.190
0.097
0.000
-0.008
-0.012
-0.050
13.77
24.78
17.88
6.62
6.12
7.33
11.63
11.88
ppm

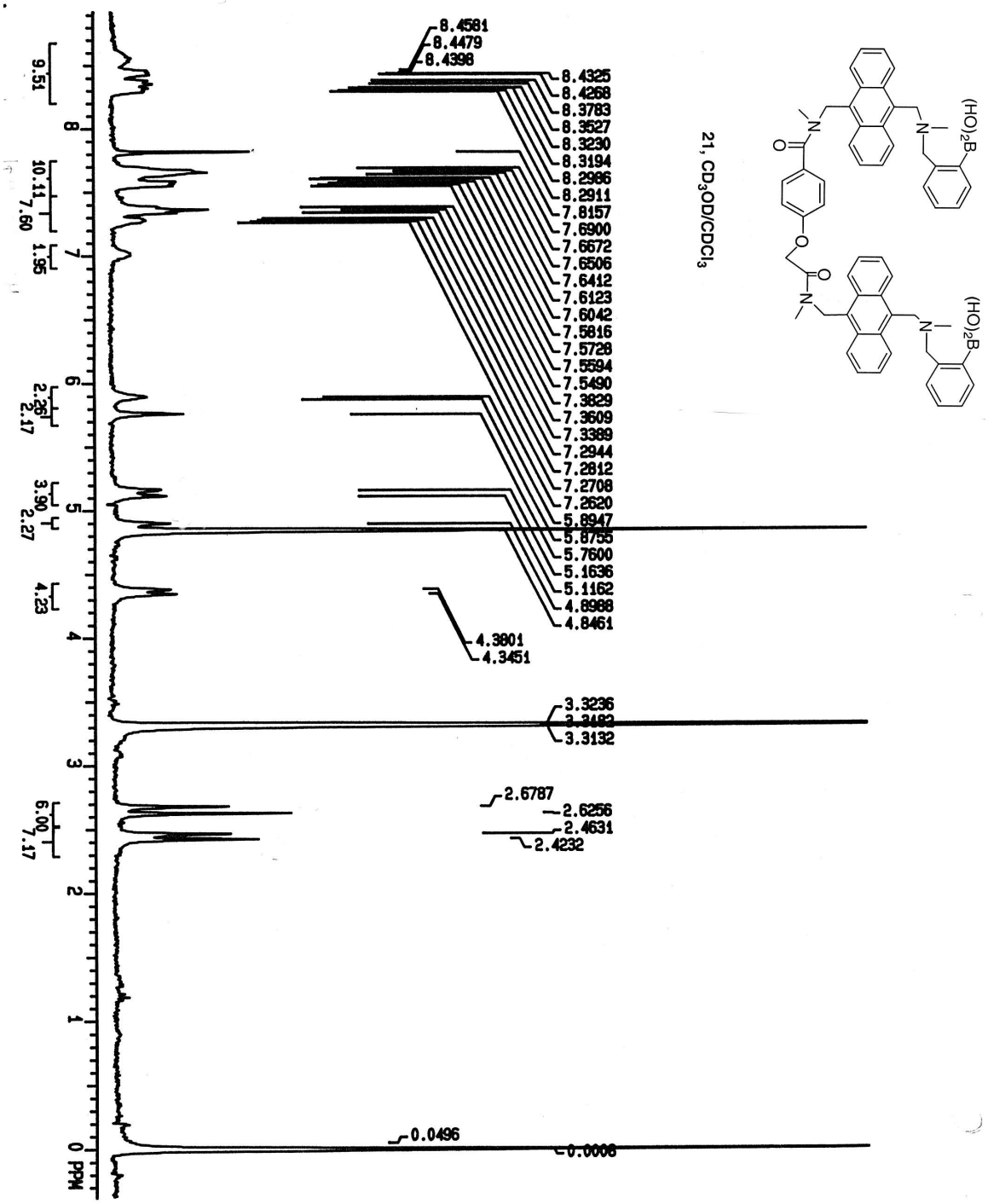
21, $CD_3OD/CDCl_3$
$(HO)_2B$
$(HO)_2B$
8.4581
8.4479
8.4398
8.4325
8.4268
8.3783
8.3527
8.3230
8.3194
8.2986
8.2911
7.8157
7.6900
7.6672
7.6506
7.6412
7.6123
7.6042
7.5816
7.5728
7.5594
7.5490
7.3829
7.3609
7.3389
7.2944
7.2812
7.2708
7.2620
5.8947
5.8755
5.7600
5.1636
5.1162
4.8988
4.8461
4.3801
4.3451
3.3236
3.3132
2.6787
2.6256
2.4631
2.4232
0.0496
0.0000
9.51
10.11
7.60
1.95
2.36
2.17
3.90
2.27
4.23
6.00
7.17
PPM

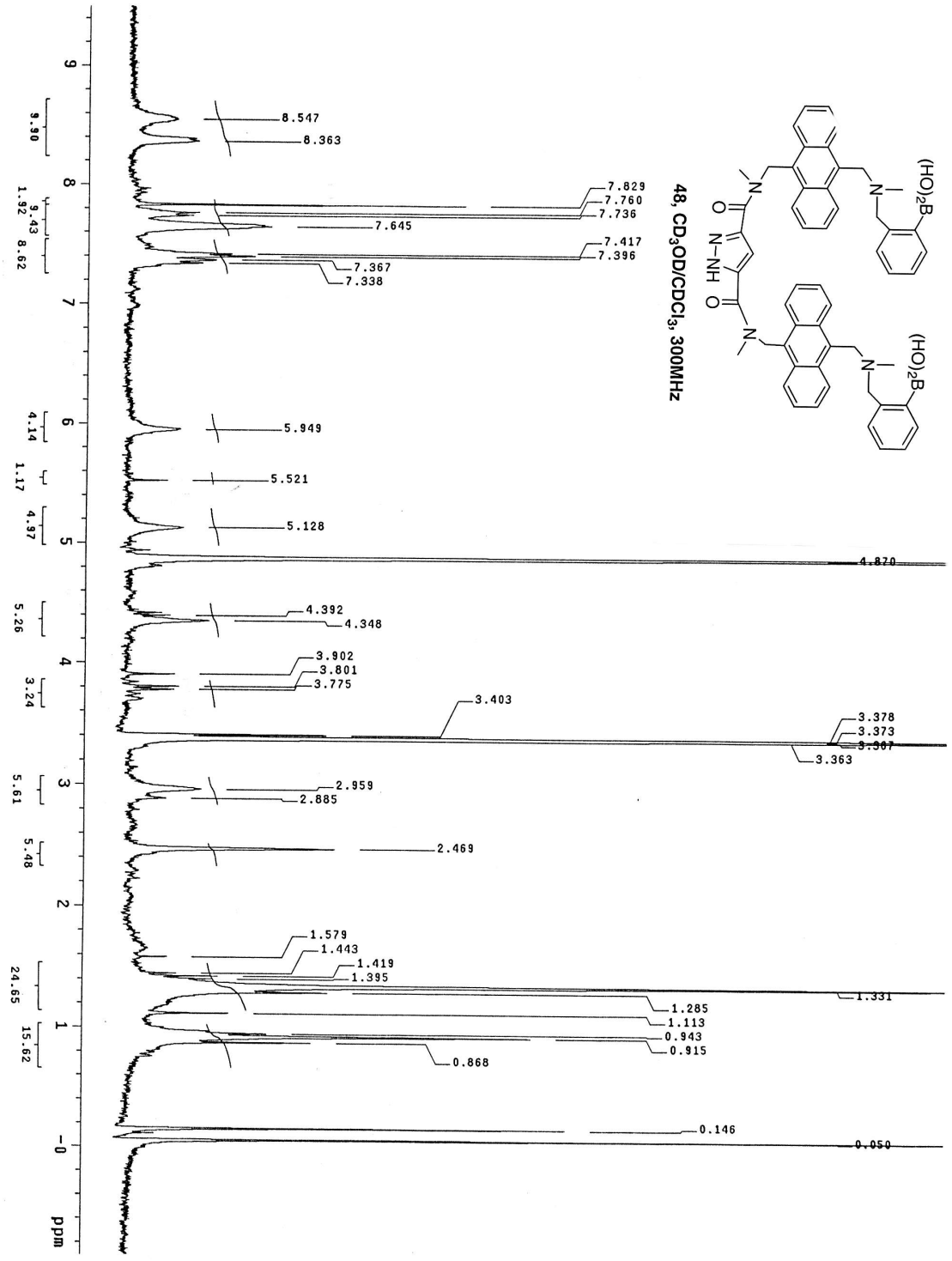
48, CD3OD/CDCl3, 300MHz
(HO)2B
(HO)2B
N
O
N–NH
O
8.547
8.363
7.829
7.760
7.736
7.645
7.417
7.396
7.367
7.338
5.949
5.521
5.128
4.870
4.392
4.348
3.902
3.801
3.775
3.403
3.378
3.373
3.367
3.363
2.959
2.885
2.469
1.579
1.443
1.419
1.395
1.331
1.285
1.113
0.943
0.915
0.868
0.146
0.050
9.90
9.43
1.92
8.62
4.14
1.17
4.97
5.26
3.24
5.61
5.48
24.65
15.62
ppm

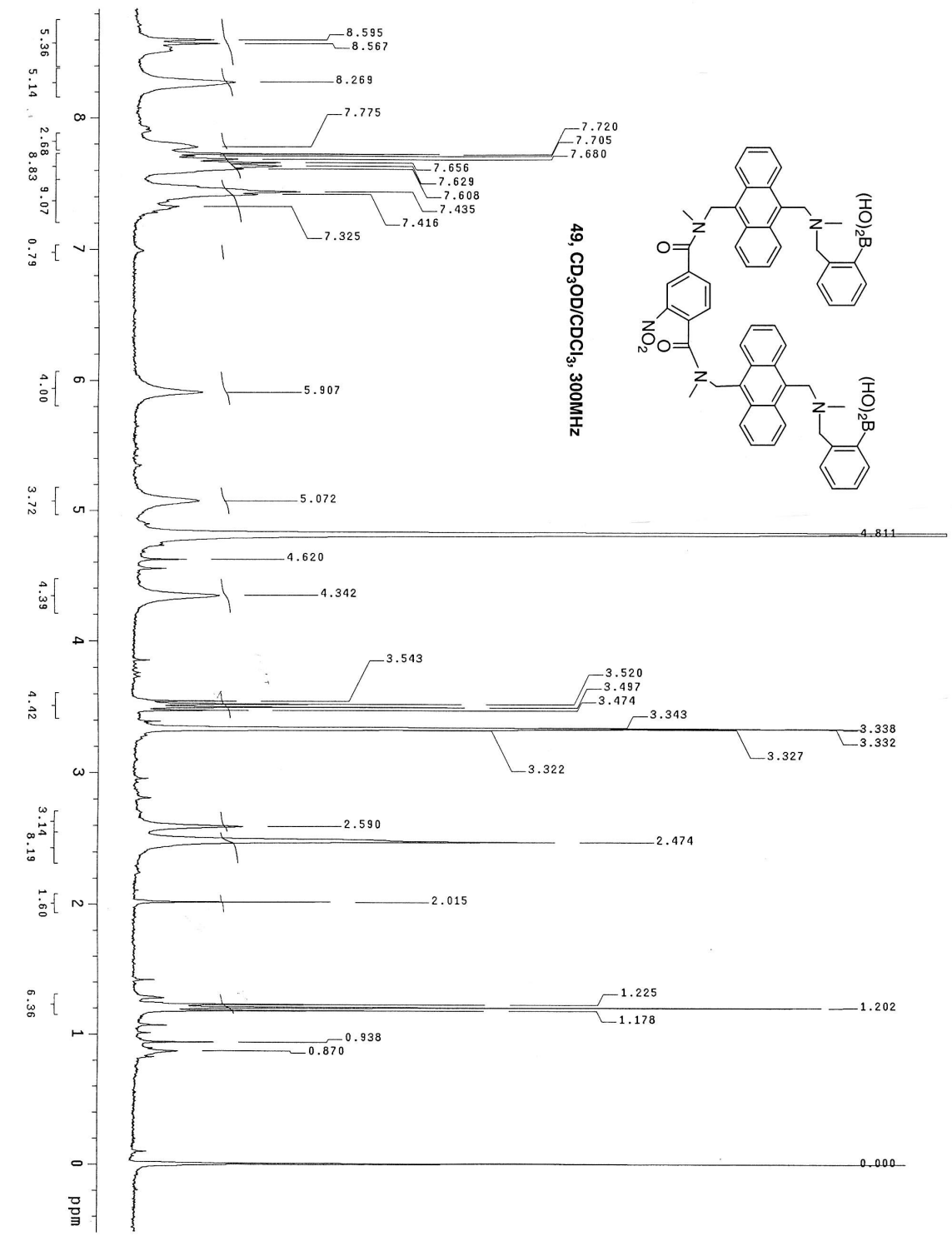
49, CD3OD/CDCl3, 300MHz
8.595
8.567
8.269
7.775
7.720
7.705
7.680
7.656
7.629
7.608
7.435
7.416
7.325
5.907
5.072
4.811
4.620
4.342
3.543
3.520
3.497
3.474
3.343
3.338
3.332
3.327
3.322
2.590
2.474
2.015
1.225
1.202
1.178
0.938
0.870
0.000
ppm

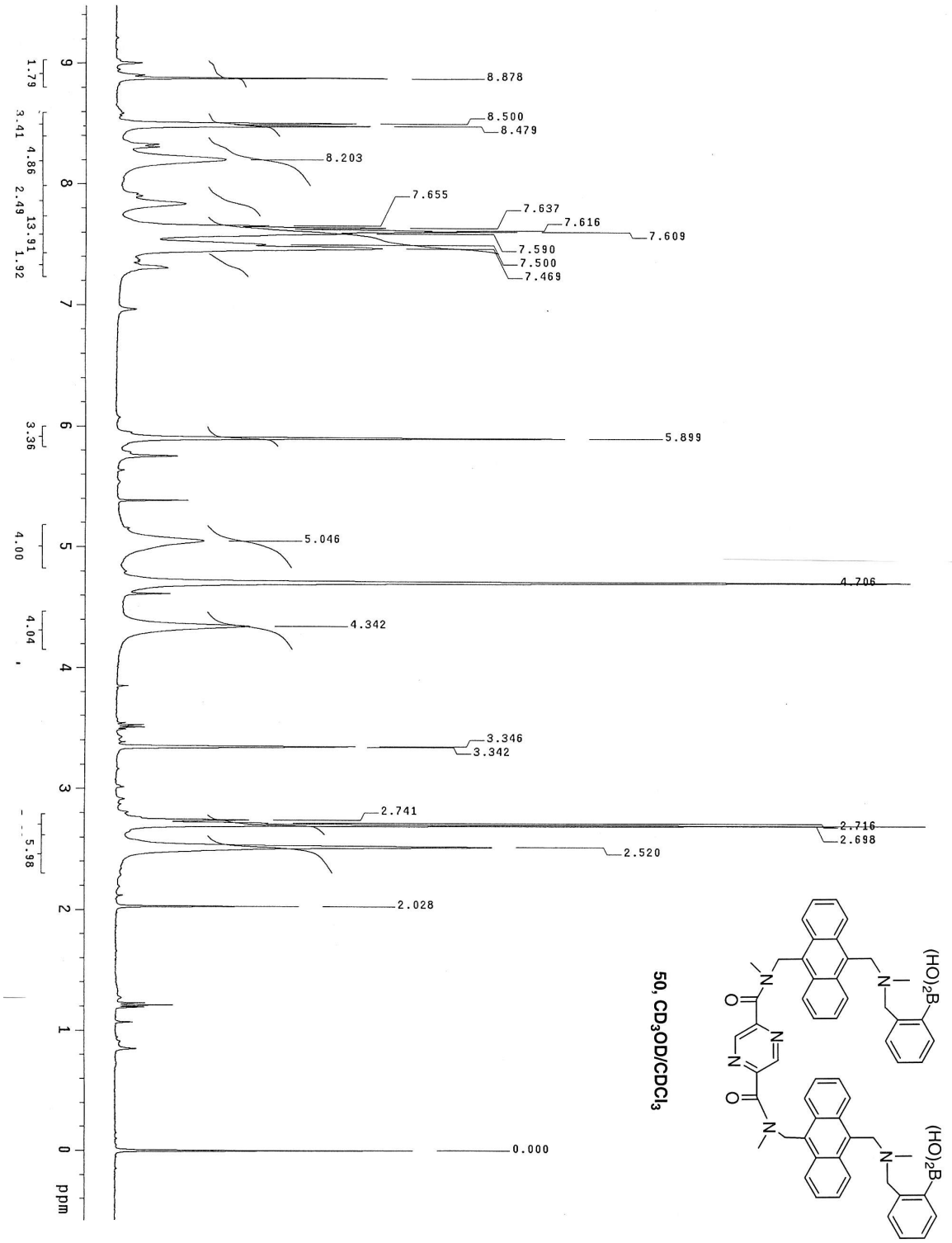
8.878
8.500
8.479
8.203
7.655
7.637
7.616
7.609
7.590
7.500
7.469
5.899
5.046
4.706
4.342
3.346
3.342
2.741
2.716
2.698
2.520
2.028
0.000
1.79
3.41
4.86
2.49
13.91
1.92
3.36
4.00
4.04
5.98
ppm
50, CD3OD/CDCl3
(HO)2B
(HO)2B

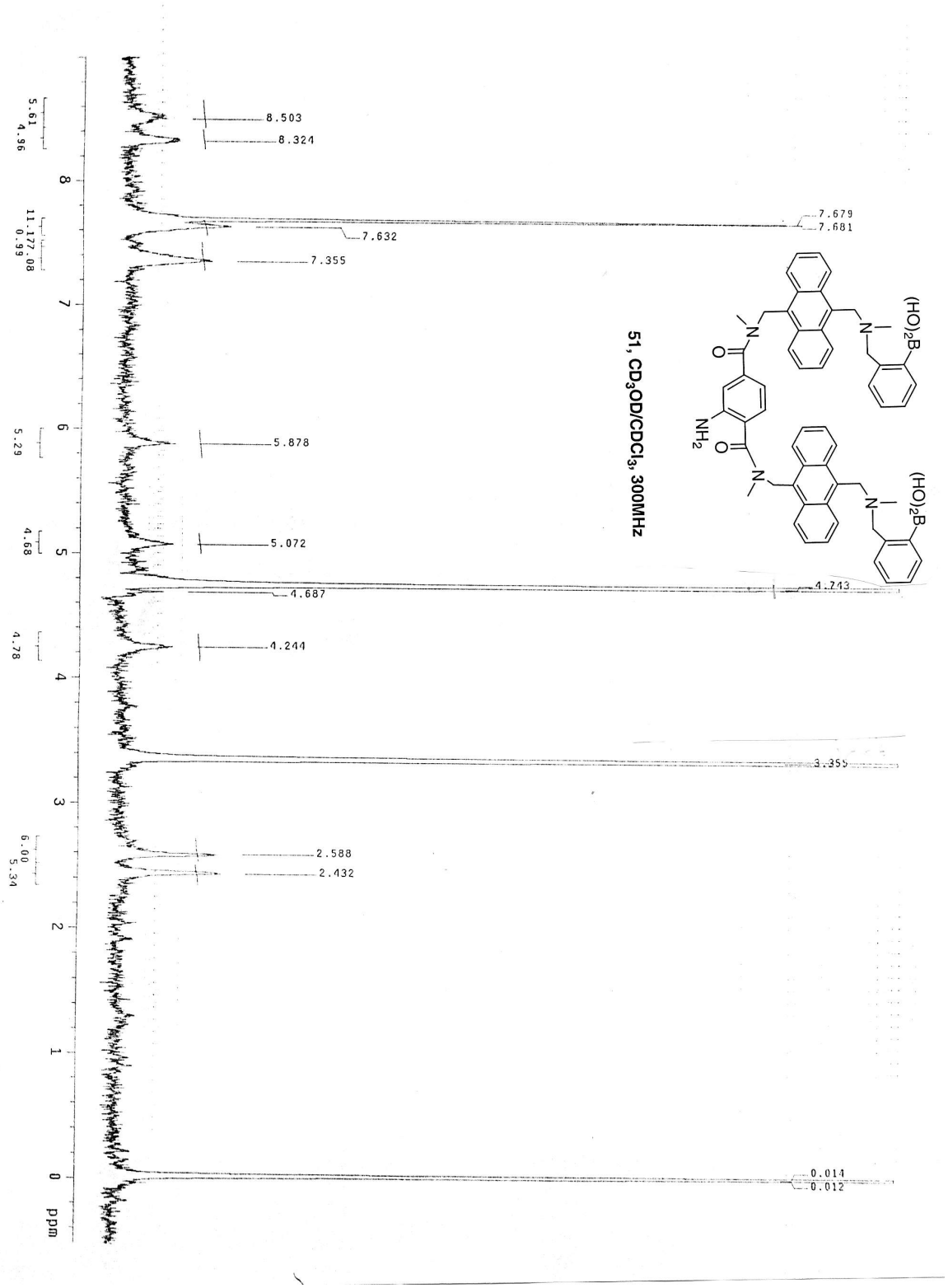
51, CD3OD/CDCl3, 300MHz
8.503
8.324
7.679
7.681
7.632
7.355
5.878
5.072
4.687
4.244
4.243
3.355
2.588
2.432
0.014
0.012
(HO)2B
NH2
O
N
ppm

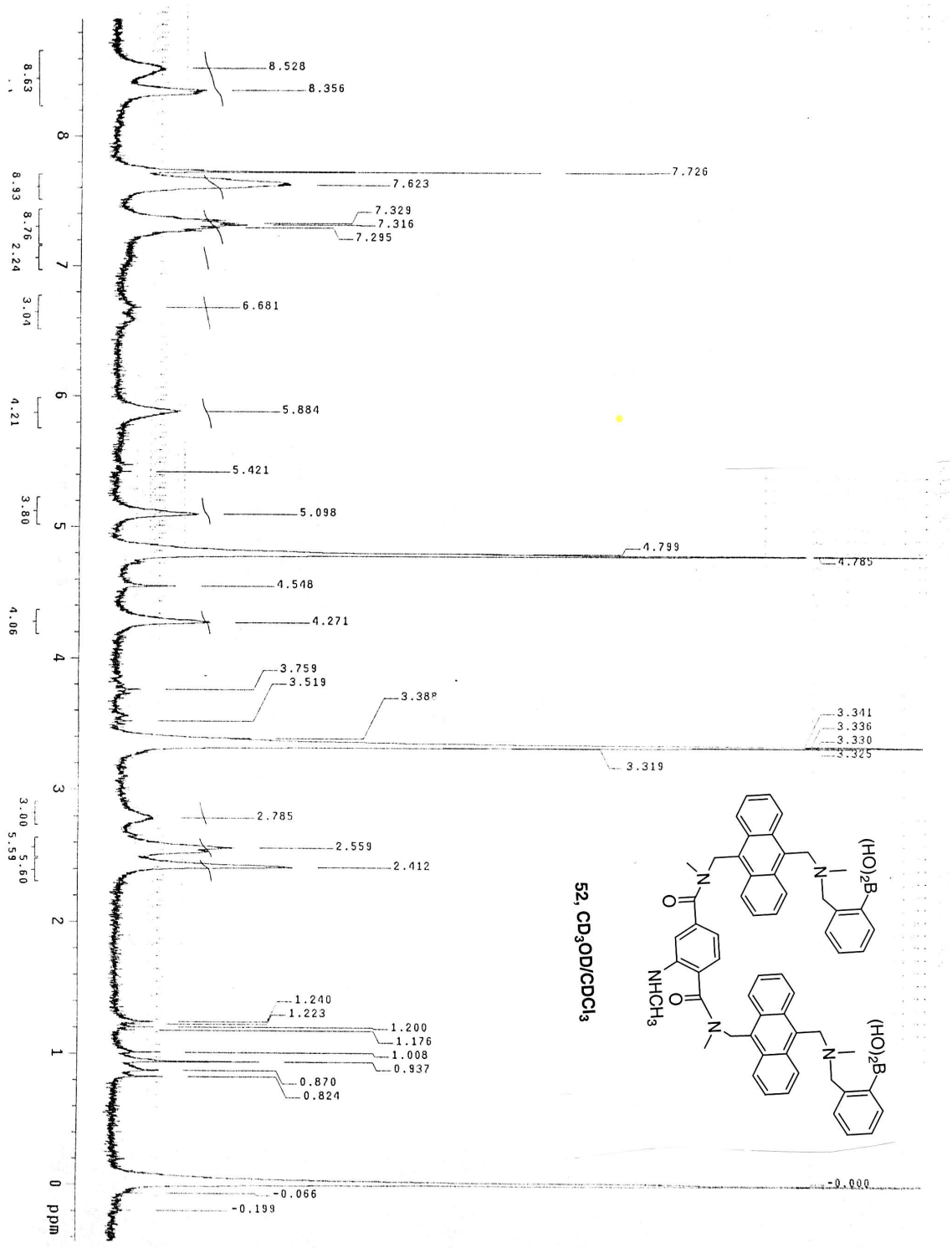
8.528
8.356
7.726
7.623
7.329
7.316
7.295
6.681
5.884
5.421
5.098
4.799
4.785
4.548
4.271
3.759
3.519
3.388
3.341
3.336
3.330
3.325
3.319
2.785
2.559
2.412
1.240
1.223
1.200
1.176
1.008
0.937
0.870
0.824
-0.000
-0.066
-0.199
ppm
52, CD3OD/CDCl3
(HO)2B
NHCH3
(HO)2B

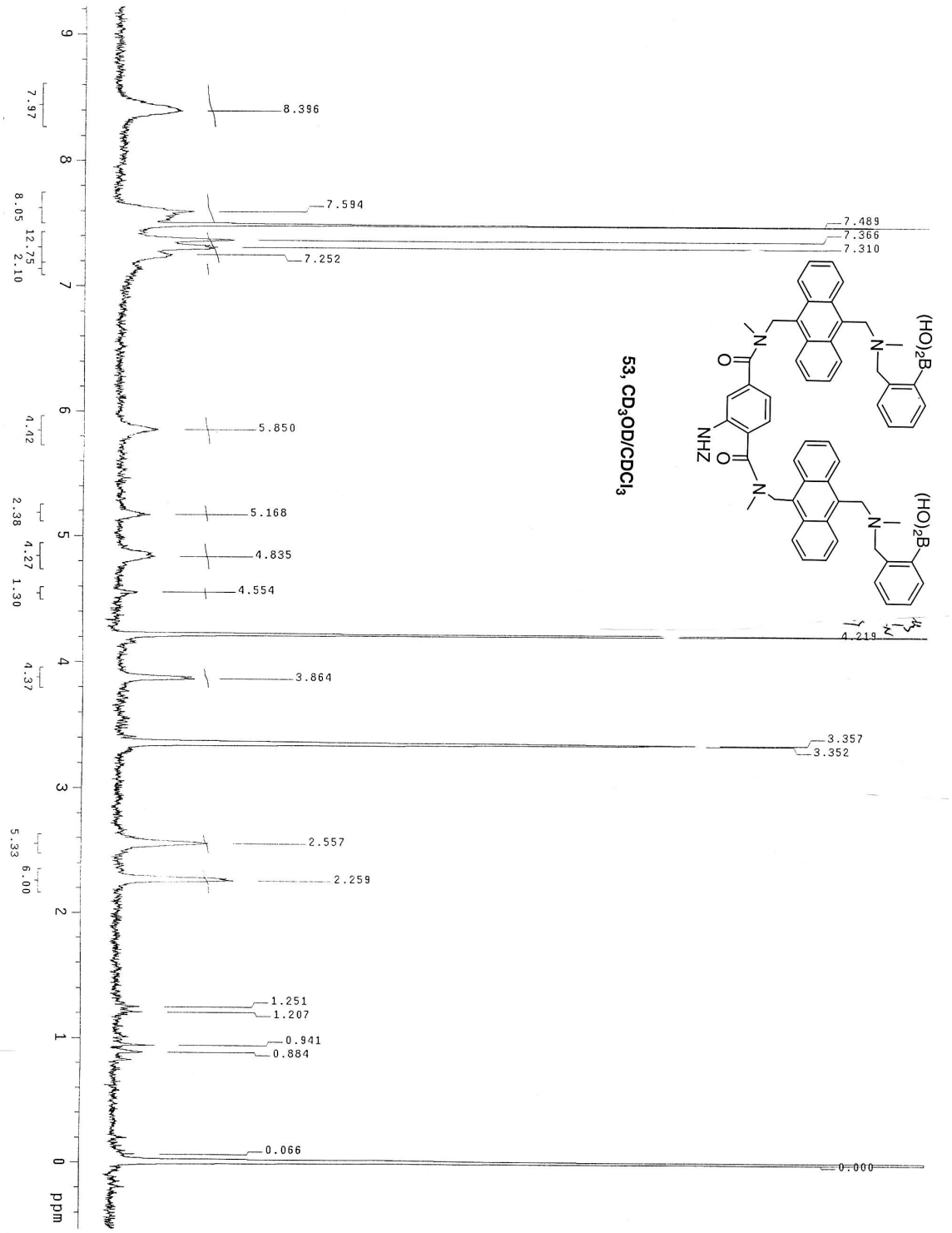
53, CD3OD/CDCl3
8.396
7.594
7.489
7.366
7.310
7.252
5.850
5.168
4.835
4.554
4.219
3.864
3.357
3.352
2.557
2.259
1.251
1.207
0.941
0.884
0.066
0.000
ppm

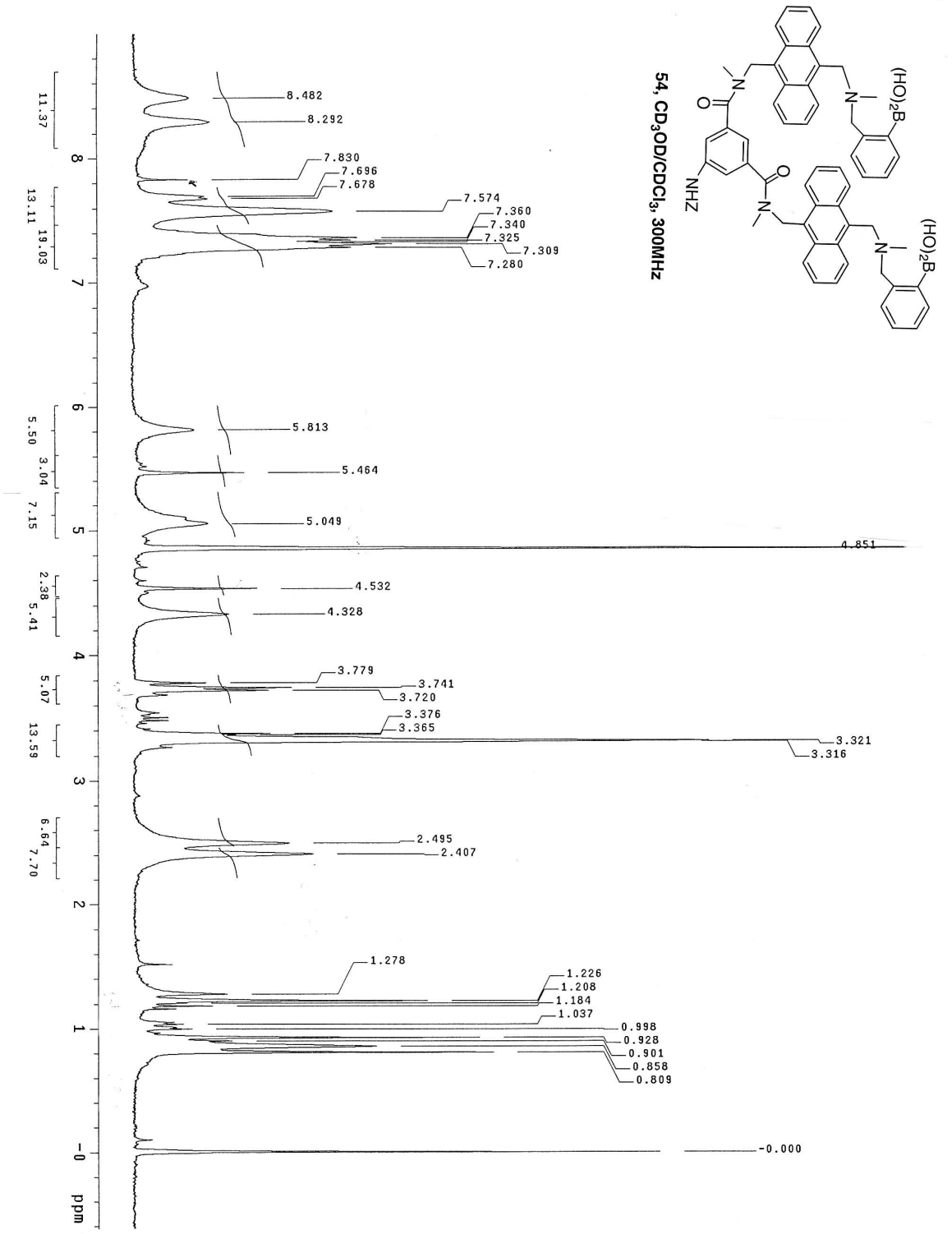
54, CD3OD/CDCl3, 300MHz
(HO)2B
NHZ
(HO)2B
8.482
8.292
7.830
7.696
7.678
7.574
7.360
7.340
7.325
7.309
7.280
5.813
5.464
5.049
4.851
4.532
4.328
3.779
3.741
3.720
3.376
3.365
3.321
3.316
2.495
2.407
1.278
1.226
1.208
1.184
1.037
0.998
0.928
0.901
0.858
0.809
-0.000
11.37
13.11
19.03
5.50
3.04
7.15
2.38
5.41
5.07
13.59
6.64
7.70
ppm

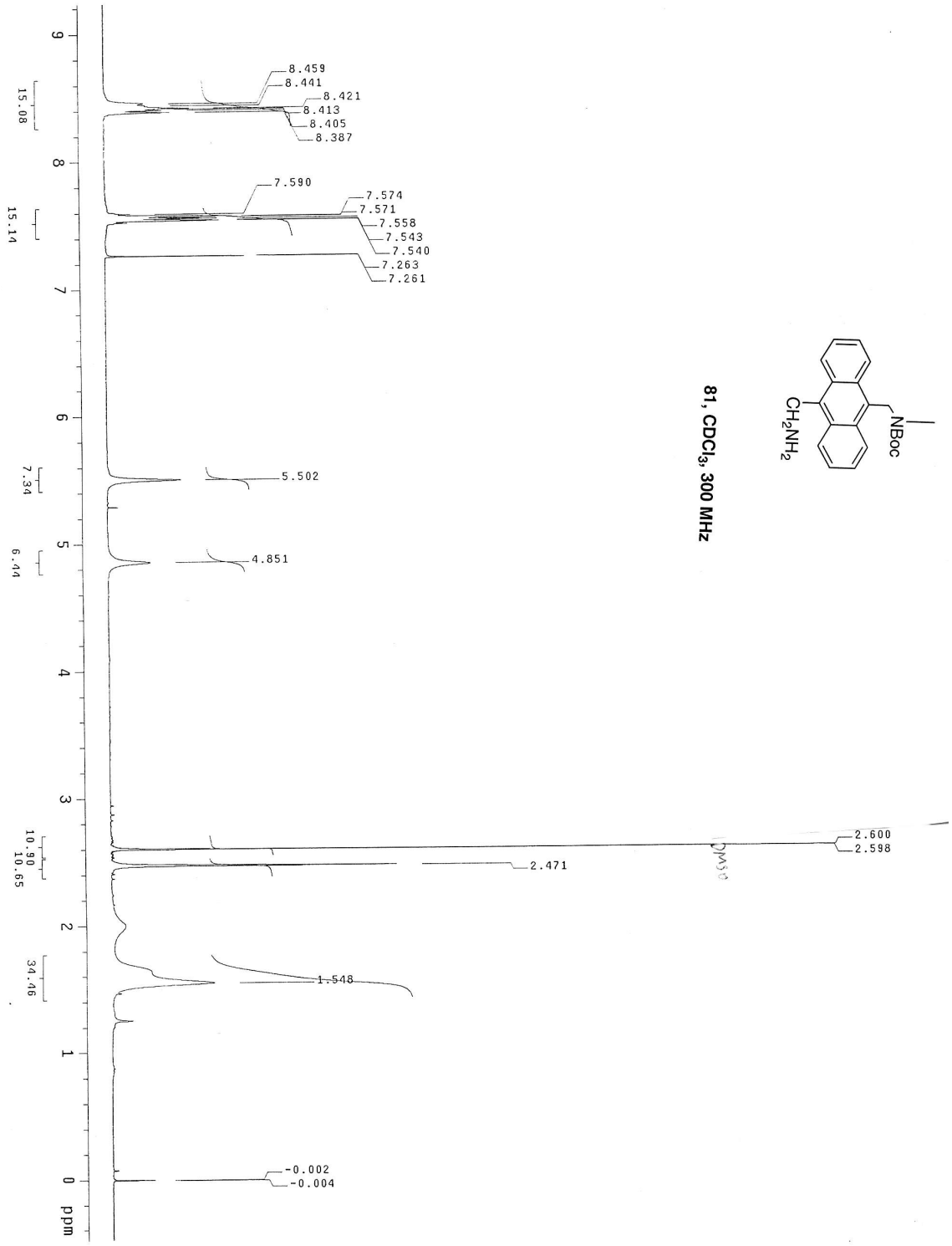
81, CDCl3, 300 MHz
CH2NH2
NBoc
8.459
8.441
8.421
8.413
8.405
8.387
7.590
7.574
7.571
7.558
7.543
7.540
7.263
7.261
5.502
4.851
2.600
2.598
2.471
1.548
-0.002
-0.004
15.08
15.14
7.34
6.41
10.90
10.65
34.46
ppm

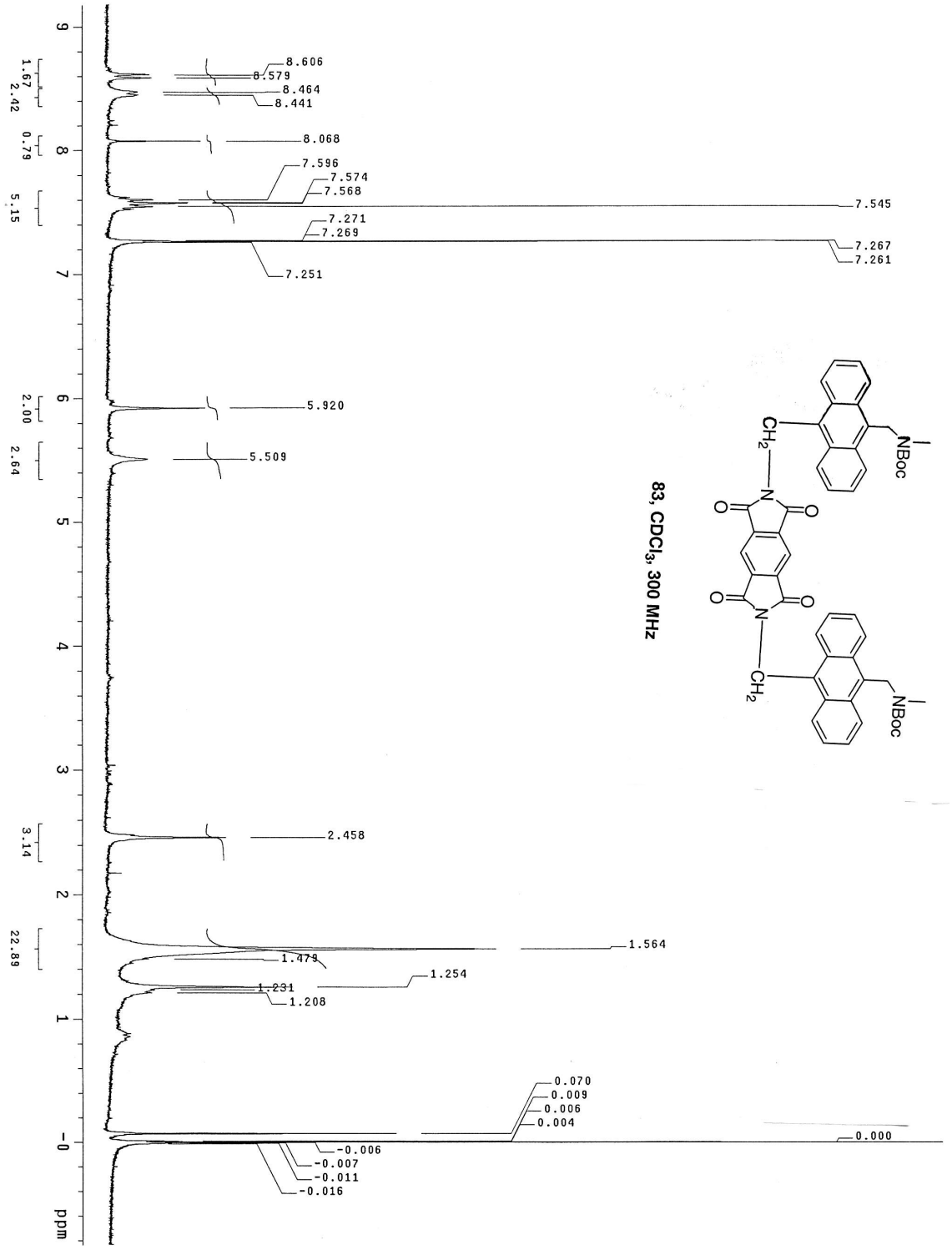
8.606
8.579
8.464
8.441
8.068
7.596
7.574
7.568
7.545
7.271
7.269
7.267
7.261
7.251
5.920
5.509
2.458
1.564
1.479
1.254
1.231
1.208
0.070
0.009
0.006
0.004
0.000
-0.006
-0.007
-0.011
-0.016
1.67
2.42
0.79
5.15
2.00
2.64
3.14
22.89
ppm
83, CDCl3, 300 MHz
NBoc
CH2
N
O

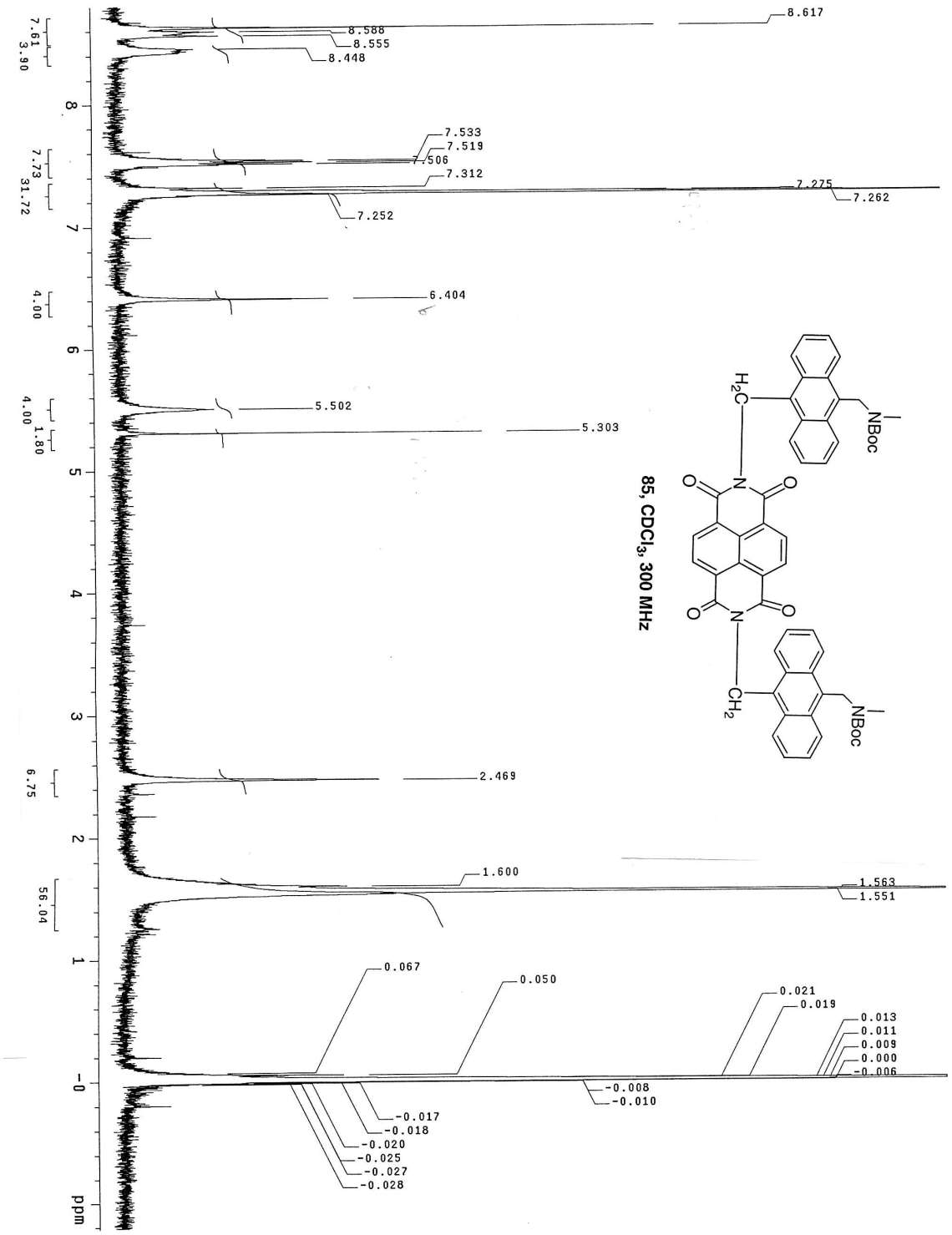
8.617
8.588
8.555
8.448
7.533
7.519
7.506
7.312
7.275
7.262
7.252
6.404
5.502
5.303
2.469
1.600
1.563
1.551
0.067
0.050
0.021
0.019
0.013
0.011
0.009
0.000
-0.006
-0.008
-0.010
-0.017
-0.018
-0.020
-0.025
-0.027
-0.028
7.61
3.90
7.73
31.72
4.00
4.00
1.80
6.75
56.04
ppm
85, CDCl3, 300 MHz
H2C
NBoc
N
O
CH2
NBoc

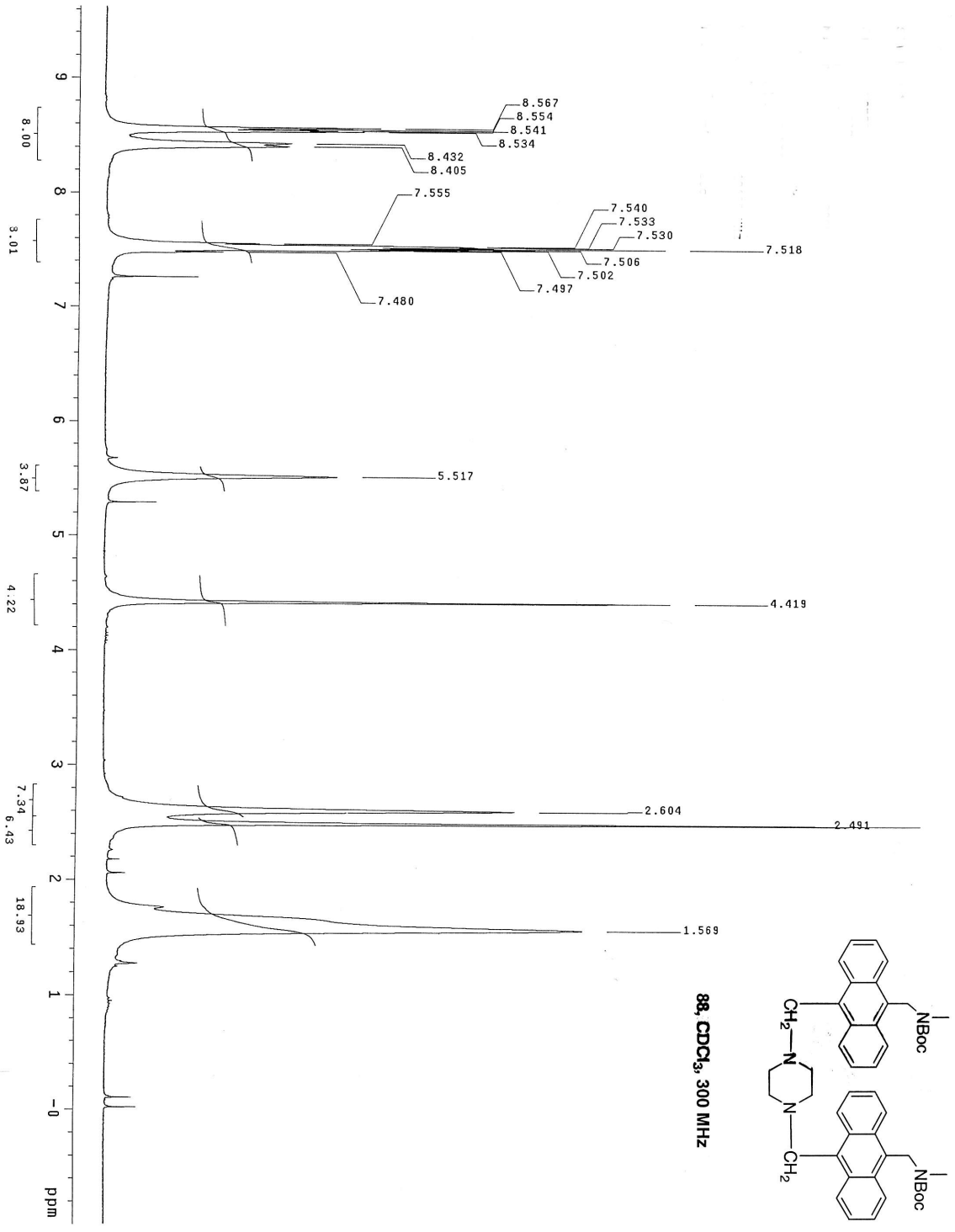
8.567
8.554
8.541
8.534
8.432
8.405
7.555
7.540
7.533
7.530
7.518
7.506
7.502
7.497
7.480
5.517
4.419
2.604
2.491
1.569
8.00
3.01
3.87
4.22
7.34
6.43
18.93
ppm
88, CDCl3, 300 MHz
CH2
N
NBoc

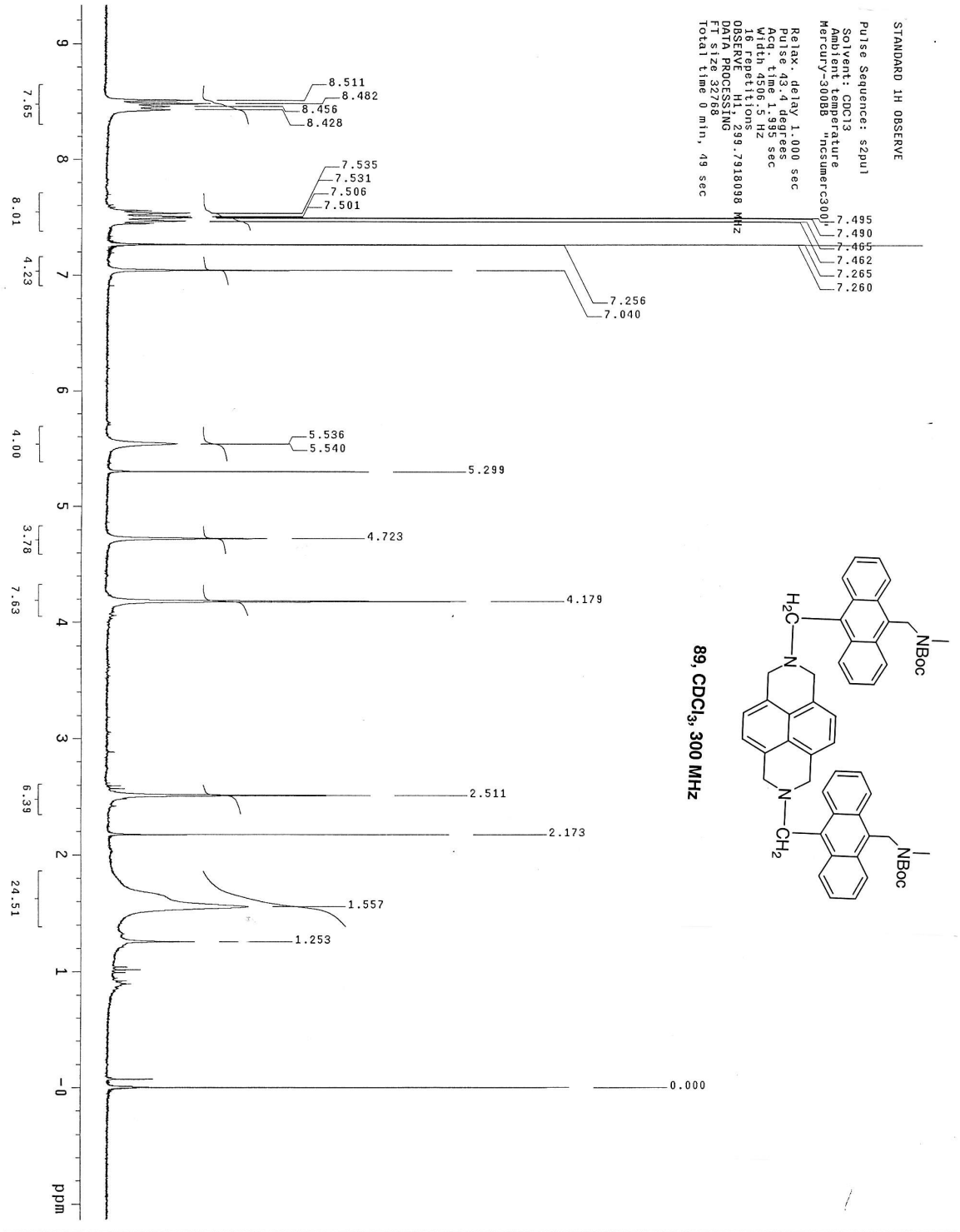
STANDARD 1H OBSERVE
Pulse Sequence: s2pul
Solvent: CDCl3
Ambient temperature
Mercury-300BB "ncsumerc300l"
Relax. delay 1.000 sec
Pulse 43.4 degrees
Acq. time 1.995 sec
Width 4506.5 Hz
16 repetitions
OBSERVE H1, 299.7918098 MHz
DATA PROCESSING
FT size 32768
Total time 0 min, 49 sec
8.511
8.482
8.456
8.428
7.535
7.531
7.506
7.501
7.495
7.490
7.465
7.462
7.265
7.260
7.256
7.040
5.536
5.540
5.299
4.723
4.179
2.511
2.173
1.557
1.253
0.000
7.65
8.01
4.23
4.00
3.78
7.63
6.39
24.51
ppm
89, CDCl3, 300 MHz
H2C
N
NBoc
N
CH2
NBoc

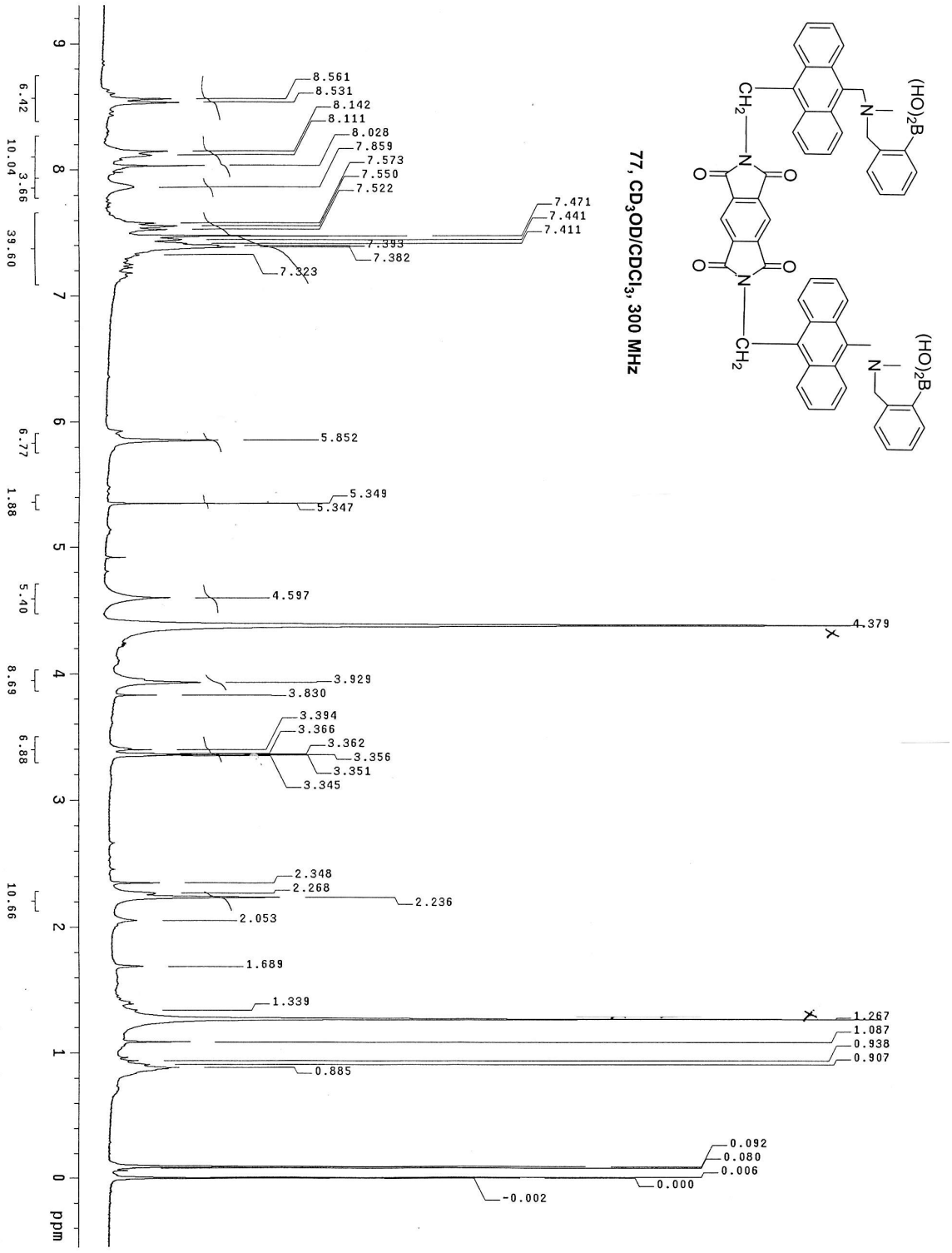
77, CD3OD/CDCl3, 300 MHz
8.561
8.531
8.142
8.111
8.028
7.859
7.573
7.550
7.522
7.471
7.441
7.411
7.393
7.382
7.323
5.852
5.349
5.347
4.597
4.379
3.929
3.830
3.394
3.366
3.362
3.356
3.351
3.345
2.348
2.268
2.236
2.053
1.689
1.339
1.267
1.087
0.938
0.907
0.885
0.092
0.080
0.006
0.000
-0.002
6.42
10.04
3.66
39.60
6.77
1.88
5.40
8.69
6.88
10.66
ppm
CH2
N
O
(HO)2B

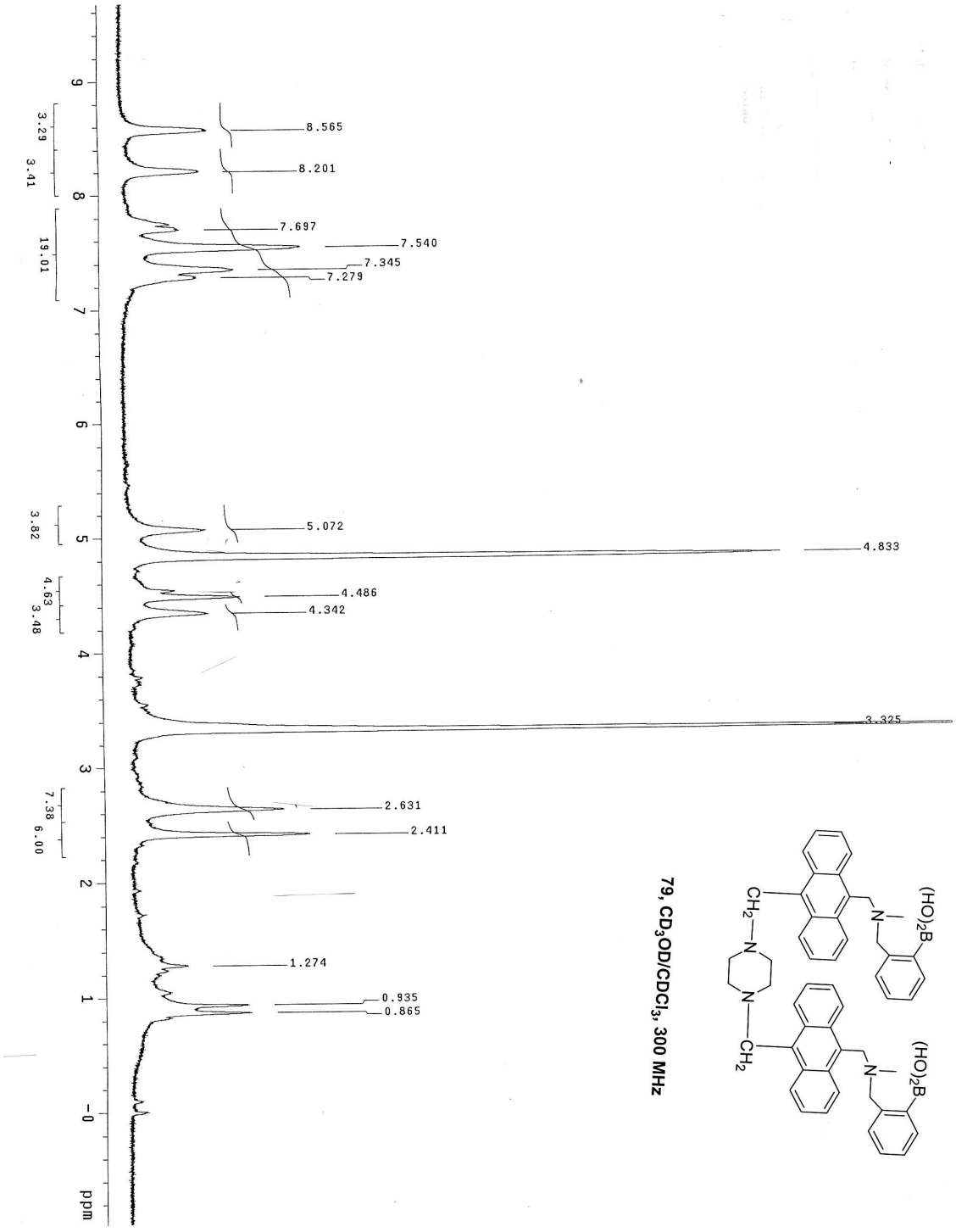

79, $CD_3OD/CDCl_3$, 300 MHz

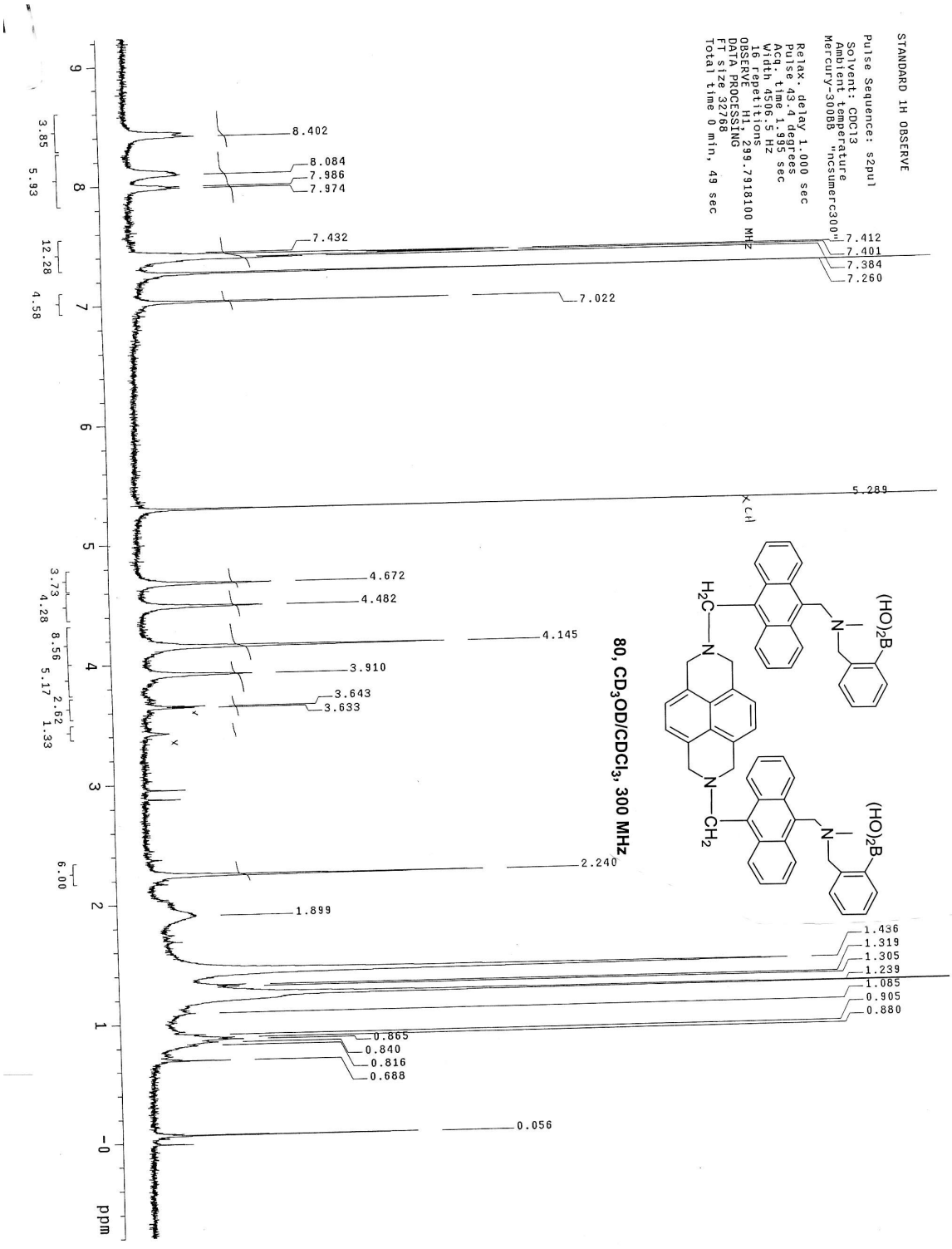
STANDARD 1H OBSERVE
Pulse Sequence: s2pul
Solvent: CDCl3
Ambient temperature
Mercury-300BB "ncsumerc300"
Relax. delay 1.000 sec
Pulse 43.4 degrees
Acq. time 1.995 sec
Width 4506.5 Hz
16 repetitions
OBSERVE H1, 299.7918100 MHz
DATA PROCESSING
FT size 32768
Total time 0 min, 49 sec
8.402
8.084
7.986
7.974
7.432
7.412
7.401
7.384
7.260
7.022
5.289
4.672
4.482
4.145
3.910
3.643
3.633
2.240
1.899
1.436
1.319
1.305
1.239
1.085
0.905
0.880
0.865
0.840
0.816
0.688
0.056
80, CD3OD/CDCl3, 300 MHz
(HO)2B
(HO)2B
ppm

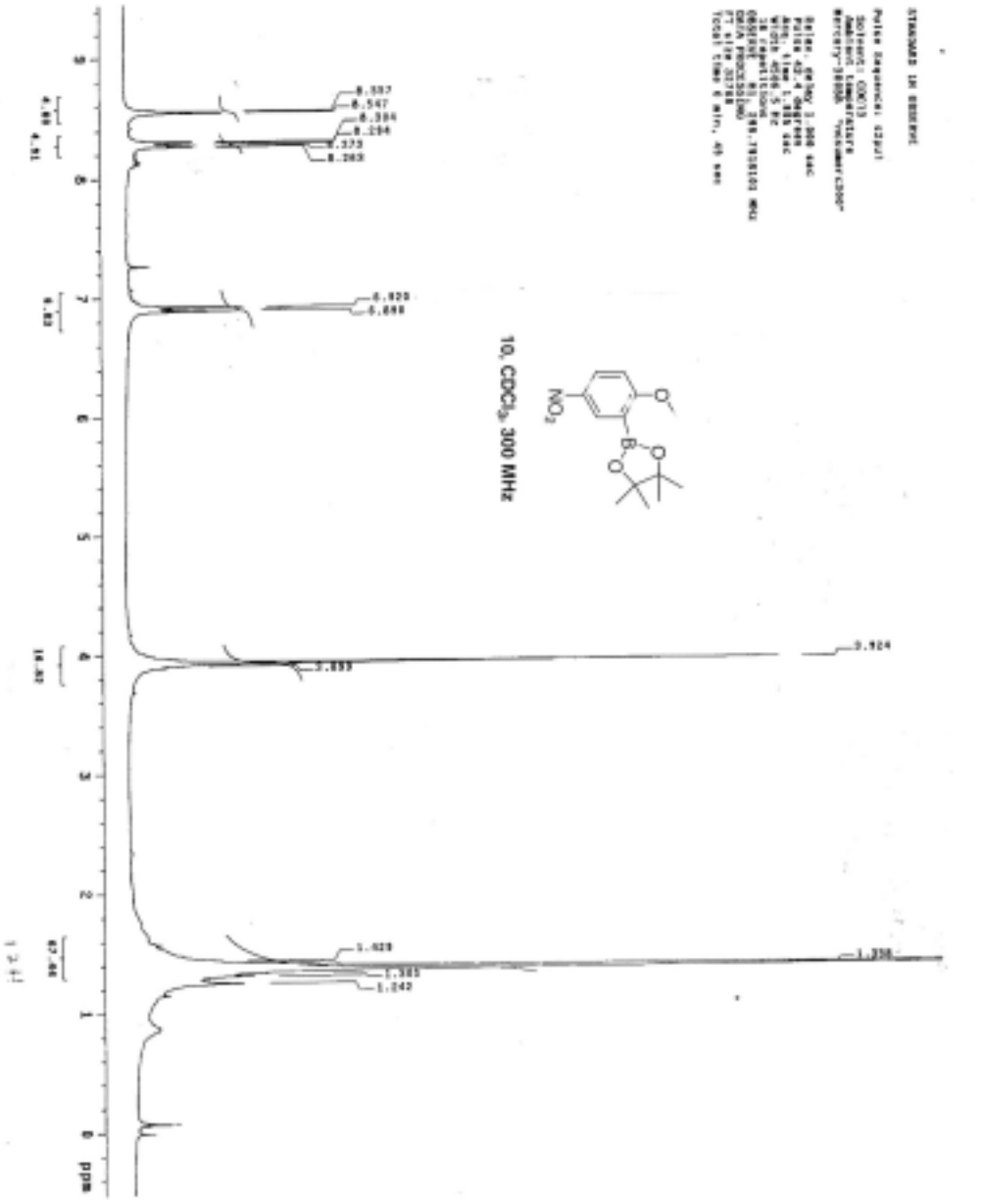
10, CDCl3, 300 MHz
NO2
B
O
O
O
8.557
8.547
8.304
8.294
8.273
8.263
7.929
7.888
7.853
1.929
1.385
1.242
1.338
ppm

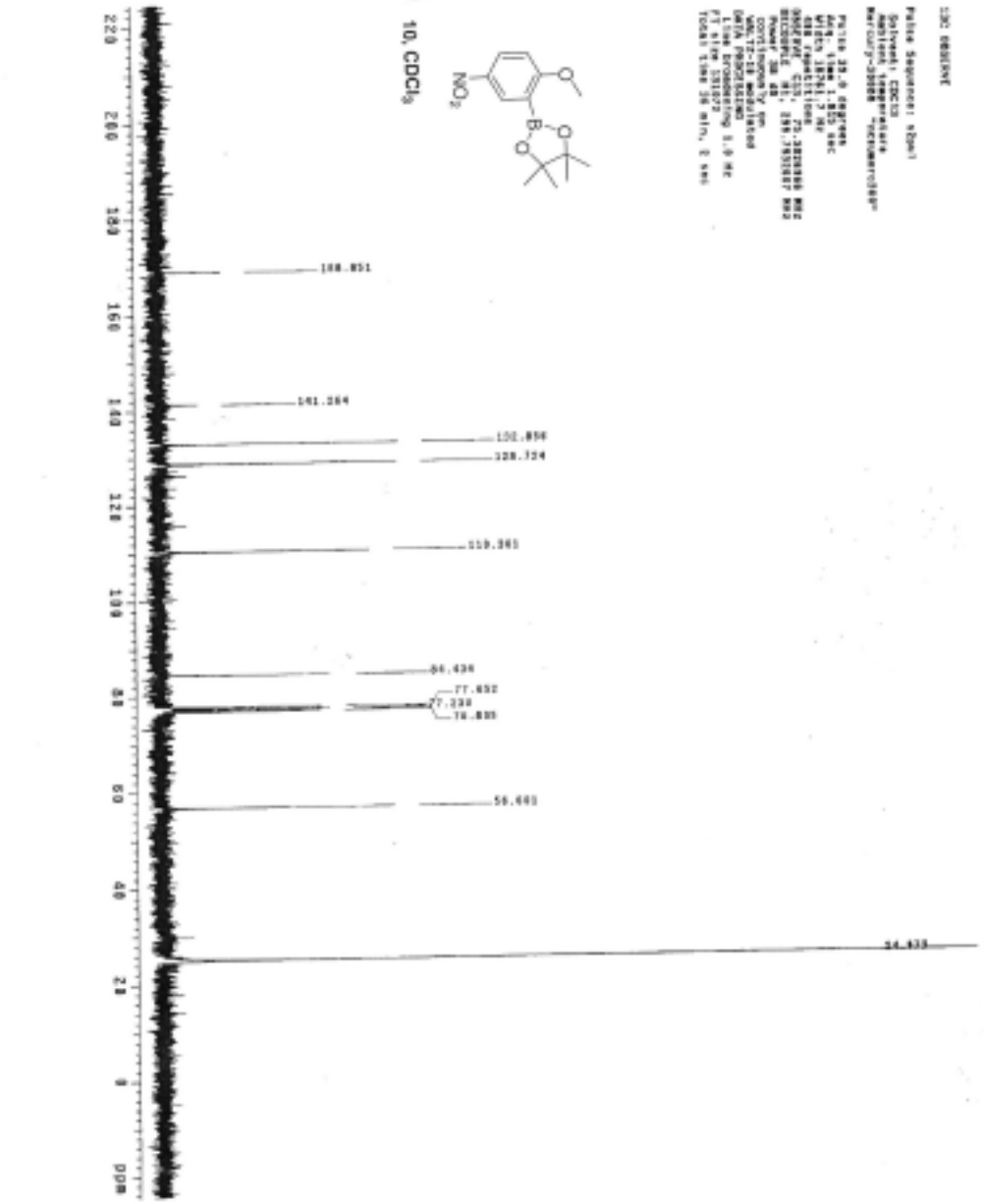
10, $CDCl_3$
NO_2
O
B
O
O
188.851
161.264
132.856
128.724
119.361
84.434
77.652
77.334
76.885
58.661
24.433
220
200
180
160
140
120
100
80
60
40
20
0
-20

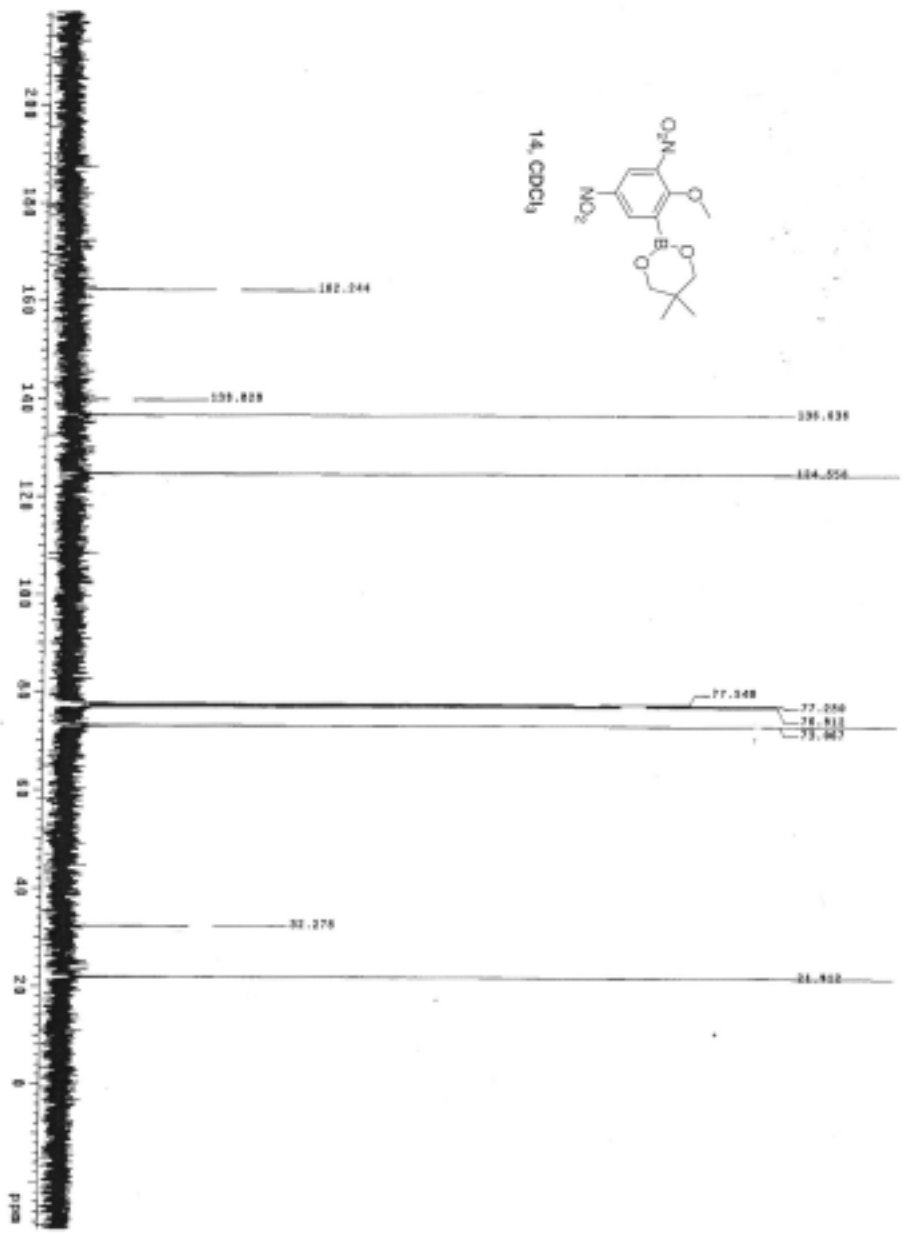
14, CDCl3
O2N
NO2
O
B
O
O
182.244
150.828
135.635
134.554
77.348
77.250
76.933
73.967
32.278
24.902
ppm

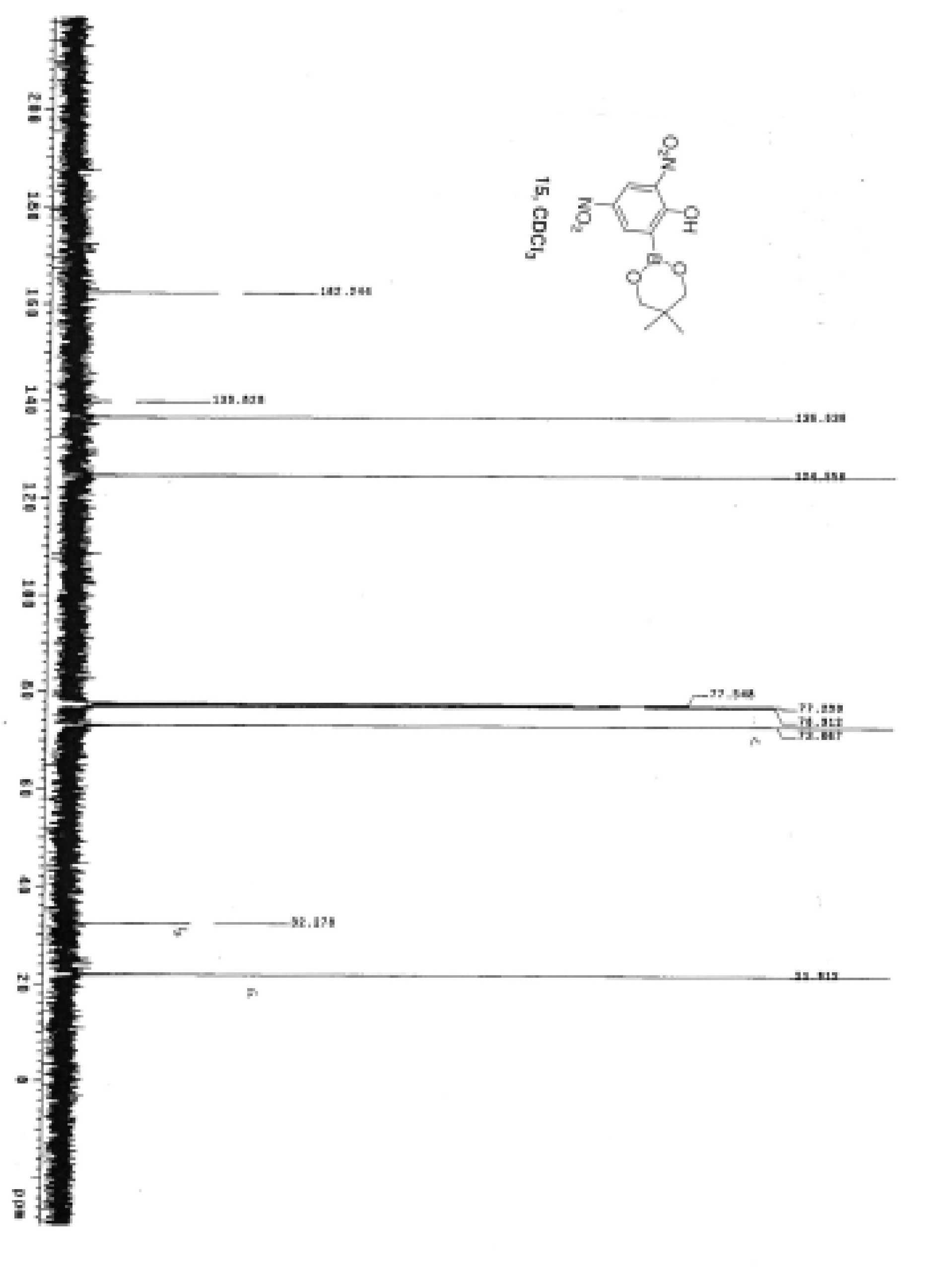
15, CDCl3

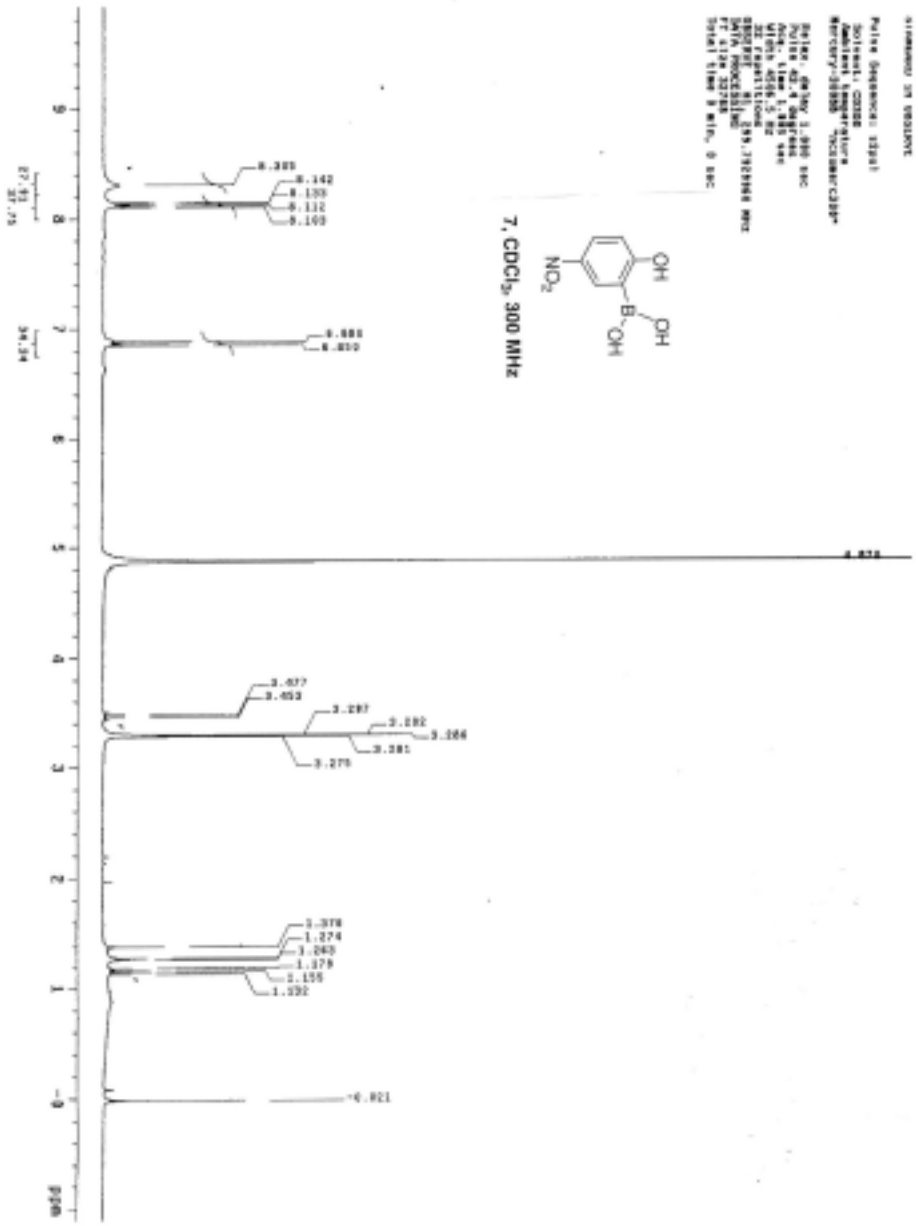
7, CDCl3, 300 MHz
OH
OH
B
OH
NO2
8.305
8.142
8.133
8.112
8.103
8.001
8.000
4.978
3.457
3.453
3.287
3.282
3.266
3.261
3.275
1.378
1.274
1.265
1.179
1.155
1.152
0.021
ppm